

Earth Explorer 9 Candidate Mission FORUM — Report for Mission Selection



Reference	ESA-EOPSM-FORM-RP-3549
Issue/Revision	1.0
Date of Issue	21/06/2019
Status	Issued



ACKNOWLEDGEMENTS

This report is based on contributions from the FORUM Mission Advisory Group (MAG):

Helen Brindley (Imperial College London, UK)
Stefan A. Buehler (University of Hamburg, DE)
Dorothee Coppens (EUMETSAT, INT)
Adrien Deschamps (CNES, FR)
Steven Dewitte (Royal Meteorological Institute of Belgium, BE)
Bianca M. Dinelli (ISAC-CNR, IT)
Laurent Labonnote (University of Lille, FR)
Quentin Libois (Météo-France, FR)
Martin Mlynczak (NASA Langley Research Center, US)
Luca Palchetti (INO-CNR, IT)
Marco Ridolfi (University of Bologna, IT)
Martin Riese (Forschungszentrum Jülich, DE)
Roger Saunders (Met Office, UK)

The scientific content of the report was compiled by Hilke Oetjen (Scientific Coordinator), based on inputs derived from the MAG, supporting scientific studies, and campaign activities, with contributions from Richard Bantges, Marco Barucci, Claudio Belotti, Giovanni Bianchini, Elisa Castelli, Simone Ceccherini, Bertrand Cluzet, Mathieu Compiègne, Ugo Cortesi, William Cossich, Francesco D'Amato, Samuele Del Bianco, Mohamadou Abdoulaye Diallo, Gianluca Di Natale, Alessio Di Roma, Marie Dumont, Marco Gai, Dina Khordakova, Lukas Kluff, Tiziano Maestri, Davide Magurno, Alessio Montori, Jonathan E. Murray, Piera Raspollini, Markus Rettinger, Christian Rolf, Jacqueline E. Russell, Luca Sgheri, Ralf Sussmann, Silvia Viciani, Jérôme Vidot, Hannes Vogelmann, Laura Warwick, the UK FAAM team, the UK MetOffice, and Dirk Schuettemeyer.

The technical content of the report was compiled by Bernardo Carnicero Domínguez (Technical Coordinator) and Charlotte Pachot (Payload Technical Coordinator) with contributions from Itziar Barat, Paolo Bensi, Christophe Caspar, Miguel Copano, Mauro Federici, Dulce Lajas, Flavio Mariani, Vasco Pereira, Stefanie Riel, Gonçalo Rodrigues, Bernd Sierk, Kate Symonds and Andrea Tromba, based on inputs derived from the industrial Phase A system and technical activities and the FORUM end-to-end performance simulator activity under the responsibility of the Future Missions and Instruments Division. Special thanks go to the industrial teams who have supported ESA to bring this report together in a very short time after the Phase A Preliminary Requirements Review.

Recommended citation:

ESA (2019). *Report for Mission Selection: FORUM*, European Space Agency, Noordwijk, The Netherlands, ESA-EOPSM-FORM-RP-3549, 263pp.

Cover image design: Earth Observation Graphics Bureau (EOGB)
Copyright: @ 2019 European Space Agency

TABLE OF CONTENTS:

ACKNOWLEDGEMENTS.....	2
TABLE OF CONTENTS:	3
EXECUTIVE SUMMARY	7
1 INTRODUCTION.....	11
2 BACKGROUND AND SCIENTIFIC JUSTIFICATION	14
2.1 The Far-Infrared Earth: the Benefit of FORUM	19
2.1.1 The Greenhouse Effect, Atmospheric Cooling, Water Vapour and the Critical Contribution of the FIR	19
2.1.2 The Role of Spectroscopy	23
2.1.3 Ice Clouds and Radiative Impacts.....	25
2.1.4 Climate Forcing and Feedbacks: the Power of Spectral Resolution.....	27
2.1.5 Numerical Weather Prediction and Climate Model Evaluation.....	29
2.2 Readiness and Unique Contribution	32
2.2.1 Space-Based Heritage	32
2.2.2 Lessons Learned from Campaigns.....	33
2.2.3 Unique Contribution: Why Now?	34
2.3 Filling the Knowledge Gap.....	35
3 RESEARCH OBJECTIVES	36
3.1 Mission Objectives	38
3.1.1 Primary Objectives	38
3.1.2 Secondary Objectives	40
4 OBSERVATIONAL REQUIREMENTS	41
4.1 General Observational Concept.....	41
4.2 Observational Requirements Related to the FSI.....	41
4.2.1 Measurement of the Full Infrared Spectrum at TOA	41
4.2.2 Spectral Resolution	42
4.2.3 Noise Requirements	44
4.2.4 Spectral Calibration.....	46
4.2.5 Requirements for the Calibration Absolute Radiometric Accuracy	47
4.2.6 Requirements on Stability and Pointing of the Line-of-Sight.....	49
4.3 Observational Requirements related to FEI.....	51
4.3.1 Measurement of Thermal Colocated Images.....	51
4.3.2 Size and Spatial Resolution, Spectral Range, Noise and Accuracy Requirements	52



4.4 Spatial and Temporal Sampling Requirements	56
4.4.1 Spatial Coverage Requirements	56
4.4.2 Spatial Sampling Requirement and Ground Pixel Size	56
4.4.3 Mission Duration and Orbit	57
4.5 Loose Formation Mission Concept with an Operational Mission.....	57
4.5.1 Advantages of Flying in Loose-Formation with IASI-NG	58
4.5.2 Temporal and Spatial Co-registration Requirements with IASI-NG.....	59
4.6 FORUM Products.....	60
4.6.1 Level-1 Products	60
4.6.2 Level-2 Products and Potential Higher-Level Products.....	61
4.6.3 Data Latency.....	61
5 MISSION ELEMENTS	63
5.1 Mission Architecture Overview.....	63
5.2 Mission Analysis	64
5.2.1 Orbit Selection.....	64
5.2.2 Loose Formation Flying and Orbit Maintenance	65
5.3 Space Segment	67
5.3.1 Overview	67
5.3.2 Satellite Configuration	67
5.3.3 Payload	70
5.3.4 Platform.....	105
5.3.5 Budgets	118
5.4 Launcher	121
5.5 Ground Segment and Data Processing.....	123
5.5.1 Overview of Ground Segment Elements.....	123
5.5.2 Flight Operation Segment	123
5.5.3 Payload Data Ground Segment	127
5.5.4 Level-0 to Level-1 Data Processing.....	129
5.6 Operations, Utilisation and Disposal Concept	132
5.6.1 Overview	132
5.6.2 LEOP and Commissioning.....	132
5.6.3 Nominal Operations and Calibrations	133



5.6.4 Contingency Operations.....	134
5.6.5 Disposal	135
6 SCIENTIFIC DATA PROCESSING AND VALIDATION CONCEPT	137
6.1 Retrieval Approach	137
6.1.1 Cloud Detection and Classification.....	139
6.1.2 Retrieval Method.....	140
6.1.3 Calculation of Spectrally-Resolved and Total OLR Fluxes.....	145
6.2 Validation Concept.....	147
6.2.1 Validation Organisation	147
6.2.2 Validation Methods.....	148
6.2.3 Quality Monitoring.....	150
7 MISSION PERFORMANCE ESTIMATION.....	151
7.1 FORUM End-to-End Mission Performance Simulator.....	151
7.1.1 FEES Geometry Module.....	152
7.1.2 FEES Scene Generator Module.....	152
7.1.3 FEES Instrument and Level-1 Processing Modules	154
7.1.4 FEES Level-2 Retrieval Module.....	157
7.1.5 FEES Performance Assessment Module.....	161
7.1.6 FEES Test Scenarios Description.....	161
7.2 Level-1 Mission Performance.....	163
7.2.1 Level-1 Mission Performance Summary	163
7.2.2 Level-1 Mission Performance.....	166
7.2.3 FORUM Sounding Instrument (FSI) Level-1 Performance	169
7.2.4 FORUM Embedded Imager (FEI) Level-1 Performance.....	176
7.3 Scientific Performance	179
7.3.1 FEES Performance	179
7.3.2 Complementary Scientific Performance	182
7.4 Campaign Data Analysis	198
7.4.1 Ground-based Campaign at Zugspitze.....	198
7.4.2 Airborne Measurements	202
8 MISSION CONTEXT.....	208
8.1 Science and Societal Impact	208
8.2 Global Mission Context.....	210



8.3 User Community Readiness 212

8.4 Applications 213

8.4.1 Evaluating and Improving Earth-System Models using FORUM Level-1 Radiances 213

8.4.2 The role of FORUM Level-2 Products for Climate 214

9 PROGRAMMATICS 218

9.1 Scientific Maturity, Critical Areas and Risks..... 218

9.1.1 Scientific Maturity: key questions for SRL 218

9.1.2 Critical Scientific Areas and Risks 221

9.1.3 Scientific Roadmap 222

9.1.4 Scientific Concluding Remarks 223

9.2 Technical maturity, Critical Areas and Risks 226

9.2.1 Summary 226

9.2.2 Satellite and Platform..... 227

9.2.3 FORUM Sounding Instrument and FORUM Embedded Imager 228

9.3 Development Approach and Schedule..... 231

9.3.1 Overall Development Approach and Model Philosophy 231

9.3.2 Schedule 232

9.4 Conclusion..... 233

REFERENCES 235

ACRONYMS 259



EXECUTIVE SUMMARY

This report forms the basis for the selection of the ninth Earth Explorer mission within ESA's Earth Observation Programme. Two competing 'Fast Track' candidates, the Far-infrared Outgoing Radiation Understanding and Monitoring (FORUM) mission and the Surface ocean KInematics Multiscale (SKIM) mission. Each have each undergone a rapid and compressed Phase A feasibility study. This report covers the FORUM mission.

FORUM aims to measure the Earth's top-of-atmosphere emission spectrum in the 100 to 1600 cm^{-1} (i.e. 6.25 to 100 μm) spectral region filling the observational gap in the far-infrared (100 to 667 cm^{-1} i.e. from 15 to 100 μm), which has never been observed from space, spectrally resolved, and in its entirety. This measurement will improve the understanding of the climate system by supplying, for the first time, most of the spectral features of the far-infrared contribution to the Earth radiation budget, particularly focusing on the water vapour contribution related to the continuum absorption in the rotational band, the cirrus cloud properties, and the ice/snow surface emissivity.

It has long been acknowledged that the far-infrared: defined here as wavelengths greater than 15 μm (wavenumbers smaller than 667 cm^{-1}) plays a pivotal role in determining the planet's energy budget. Under clear-sky conditions, this region contributes a quarter to one-third of the Earth's greenhouse effect. Under all-sky conditions its influence on Earth's emitted energy is even larger, with the typically colder emitting temperatures of mid- and high-level clouds shifting the peak of the Planck function to longer wavelengths such that, in the global mean, approximately half of Earth's emission to space occurs within the far-infrared.

The dominant role of the far-infrared in determining Earth's outgoing longwave radiation is in part due to the strong water vapour rotation band at wavelengths greater than 16.5 μm . This in turn means that radiative emission in the far-infrared is particularly sensitive to water vapour in the climatically important upper troposphere/lower stratosphere region. Similarly, clear-sky longwave radiative cooling through the mid and upper troposphere is dominated by the contribution from the far-infrared.

For much of the globe this water vapour absorption means that far-infrared surface emission cannot be sensed from space, but in very dry, clear-sky conditions experienced in the Arctic and Antarctica this is no longer the case. Here, the outgoing longwave radiation becomes sensitive to surface emission within the far-infrared through a number of micro-windows which become progressively more transmissive as water vapour concentration reduces. Very recent studies show that better understanding of this unexplored phenomenon may play a critical role in both reducing persistent climate model biases and determining the pace of Arctic and Antarctic climate change.

Moreover, cirrus clouds (or cirri), typically poorly constrained by observations yet crucial players in determining current and future climate, have emitting temperatures that place the peak of their radiative emission within the far-infrared. The ability to correctly simulate the

interaction of the radiation spectrum with cirri relies on the capability of optical models to adequately represent their scattering and absorption properties. These are crucially dependent on the complex ice-crystal shapes and their size distributions within the clouds. Recent advances in cirrus cloud modelling have attempted to capture the bulk microphysical properties of cirri spanning the entire electromagnetic spectrum. However, while there are many satellite observations of the reflected visible and emitted near- and mid-infrared radiation in the presence of cirrus clouds that can be exploited to test these developments, there are no such observations that span the far-infrared. This represents a major barrier to improving the confidence in the ability to understand and monitor cirrus properties and their interaction with Earth's outgoing longwave energy, particularly since the contrast in ice and water refractive indices between the far-infrared and mid-infrared implies that unique information relating to cloud classification and microphysics can be leveraged only from measurements of the far-infrared spectrum.

The FORUM mission directly addresses several of ESA's Living Planet Challenges particularly with Challenge A1: *Water vapour, cloud, aerosol and radiation processes and the consequences of their effects on the radiation budget and the hydrological cycle*. The mission will supply multi-annual "accurate and stable measurements of the long-wave radiation at the top of the atmosphere to assess the contributions of clouds and aerosols, greenhouse gases, in particular water vapour, and surface optical properties to the radiation budget", which are required to reduce the "largest uncertainty (still present) to estimates and interpretations of Earth's changing energy budget" (IPCC, 2013). The "accurate descriptions of the properties of clouds and the distribution of water and ice in the atmosphere", supplied by FORUM, will give a better understanding of the role of clouds in the climate system, including cloud–radiation feedback.

The overarching research goal of the FORUM mission is the evaluation of the role of the far-infrared in shaping the current climate and thus reduce uncertainty in predictions of future climate change. This will be addressed by: a) building a highly accurate global dataset of far-infrared radiances to validate present-day state as captured by Earth system models; b) using these measurements to understand and constrain the processes that control far-infrared radiative transfer and hence Earth's greenhouse effect; c) updating the parameterisations of these processes for implementation in radiative transfer codes, and ultimately in Earth system models; and d) characterising critical feedback mechanisms.

While the primary focus of FORUM will exploit the high radiometric accuracy, instantaneous radiance observations will also be used for the following applications: a) retrieval of far-infrared surface emissivity in appropriate conditions (clear-sky, low precipitable water vapour); b) assessment of additional benefit of far-infrared compared to state-of-the-art hyperspectral mid-infrared radiances for upper troposphere/lower stratosphere H₂O retrieval; c) detection of thin cirrus cloud; and d) retrieval of ice-cloud optical depth, ice water path cloud top height, cloud geometrical thickness (or equivalently cloud bottom height) and particle size.

The FORUM mission consists of a single satellite carrying two optical instruments: the FORUM Sounding Instrument (FSI) and the FORUM Embedded Imager (FEI). The satellite flies in a loose formation with MetOp-SG(A1) in a 29-day repeat-cycle Sun-synchronous



orbit, with a Mean Local Solar Time at the descending node of 09:30 and an average orbit altitude of 830 km. Vega-C is the baseline launcher in a dual-launch configuration.

FORUM performs continuous step-and-stare nadir-looking observations of spectrally-resolved top of atmosphere radiances in the mid-infrared and far infrared region of the spectrum. The primary instrument is the FSI, a single-pixel Fourier Transform Spectrometer (FTS) sampling the electromagnetic spectrum from 1600 cm^{-1} to 100 cm^{-1} ($6.25\text{ }\mu\text{m}$ to $100\text{ }\mu\text{m}$) with a spectral resolution better than 0.5 cm^{-1} . The FSI single pixel is co-located with the footprint of the FEI, a single-band-infrared-imager centred at $10.5\text{ }\mu\text{m}$ with a bandwidth of $1.5\text{ }\mu\text{m}$ and used for scene heterogeneity determination. Both instruments share several common units, such as the entrance aperture, the pointing mechanism, the thermal and mechanical framework and the radiometric calibration devices. The FORUM payload data will be downlinked to the ground station with a radio link in the X-band. The generic Earth Explorer ground segment infrastructure is used for the FORUM mission.

The space segment is designed for a nominal lifetime of four years with sufficient propellant to last six years. The FORUM satellite is largely based on a recurrent three-axis stabilised Earth-pointing platform, with specific mission adaptations, which ensure a streamlined satellite development approach to meet the stringent programmatic boundary conditions for this Earth Explorer Fast Track mission while minimising the development risks.

FORUM is considered a technically feasible mission. Critical technologies have been identified and dedicated pre-development activities have been initiated during Phase A. Based on the results of pre-developments achieved so far, and assuming successful completion of the pre-developments planned to be initiated in phase B1, it is expected to reach at least a Technology Readiness Level of 5 or 6 by the end of Phase B1. The main critical technologies and pre-developments initiated during the Phase A are:

- beamsplitter
- calibration blackbody
- detection chain
- interferometer mechanism.

In terms of scientific readiness, the critical scientific areas of maturity and risk have been assessed and there are no major issues of concern with respect to the scientific development of FORUM. The mission and research objectives have remained stable with respect to the original proposal. However they have been significantly refined within dedicated science activities and can be considered consolidated. During the Phase A, two measurement campaigns were performed, one ground-based at Zugspitze summit in Germany, and one airborne over the UK. The results will undergo further investigation. The first ever measurements of far-infrared emissivity with simultaneous characterisation of the studied snow sample, already delivered impressive results confirming, in parts, theoretical calculations. A complex end-to-end performance simulator has been developed. Based on simulations and dedicated campaign activities, FORUM was demonstrated to be compliant with its scientific mission requirements.



Numerous studies have been performed, demonstrating the impact of far-infrared radiances and fluxes for weather and climate. A diverse range of researchers (climate scientists, numerical weather prediction and climate modellers, atmospheric chemists, spectroscopists) are anticipating real FORUM data to test and improve this understanding. The interest from the user community has been demonstrated by the participation of about 90 international researchers at the first FORUM user workshop held in 2018.

On the basis of the above, it is considered that FORUM has reached the required Scientific Readiness Level of 5 at the end of Phase A.

Assuming the expected successful outcome of on-going and planned technology pre-developments, the maturity of critical technologies will reach the required level prior to the start of the implementation phase. The development schedule is driven by the instrument development, calibration & characterisation and test phases. The Design Development and Verification Plan and the associated schedule are not yet fully consolidated and further improvements would be necessary to recover - with margins - the launch date by the end of 2025.

FORUM will be the first satellite mission to provide spectrally-resolved measurements in the far-infrared range, enabling climate research and acquiring knowledge with which to reduce uncertainty in predictions of future climate change.

It is judged that the FORUM mission concept has reached the expected scientific and technical readiness level at the end of Phase A, and is sufficiently mature for implementation as Earth Explorer 9. The development schedule is compatible with a launch in the 2026 timeframe.



1 INTRODUCTION

The Earth Observation Envelope Programme is a rolling programme designed to underpin European efforts in Earth Observation from space. The Earth Explorer element of the programme consists of a series of space missions addressing critical Earth science issues. To date ESA has developed and launched five such Earth Explorer research missions:

- GOCE - Gravity field and steady-state Ocean Circulation Explorer
- SMOS - Soil Moisture and Ocean Salinity
- CryoSat - Polar Ice Monitoring
- Swarm - Earth's Magnetic Field and Environment Explorer
- Aeolus - Doppler Wind Lidar

and is currently implementing a further three:

- EarthCARE - Clouds, Aerosols and Radiation Explorer
- Biomass - to take global measurements of forest biomass
- FLEX – Fluorescence Explorer

The Agency aims to achieve a clear appreciation of the science community's views on what mission concepts will give the highest scientific return and best response and solution to scientific challenges and issues facing society (Earth Observation Science Strategy for ESA: A New Era for Scientific Advances and Societal Benefits, ESA SP-1329/1 and ESA's Living Planet Programme: Scientific Achievements and Future Challenges – Scientific Context of the Earth Observation Science Strategy for ESA, ESA SP-1329/2, European Space Agency, Noordwijk, the Netherlands, 2015).

This series of pioneering Earth Explorer satellite missions represents the epitome of Europe's technical endeavour in conceiving and realising new Earth-observing capabilities. Each of these research missions offers new innovative measurement techniques to explore and understand different aspects of the Earth system. Meanwhile, the guiding principle remains to define, develop and operate these Earth Explorer missions in close cooperation with the scientific community to address the most critical Earth-science questions in as comprehensive and effective a manner as possible.

In 2016, ESA initiated a call to invite proposals for mission concepts that exhibit a certain degree of maturity, or 'readiness', and that demonstrate the potential of new innovative Earth Observation techniques of relevance to both the scientific and the applications communities. Mission Proposers were encouraged to make use of recurrent hardware and software, of formation and constellations (possibly via national and/or international partnerships), and launch opportunities. Specific to this Call, the scope of the EE-9 mission was to address science questions that have a direct bearing on societal issues such as:

- Food security
- Availability of fresh water
- Management of the Earth's resources and energy
- Health of the planet and humankind
- Disaster risk reduction and improvement of disaster resilience



- Climate change

Not only the feasibility of the concept in terms of realising its scientific objectives and meeting its technical challenges has to be demonstrated, but also the capacity of the mission to address scientific questions in the context of above major societal issues.

In 2017, two Earth Explorer 9 candidates were selected for feasibility study (Phase A): FORUM and SKIM.

The Far-infrared Outgoing Radiation Understanding and Monitoring (FORUM) mission aims to measure the Earth's top-of-atmosphere emission spectrum in the 100 to 1600 cm^{-1} (6.25 μm to 100 μm) spectral region covering the observational gap of the far-infrared 100 – 667 cm^{-1} (15 μm to 100 μm), which has never been observed from space, spectrally resolved, and in its entirety. This measurement will provide an improved understanding of the climate system by supplying, for the first time, most of the spectral features of the far-infrared contribution to the Earth radiation budget, particularly focusing on the water vapour contribution related to the continuum absorption in the rotational band, cirrus cloud, and ice/snow surface emissivity.

The Sea surface Kinematics Multiscale monitoring (SKIM) mission aims to observe directly and simultaneously, Ocean Total Surface Current Velocity and wave-spectra to characterise and quantify their role in ocean/atmosphere processes and their societal impact at the global and regional scale.

Owing to the fact that concepts were invited where scientific as well as technological investigation/validation have progressed, the Agency has implemented a streamlined schedule as compared to previous Earth Explorer missions.

The Reports for Mission Selection capture the status of the respective mission concept at the end of Phase A activities. The two volumes will be provided to the Earth-observation community as a basis for the User Consultation Meeting held in July 2019, and for the subsequent recommendation for selection of a single Earth Explorer 9 mission by the Advisory Committee for Earth Observation.

Each Report for Mission Selection follows a common format and logic. Each identified the scientific questions and related key societal issues motivating the mission and its research objectives. After establishing the scientific basis and rationale, the specific mission objectives are outlined and traced to a set of requirements used for system concept definition. Consolidated descriptions of two competing technical concepts are provided for each candidate mission, the designs of which are optimised to respond to the mission requirements. Based on each design concept, the end-to-end performance is simulated and the maturity of the geophysical data processing is outlined. The results are used to establish the feasibility and maturity of the concept as well as to evaluate the capability to fulfil the mission requirements and scientific objectives.

Each report comprises this introductory first chapter and eight subsequent chapters as follows:



Chapter 2 identifies the background and scientific issues to be addressed by the mission. It provides justification for the mission and includes a review of the current scientific understanding of the issue in question while identifying the potential advances in knowledge that the mission could provide.

Chapter 3 draws on arguments presented in Chapter 2, and summarises specific research objectives and related mission objectives.

Chapter 4 outlines the mission requirements, including required Level-2 geophysical data products and observational parameters, the need for these observations to be made from space, and aspects of timeliness and timing of the mission.

Chapter 5 provides an overview of the system elements, including the space and ground segments, operations, calibration and the data processing up to Level-1b.

Chapter 6 details the scientific data processing and validation concept, including processing and calibration/validation as well as the data processing techniques that need to be implemented to meet the data product requirements.

Chapter 7 makes a comparison of the expected versus the required performance and ability to fulfill the research/observational objectives based on the documented system concept.

Chapter 8 documents the readiness of the scientific user community in respect to planned use of the unique scientific products, the global context in terms of complementary missions as well as the operational or applications potential of the data products. This chapter also outlines the societal benefit of the mission.

Chapter 9 outlines a programme of implementation. It also addresses the technical maturity, the development status of key technologies, and schedules.

2 BACKGROUND AND SCIENTIFIC JUSTIFICATION

Climate and its variability shapes human well-being. Emerging interdisciplinary research demonstrates how it determines the nature of societies, affects the characteristics and functioning of ecosystems and impacts worldwide economic performance (e.g. Carleton and Hsiang, 2016). Many societal decisions – governing financial investments, infrastructure design, resource management, and policy – require information about the current climate, and use predictions concerning how it may change. By improving the understanding of the current and future state of the climate, society's basis for decision making is enhanced and strengthened, benefiting people and communities across the globe.

Climate change has been identified as one of the greatest challenges of this time (United Nations, 2015). Observations show that some of the most fragile areas of the planet are changing at a faster rate than has ever been seen in history, with perhaps irreversible, decline in biodiversity, and implications for water and food security. With its global reach, Earth observation from space plays a critical role in monitoring climate, providing key measurements that can be used to both pinpoint and document how it is changing, while simultaneously confronting the modelling tools that are used to predict the future.

In the climate community, perhaps the most well established metric used to characterise the climate state is the global near-surface temperature. A critical finding from the early 2000s was that state-of-the-art climate models could only replicate the historical near-surface temperature record through the 20th Century if the anthropogenic emissions of greenhouse gases and aerosols were included in the model simulations (Jones et al., 2013). However, progress in reducing the spread of future climate predictions from the same modelling tools has been less forthcoming despite improvements in the understanding of the complexity of the Earth system (Knutti and Sedláček, 2013). Earth system models today incorporate a large array of interlinked processes, representing the best efforts to capture this complexity. However, the range of predictions of future changes in global mean surface temperature in response to a doubling of carbon dioxide – the climate sensitivity (Box 2.1) – remains stubbornly high (Intergovernmental Panel on Climate Change (IPCC) reports; IPCC, 1990, Stocker et al., 2013). Economic modelling suggests that reducing uncertainty in climate sensitivity by a factor of two would have a tremendous economic value, of between \$5 – 20 trillion (Cooke et al., 2014, 2017; Hope, 2015).

Box 2.1: Climate sensitivity

At the global, multi-annual scale, the energy balance at the top of Earth's atmosphere can be considered to be in equilibrium such that the net incoming energy from the Sun is balanced by the terrestrial radiation escaping to space (also termed outgoing longwave radiation, OLR). Perturbations to this balance will result in climate adjustments so that equilibrium at the top of the atmosphere is restored. For example, increases in carbon dioxide (CO₂) will result in additional absorption of surface emitted radiation by the atmosphere, reducing the OLR and leading to warming, such that Earth emits more radiation which re-establishes the balance. In reality this readjustment process takes time. Because of the long timescales of ocean mixing and the large thermal inertia of the ocean, it can take centuries for the balance to re-establish and for temperatures to reach a new

equilibrium state. During this period of adjustment, Earth's energy imbalance is a heat loss or gain that will ultimately be realised as a change in temperature at equilibrium.

Equilibrium climate sensitivity is defined as the equilibrium global surface temperature change to a sustained doubling of atmospheric CO₂ concentration and provides a relatively simple means of comparing the response of a wide array of different climate models. Mathematically it is defined as:

$$\Delta T_s = \Delta F / \lambda \quad 2.1$$

where ΔF is the radiative forcing or change in the net incoming energy (incident solar radiation minus reflected solar radiation minus OLR) at the top of the atmosphere (TOA) owing to a doubling of atmospheric CO₂ concentrations with respect to pre-industrial levels, ΔT_s is the resulting change in global mean surface temperature required to restore equilibrium and λ is the climate feedback parameter. In this formulation, λ contains the effects of all the feedback processes that contribute to restore the radiative balance at the TOA. This includes the response of clouds, water vapour, surface radiative properties and vertical temperature profiles to the surface temperature change caused by the original radiative forcing.

The first IPCC report in 1990 estimated an equilibrium climate sensitivity of between 1.5 and 4.5 K, with a 'best guess' estimate of 2.5 K. Subsequent reports have updated these values slightly but the latest published estimates, in 2013, give an identical range. Estimates emerging from the current Coupled Model Intercomparison Project (CMIP6), which will contribute to the next IPCC report in 2021, hint at a higher value, suggesting Earth will warm faster than thought (Voosen, 2019). However, there has been a rather depressing lack of progress in pinning down an exact value for the Earth's equilibrium climate sensitivity, principally because of uncertainties associated with the feedbacks in the system. The large uncertainty in equilibrium climate sensitivity is one of the largest uncertainties in predicted future economic impacts of any given scenario of future anthropogenic emissions (Interagency Working Group on Social Cost of Carbon Memo, 2010, or SCC, 2010).

It is commonly accepted that the range in climate sensitivity is driven mainly by uncertainties associated with the magnitude and, in some cases, sign of feedbacks in the system (Stocker et al., 2013). In this context, climate feedbacks are defined as physical processes that respond to the surface-temperature change induced by a radiative forcing, such as an anthropogenic increase in CO₂. They can amplify or reduce the original temperature change. At the global scale, the most critical feedbacks are related to cloud, water vapour and the vertical temperature profile. To reduce uncertainty in future predictions of climate, observations that are able to test the understanding of the link between the drivers of change (the radiative forcings) and the climatic response (the feedbacks) are urgently needed. Moreover, as increasingly recognised by organisations such as the World Meteorological Organization's Global Climate Observing System (GCOS), these observations should be made with an accuracy that allows them to be used, with confidence, as a benchmark against which future measurements can be compared.

This basic principle lies behind the concept of GCOS's Essential Climate Variables (ECVs) and the emergence of dedicated projects to characterise and develop fundamental climate data records (e.g. <http://www.fiduceo.eu/>). Of these, perhaps the most fundamental ECV is Earth's Radiation Budget (ERB), measured at the top of the Earth's atmosphere. Consisting of two components, the net incoming solar radiation and the outgoing terrestrial radiation, it measures the flow of energy into and out of the Earth system. At equilibrium, on global multi-annual scales these components balance, and during a transition to a new equilibrium their imbalance determines the heating or cooling yet to be realised, as a temperature change. Measurements of the ERB from space thus contain a wealth of information about the present and future climate and are essential to understand the climate and how it is evolving with time.

Outgoing terrestrial radiation is the energy emitted by the Earth-system that escapes to space. Because of the typical temperatures of Earth's surface and the overlying atmosphere, more than 97 % of this emitted energy occurs in the wavelength range 4–100 μm (100–2500 cm^{-1}) and is commonly termed outgoing longwave radiation or OLR. Greenhouse gases such as CO_2 have strong absorption bands over this wavelength range. Increases in their atmospheric concentrations lead to enhanced trapping of longwave radiation and a reduction in OLR in these bands (Fig. 2.1a). All other properties remaining unchanged, the additional heat trapped in the system will ultimately result in an increase in surface temperature. This increase leads to enhanced OLR as the Earth system attempts to regain equilibrium at the top of the atmosphere. Interestingly, this increase is manifested across a quite different spectral range to the original forcing (Fig. 2.1b). In fact it is possible to decompose different forcings and feedbacks into an associated *spectral signature* (Box 2.2). In this way, the distribution of Earth's emitted energy to space with wavelength implicitly

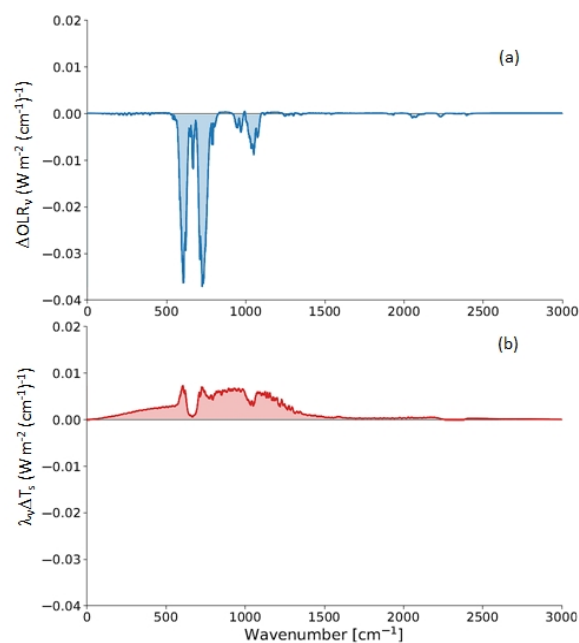


Figure 2.1 Spectral variation of (a) change in OLR due to a doubling of CO_2 after stratospheric adjustment; (b) the spectral climate response, $\lambda_w \Delta T_s$, in restoring equilibrium at the top of the atmosphere. Calculations by clear-sky Radiative Convective Equilibrium model KONRAD. (L. Kluft, Max Planck Institute for Meteorology, Hamburg)

contains the imprint of multiple forcing and feedback processes. Highly accurate measurements across the OLR spectrum thus provide a means of directly linking changes in Earth’s energy balance to the underlying mechanisms behind the change. Such measurements can only be made from space.

Box 2.2: The spectral signature of radiative forcing and feedbacks

The top of atmosphere broadband radiation flux measurements comprising the ERB provide key observational constraints for understanding the energy balance of the climate system and its evolution in time. However, it is difficult to diagnose specific perturbations to, and responses of, the climate system from such measurements because they integrate the contribution from these different effects into a single number. Cancellation effects can, and do, occur (Hansen, 2005), masking the competing signals. In contrast, by measuring the OLR spectrum, the impact of different controlling factors on the radiation energy budget can be disentangled (e.g. Harries et al., 2005; Kiehl, 1983; Leroy et al., 2008; Slingo and Webb, 1997).

Fig. 2.2 provides examples of the type of spectral signatures that might be expected to emerge owing to specific forcing and feedbacks in the climate system. These have been calculated using climate model simulations for a double-CO₂ climate run, comparing spectra representative of pre-industrial conditions (atmospheric CO₂ concentrations set at

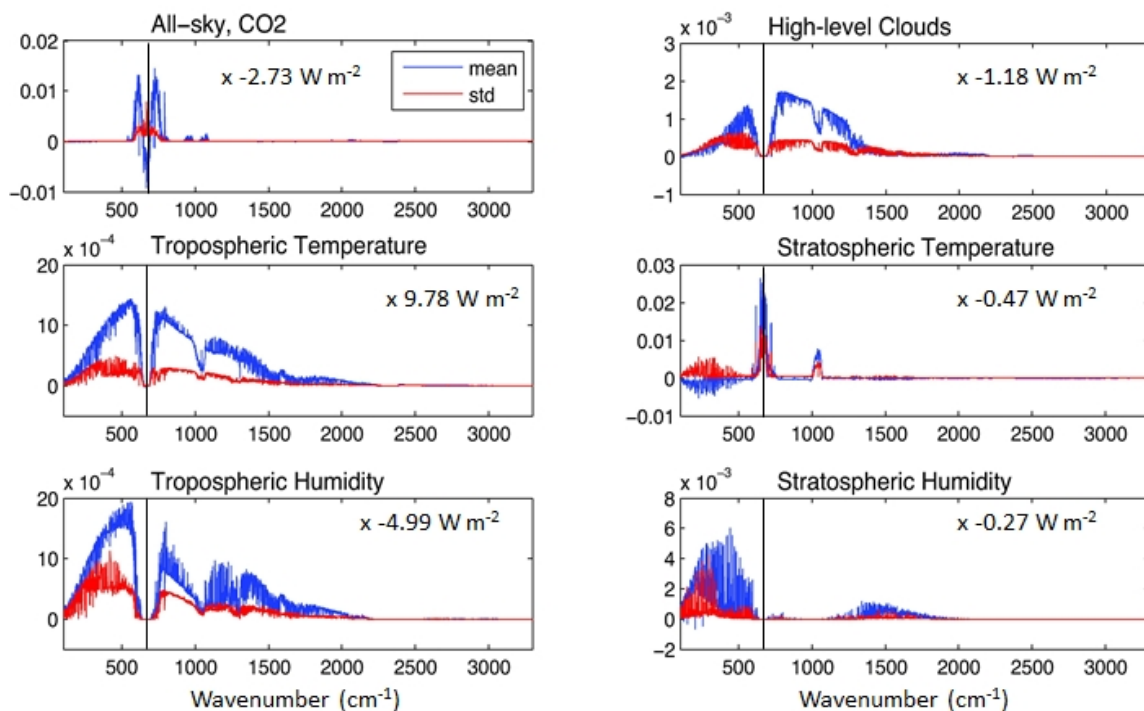


Figure 2.2 Spectral fingerprint in OLR associated with a doubling of CO₂ (top left) and the resulting OLR signal owing to the response of different climate parameters. In each case the blue line shows the global mean fingerprint while the red curve is the associated 1σ standard deviation due to spatial variation in the signal. To obtain the correct magnitude and sign of the radiative signal in W m⁻² the values on each y-axis have to be multiplied by the number in each panel. The black line in each panel is at 667 cm⁻¹. Values to the left of this line lie within the far-infrared. (Adapted from Y. Huang et al., 2010)



280 ppm) to those that were simulated after the model had responded to a doubling of atmospheric CO₂ (Yi Huang et al., 2010). The focus is specifically on the signatures down to the CO₂ doubling (the original forcing) and the response (feedback) of water vapour, temperature, distinguishing in both cases between the stratosphere and the troposphere, and high (ice) clouds. It is apparent that the original forcing has a quite distinct signal compared to the feedback signals. Moreover, while certain feedbacks show a broadly similar shape (e.g. tropospheric temperature and humidity) there are subtle differences which can be discerned given sufficient spectral coverage and accuracy. Finally, and perhaps most critically, a substantial proportion of all of the feedbacks, and indeed the CO₂ forcing, occurs within the far-infrared (FIR) at wavenumbers less than 15 μm (667 cm⁻¹).

How well is Earth's OLR spectrum known? At mid-infrared (MIR) wavelengths between 4–15 μm (667–2500 cm⁻¹), continuous, global, hyper-spectral observational records from space spanning almost 20 years exist (e.g. Chahine et al., 2006; Hilton et al., 2012). Moreover, satellite observations within specific wavelength bands in the MIR have existed for twice as long (e.g. Scott et al., 1999). However, as of today, there is less than a year's worth of observations of Earth's OLR spectrum at wavelengths between 15–25 μm (400–667 cm⁻¹) (Section 2.2.1) and no measurements at all of the spectrum between 25–100 μm (100–400 cm⁻¹). Fig. 2.2 shows that a large proportion of the expected feedback signatures owing to changes in temperature, water vapour and high cloud is predicted to occur in this FIR region from 15–100 μm (100–667 cm⁻¹). In several cases such as high cloud, tropospheric water vapour and temperature, the contrast between the FIR and MIR signals holds the key to distinguishing between different effects. This demonstrates that spectral observations of the OLR across the FIR from space are urgently needed, to test and refine the understanding of the links between these parameters and their role in shaping future climate.

More fundamentally, as will be shown, observations in the FIR have the potential to deliver new insight into the interplay between water vapour, temperature, ice cloud and, in very dry regions, surface properties, and their radiative impact. It will be shown that the large contribution that the FIR makes to Earth's OLR and atmospheric cooling, coupled with its sensitivity to these critical climate parameters, means that the absence of such measurements constitutes the major remaining observational gap in the knowledge of Earth system energetics. The Far-infrared-Outgoing-Radiation Understanding and Monitoring (FORUM) mission will fill this gap by providing systematic, global, spectral measurements spanning the FIR and MIR and quantify, for the first time, how these parameters and their interactions combine to modulate the total energy emitted by Earth, and its variability over space and time. In this way, the mission directly addresses the most urgent observational requirement as identified by Atmosphere Challenge A1 of the science strategy within the ESA Earth Observation Living Planet Programme (ESA, 2015a):

Challenge A1: Water vapour, cloud, aerosol and radiation processes and the consequences of their effects on the radiation budget and the hydrological cycle.

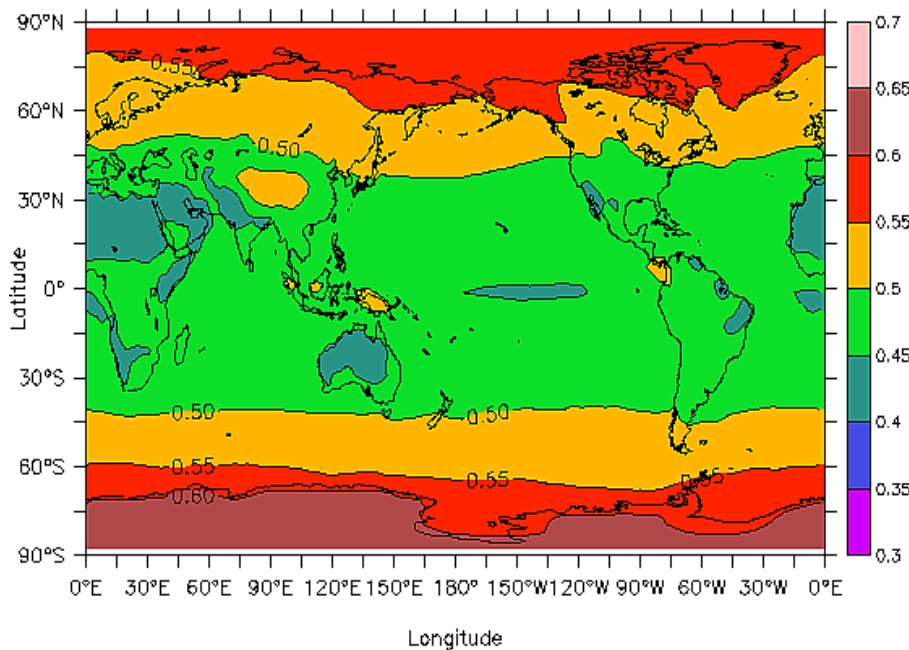


Figure 2.3 Ratio of TOA annual mean all-sky FIR flux (15–100 μm) to total OLR as calculated using the NCAR Community Atmosphere Model: 40 % or more of the OLR is in the FIR at all global locations. (W. Collins Lawrence Berkeley National Laboratory, US and M. Mlynchzak, NASA, US)

2.1 The Far-Infrared Earth: the Benefit of FORUM

The global annual mean spectrally integrated, or broadband OLR over the period 2000–2010 has been estimated as $239.7 \pm 3.3 \text{ W m}^{-2}$ (Stephens et al., 2012). Assuming blackbody emission, this implies that, viewed from space, Earth has a global mean effective emitting temperature of around 255 K such that the peak of its emission lies within the FIR. The key role that the spectral region plays in modulating the TOA energy budget can be seen in its contribution to the total OLR as a function of latitude and longitude, with climate model simulations suggesting that between 40–65 % of Earth’s all-sky OLR is found in the FIR as shown in Fig. 2.3.

2.1.1 The Greenhouse Effect, Atmospheric Cooling, Water Vapour and the Critical Contribution of the FIR

The 255 K global mean effective emitting temperature of Earth is in marked contrast to its global mean surface temperature of around 288 K. The difference is due primarily to strong absorption by water vapour and CO_2 with much of this absorption occurring within the FIR (Harries et al., 2008). There are several ways to demonstrate the importance of FIR absorption. One simple, but powerful way is to display Earth’s greenhouse effect, defined as the difference between the surface emission and the OLR (Raval and Ramanathan, 1989), as a function of wavenumber, or the amount of radiation trapped within the atmosphere. Simulations of this quantity for clear-sky conditions for two extreme cases: a tropical (warm, wet) and a sub-Arctic winter (cold, dry) profile, show that around one-quarter of the total greenhouse effect occurs within the FIR for the tropical case, increasing to one-third for the sub-Arctic winter case (Brindley and Harries, 1998).

The importance of FIR absorption and emission is not confined to its impact at the TOA. Clear-sky longwave radiative cooling in the mid-upper troposphere is dominated by the contribution from the FIR, primarily due to the strong absorption and emission by water vapour at FIR wavelengths (Fig. 2.4). In this way the FIR has a critical role not only in regulating Earth's clear-sky cooling to space but also in influencing atmospheric dynamics.

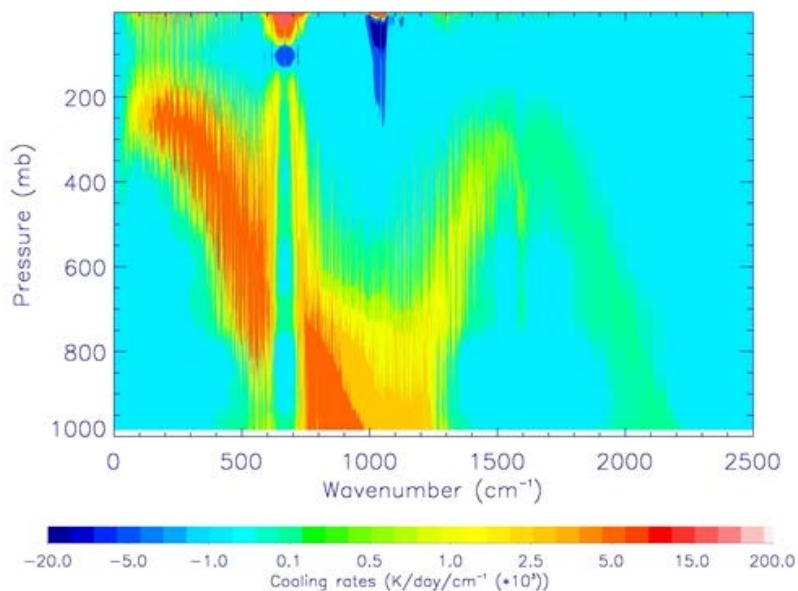


Figure 2.4 Simulated atmospheric longwave radiative cooling rates in $\text{K day}^{-1} (\text{cm}^{-1})^{-1} \times 10^3$ as a function of wavenumber and pressure for a standard tropical profile. The cooling in the mid-upper troposphere (pressure levels between 150 and 700 hPa) is dominated by the contribution from the FIR. (Adapted from Harries et al., 2008)

A direct corollary of this behaviour is that in clear-sky conditions, or in the presence of low cloud, outgoing radiation in the FIR is particularly sensitive to changes in mid-upper tropospheric water vapour (Sinha and Harries, 1995). Fig. 2.5 gives a simple demonstration of this sensitivity by showing the simulated impact of a 12 % perturbation to water vapour concentrations on the greenhouse effect for four distinct layers in a standard tropical profile. As the height of the perturbation shifts from lower to higher layers, the peak response, in terms of the change in greenhouse effect, also shifts from the MIR to the FIR. It is worth making several further points here: (1) for this atmospheric profile the 12 % increase in water vapour concentration results in the same reduction in total OLR as a doubling of CO_2 ; (2) the typical uncertainty in current estimates of upper tropospheric water vapour is of the order 10 %; (3) the use of a constant percentage change means that the absolute perturbation to water vapour amounts in the lower stratosphere is very small (~ 0.3 ppmv); (4) looking down on Earth, these changes in lower stratosphere water vapour can only be observed in the FIR, and require high radiometric accuracy and spectral resolution ($\sim 0.5 \text{ cm}^{-1}$).

The relatively small change in water vapour required to match the integrated effect of a doubling in CO_2 highlights its status as the most important greenhouse gas (Held and Soden, 2000). As shown in Figs. 2.4 and 2.5, a given perturbation to water vapour will have a strong effect throughout the mid-upper troposphere and into the lower stratosphere. In particular, the atmospheric radiation balance is highly sensitive to greenhouse gas changes in the

cold tropopause region (Riese et al., 2012). Even slight variations in water vapour (less than 1 ppm) in the lower stratosphere therefore represent an important source of the decadal variability in the surface temperature (Solomon et al., 2010).

In addition to its influence on the radiation budget, upper troposphere/lower stratosphere (UTLS) water vapour also significantly affects, and is affected by, atmospheric dynamics (Chung et al., 2011), transport (Ploeger et al., 2013), cloud formation and lifetime (Collins, 2002; Sherwood et al., 2010), and, through its strong feedback effect it plays a key role in

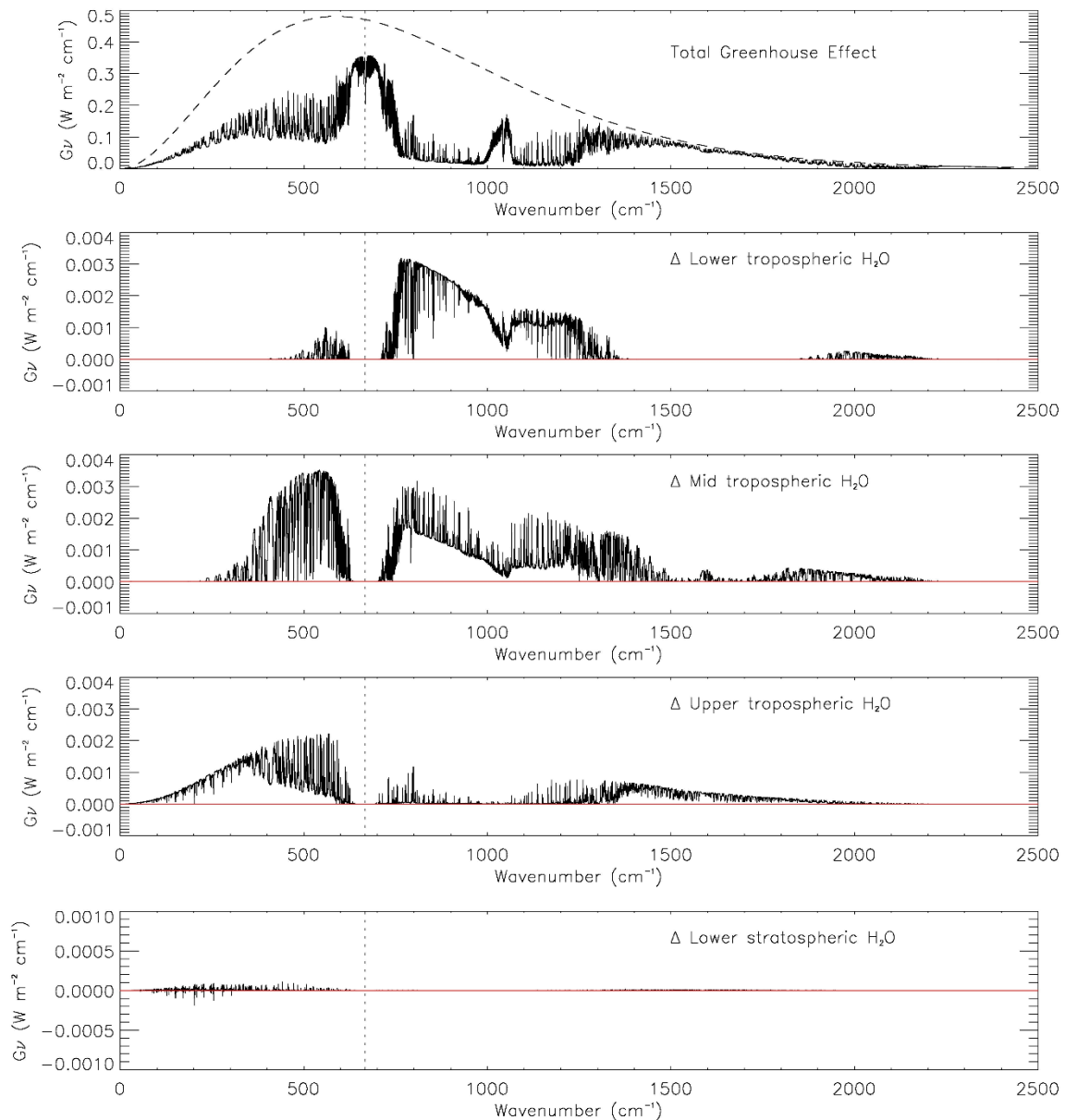


Figure 2.5 Top panel: simulated spectral greenhouse effect, $G\nu$, for a tropical standard atmosphere. The surface emission is shown by the dashed line. The lower panels show the simulated change in $G\nu$ given a 12 % increase in water vapour in the specified atmospheric layer. In each case values to the left of the dotted line are within the FIR. (H. Brindley, Imperial College, London)



shaping the future evolution of the climate (Dessler et al., 2008, 2013). The measurement accuracy and resolution required to improve the understanding of water vapour radiative effects, interaction with cloud processes, and transport within the atmosphere strongly depend on the target application. For example, cirrus cloud properties are strongly dependent on the environment in which they form (Comstock et al., 2004; Jensen et al., 2005) such that a 10% uncertainty in relative humidity with respect to ice has significant implications for the resulting cloud microphysics.

Given these dependencies, over the last couple of decades there have been substantial efforts to improve the characterisation of UTLS water vapour. A prominent example is the Water Vapour Assessment 2 (WAVAS-2) by the World Climate Research Programme (WRCP) and Stratosphere-troposphere Processes And their Role in Climate (SPARC) initiative. WAVAS-2 aims to update the first SPARC Water Vapour Assessment (Kley et al., 2000) by including recent satellite, field, and laboratory measurements and assessing processes affecting stratospheric water vapour and its evolution (see ACP/AMT/EESD inter-journal special issue, 2016). In-situ airborne hygrometer inter-comparisons within the UTLS suggest that, at least over the limited geographical and altitude regions sampled, agreement between different instruments is within their total uncertainty budgets at $\pm 10\text{--}15\%$. However, systematic biases between instruments of the same order of magnitude as this budget are noted in very low humidity regimes (water vapour <10 ppm) (Kaufmann et al., 2018). Similarly, recent estimates of water vapour trends and variability within the lower stratosphere recognise that these are still poorly constrained and subject to large uncertainties (Hegglin et al., 2014; Hurst et al., 2011).

Moreover, despite the substantial effort that has been made to assess, improve and homogenise upper tropospheric water vapour estimates from radiosondes (McCarthy et al., 2008, 2009; Miloshevich et al., 2006) and satellite sounders (Shi and Bates, 2011) best-case uncertainties from the GCOS Reference Upper Air Network (GRUAN) radiosondes are still of the order 5%, reaching 15% near the tropopause (Dirksen et al., 2014). These uncertainties are still significant because all current measurement techniques have shortcomings over the upper tropospheric altitude range. Limb sounding instruments, which offer high vertical resolution, are affected by the variable nature of the water vapour horizontal distribution; narrow-band nadir sounding instruments have poor vertical resolution and can suffer from clear sky and dry biases (Chung et al., 2014; John et al., 2011); MIR hyperspectral sounders have limited sensitivity to the region and underestimate humidity extremes (Chou et al., 2009); current Global Positioning System (GPS) radio-occultation based approaches have reduced sensitivity in the upper troposphere (Kursinski and Gebhardt, 2014) and radiosondes need corrections to be applied to account for biases induced by daytime solar heating, instrument time-lags and calibration (Dirksen et al., 2014).

Studies have shown that the enhanced sensitivity in the FIR to small changes in water vapour concentration in the UTLS can be exploited to improve the knowledge of water vapour concentrations in this climatically critical region (e.g. Merrelli and Turner, 2012). Simultaneous measurements of the full OLR spectrum from FORUM will allow this water vapour distribution to be related directly, for the first time, to its associated radiative signature and greenhouse effect.

2.1.2 The Role of Spectroscopy

Outgoing long-wave radiation to space is the fundamental cooling mechanism of the Earth-atmosphere system. Simulations based either on idealised profiles (Clough et al., 1992; Sinha and Harries, 1995) or estimates of global water vapour fields (Allan et al., 1999; Allan, 2004) suggest that much of this cooling occurs within the FIR water vapour absorption band (Fig. 2.4). All such simulations make use of radiative transfer codes that can range from highly detailed, but relatively slow 'line-by-line' models, which consider individual spectral lines (e.g. Clough et al., 2005), to the rapid, but highly parameterised codes typically used in state-of-the-art general circulation models (GCM) (e.g. Iacono et al., 2000). The accuracy of all of these codes is ultimately dependent on the underlying spectroscopy, or detail of the position, width and strength of individual gaseous absorption lines and any associated broad-band features or continua (e.g. Shine et al., 2012). In this way, accurate spectroscopy and its representation in radiative transfer algorithms fundamentally affects the ability to model current, and predict future, climate.

Spectroscopy underpins the knowledge of the climate in another, subtly different way. The long-term records that have been, and are currently being, derived of a multitude of essential climate variables rely on radiative transfer codes to translate the raw measurements made by satellites, into the physical properties of the surface and the atmosphere and its constituents relevant to scientists, policy makers and the general public.

Likewise, modern data assimilation systems used in numerical weather prediction (NWP) make extensive use of the information related to temperature, water vapour, and other trace gases provided by satellite observations (e.g. Collard and McNally, 2009). They either ingest geophysical quantities retrieved from satellite observations, or, increasingly, use radiances measured directly. In both cases, the quality of the final NWP forecasts will critically depend on the ability of the radiative transfer model used in the data assimilation to accurately convert physical quantities into radiances (Saunders et al., 2018) and hence the accuracy of the underpinning spectroscopy.

Recognising their importance, detailed compilations of spectroscopic parameters have been built up over time and are continuously updated as new, improved information becomes available either from laboratory or field measurements (e.g. Gordon et al., 2017; Jacquinet-Husson et al., 2016). Nonetheless, uncertainties in the knowledge of spectroscopic line parameters and continua are the primary limitations on the accuracy of leading edge radiative transfer models (e.g. Mlawer et al., 2019; Turner et al., 2012). Reducing these uncertainties is therefore an important step towards improving the impact of satellite data on weather forecasting and climate studies.

Radiative closure studies, where observations of spectrally resolved infrared radiance are compared to simulations in a tightly constrained environment, can highlight systematic differences between the calculated and measured spectral radiances. They provide a means of assessing the consistency of the input spectroscopic parameters within different absorption bands of the same trace gas, and between different gaseous absorbers. Such studies have shown how, for example, observations from Infrared Atmospheric Sounding Interferometer (IASI) can be used to assess the knowledge of the spectroscopy of

water vapour, carbon dioxide and other trace gases across the MIR (e.g. Shephard et al., 2009).

Measuring water vapour line parameters in the FIR region in a controlled environment is challenging because FIR water vapour absorption lines originate from high quantum number energy levels which are hard to observe at the pressures and temperatures that can be reached in the laboratory. Therefore, estimates of water vapour FIR line strengths and positions have been derived through theoretical calculations based on high temperature laboratory measurements (e.g. Coudert et al., 2014; Lodi and Tennyson, 2012; Yu et al., 2012) and the spectroscopic uncertainties associated with them are significant.

Ground-based measurement campaigns, observing the atmospheric downwelling radiation can be used to assess the quality of water vapour FIR spectroscopic parameters. However, as shown in Fig. 2.6 the transparency of the atmosphere in the FIR reduces dramatically as the amount of water vapour in the atmospheric column, or *precipitable water vapour* increases. For the majority of locations around the globe, precipitable water vapour exceeds 1 cm, with much of this water vapour in the lowest layers of the atmospheric column. This limits what can be sensed about the atmosphere from the surface, limiting the altitude range that can be sampled and completely precluding useful measurements at many FIR wavelengths. Campaigns designed to test FIR spectroscopy are therefore limited to very dry environments in order to observe absorption features over the widest possible spectral range, covering the largest altitude range.

Over time, a number of such campaigns have refined and tested the knowledge of water vapour spectroscopy within the FIR (e.g. Delamere et al., 2010; Liuzzi et al., 2014; Tobin et al., 1999; Turner and Mlawer, 2010). Very recent work has exploited the exceptionally low water vapour contents at Cerro Toco, Chile (precipitable water vapour between 0.3 and 0.5 mm) to provide an updated estimate of the water vapour spectroscopic

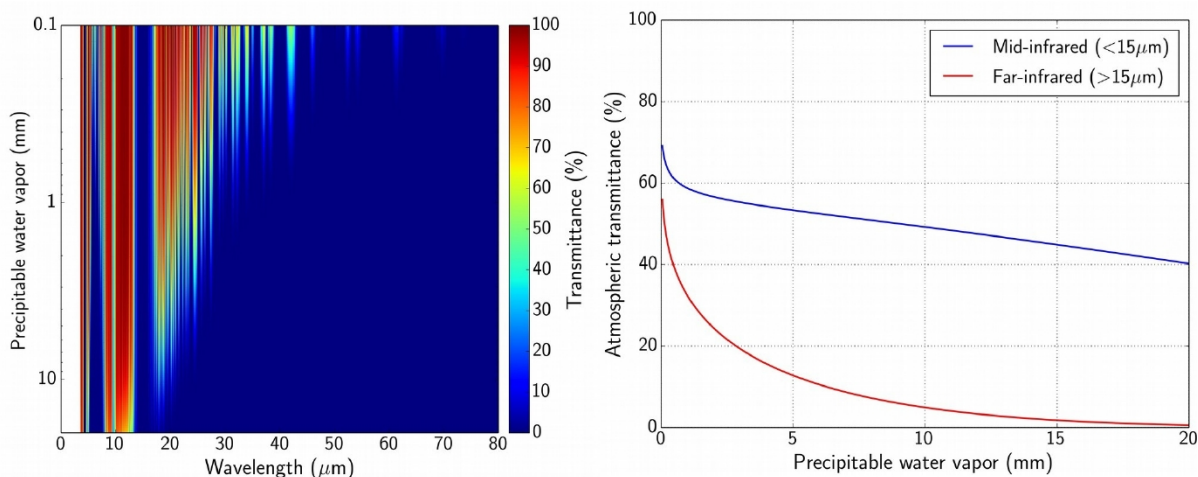


Figure 2.6 Left: atmospheric transmittance as a function of wavelength and precipitable water vapour. As the amount of water vapour in the atmosphere increases (moving down the y-axis), micro-windows in the FIR (wavelength > 15 μm) close, meaning that, when looking up from the surface the downwelling FIR radiation originates from lower in the atmosphere. Right: atmospheric transmittance as a function of precipitable water vapour integrated over the MIR and FIR. The FIR becomes almost opaque when the precipitable water vapour exceeds 1 cm. (Q. Libois, Meteo-France)

parameters across the FIR (Mlawer et al., 2019) and agreement between state-of-the-art line-by-line simulations of the downwelling radiance at the surface and available measurements is now sufficient to identify biases in the input water vapour profiles themselves (Rizzi et al., 2018).

However, ground-based FIR measurements sample atmospheric layers with pressure and temperature conditions very different from those that can be sampled from space. High-altitude aircraft and balloon measurements give a more representative picture of what might be seen from a satellite's perspective, albeit over a limited geographical range. Such measurements have demonstrated their value to study water vapour spectroscopy deep into the FIR (wavenumbers $<400\text{ cm}^{-1}$) (Green et al., 2012).

It has, however, still to be demonstrated that the assessed quality of the water vapour spectroscopy can be extended over the full range of global conditions that can be sampled from space. In fact, the uncertainties associated with state-of-the-art ground-based estimates of water vapour spectroscopy are still large. For example, the most recent estimates of water vapour continuum coefficients have uncertainties of the order 20–30% at wavelengths 100–400 cm^{-1} (Mlawer et al., 2019). By observing the spectrally resolved OLR in the FIR, FORUM will provide the first measurements capable of validating and improving these estimates on a global scale.

FORUM will also make the first high-quality observations of the complete 15 μm (667 cm^{-1}) CO_2 band. Observations from IASI show that the 700–750 cm^{-1} region can be matched within instrumental noise by model simulations using state-of-the-art spectroscopy and collocated high-quality radiosonde and reanalysis data (e.g. Serio et al., 2019). FORUM measurements, covering the longwave side of the band (wavenumbers $<645\text{ cm}^{-1}$), will provide the first opportunity to perform a similar validation exercise in this spectral region. Confirmation of the spectroscopy in this range is important to properly characterise the radiative forcing owing to enhanced CO_2 concentrations (Section 2.1.4) and may also prove beneficial for improving CO_2 and temperature retrievals using the 15 μm band.

2.1.3 Ice Clouds and Radiative Impacts

Clouds affect the radiative balance of Earth's atmosphere through competing greenhouse and albedo effects. The balance between these effects is of fundamental importance to Earth's climate system and varies with cloud height, microphysical properties, phase, geometrical thickness and the background atmosphere in which the cloud is embedded. Insufficient knowledge of cloud fields, their radiative properties, their contribution to the radiation budget and how this may evolve in a changing climate is the primary reason why predictions of future climate from different state-of-the-art models show a substantial variation (Stocker et al., 2013).

One measure of the degree to which a cloud interacts with radiation is its *opacity* given by the optical depth, which is a function of wavelength. The larger this number, the greater the attenuation of radiation by the cloud. It has been understood for some time that the greenhouse effect of sub-visual or optically thin, high ice cloud or cirrus (Hong et al., 2016; Sassen and Cho, 1992) exceeds their albedo effect, resulting in a net warming radiative effect

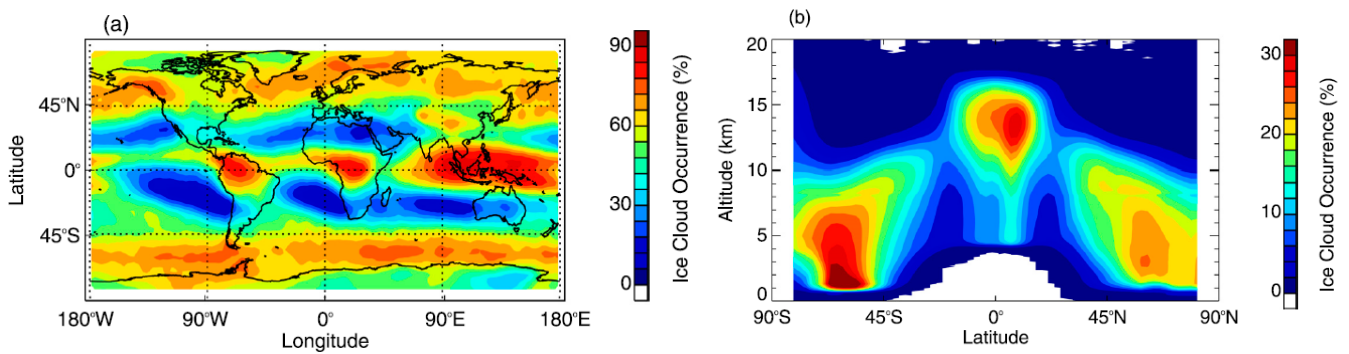


Figure 2.7 Global ice cloud occurrence frequency derived from four years of CloudSat and CALIPSO observations as (a) a function of latitude and longitude and (b) a function of latitude and height. Note the different colour scales. (Hong and Liu, 2015, © Copyright [2015] American Meteorological Society (AMS))

with peak values in the Tropics. As a consequence, any change of these cloud parameters (e.g. opacity, cloud height, geometrical thickness or even geographical distribution) in a warming world could enhance or reduce projected warmings.

There is no clear understanding of how clouds will change in the future, both in terms of location and extent and their microphysical properties, although some different mechanisms have been proposed (e.g. Bony et al., 2016). Indeed the most recent IPCC report states: ‘The role of thin cirrus clouds for cloud feedback is not known and remains a source of possible systematic bias... the representation of cirrus in GCMs appears to be poor’ (Stocker et al., 2013). More recent studies have also highlighted the prevalence of sub-visual, low-altitude ice cloud, and simulations have suggested that these too have a substantial radiative impact (Hong et al., 2016). A notable finding is that, overall, the global net radiative effect of ice clouds is warming owing to a much higher occurrence of thin cloud compared to thick ice cloud.

Ice cloud climatologies, built up from multi-year satellite observations from active sensors, show that ice clouds are extremely widespread, particularly in regions of tropical deep convection and over the mid-latitudes (Fig. 2.7). Of these ice cloud occurrences, thin and sub-visual clouds (visible optical depth <0.3) contribute around 40% to the total cloud occurrence (Hong and Liu, 2015), showing a similar geographical distribution to that seen in Fig. 2.7. Optically thicker cloud, with visible optical depths of between 0.3 and 3 contribute a further 39 % to the total ice cloud occurrence. According to this global picture, sub-visual ice clouds tend to be preferentially located at low altitudes in the northern and southern mid-latitudes while thin ice clouds are more often found in the tropical UTLS, in the form of detraining or overshooting cirrus anvils.

The impact of ice clouds on the radiation balance is complex. It depends on several parameters such as surface albedo, emissivity and temperature; cloud height and thickness; and ice crystal size distribution and shape (Baran, 2012; Fusina et al., 2007; Maestri et al., 2005; Yang et al., 2015), and their geographical location. Unlike the spherical droplets found in liquid water clouds, the highly complex shapes of ice crystals observed in cirrus clouds (the crystal habits) makes modelling their impact on radiation particularly challenging. For example, early work by Stephens et al. (1990) using a simple mechanistic climate model

concluded that predictions of cirrus feedback on climate were limited by a lack of understanding of the relationship between the size and shape of ice crystals and the bulk optical properties of the cirrus clouds. More recent work by Baran (2012) and Baran et al. (2014) reinforces this statement by showing that significant GCM-simulated longwave and shortwave radiative flux differences resulting from different crystal models and parameterisations are widespread, reaching 10–30 Wm^{-2} and from -10 to -35 Wm^{-2} , respectively.

Efforts to constrain the radiative impact of cirrus clouds have primarily focused on the visible and MIR spectral regions where the abundance of data from both aircraft and satellite observations has enabled the development, iteration and validation of cirrus scattering models (Baran, 2012; Baum et al., 2014; Yang et al., 2015). However, to date, there have been very few spectral observations of cirrus clouds spanning the FIR, precluding a rigorous test of how well these models are able to capture the radiative signature of cirrus within this spectral region (Baran, et al., 2014). The limited aircraft-based radiative measurements of cirrus spanning the FIR and MIR that do exist imply that current optical models are unable to match the observed signals consistently across the infrared spectrum (Cox et al., 2010). In order to quantify and reduce the uncertainties associated with current cirrus optical models in the FIR it is imperative to measure a comprehensive set of spectra, sampling different meteorological regimes covering the full infrared spectrum. This will enable improved optical models with quantified uncertainties to be developed, greatly enhancing confidence in the ability of both climate and NWP models to accurately represent these radiatively important, widespread clouds. FORUM will provide these measurements for the first time.

2.1.4 Climate Forcing and Feedbacks: the Power of Spectral Resolution

As described in Box 2.1, a radiative forcing, ΔF refers to the deviation from radiative balance at the top of atmosphere resulting from a perturbation to the climate system. Examples of natural perturbations include changes in solar radiation related to variations in solar activity or the worldwide dissemination of volcanic aerosol after an eruption. Anthropogenic forcings include those owing to changes in the atmospheric concentration of greenhouse gases arising from human activities.

Although radiative forcing is generally summarised by a single value, each specific forcing will also have its own spectral signature. For instance the greenhouse effect of CO_2 mostly operates in its strong absorption band centred at 15 μm . Likewise, methane (CH_4) and nitrous oxide (N_2O) have localised absorption bands at around 7.7 μm and 17 μm , respectively. Aerosol interactions with radiation are also strongly wavelength dependent. As a consequence, discriminating between and accurately assessing anthropogenic radiative forcings requires detailed spectral information that only satellite-based hyperspectral observations across the whole infrared (IR) range can provide.

Because of the confidence in the knowledge of both CO_2 spectroscopy and line-by-line radiative transfer codes, the radiative forcing owing to CO_2 has been considered to be well-understood and well-constrained for some time (Stocker et al., 2013), (IPCC 2008). Nonetheless, recent studies have challenged this view (Pincus et al., 2015; Soden et al.,

2018). Comparisons of ΔF resulting from the same change in CO_2 across models participating in the Coupled Model Intercomparison Project 5 (CMIP5) show a spread of up to 3 W m^{-2} in ΔF (Chung and Soden, 2015a) directly affecting calculations of the resulting climate sensitivity (Chung and Soden, 2015b). Indeed, as originally pointed out over 30 years ago, the impact of inconsistencies in the calculation of radiative forcing on estimates of climate sensitivity “is nearly half of the often quoted range of uncertainty of 1.5° to 4.5°C ” (Cess et al., 1993). Hence, even if all other aspects of the climate models were perfect, the spread in projections of CO_2 -induced climate change would only be reduced by 50 % because of the differences in radiative forcing. Part of the issue is because of differences in parameterisations of the radiative transfer used in the various models. However, as described in Section 2.1.2, as yet there are no high-quality observations spanning the entire $15 \mu\text{m}$ CO_2 band. FORUM measurements will enable the assessment of the spectroscopy across the band for the first time, as well as providing benchmark observations against which climate models can be compared.

Although a radiative forcing will ultimately result in a change in surface temperature, its overall effect can be substantially modified by feedback processes operating within the climate system. Prominent examples of positive feedbacks – or responses that amplify the original surface temperature change – include those owing to water vapour and surface albedo. Conversely, since a warmer surface will naturally emit more IR radiation, leading to a cooling, the largest negative feedback is termed the Planck feedback. Climate models also tend to predict that the gradient of the tropical temperature lapse rate will lessen with surface warming, resulting in a negative ‘lapse rate’ feedback (e.g. Soden and Held, 2006). Water vapour and lapse rate feedback do not act independently, but have a significant cross-component. Since the upper troposphere warms more than the surface, the water concentration there also increases more, resulting in additional positive feedback. Finally, cloud feedbacks comprise all the radiative changes resulting from modifications of cloud occurrence and physical properties in response to a warming climate. Current climate models show the largest spread in their estimates of cloud feedback with even the sign of the feedback still open to question (Vial et al., 2013).

While all of the above feedbacks have been recognised for some time, recent work has identified a new amplification mechanism that has particular relevance for polar regions and the FIR. As shown by Fig. 2.6, as the atmosphere becomes drier, transparent micro-windows within the FIR begin to open up such that in clear-skies the effects of changes in surface conditions can be sensed from space. The importance of this effect is exacerbated by cold surface temperatures, which shift the peak of the surface emission to longer wavelengths, within the FIR. Both of these conditions are commonly met in polar environments. Typically climate models have assumed that the surface emissivity in the FIR is that of an ideal blackbody (i.e. equal to 1 at all wavelengths). Studies using the Community Earth System Model (CESM) show that accounting for spectrally varying surface emissivity in the FIR compared to assuming blackbody surface emission results in increases in decadal average Arctic surface temperatures of up to 2 K, concomitant with decreases of up to 15 % in Arctic sea-ice extent by the 2030s (Feldman et al., 2014). The authors use these results to introduce a new positive feedback mechanism, termed the ‘ice-emissivity’ feedback, whereby sea ice melt in response to an initial surface warming exposes the less emissive ocean below, resulting in additional warming. Further analyses with CESM have also shown that (1) the inclusion of



more realistic spectrally varying surface emissivities can significantly reduce the winter-time Arctic cold-pole bias (Kuo et al., 2018), which has been a long-standing issue for climate models in general (Flato et al., 2013) and (2) the sign of the ice-emissivity feedback appears to be dependent on the detailed characteristics of the underlying surface (X. Huang et al., 2018). All the above studies rely on estimates of the surface emissivity that have been derived theoretically and have not been extensively validated in the FIR (Chen et al., 2014). A key goal of the FORUM mission is to use spectra measured over suitably selected high-latitude scenes to derive a database of FIR surface emissivities for both the Arctic and Antarctic, including an assessment of seasonal and, in particular, inter-annual variability.

Because of their uncertainty and influence on climate sensitivity, quantifying feedbacks has been one of the holy grails of climate researchers for several decades. A better understanding of how the hydrological cycle, clouds and the general circulation couple to influence climate sensitivity is one of the WCRP's current Grand Scientific Challenges (Bony et al., 2015). Several authors have shown how short term variability, on the timescale of monthly or annual means, can be used to probe cloud feedback mechanisms (e.g. Zelinka and Hartmann, 2011; Zhou et al., 2014) and to develop emergent constraints on equilibrium climate sensitivity (e.g. Klein and Hall, 2015). As highlighted by Box 2.2, highly accurate, global observations of the Earth's spectrally resolved emission to space provide a novel and powerful route for identifying and quantifying the effect of different feedbacks that can complement these approaches because each feedback bears its own spectral signature which is intrinsically tied to the overall energetic response of the planet.

Since estimates of climate feedbacks are typically derived from climate model simulations, and since the vertical structure of the atmosphere is reflected in the spectral distribution of the outgoing fluxes, it is imperative that the models employed can accurately simulate both spectrally resolved, and integrated TOA fluxes. Several studies have shown that uncertainties associated with water vapour spectroscopy, ice clouds and, in polar regions, the surface emissivity, have a major impact on the ability to assess accurately the radiative impact of changes in these parameters (Baran, et al., 2014b; X. Huang et al., 2018; Turner et al., 2012). This represents a fundamental gap in the knowledge of the Earth system and undermines confidence in the ability of climate models to correctly estimate climate sensitivity. Comprehensive observations of the full IR spectrum, including the FIR, are urgently needed. This is the main objective of the FORUM mission.

2.1.5 Numerical Weather Prediction and Climate Model Evaluation

Satellite data, and in particular IR sounder measurements, now provide the largest contribution to the skill of NWP models (Fig. 2.8) as shown by several operational centres that routinely assimilate radiances from a number of the advanced IR sounders (e.g. IASI, Cross-track Infrared Sounder or CrIS, Atmospheric Infrared Sounder or AIRS). The measurements from these sounders contribute to improving the analysis of the model initial state of temperature, water vapour and ozone fields from which the forecasts are run. Simulations suggest that FIR measurements will add information on the model UTLS water vapour fields, which will in turn improve the model radiative heating profiles and representation of upper-level clouds.

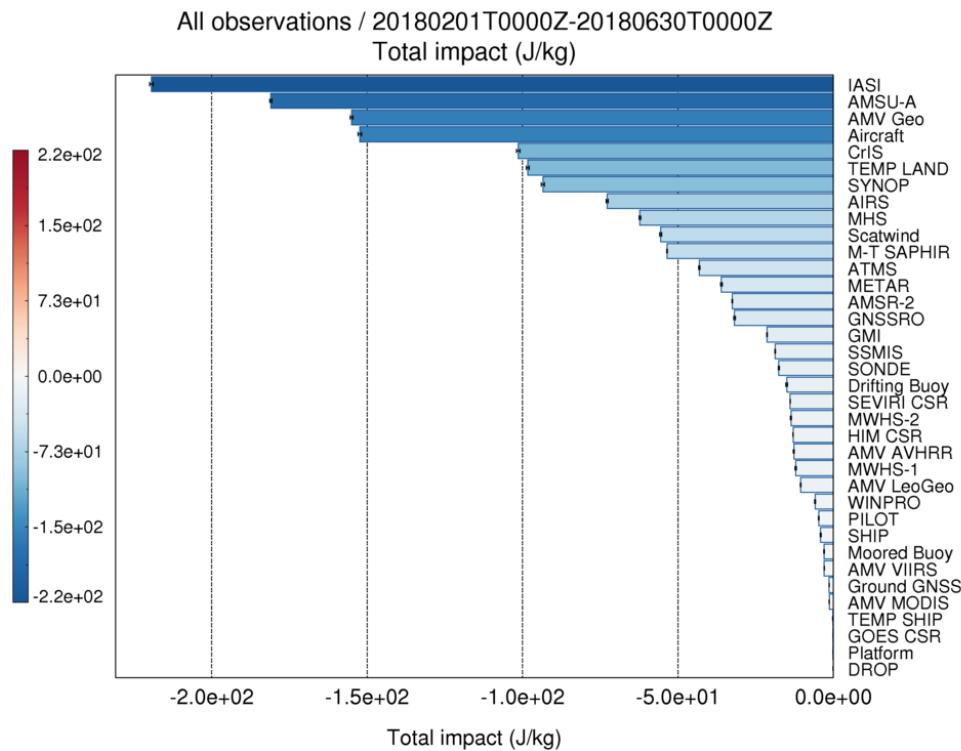


Figure 2.8 The 24hr forecast error reduction for all the different categories of observations assimilated in the Met Office global forecast model averaged over the period February to June 2018. (Adapted from Joo et al., 2013)

Climate models should always be confronted with observations for current and past scenarios to give confidence as to their ability to forecast the climate. The direct use of spectrally-resolved radiances and fluxes in climate model evaluation is an exciting, emerging field. Hyperspectral MIR observations have been exploited to diagnose biases in model temperature and moisture fields and, critically, to relate them to the underlying causes (Huang et al., 2007). Similarly, they have been used to evaluate model representations of cloud cycles and phenomena such as the super-greenhouse effect (Huang and Ramaswamy, 2008), but there is much that could still be done (e.g. Huang et al., 2011).

Recognising the critical importance of the FIR, several attempts have been made to estimate spectrally-resolved fluxes spanning the full IR by using physical or statistical relationships between MIR observations and the unmeasured FIR spectrum (X. Huang et al., 2008, 2010). These synthetic fluxes have been compared with output from reanalyses, showing reasonable agreement at the global scale, but more significant discrepancies for specific regimes and between day and night (Chen et al., 2013). When used to evaluate climate-model performance (Huang et al., 2013) they illustrate how broadband flux can be insensitive to important discrepancies within individual spectral bands, because differences in the FIR and MIR water vapour bands are of opposite sign (Fig. 2.9). Because of the coupling between FIR radiative signatures and water vapour feedback and dynamics (e.g. Kahn et al., 2016), it is imperative to assess whether such compensation effects and biases are seen in comparisons with real observations across the FIR.

Successive generations of the climate models contributing to CMIP struggle to capture the observed water vapour vertical distribution, particularly in the upper troposphere where the largest model spread and deviation from observations is reported (Jiang et al., 2012). Similarly, large systematic biases also exist in NWP models (Dyroff et al., 2015; Kaufmann et al., 2018) and reanalyses (Jiang et al., 2015; Poshyvailo et al., 2018) particularly in the tropical UTLS. Highly accurate FIR radiances will bear the imprint of annual and inter-annual variations in mid-upper tropospheric/lower stratospheric water vapour giving insight into the coupling between these variations and their radiative impact, and permitting an assessment of how well this relationship is captured in current models and the scope to drive improvements.

Recent analyses have also revealed large discrepancies between GCMs and satellite observations in the frequency and spatial distribution of ice cloud occurrence, and their ice content (Eliasson et al., 2011; Hong and Liu, 2015; Li et al., 2012; Waliser et al., 2009). These discrepancies are highlighted as making an important contribution to the sizeable broadband radiation biases seen across CMIP models (Li et al., 2013). Current GCMs also struggle with correct partitioning between ice and water cloud and simulating mixed phase cloud (e.g. Lacour et al., 2018; Tan et al., 2016). The refractive indices determine the intrinsic scattering and absorption properties of a substance, and for water and ice these show a strong contrast between the FIR and MIR, and liquid clouds are around 10 times more absorbing than ice clouds in the FIR. This implies that: (1) FIR observations offer the potential for improved cloud phase determination (Rizzi et al., 2016; Turner et al., 2006); (2) ice is so transparent in the FIR that scattering becomes significant, meaning that ice cloud radiative properties in the FIR are very sensitive to ice particle size and habit, i.e. the characteristic external shape of an individual crystal (Merrelli and Turner, 2013); (3) the neglect of FIR scattering in the radiative transfer parameterisations currently employed in most GCMs may lead to systematic biases (Chen et al., 2014). FORUM observations will thus not only measure the radiative signature of ice clouds consistently across the IR for the first

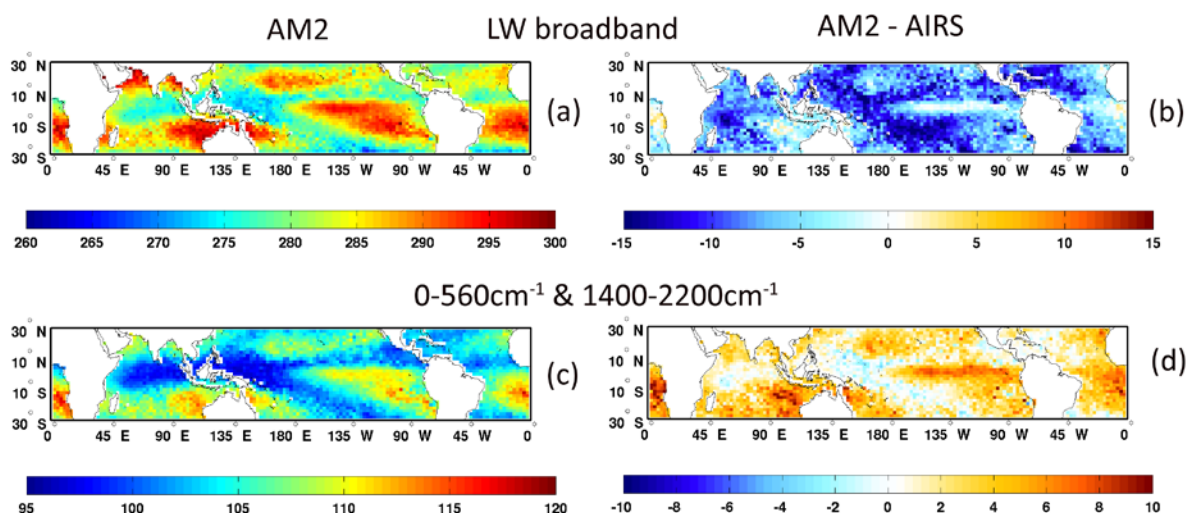


Figure 2.9 (a) Broadband OLR simulated by GFDL AM2 model for the Tropics; (b) Difference between broadband OLR simulated by GFDL AM2 and estimated from AIRS; (c) as (a) for a spectral band between 0–560 and 1400–2200 cm⁻¹; (d) as (b) for a spectral band between 0–560 and 1400–2200 cm⁻¹. (Adapted from Huang et al., 2008).



time, but also simultaneously provide a means to better constrain cloud phase, crystal habit and size: both aspects will allow a rigorous test of current ice cloud microphysical parameterisations within GCMs and drive improvements that are rooted in observed behaviour.

Finally, as noted in Section 2.1.4, observations of the FIR emissivity of different surface types and how these vary with time will allow the incorporation of more realistic representations of surface properties within GCMs, enabling an improved understanding and quantification of the interplay between the cryosphere, ocean, atmosphere and radiation budget in some of Earth's most fragile locations.

2.2 Readiness and Unique Contribution

2.2.1 Space-Based Heritage

Global, spectrally integrated measurements of Earth's OLR have been made by a variety of satellite sensors for almost four decades (Barkstrom, 1984; Wielicki et al., 1996). Similarly, there is an unbroken record of global TOA hyper-spectral MIR radiances from 2000 onwards (e.g. Chahine et al., 2006; Han et al., 2013; Hilton et al., 2012). In contrast, the only spectrally-resolved satellite measurements of Earth's emission extending some way into the FIR were made for a few brief periods over 25 years ago.

Launched by the US in 1969, the Infrared Interferometer Spectrometer (IRIS) B instrument on Nimbus-3 (Conrath et al., 1970) obtained short-lived (less than 1 month) measurements of the OLR spectrum between 400–2000 cm^{-1} (5–25 μm) with a resolution of 5 cm^{-1} and a footprint of 150 km diameter. Its successor, IRIS-D, launched on Nimbus-4 in 1970, covered a more limited spectral range (400–1500 cm^{-1}) but with higher spectral resolution (2.8 cm^{-1}) and a smaller ground footprint of ~ 100 km diameter (Hanel et al., 1972), gathering measurements over a 10 month period between April 1970 and January 1971. In Europe, between 1976 and 1979 three Soviet Meteor satellites (25, 28 and 29) carried the East German Spektrometer Interferometer-1 (SI-1). Designed to provide temperature and humidity profiles and total ozone (Feister, 1980; Spankuch, 1980), this instrument covered the spectral range 400–1600 cm^{-1} with a spectral resolution of 5 cm^{-1} , a ground footprint of $\sim 2 \times 2^\circ$ and an along-track sampling distance of between 100 and 400 km. Due to technical issues observations from SI-1 on Meteor-25 were unusable, while those available from Meteor-28 and 29 only represent 19 and 40 days between July and September 1977 and January and June 1979, respectively (Théodore et al., 2015).

These instruments were ahead of their time, permitting preliminary investigations into water vapour and CO_2 radiative transfer (Kunde et al., 1974), total ozone and upper tropospheric circulation (Prabhakara et al., 1973), and the seasonality and structure of optically thin cirrus cloud (Prabhakara et al., 1988, 1990). Given the size of their footprints, their relatively coarse spectral resolution, their lifetime, issues with their geographical sampling, radiometric calibration and in-orbit stability (Aumann et al., 2011; Bantges et al., 2016; Kunde et al., 1974), and their limited spectral coverage of the FIR, this gives confidence regarding the scientific insights that the much-enhanced capabilities of FORUM will deliver.

2.2.2 Lessons Learned from Campaigns

To date, only a few instruments in the world have measured hyperspectral radiances across the FIR extending to a wavenumber (wavelength) of at least 100 cm^{-1} ($100\text{ }\mu\text{m}$). These are the Italian Radiation Explorer in the Far InfraRed – Prototype of Applications and Development (REFIR-PAD) (Bianchini et al., 2019), the British Tropospheric Airborne Fourier Transform Spectrometer (TAFTS) (Canas et al., 1997) and the US Far-InfraRed Spectroscopy of the Troposphere (FIRST) instrument (Mlynczak et al., 2006).

REFIR-PAD, a Fourier Transform Spectrometer covering the $100\text{--}1500\text{ cm}^{-1}$ spectral range with 0.4 cm^{-1} native resolution can be considered a field demonstrator of the FORUM measurement concept. In 2005 it performed the first FIR observations from a stratospheric balloon using an uncooled system (Palchetti et al., 2006), with the resulting measurements used to assess the current knowledge of water vapour spectroscopy (Bianchini et al., 2008). The spectrally resolved measurements were also used to retrieve the underlying atmospheric state and to calculate consistent integrated outgoing FIR fluxes. Comparisons with similar calculations using temporally and spatially collocated operational analyses from the European Centre for Medium-Range Weather Forecasts (ECMWF) as input showed significant differences of up to 3.5 W m^{-2} , highlighting how spectral radiances can benefit flux estimation (Palchetti et al., 2008). Participation in the US Radiative Heating in the Underexplored Bands Campaign – II (RHUBC-II), a ground-based campaign in the Chilean Andes, with several other ground-based spectrometers saw measurements of the downwelling spectral radiance which, for the first time, spanned the entire terrestrial spectrum (Turner et al., 2012). As noted in Section 2.1.2, these observations have been exploited to provide significant updates to water vapour spectroscopy across the FIR, and have been incorporated in leading radiative transfer models, with a notable impact on atmospheric radiative heating rates (Mlawer et al., 2019).

In December 2011, REFIR-PAD was installed in the Italian–French Antarctic station Concordia, near Dome C. Since 2012, the instrument has been operating autonomously with almost complete data availability (Palchetti et al., 2015). Among other applications the measurements have been used to develop and test cloud-classification algorithms (Rizzi et al., 2016), obtain simultaneous retrievals of water vapour, temperature and cirrus properties (Di Natale et al., 2017) and assess the performance of schemes designed to synthetically produce FIR radiances (Bellisario et al., 2018). The time series of atmospheric parameters retrieved from the REFIR-PAD measurements is a unique tool for characterising the thermal structure and composition of the Antarctic troposphere (Bianchini et al., 2019), and gives a taste of what FORUM could deliver on the global scale.

Envisaged as a satellite instrument demonstrator, FIRST, covering the spectral region $50\text{--}2000\text{ cm}^{-1}$ at 0.625 cm^{-1} resolution, is designed to operate from a gondola on a high-altitude balloon (Mlynczak et al., 2006). To date the instrument has participated in two flights during 2005 and 2006, reaching altitudes of 28 and 33 km respectively, and recording approximately 16000 spectra in total (Harries et al., 2008). It has been through a rigorous laboratory calibration with warm and cold sources to simulate the range of scene temperatures observed in the atmosphere (Latvakoski et al., 2013, 2014). FIRST has also participated in several ground-based campaigns, including RHUBC-II, providing a rigorous test of the ability of radiative transfer models to match the spectroscopic signals measured



in the FIR (Mast et al., 2017; Mlawer et al., 2019; Mlynczak et al., 2016) and an independent assessment of the spectroscopic updates reported in (Mlawer et al., 2019).

The TAFTS is the only instrument capable of making hyperspectral FIR observations from aircraft, covering the spectral region from 80–600 cm^{-1} with a nominal resolution of 0.12 cm^{-1} . Airborne measurements from TAFTS have been used to probe water vapour spectroscopy (Green et al., 2012), assess the radiative signature of cirrus across the IR (Cox et al., 2010) and, most recently, exploited to enable the first airborne retrievals of snow/ice surface emissivity in the FIR (Bellisario et al., 2017). Campaign results from TAFTS, discussed in Section 7.4 highlight aspects of the science that FORUM will enable.

2.2.3 Unique Contribution: Why Now?

The deployment, and successful operation of a number of FIR spectrometers in the field indicates that the technology needed to make high-precision measurements across the region is robust. Similarly, recent advances in calibration techniques can be exploited to bring the absolute in-orbit accuracy of such measurements to an unprecedented level, allowing small changes in the atmospheric state to be discerned from the radiative signals. The long heritage of space-borne MIR spectra gives a good appreciation of many of the challenges that will be encountered in interpreting the data optimally. Similarly, the experience gained processing and analysing FIR spectra from these field instruments means that the requisite tools have already been prepared and tested on real observations.

Measurements in the field have very recently refined the spectroscopy of the FIR region. FORUM is ideally placed to leverage these advances, testing whether the updates are robust from a satellite view before exploiting the new insights gained via radiative transfer modelling and state-of-the-art retrievals. Moreover, the goal to make direct use of the measured FORUM radiances for climate model evaluation is also timely given the development of satellite simulators (Bodas-Salcedo et al., 2011) designed exactly for this purpose.

Recent interest in FIR remote sensing, strongly tied to the availability of innovative uncooled detectors sensitive to FIR radiation, has also fostered the development of satellite missions in the US and Canada. The NASA Polar Radiant Energy in the Far Infrared Experiment (PREFIRE) aims to study the detailed energy budget of the polar regions. The baseline mission design consists of two 3U Cubesats, flying for one year, covering the spectral range 5–54 μm with a spectral resolution of 0.84 μm . A key goal is to make diurnally resolved measurements of the outgoing infrared spectrum to improve knowledge of the surface energy budget and its influence on the dynamic response of, in particular, the Greenland ice-sheet. The PREFIRE instrument must be delivered by 2021, but as yet there is no dedicated launch date. The Thin Ice Clouds in the Far Infrared Experiment (TICFIRE) sponsored by the Canadian Space Agency (ASC) is similarly focused on the polar regions, but its aims are to observe optically thin ice clouds, light precipitation and water vapour in the UTLS to document and better predict the cooling rates of the atmosphere, known to be key for the dynamics of cold and stable polar air masses (Blanchet et al., 2011). Covering the spectral range 8–50 μm using eight narrow bands, TICFIRE is supported by Environment and Climate Change Canada, and is expected to be highly beneficial for the prediction of mid-latitude winter storms via the assimilation of these new observations. The mission is not yet



scheduled but discussions are ongoing between NASA and ASC. Both PREFIRE and TFCFIRE are highly process-oriented missions and are characterised by much lower spectral resolution than FORUM. As such, if launched prior to FORUM, they can be pathfinders for the broader, global ambitions of FORUM and will provide valuable feedback for the preparation of the mission.

It is worth re-emphasising that the observations provided by FORUM will address pressing scientific questions identified by the international climate community. For example, as climate models move towards resolving convection, new opportunities arise to understand what governs atmospheric water vapour and cloud distributions. With its capability to provide new and unique observational constraints on upper tropospheric water vapour and cloud feedbacks, FORUM will allow these new modelling capabilities to be fully exploited and will thus contribute significantly to meeting WCRP's *grand challenge* on clouds, circulation and climate sensitivity (Bony et al., 2015). The observations will also speak directly to the goal of the Global Energy and Water Cycle Experiment (GEWEX) Upper Tropospheric Clouds and Convection Process Evaluation Studies initiative to understand the relation between convection, cirrus anvils and radiative heating.

More generally, the Committee on the Decadal Survey for Earth Science and Applications from Space highlight that reducing the uncertainty in cloud, water vapour and lapse rate feedbacks, and specifically quantifying the role of the UTLS are *most or very important* targets in their most recent report (Committee on the Decadal Survey for Earth Science and Applications from Space et al., 2018). ESA itself identifies improving the understanding and quantification of water vapour, cloud, aerosol and radiation processes and the consequences of their effects on the radiation budget and the hydrological cycle as one of its key challenges (key challenge A1, ESA, 2015a). ESA recommend that the most urgent observations needed to meet this goal are sustained, accurate and stable measurements of radiation at the TOA, that are capable of distinguishing between the contributions from clouds, greenhouse gases (with an emphasis on water vapour) and surface properties. FORUM meets this requirement.

2.3 Filling the Knowledge Gap

As demonstrated above, FIR radiation plays a fundamental role in modulating the current climate and responding to change and holds critical information about key climate components and processes. Theory suggests that systematic, global observations of Earth's outgoing FIR spectrum will provide new insight into the radiative cooling of the planet and its controls, testing and refining the understanding of how these operate from the local to global scale, and how they respond in a changing climate. Despite this, there are still no dedicated satellite based measurements of outgoing FIR radiation beyond a few isolated spectra from the 1970s, and even these only extend a limited way into the region. By providing highly accurate measurements of the OLR spectrum across the FIR, FORUM will address this shortcoming, making a truly unique contribution to the knowledge of the climate and how it is responding to change.

3 RESEARCH OBJECTIVES

Observing how Earth's outgoing longwave radiation (OLR) varies with time continues to be a key element of the global Earth Observation programme, with the measurements playing a crucial role in calibrating and evaluating state-of-the-art Earth system models (e.g. Baker and Taylor, 2016). Current missions measuring OLR include NASA's Cloud's and the Earth's Radiant Energy Systems (CERES) programme (Wielicki et al. 1996), EUMETSAT's Geostationary Earth Radiation Budget (GERB) mission (Harries et al., 2005) and the French/Indian Scanner for Radiation Budget (ScaRaB) (Roca et al., 2015). Looking further ahead, ESA's EarthCARE mission (Illingworth et al., 2015) promises to provide new insight into the coupling of cloud, aerosol and precipitation processes with the energy budget, while in the US, a CERES follow-on mission is currently being proposed.

Similarly, instruments designed to characterise the Earth's atmosphere and surface by making hyperspectral observations of OLR have been, and are continuing to be deployed. For example, spectrally resolved observations across the MIR from EUMETSAT's Infrared Atmospheric Sounding Instrument (IASI) and NASA's Atmospheric InfraRed Sounder (AIRS) and Cross-track Infrared Sounder (CrIS) have significantly improved operational weather forecasting skill (see Fig. 2.8), while also being exploited to develop long-term records of important climate parameters such as temperature, water vapour, cloud cover, cloud top temperature and cloud phase, ozone, carbon dioxide, nitrous oxide, methane, carbon monoxide and many other trace gases. This capability will be continued by, other instruments such as, IASI-NG on MetOp Second Generation A (MetOp-SG-A).

While all of these missions do, or will provide cutting-edge observations of either the total integrated OLR, or the outgoing spectrum across the mid-infrared (MIR), none provide the spectral detail necessary to test the understanding of key physical processes in the energetically significant far-infrared (FIR). FORUM will provide these observations for the first time. As demonstrated in Chapter 2, current theory predicts that such measurements are key for understanding exactly how Earth currently cools to space, and, critically, how it responds to both natural and anthropogenic change. Therefore, the overarching research goal of the FORUM mission is,

- evaluating the role of the FIR in shaping the current climate and thus reduce uncertainty in predictions of future climate change.

This will be addressed by:

- building a highly accurate global dataset of FIR radiances to validate present-day state as captured by Earth system models
- using these measurements to understand and constrain the processes that control FIR radiative transfer and hence Earth's greenhouse effect
- updating the parametrisations of these processes for implementation in radiative transfer codes, and ultimately in Earth system models
- characterising critical feedback mechanisms.

Because the OLR FIR spectrum has never been measured in its entirety from space, predicting exactly what can be additionally leveraged from the observations depends on a number of assumptions. Nonetheless, the current understanding, based on a combination of theoretical calculations and field measurements, suggests that highly accurate space-based FIR observations are required to provide:

- an improved characterisation of mid-upper tropospheric/lower stratospheric water vapour which is critical for climate sensitivity and trends, and with potential benefit for numerical weather prediction (NWP).
- the ability to detect thin ice cloud (optical depth at 10 μm between ~ 0.03 to ~ 0.4) from passive observations. Current passive observations are inefficient at detecting these clouds, causing biases in the long-term climatologies used to evaluate current climate models. Better detection may also benefit NWP by enabling improved discrimination between clear and cloudy radiances, and can also benefit surface parameter retrievals by removing any contamination from this kind of cloud.
- enhanced sensitivity to ice cloud particle size and shape – these clouds are widespread, yet assessment of their FIR radiative impact relies on theoretical estimates. The optical properties of ice imply that the FIR will be more sensitive to ice crystal shape and size than the MIR, providing additional information for the retrieval of these properties.
- enhanced capability for cloud phase discrimination owing to the large contrast of optical properties between liquid water and ice.
- the ability to retrieve and monitor FIR surface emissivity in low-humidity areas (polar regions, high altitude regions and deserts). To date, reported estimates of FIR surface emissivity are extremely limited, however the incorporation of realistic (theoretical) values in Earth system models has been shown to have important implications for Arctic surface-temperature bias correction and the future evolution of the region. In suitable conditions, FORUM measurements can be inverted to obtain a much wider, observationally based database of FIR emissivity and how it varies with space and time.

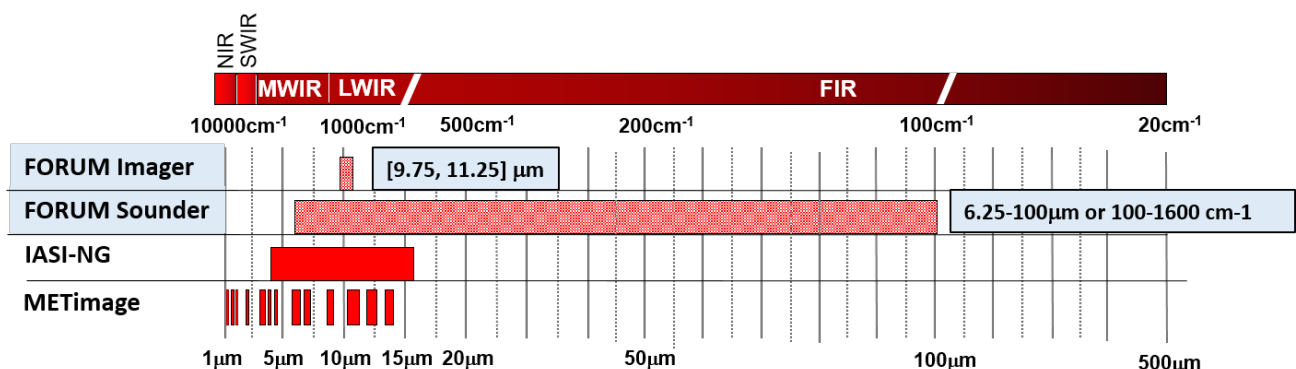


Figure 3.1 Spectral range of the FORUM instruments in comparison to IASI-NG and METImage on MetOp-SG(1A). (ESA)

3.1 Mission Objectives

3.1.1 Primary Objectives

The FORUM mission will observe, for the first time, the distribution of Earth's OLR across the IR spectrum, encompassing FIR. Perhaps uniquely in the context of prior Earth Explorer missions, these measurements are valuable in their own right since the measured radiances can be used directly to (1) assess and improve the underlying spectroscopy in the FIR; (2) tie the observed radiative signatures directly to variability, in particular, in water vapour, greenhouse gases, cloud and surface properties; (3) provide a stringent evaluation of radiative processes in climate models via the use of satellite simulators. Hence, the primary goal of FORUM is to enable these measurements to be made with sufficient spectral coverage and resolution, and with high enough radiometric accuracy that each of these goals can be met. These high-accuracy measurements can also serve as a benchmark against which future IR radiance observations can be compared.

Given these aims, the spectral coverage needs to encompass the range over which the Earth's energetic emission is significant. While the FORUM payload will focus on this range, covering 100–1600 cm^{-1} (contributing ~95 % or more to the total OLR), coverage across the IR necessitates flying in loose formation with a dedicated MIR sounder of similar spectral resolution. The Infrared Atmospheric Sounding Interferometer-Next Generation (IASI-NG) on MetOp Second Generation (SG) A1 is the logical choice due to its heritage, timeliness and operational status. By extending a substantial way into the MIR, cross-calibration between FORUM and IASI-NG (coverage 645–2760 cm^{-1} , Fig. 3.1) can be performed routinely, a major benefit for both instruments given FORUM's radiometric accuracy. The mission goals also strongly complement those of other MetOp-SG(1A) instruments, particularly the METimage radiometer (high resolution scene identification), Microwave Sounder (temperature, humidity and cirrus) and Multi-viewing, Multi-channel, Multi-polarisation Imager, 3MI (cirrus), potentially also benefitting the first of these instruments via cross-calibration of its MIR channels.

While the infrared signatures of perturbations to surface and cloud properties are relatively broadband, the radiative impact of changes in water vapour, particularly in the upper troposphere/ lower stratosphere (UTLS) are manifested at significantly higher spectral resolution (Box 2.1), driving this aspect of the mission design. To distinguish spectral signatures owing to seasonal and longer-term variations in UTLS water vapour and allow assessment of the underlying spectroscopy at a level commensurate with prior ground-based campaigns a spectral resolution of 0.5 cm^{-1} is required.

Since the goal of the mission is to characterise the Earth's infrared spectral emission over the full range of atmospheric conditions, the proposed coverage is global. Flying in formation with MetOp-SG(1A) meets this requirement. Based on the variability seen in the parameters to which the OLR is sensitive, the mission duration should be long enough that, at the minimum, the seasonality in the FIR spectral signatures can be evaluated, with the goal to quantify longer-term variability associated with large scale modes of climate variability such as the El Niño Southern Oscillation (ENSO) or the Quasi-Biennial Oscillation (QBO).

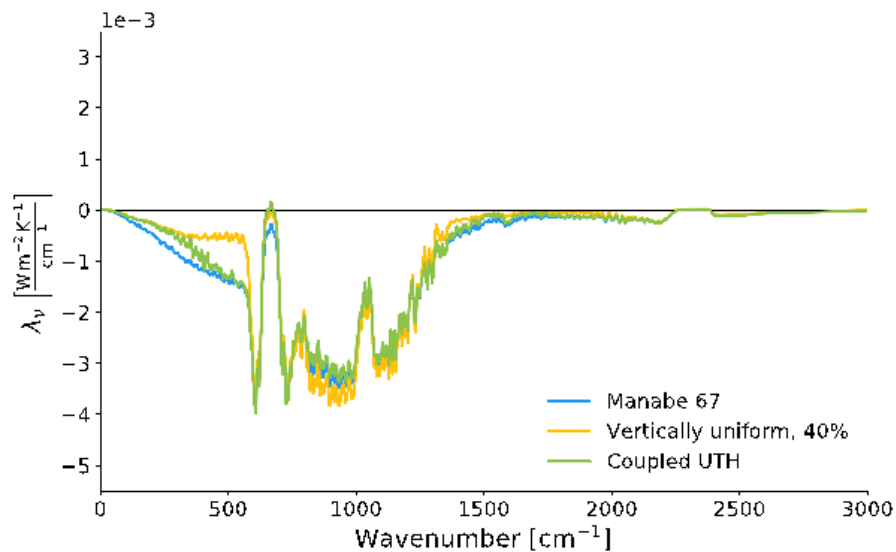


Figure 3.2 Total spectral climate feedback (expressed in terms of climate feedback parameter, λ_v , or change in spectral OLR flux per unit surface temperature warming) for the KONRAD model. Different coloured curves represent different assumptions concerning the vertical distribution of relative humidity, which lead to large feedback differences, particularly in the FIR region of the spectrum (L. Kluft, MPI-M, Hamburg).

In terms of measurement accuracy, as a climate explorer the emphasis of FORUM is more on radiometric accuracy than instantaneous noise in order to minimise measurement bias. By averaging over spatio-temporal scales, or over specific climatic regimes (e.g. cloud type), the effects of noise can be reduced in order to isolate the true, subtle radiative signatures of different processes. For example, the radiative impact of variability in UTLS water vapour on the measured spectrum is small and occurs relative to a cold background signal, making its detection extremely challenging. However, analyses of annual and inter-annual variability of stratospheric water vapour mainly build on monthly and zonally averaged values (Davis et al., 2016). The proposed sampling strategy of FORUM is sufficient to reduce the uncertainty associated with a 10° zonal, monthly mean spectrum to the underlying radiometric accuracy by eliminating random noise. Therefore, an absolute radiometric accuracy of at least 0.25 K at 3σ (200–1300 cm^{-1}) across all realistic scene temperatures (190–300 K) will enable the effects of typical perturbations in UTLS water vapour associated with ENSO and the QBO to be detected, with finer discrimination possible given the goal accuracy of 0.1 K (300–1100 cm^{-1}). The same sensitivity will easily provide the means to evaluate and improve current models of cirrus optical properties consistently across FIR and MIR and to derive surface emissivity. Importantly, this level of accuracy will also allow the observations to be used, with confidence, as a benchmark against which future spectrally-resolved measurements can be compared (Wielicki et al., 2013). A noise equivalent spectral radiance (NESR) of 0.4 $\text{mW m}^{-2} \text{sr}^{-1} (\text{cm}^{-1})^{-1}$ between 200–800 cm^{-1} and 1.0 $\text{mW m}^{-2} \text{sr}^{-1} (\text{cm}^{-1})^{-1}$ outside this range is sufficient to meet these goals given the instrument sampling.

Recent work has shown that it is possible to exploit short-term variability to probe feedback mechanisms and potentially to develop emergent constraints on equilibrium climate sensitivity (Klein and Hall, 2015). For example, the amplitude of natural variability in monthly tropical mean surface temperature is approximately 1 K. Although small, this is

large enough to detect surface temperature dependent feedback mechanisms such as that caused by the changes in altitude and fractional coverage of tropical high cloud in response to the inter-annual temperature variability (Zelinka and Hartmann, 2011). Model calculations imply that the spectral feedback for a 1 K surface temperature change has an amplitude of close to $3\text{--}4 \text{ mW m}^{-2} (\text{cm}^{-1})^{-1}$ in spectral OLR flux, corresponding to approximately $1 \text{ mW m}^{-2} \text{ sr}^{-1} (\text{cm}^{-1})^{-1}$ in spectral radiance, with humidity induced differences in feedback of around $0.3 \text{ mW m}^{-2} \text{ sr}^{-1} (\text{cm}^{-1})^{-1}$ in the FIR (Fig. 3.2). Signals of this magnitude will be easily detectable by FORUM on the monthly mean scale.

Because climate modellers have traditionally worked in terms of outgoing energy flux, and because this is also the quantity traditionally reported by dedicated Earth Radiation Budget (ERB) missions, the Level-1c spectral radiances will be converted to spectral fluxes using standard techniques (Section 6.1.3). In concert with estimates of surface temperature and emissivity, both of which can be obtained using the FORUM mission architecture, these fluxes will be used to derive the first ever observational estimates of Earth's greenhouse effect with wavelength across the IR spectrum, and how this varies in space and time. Similarly, the fluxes will allow the spectral longwave forcing of cloud and its variability to be diagnosed observationally for the first time. Both metrics will shed new light on the role of cloud and water vapour in controlling radiative transfer within the atmosphere. Because of the spectral coverage, the resolved fluxes, greenhouse effect and cloud forcing can also be tied directly to their integrated broadband impact, which is important in the context of cross-comparisons with concurrent ERB missions.

3.1.2 Secondary Objectives

While the primary focus of FORUM will exploit its high radiometric accuracy, the NESR is such that instantaneous radiance observations will also be used for the following applications:

- retrieval of FIR surface emissivity in appropriate conditions (clear-sky, low precipitable water vapour)
- assessment of additional benefit of FIR compared to state-of-the-art hyperspectral MIR radiances for UTLS H₂O retrieval
- detection of thin cirrus cloud
- retrieval of ice-cloud optical depth, ice water path (which is the total amount of ice in the cloudy column in g/m^2) cloud top height, cloud geometrical thickness (or equivalently cloud bottom height) and particle size

More detail on each of these aspects will be provided in Chapters 4, 6 and 7.

4 OBSERVATIONAL REQUIREMENTS

This chapter provides the observational requirements for the FORUM mission. All the main requirements, including requirements on spatial and temporal sampling, on geophysical parameters and the associated data products necessary to meet the scientific goals, are derived and justified based on the research objectives outlined in Chapter 3. The requirements on the FORUM Level-1 and Level-2 products are given.

4.1 General Observational Concept

The FORUM mission requires an instrument able to measure Earth's spectrally-resolved outgoing longwave energy across the far-infrared (FIR) spectral range with high absolute accuracy. Characterisation of the surface, atmospheric and cloud homogeneity in the observed field-of-view is also required to help interpret the resolved radiance observations. These needs dictate the use of two instruments, which are:

- a spectrometer, the FORUM Sounding Instrument (FSI). The FSI is the core instrument measuring the spectrally-resolved top-of-atmosphere (TOA) outgoing longwave radiation (OLR) radiance
- a co-aligned imager, the FORUM Embedded Imager (FEI), sharing the same bore-sight as the FSI, operating in the thermal infrared (TIR) atmospheric window with higher spatial resolution than the FSI to characterise scene homogeneity

Observations are performed at nadir to minimise the atmospheric path-length to the surface and hence maximise the atmospheric transmittance, enhancing the sensitivity to the surface and facilitating the retrieval of surface emissivity. Nadir observations are also required to reduce horizontal smearing of different air masses which would introduce uncertainty into retrievals and hence flux calculations.

The loose formation concept necessitates a Sun-synchronous orbit (SSO) at an altitude of about 830 km, as anticipated for MetOp-SG(1A). This choice has a consequent fixed overpass time, which provides a consistent set of observations for climatological assessments.

4.2 Observational Requirements Related to the FSI

In the following subsections, the main requirements for the FSI, related to its spectral coverage, spectral resolution, noise and radiometric calibration accuracy are derived.

4.2.1 Measurement of the Full Infrared Spectrum at TOA

The OLR at the TOA is dominated by the spectral features of atmospheric constituents, clouds and surface properties. Fig. 4.1 shows a typical spectrum calculated for a mid-latitude scenario in clear-sky conditions and in the presence of cirrus clouds. As demonstrated by the figure, the TOA spectrum contains the signature of many different greenhouse gases that are relevant for Earth's radiative budget, including water vapour (H₂O), carbon dioxide (CO₂), ozone (O₃), nitrous oxide (N₂O) and methane (CH₄).

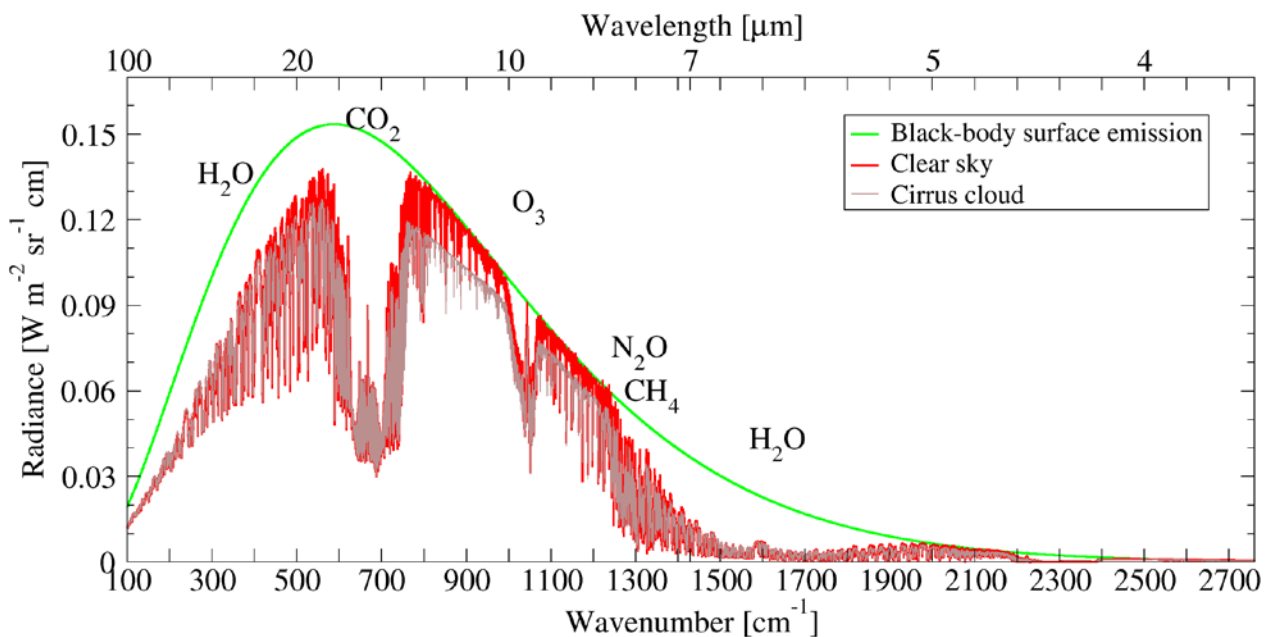


Figure 4.1. Spectral OLR at TOA in clear sky (red line) and in the presence of a cirrus cloud (grey line) for a mid-latitude scenario. The green curve is the blackbody emission at the surface temperature of 26°C which approximates the surface emission. (L. Palchetti, CNR, Italy)

Clouds and their properties can be sensed when the atmospheric transmittance above the cloud is sufficiently high to allow the radiation that they emit and scatter to reach the TOA. Fig. 4.1 also shows that in the absence of clouds, the spectrum contains information about the surface emission, represented by the green curve, inside the highly transparent, ‘atmospheric windows’ from 800–1000 cm^{-1} and 1100–1250 cm^{-1} .

A requirement on the spectral range of 100–1600 cm^{-1} is set to allow FORUM to cover the range over which Earth’s energetic emission to space is most significant (Fig. 4.2). While FORUM will focus on this range, providing the first-ever observations of spectral FIR OLR, coverage across the full infrared necessitates flying in loose formation with a dedicated MIR sounder of similar spectral resolution such as IASI-NG.

4.2.2 Spectral Resolution

The spectral resolution is driven by the necessity to provide the spectrum with sufficient resolution to distinguish the spectral signatures due to seasonal and longer term variations in upper troposphere/ lower stratosphere (UTLS) water vapour (see Fig. 2.5) and to allow assessment of the underlying water vapour spectroscopy. To meet this aim a threshold spectral resolution with full-width half-maximum (FWHM) of 0.5 cm^{-1} is required.

Fig. 4.3 reinforces this requirement by showing simulations of clear-sky TOA brightness temperature spectra for the FIR region, where water vapour has very strong absorption features. The same atmospheric profiles of temperature and humidity have been used as input in each case but the TOA spectra have been simulated at a variety of different spectral resolutions. The left panel of the figure shows how the degradation of resolution broadens

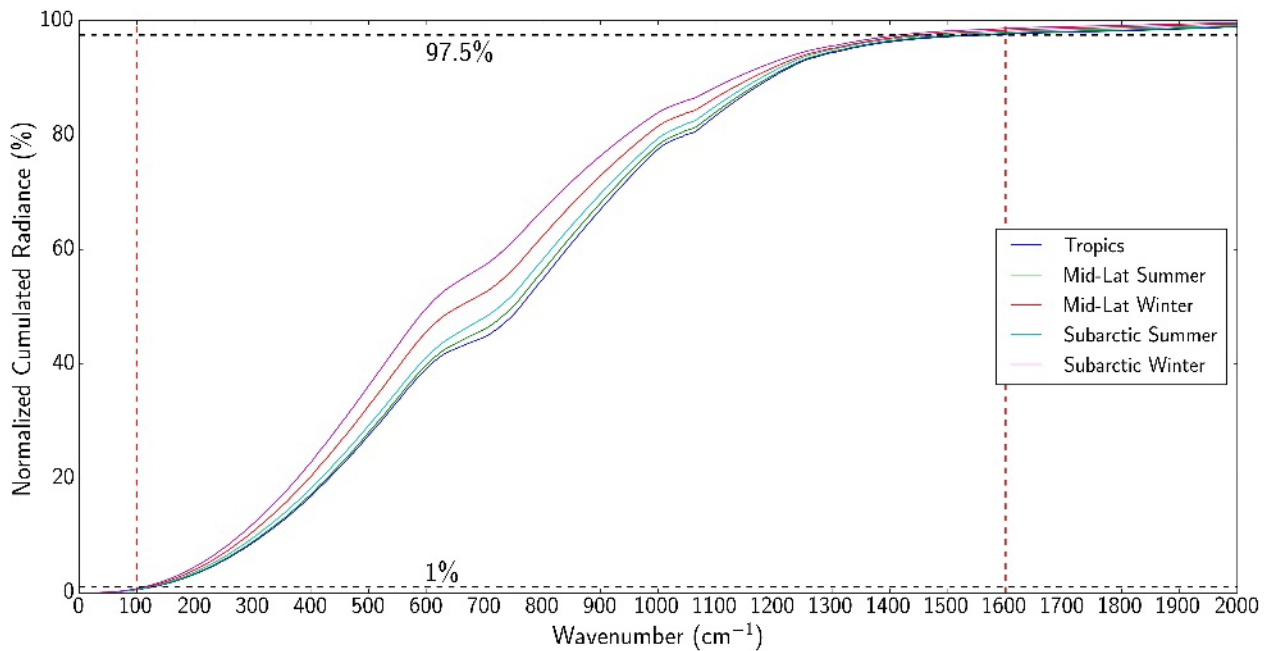


Figure 4.3. Normalised clear-sky cumulative radiance for a nadir view over the full IR spectrum. The figure shows that dependent on atmospheric conditions, 95 % or more of the total TOA OLR lies within the 100–1600 cm^{-1} range covered by FORUM. (Q. Libois, Meteo-France)

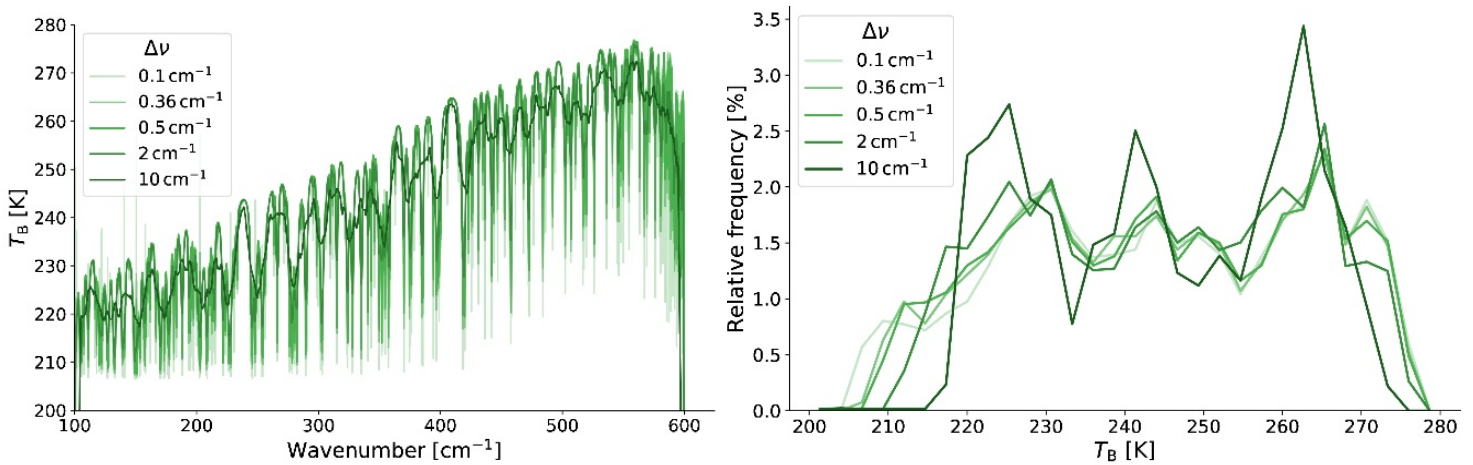


Figure 4.2. Brightness temperature (T_B) spectra at TOA calculated in the FIR region (left panel) and frequency occurrence of the T_B values as a function of the different spectral resolutions (right panel). As the spectral resolution is degraded the shape of the frequency distribution changes and the *cold-tail* is lost, indicating a lack of ability to capture the signature of the strong water vapour absorption features. (L. Klufft, MPI-M, Hamburg, Germany)

the narrow water vapour absorption features, reducing the ability to properly characterise their spectral signature. The degradation is more clearly shown by the right panel, where the frequency with which different brightness temperature values occur in the simulations is plotted for different resolutions. As the spectral resolution is degraded, the capability to sound the coldest lines of the spectrum, originating from the UTLS, is lost. However, Fig. 4.3, right panel shows that increasing the resolution beyond 0.5 cm^{-1} does not markedly increase the amount of information retained in the *cold-tail* of the frequency distribution.

As will be described in Section 7.3, this spectral resolution is also sufficient for the retrieval of water vapour profiles, cloud and surface parameters that are required to meet the secondary research objectives stated in Chapter 3.

4.2.3 Noise Requirements

The Noise Equivalent Spectral Radiance (NESR) is a suitable parameter to characterise the instrument noise performance.

The requirement on the NESR value is chosen to have sufficient sensitivity to meet the primary research objectives of FORUM, which are related to the capability of identifying FIR features of water vapour, thin cirrus clouds and surface properties, as stated in Section 3.1.1. It is worth reiterating that these primary research objectives require high radiometric accuracy (see Section 4.2.5) at the ‘climatological’ scale (defined here as 10° zonal, monthly mean, but not precluding other, commensurate binning strategies). To meet these objectives significant averaging of the spectra will be performed. Given this, the primary driver on NESR is the necessity that it is small enough that, given the FORUM temporal and spatial sampling, the uncertainty on a ‘climatological’ spectrum will reduce to the radiometric accuracy. Focusing more on the use of instantaneous measurements, the key secondary driver on the NESR is the desire to retrieve FIR surface emissivity (Section 3.1.2). Lastly, instantaneous measurements will also be used to investigate the potential for improved ice-cloud detection, and water vapour, and ice-cloud microphysical property and height retrievals, exploiting FIR information.

For the primary mission objectives the NESR requirement is thus intrinsically linked to the FORUM orbit (Sun-synchronous orbit, 830 km altitude) and spatial sampling and ground pixel size (Section 4.4.2). In addition to work on forcing and feedbacks (e.g. Leroy et al., 2008, Y. Huang et al, 2010), climate observing system simulation experiments by Feldman et al. (2015) show how monthly, zonally-averaged spectra could be used for model evaluation, including the identification of both long and short-term climate trends and variability. Wielicki et al. (2013) identify a target absolute radiometric accuracy of 0.1 K (3σ) for the resolved TOA infrared radiance spectrum to be able to characterise natural variability in the climate system and hence identify signals of change. Given both findings, the proposed orbit and sampling, and the FIR focus of the mission, the NESR for FORUM has to be lower than $0.6 \text{ mW}/(\text{m}^2 \text{ sr cm}^{-1})$ in the spectral range $200\text{--}800 \text{ cm}^{-1}$. A goal of $0.4 \text{ mW}/(\text{m}^2 \text{ sr cm}^{-1})$ would allow a higher temporal and spatial averaging to be employed to meet the same absolute accuracy. Outside the $200\text{--}800 \text{ cm}^{-1}$ range, the threshold requirement on the NESR is relaxed to $2 \text{ mW}/(\text{m}^2 \text{ sr cm}^{-1})$, with $1 \text{ mW}/(\text{m}^2 \text{ sr cm}^{-1})$ as the goal.

For the secondary research objectives, it is useful to note that, given current FIR models of water vapour spectroscopy, simulations suggest that it will be possible to retrieve water vapour profiles between 0–20 km at a 2 km vertical resolution with a precision of 15 % (Section 7.3.3). This level of precision is quite commensurate with current satellite capability, particularly in the UTLS, as identified by the ESA Water Vapour CCI Project (e.g. Hegglin et al., 2013, 2019). With the insight that FORUM will bring for water vapour spectroscopy in the FIR, it is possible that this simulated performance could improve in practice.

Similarly, for cloud, a rigorous information content analysis (Labonnote, 2019) suggests that the threshold (goal) NESR will allow instantaneous retrievals of ice water path (IWP) to within 20 % (15 %), cloud top height (CTH) to within 10 % (10 %) and cloud base height (CBH) to within 30 % (20 %) for clouds with an infrared optical depth of between 0.5 and 3. For thinner clouds, with an optical depth of below 0.5, the CTH is still defined to within 15 % but the IWP and CBH are predicted to be more uncertain. It is worth making the point that the IWP is very low in these cases so the percentage error appears high for a small absolute difference. In both absolute and percentage terms, several of these results meet the requirements laid out by the Global Climate Observing System (GCOS) Implementation Plan (WMO, 2016) and the WMO Observing Systems Capability Analysis and Review Tool (OSCAR, <https://www.wmo-sat.info/oscar/observingrequirements>).

The required NESR will also allow surface emissivity to be retrieved within 0.01 across much of the FIR. According to current theoretical models of FIR snow emissivity (Chen et al., 2014)

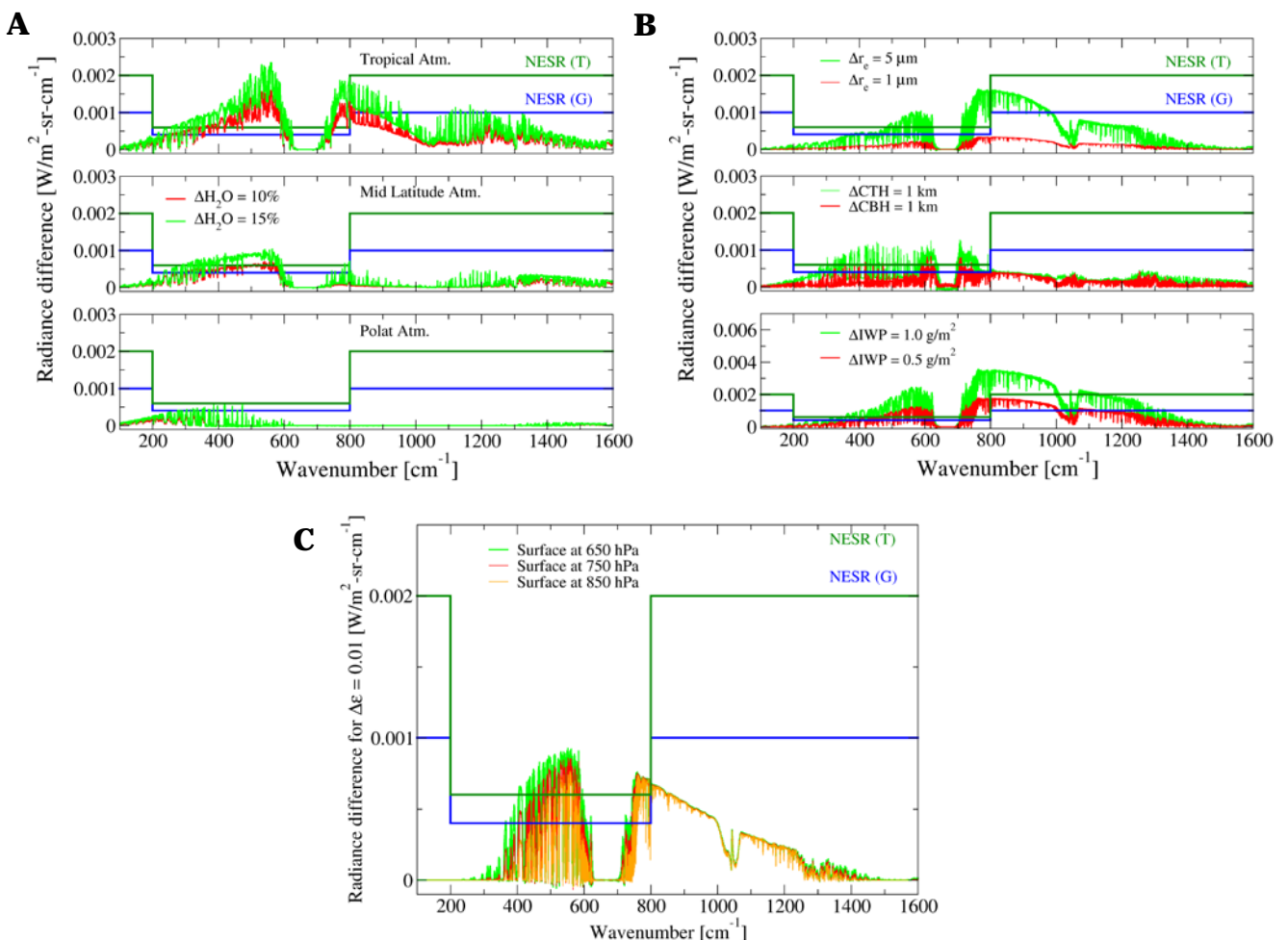


Figure 4.4. A: spectral radiance sensitivity to 10 and 15 % variation in water vapour for three standard atmospheres. B: spectral radiance sensitivity to cirrus cloud parameters for a thin cirrus cloud with cloud optical depth of 0.3 at 8–10 km altitude for a mid-latitude scenario. C: spectral radiance difference for a variation of surface emissivity $\Delta\epsilon = 0.01$ for a polar atmosphere and three different surface elevations. (L. Palchetti, CNR, Italy)

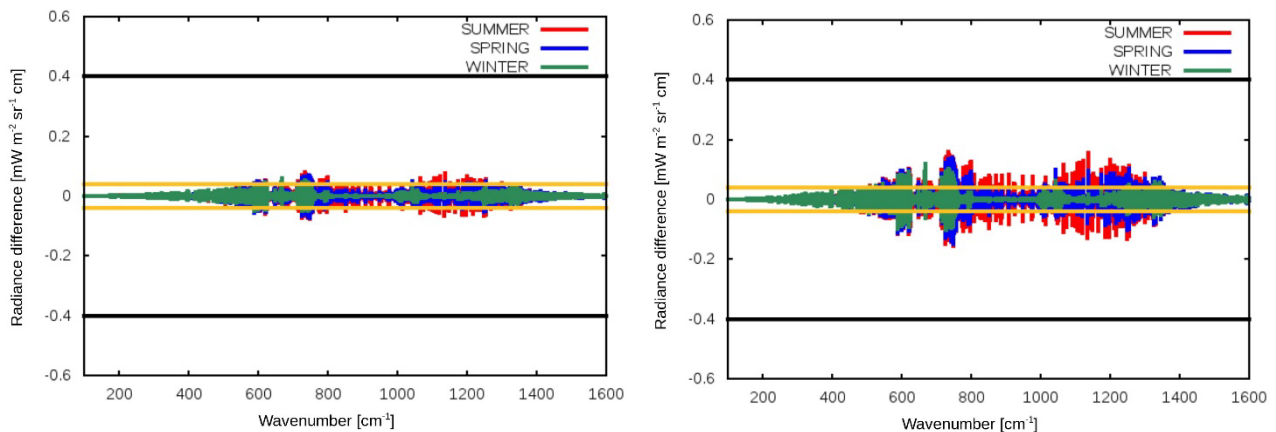


Figure 4.5. Spectral differences due to a shift of the spectral channel position of 1 ppm (left panel) and 2 ppm (right panel) compared to NESR/10 (yellow line). The NESR goal requirement is also shown in black. (B. M. Dinelli, CNR, Italy)

this level of accuracy is sufficient to discriminate between different snow grain sizes and density, information that is important in the context of sign and magnitude of the ice-emissivity feedback mechanism (Huang et al., 2018).

Fig. 4.4 shows simulations of the sensitivity of an instantaneous FORUM observation to variations in water vapour, cloud and surface emissivity corresponding with the retrieval capabilities discussed above. The simulations were performed using the radiative transfer codes KLIMA (Cortesi et al., 2014) for clear sky and RTTOV (Saunders et. al. 1999) for the cloudy sky. In each case the results reinforce that instantaneous FORUM measurements have sensitivity to these geophysical parameters above the level of the required NESR. More information about the retrieval performance of the Level-2 geophysical products, using this requirement on the NESR, will be provided in Chapter 7.

4.2.4 Spectral Calibration

The knowledge of the frequency (or wavelength) of each FORUM spectral channel has to be known with an accuracy that will produce a negligible distortion when the observed spectrum is compared with simulations. This translates into requiring that the difference between simulated spectra, one at the nominal frequency grid and one using a grid perturbed by the error in the position of the central frequency of FSI channels, should be equal or lower than the NESR value divided by 10.

To evaluate this requirement, the effects of a shift in the position of the central frequency have been calculated in clear sky, which has narrower spectral lines and is prone to the largest errors, for three scenarios: tropical summer, mid-latitude spring and polar winter. The spectra have been simulated at very high resolution (0.0005 cm^{-1}) and then convolved with a sine cardinal (sinc) function that approximates the FSI instrumental line shape. The centre of the sinc function has been shifted by different amounts expressed as ppm of the nominal frequency, and the resulting perturbed spectra have been compared with the unperturbed ones. Fig. 4.5 shows that the differences produced by a shift of 1 ppm are almost completely below a tenth of the required NESR goal, whereas a shift of 2 ppm produces differences that are almost completely below a tenth of the required NESR threshold.

Therefore, the requirement is that the position of the spectral channel centre will be known with an absolute accuracy of better than 2 ppm (threshold) and with a goal of 1 ppm.

4.2.5 Requirements for the Calibration Absolute Radiometric Accuracy

The overarching research goal of the FORUM mission – to evaluate the role of the FIR in shaping current and future climate – will be addressed by building a highly accurate global dataset of FIR radiances. Since climate is, by definition, a statistical description of high frequency weather events it is appropriate to consider building spatial and temporal averages of the instantaneous FORUM measurements for climate model evaluation (e.g. Feldman et al., 2015). As noted in Section 4.2.3, the baseline is monthly mean, 10° zonal averages, although this does not preclude employing other averaging strategies (e.g. by cloud regime). When taking averages over a large enough sample, the only source of uncertainty on an averaged spectrum will come from the calibration absolute radiometric accuracy (ARA), because the statistical noise (NESR) is reduced by the square-root of the number of averaged measurements (about a factor of 80 for monthly mean, 10° zonal averages). As discussed in Chapter 3, feedback signals associated with a 1 K change in surface temperature, typical of the level of variability in tropical monthly mean values, is estimated to be around $1 \text{ mW}/(\text{m}^2 \text{ sr cm}^{-1})$ in spectral radiance, with humidity induced differences in the feedback signal of around $0.3 \text{ mW}/(\text{m}^2 \text{ sr cm}^{-1})$, peaking in the FIR (see Fig. 3.2). Similarly, changes in TOA radiance induced by perturbations in water vapour as a result of ENSO variability are greater than $0.4 \text{ mW}/(\text{m}^2 \text{ sr cm}^{-1})$ (see Chapter 7, Fig. 7.3-14)

Fig. 4.6 shows that an accuracy of at least $0.3 \text{ mW}/(\text{m}^2 \text{ sr cm}^{-1})$ in the FIR is required to capture these climate signatures. This level of accuracy can be reached with a threshold

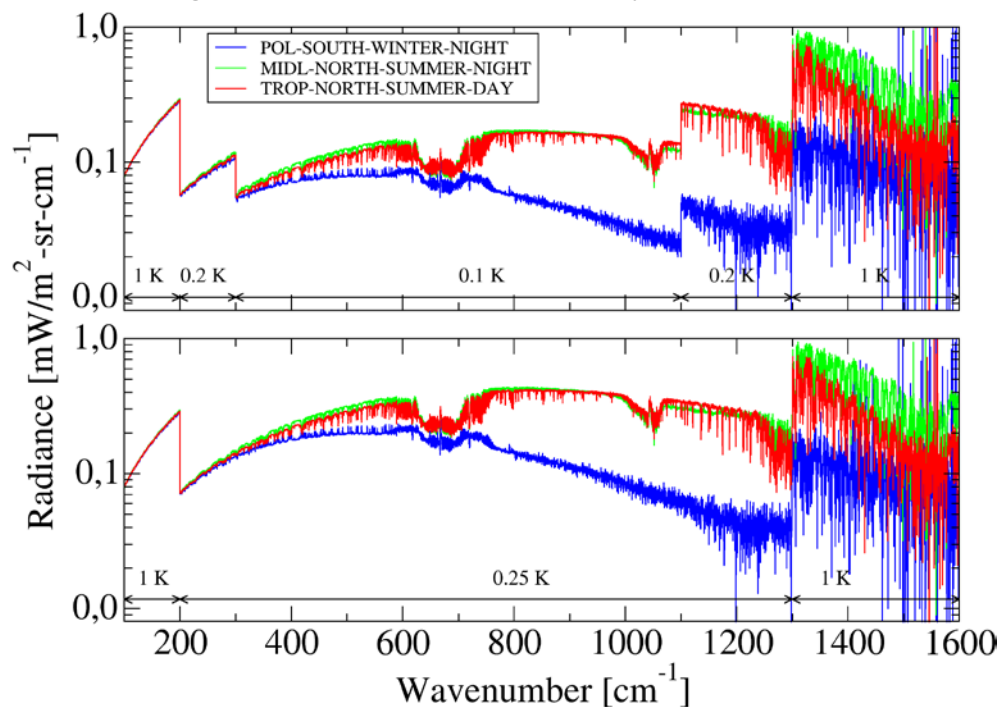


Figure 4.6 ARA requirement (goal in the top panel and threshold in bottom panel) converted to radiance for three scenarios (polar night, mid latitude, tropical day). (L. Palchetti, CNR, Italy)

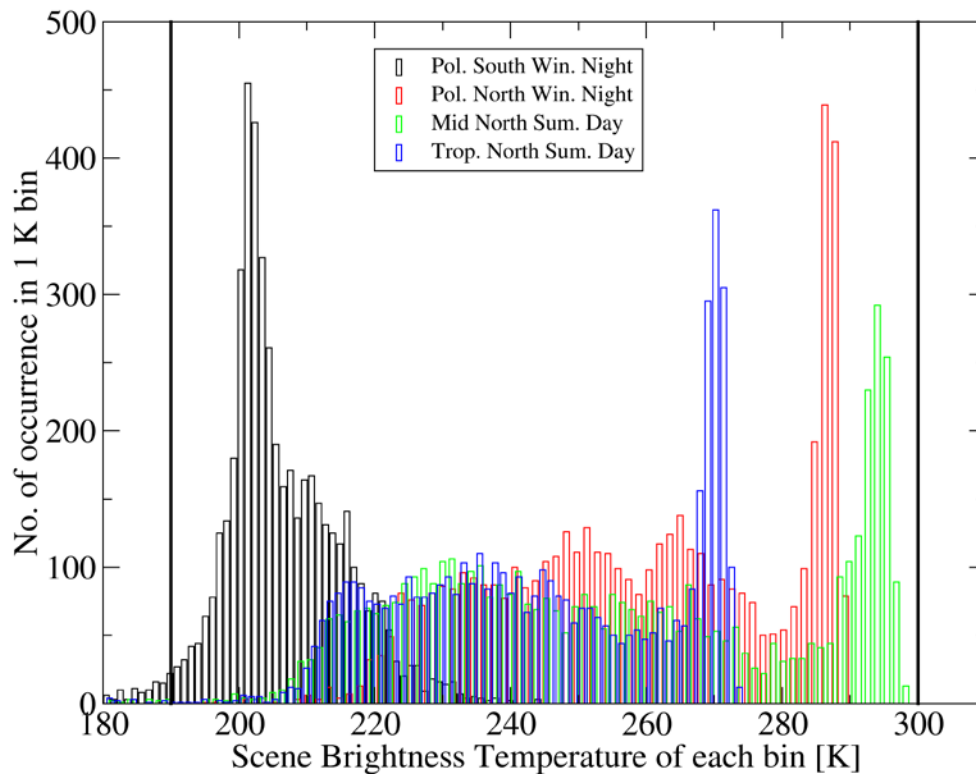


Figure 4.7 Distribution of channel brightness temperature for different scenarios. (L. Palchetti, CNR, Italy)

requirement on ARA, expressed in brightness temperature, of at least 0.25 K in the 200–1300 cm^{-1} range and 1 K elsewhere. To show that this requirement is commensurate with the signal sizes highlighted above it has been converted into radiance accuracy and is shown in the bottom panel of Fig. 4.6. The top panel shows the goal radiance accuracy, which will allow a finer discrimination of the spectral signatures. This corresponds to the following ARA requirement: 0.1 K between 300–1100 cm^{-1} , 0.2 K between 200–300 and 1100–1300 cm^{-1} , and 1 K outside these ranges.

Since FORUM aims to provide a record of high-quality spectral measurements with the goal of reducing uncertainty in climate predictions, the ARA is required with 3σ standard deviation (Wielicki et al., 2013). This level of accuracy needs to be reached for all realistic temperatures of the observed scenes, from between 190–300 K. Fig. 4.7 provides the motivation for this choice by showing the frequency distribution of simulated scene brightness temperatures across the FORUM spectral range for four different scenarios, covering warm (tropical day time) and cold (polar night) extreme cases. Across these scenes the vast majority of brightness temperatures range 190–300 K, with only the extreme southern polar night exhibiting values less than 190 K. Even in this case, 97% of the spectral brightness temperatures are greater than 190 K. All scenarios show maximum brightness temperatures less than 300 K.

4.2.6 Requirements on Stability and Pointing of the Line-of-Sight

To assess the dwell time stability requirement of the line-of-sight, the variation in the observed radiances caused by the displacement of the centre of a FORUM pixel (assumed to be a circle of radius r) by a given amount has been calculated. The difference is at maximum when 50 % of the pixel is in clear-sky and 50 % covered by a cloud, as shown in the left side of Fig. 4.8.

A displacement of the centre of the FOV perpendicular to the cloud edge, as shown in the right of Fig. 4.8, will cause the maximum change in the fraction of the FOV contaminated by the cloud. The radiances observed by FORUM have been evaluated for a partially cloudy FOV by combining a clear sky simulation with a simulation using exactly the same atmospheric and surface state but with a cloud inserted in the FOV. If α is the cloud fraction in the FORUM FOV, the observed spectrum \mathbf{S} can be obtained using:

$$\mathbf{S}_{\text{tot}} = \alpha \mathbf{S}_{\text{clear}} + (1 - \alpha) \mathbf{S}_{\text{cloud}} \quad (4.1)$$

For a small displacement d of the centre of the FOV, the difference in the fraction of the cloud covered area can be easily determined using:

$$\alpha - \alpha' = \frac{2d}{\pi r} \quad (4.2)$$

And the resulting difference in the spectrum will be:

$$\mathbf{S}_{\text{diff}} = \mathbf{S}_{\text{tot}} - \mathbf{S}_{\text{tot}'} = (\alpha - \alpha') (\mathbf{S}_{\text{clear}} - \mathbf{S}_{\text{cloud}}) \quad (4.3)$$

Therefore, varying the value of d , the limiting value that ensures that the change to the FORUM radiance is too small to significantly impact its quality, can be found. Tests have shown that a value of 200 m causes average differences in the radiances in the order of a tenth of the threshold NESR and a value of 100 m causes average differences in the radiances

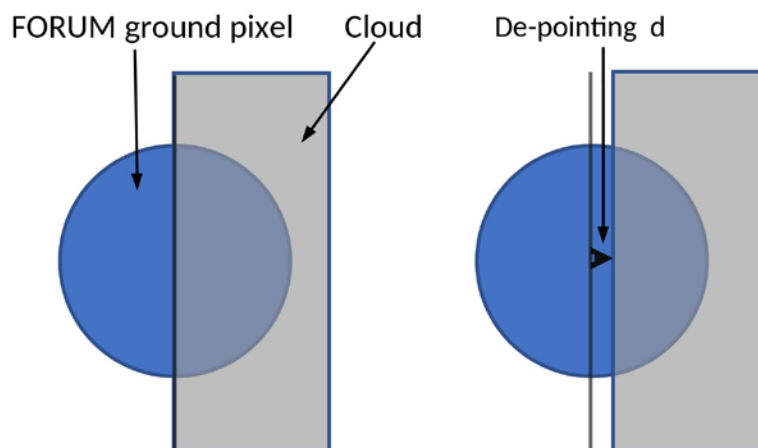


Figure 4.8 FORUM pixel covered by 50 % of a cloud and a de-pointing of distance d . (B. M. Dinelli, CNR, Italy)

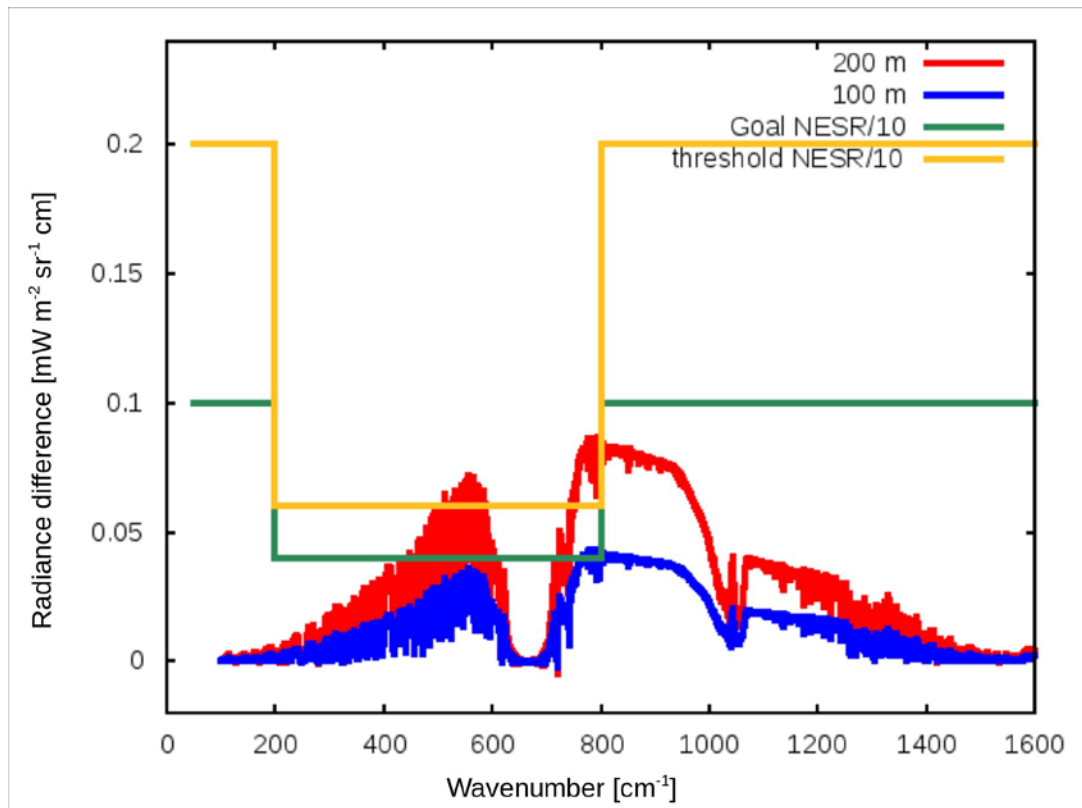


Figure 4.9 Spectral difference due to a pointing error of 100 m (blue line), 200 m (red line) in the worst case of the pixel covered by 50 % of cloud, and compared to a tenth of the NESR goal and threshold requirements. (B. M. Dinelli, CNR, Italy)

of the order of a tenth of the goal NESR, as shown in Fig. 4.9. Accordingly, the threshold requirement on the stability of FORUM pointing is set to 200 m and the goal value 100 m.

The value of the maximum accepted depointing angle should ensure that no distortions are present in the spectra recorded by FORUM. This has been translated to the requirement that the radiance observed by the FSI during the acquisition of a single scene is constant within a threshold that has been defined to be the goal NESR value divided by 10. This corresponds to $0.04 \text{ mW/m}^2 \text{ sr cm}^{-1}$ in the FIR frequency range ($200\text{--}800 \text{ cm}^{-1}$) and $0.1 \text{ mW/m}^2 \text{ sr cm}^{-1}$ elsewhere.

To evaluate the differences in the observed radiances, FORUM spectra have been simulated at high resolution over a set of different viewing angles for climatological atmospheric conditions, for all seasons and for six latitudinal bands. Fig. 4.10 shows the results of the simulations in the worst condition found, which is for a tropical atmosphere in summer, where the differences between the simulated spectra at different angles are the largest. The spectral differences are calculated for different viewing angles using the goal value for the spectral resolution.

Fig. 4.10 shows that for viewing angles up to 3.5° the differences between the radiances are below a tenth of the NESR. Therefore, from radiometric considerations only, the maximum

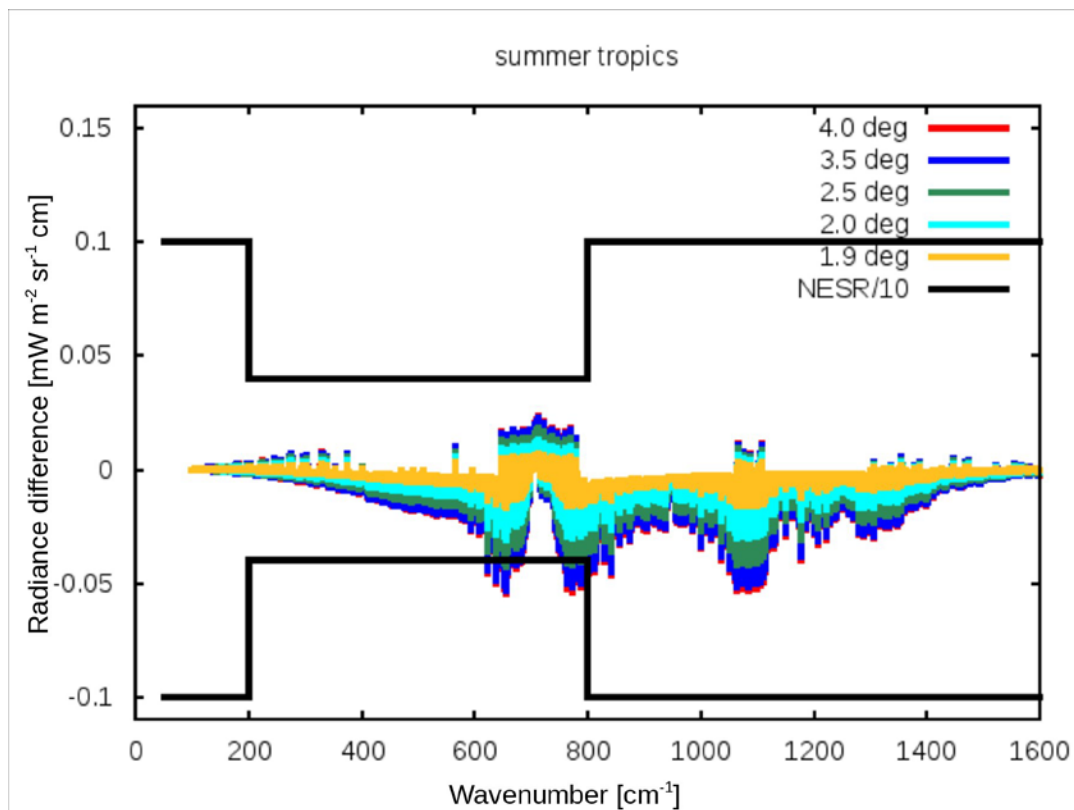


Figure 4.10 Difference between FORUM spectrum at nadir and spectra calculated at different viewing angles. The different colours represent the values of the viewing angles as given in the legend. (Bianca M. Dinelli, CNR, Italy)

dwelt time depointing angle of the line-of-sight should be less than $\pm 3.5^\circ$ with respect to the nadir direction.

The maximum depointing angle also ensures that the distortion of the ground pixel should be less than 200 m. The distortion produced by slant views has been evaluated by calculating the difference in the radius of the pixel along the orbit track owing to the different pointing angles, assuming a constant field of view half angular aperture of 0.52° (7.5 km radius for an orbit altitude of 830 km). With this field of view aperture and assuming a perfect match of the centre of the pixel for all angles, a 3.5° viewing angle produces a difference in the radius of about 32 m in one direction and 24 m in the other direction, well below the requirement of 200 m.

4.3 Observational Requirements related to FEI

4.3.1 Measurement of Thermal Colocated Images

The FSI ground scene covers an area of 7.5 km radius, and the measured spectrum will be the integral of the atmospheric and surface contribution in that area. In order to facilitate scene classification and assess the degree of homogeneity of the FSI ground scene and the cloud coverage, an imager has been added to the mission and will provide colocated measurements with the FSI.



The recorded images will also be used to monitor changes of the observed scenes, principally due to the movement of clouds, during the time needed to acquire one FSI interferogram, and between the acquisition of FORUM FSI and IASI-NG spectra to screen suitable cases for synergistic retrieval. This requires at least five images to be acquired during the dwell time.

4.3.2 Size and Spatial Resolution, Spectral Range, Noise and Accuracy Requirements

The ground pixel size of the imager must be larger than the area covered by the FSI pixel to account for mispointing between the two and to monitor both the portion of the atmosphere crossed by the FSI Line of Sight during the integration time and the area covered by the IASI-NG collocated measurement. The FSI pixel covers a circular area with a 7.5 km radius. An area across and along track of $36 \times 36 \text{ km}^2$ will always include the FSI pixel and will also enable the observation of the surrounding area that will be sampled by the FSI line of sight during dwell time because of the varying slant path needed to compensate for the satellite movement. Moreover, this coverage will also enable the observation of the area sampled by IASI-NG collocated measurements.

The spatial resolution of the FEI should be higher than that of the FSI, to help detect and assess sub-pixel inhomogeneities of the FSI in both cloudy conditions and when viewing the surface (i.e. to identify small islands, coastlines, small clouds). Typical opaque ice clouds produce detectable differences in the FSI signal when covering an area of about 1.2 km^2 inside the FSI FOV. In order to be able to clearly detect this cloud coverage, a spatial resolution of the FEI of at least two times higher than this value is needed. This corresponds to 0.6 km^2 . This requirement implies that to be able to infer the scene classification of the FSI from the FEI, the relative alignment must be known with a spatial co-registration of 300 m as goal and 600 m as threshold.

The imager should be sensitive to the surface and cloud properties, so it also has to be able to analyse any FSI scene during day and night acquisitions. As a consequence, the spectral band of the imager has been chosen in the TIR, centred in the atmospheric window at $10.5 \text{ }\mu\text{m}$ (952 cm^{-1}) where numerous studies (Inoue, 1985, Parol et al., 1991, Ackerman et al., 1995) have already shown the sensitivity to both surface and cloud property variations. The FEI spectral band width should enable sufficient coverage of the atmospheric window, which translates into a width of $1.5 \text{ }\mu\text{m}$ at around 952 cm^{-1} .

The radiometric accuracy is not an issue for the FEI if just used for monitoring scene homogeneity since only relative changes are important. However, the imager observations can also be used to help the study of the cloud properties. Therefore, the accuracy of the brightness temperature measured by the FEI should be similar to the goal noise level of the FSI in the same spectral region that is below 1K.

The precision of the FEI can be characterised by its noise equivalent delta temperature (NeDT), which is typically defined at a single reference temperature, chosen here as 210 K. This choice is based on the coldest scene that the FEI is likely to measure given its spectral width since the non-linearity of the conversion of NeDT to radiance makes the requirement most stringent for coldest scenes. To assess its threshold and goal values the following

argument is used. Typical land skin temperatures vary greatly (5 K in a range of 10 km) and cloud top temperatures have a variability of several tens of K depending on their altitude and opacity profile. The FEI NeDT should be small enough that it enables the identification of inhomogeneity in the skin temperatures or in the cloud coverage that produce detectable differences in the FSI spectrum. Therefore, to infer the NeDT, the differences in the FEI measurements that produce detectable differences (above the FSI goal NESR) in the FSI radiances need to be assessed. For clear sky, they have been evaluated by simulating the FSI measurements with varying skin temperatures and computing the differences for both the FSI and FEI measurements as a function of the skin temperature variation. For cloud coverage monitoring, the FEI should be able to detect FSI sub-pixel temperature variations that would produce an averaged FSI spectrum variation (compared to the fully clear pixel) higher than the FSI NESR. Therefore, simulations have been performed assuming a FSI pixel is half clear and half cloudy, and the differences between the FSI and FEI measurements in the clear and cloudy parts of the FSI pixel have been evaluated. In the following sections these tests are described.

Clear-sky case

FEI and FSI measurements have been simulated with LIDORT (Spurr, 2008) with skin temperature variations of 0.25, 0.5, 0.75 and 1.0 K. The measurements have been simulated for six latitudinal bands and four seasons using climatological atmospheric profiles. Fig. 4.11 reports the differences for the FSI measurements in the best and worst case scenarios. Fig. 4.11, bottom panel shows that in the worst case scenario, a skin temperature difference of 0.5 K is the maximum value that produces differences in FSI radiances that are below the NESR across the majority of the FSI spectral range. Fig. 4.12 summarises the results using a scatter plot of the differences in the simulated FEI brightness temperatures as a function of

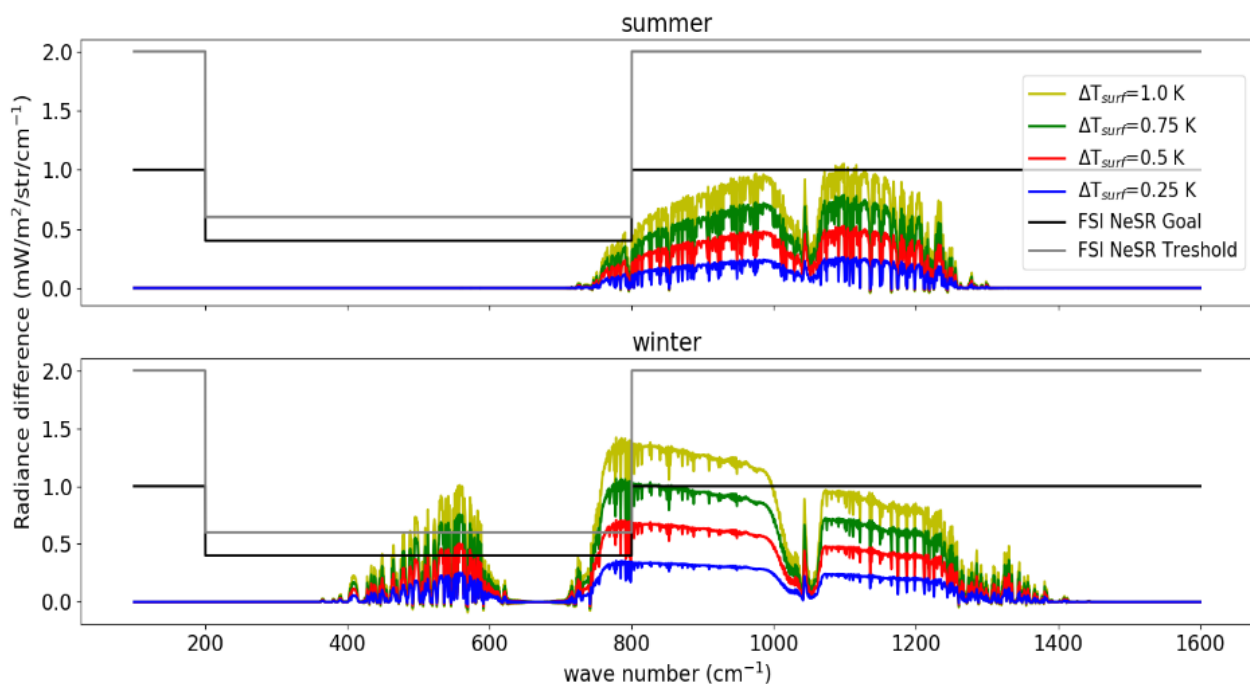


Figure 4.11. Radiance differences for the FSI measurements in the best (upper panel) and worst case (bottom panel) scenarios. (L. Labonnote, University of Lille, France)

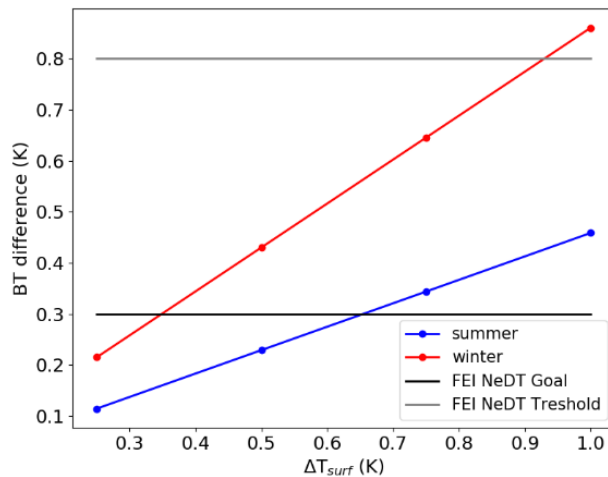


Figure 4.12 Brightness temperature differences in the FEI measurements as a function of the skin temperature differences. (L. Labonnote, University of Lille, France)

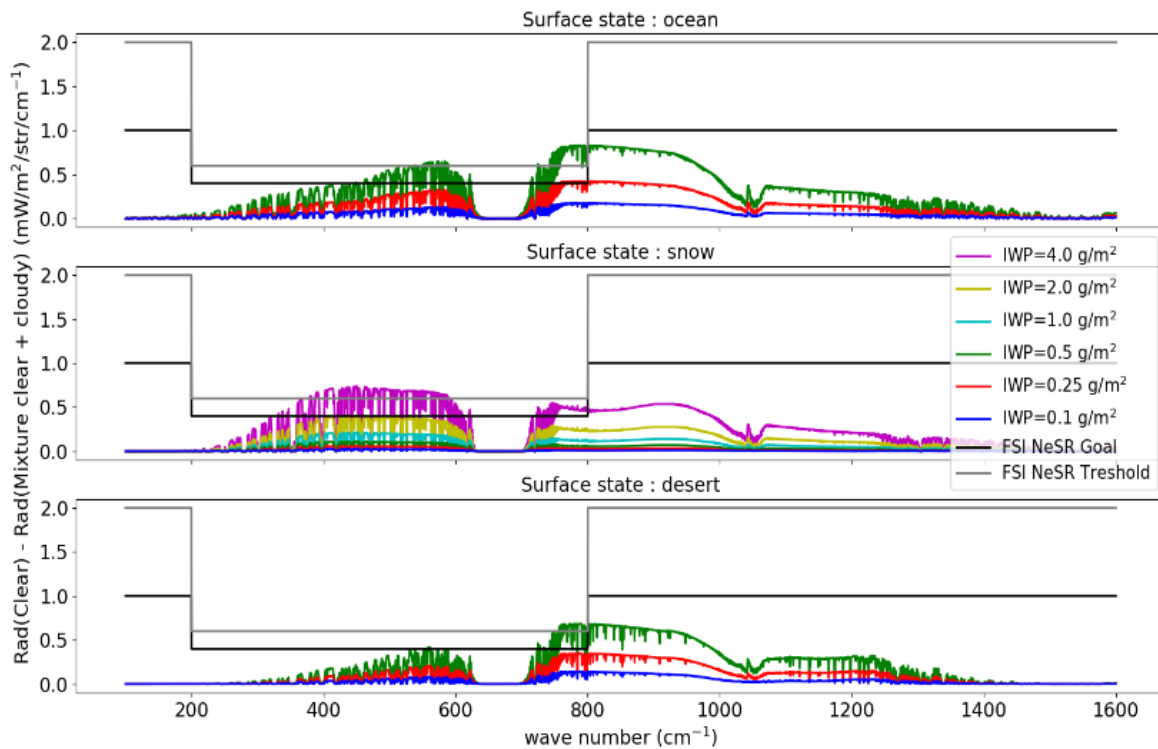


Figure 4.13 FSI radiance difference between fully clear pixel and a pixel half clear and half covered by an ice cloud. The different colour represents the opacity in terms of IWP of the covered part of the FSI pixel. The black (grey) line represents the expected FSI NESR goal (threshold). The three panels show three different surface types (L. Labonnote, University of Lille, France)

skin temperature difference. The figure indicates that a 0.5 K skin temperature difference (inhomogeneity) always corresponds to an FEI difference below 0.5 K.

Cloudy sky case

For this purpose, three atmospheric profiles in cloudy conditions above ocean, snow and desert, have been selected from the ECMWF diverse profile database

(<https://www.nwpsaf.eu/site/somware/atmospheric-profile-data/>), the last of these being representative of an extreme temperature contrast between ice cloud and the surface. A radiative transfer code has been used to simulate the measurement of fully cloudy pixels for different cloud opacity (IWP varying between 0.1 to 256 g/m²) and clear pixels for both the FSI and FEI by taking into account the expected instrument characteristics in terms of spectral band, resolution and instrument spectral response function (ISRF).

Fig. 4.13 shows the difference between a fully clear pixel and an inhomogeneous pixel (assumed half cloudy and half clear) that would be measured by the FSI, as a function of the cloud opacity in terms of IWP, together with the NESR of the FSI (black and grey lines), for the three different surface scenarios. This difference exceeds the NESR goal of the FSI for IWP greater than 0.25 g/m² above the ocean and desert, and greater than 2 g/m² above snow. If the FSI NESR threshold is considered this value becomes 0.5 g/m² for the ocean and desert scenarios, and 4 g/m² over snow.

Fig. 4.14 shows the brightness temperature difference between fully clear and cloudy pixels that would be measured by the FEI for the three different scenarios as a function of the cloud opacity expressed in terms of IWP. From this figure one can directly infer what should be the minimum signal detectable by the FEI in terms of temperature (dotted coloured lines) to detect the contrast between a clear and a cloudy pixel. For example, if the desert scenario (green line) is considered, the minimum signal detectable by the FEI with goal performance (NeDT = 0.4 K) corresponds to the temperature difference between a clear and cloudy pixel with IWP = 0.25 g/m². A value of 0.6 K (green dotted line) is found if a cloudy pixel with IWP = 0.5 g/m² is considered. Optically thicker clouds are required to produce a discernible signal over snow.

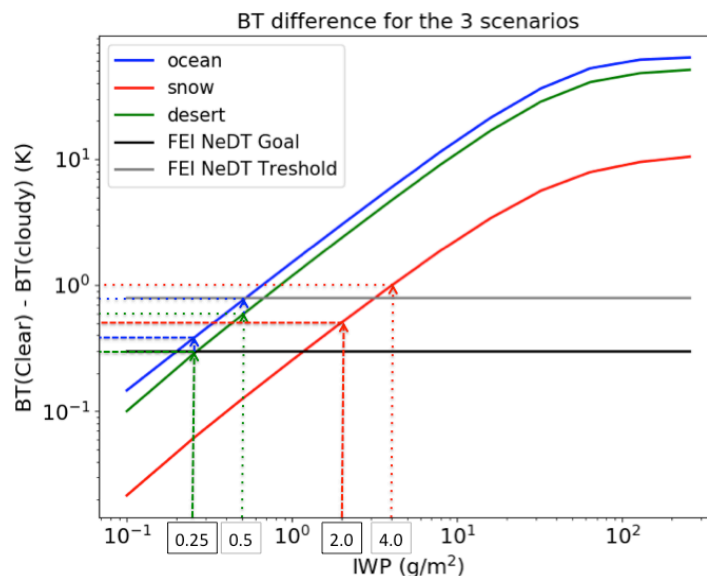


Figure 4.14. FEI brightness temperature (BT) difference between a clear and covered pixel as a function of the cloud opacity in terms of IWP. The different colours represents the three scenarios. The vertical dashed and dotted lines give the maximum opacity (in terms of IWP) of an ice cloud that would cover half of the FSI pixel and for which the difference with a fully clear pixel stay below the FSI NESR goal (threshold). The corresponding horizontal lines give the minimum signals that the FEI should be able to detect (in terms of temperature). (L. Labonnote, University of Lille, France)

4.4 Spatial and Temporal Sampling Requirements

The overarching research goal of the FORUM mission – to evaluate the role of the FIR in shaping current and future climate – requires sampling of the full range of atmospheric and surface conditions, with observations covering all regions of the globe for a long enough time period to capture interannual variability. These requirements, which align with GCOS monitoring principles for Essential Climate Variables (ECVs) (WMO, 2016) provide the basis of the mission requirements for geographical coverage, spatial and temporal sampling, and mission lifetime which are described in the following subsections.

4.4.1 Spatial Coverage Requirements

To meet the science aims described in Sections 2 and 3 FIR spectra need to be obtained over the full range of observing conditions and meteorological regimes. This means global coverage is required. The expected surface emissivity products for snow and ice fields places additional requirements on thorough sampling of high latitudes. A Sun-synchronous 82° inclination orbit allows these sampling requirements to be met, providing global coverage and excellent sampling at high latitudes. This orbit also provides the significant additional advantage of allowing FORUM to fly in loose formation with IASI-NG, thus enabling the MIR $1600\text{--}2760\text{ cm}^{-1}$ region of the OLR spectrum to be measured nearly co-incidentally with the FORUM FIR observations.

4.4.2 Spatial Sampling Requirement and Ground Pixel Size

The spatial sampling requirement is driven by the necessity to observe the variability of the OLR spectral signal and to use it to identify the spectral signatures of climate variables such as upper tropospheric water vapour. An along-track sampling of 100 km is the specified minimum required for FORUM, making its observations compatible with the 100 km horizontal resolution GCOS-recommendation for the top of the atmosphere OLR ECV for the Earth radiation budget.

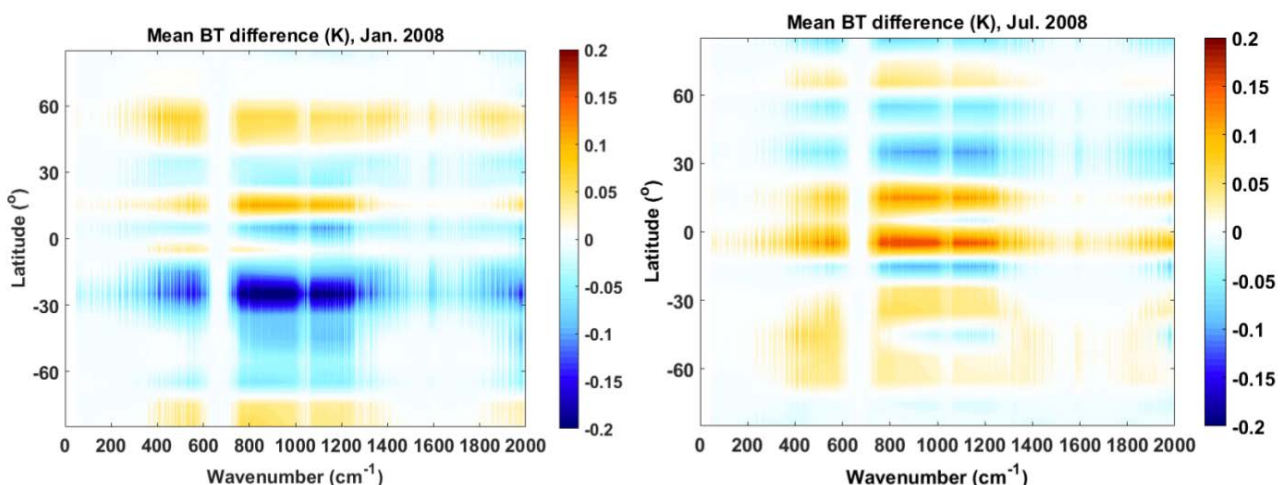


Figure 4.15 Monthly average difference between FORUM sampling and continuous sampling. Simulations computed using 6-hourly ERA5 profiles for atmospheric parameters and cloud. (Courtesy X. Huang, University of Michigan, US)

Fig. 4.15 shows the simulated difference in derived monthly mean brightness-temperature at the 10° zonal scale, between continuous sampling (true values) and the 100 km FORUM sampling. For all latitudes and spectral regions, differences are well within the 0.25 K absolute accuracy threshold requirement of the FSI measurements. This indicates that this sampling distance will still enable high-quality representative TOA spectra to be generated at the 10° zonal, monthly mean scale and will not compromise FORUM's ability to quantify the climate role of the FIR.

The FORUM field of view requirement gives a ground observation with a diameter of 15 km. This is slightly larger than the IASI-NG pixel size of 12 km, but the difference will not compromise the synergistic use of both measurements (Section 7.3.2). The probability of a cloud-free observation only decreases by about 1 % as pixel size increases from 12 km to 15 km (Krijger et al., 2007). IASI-NG measurements can therefore be used as the basis for a quantitative analysis of the expected clear and cloudy FORUM observations, using an approach originally developed by Meteo-France (Lavanant and Roquet, 2013) to assess cloud-type occurrence within the IASI FOV (Amato et al., 2014). Such analysis leads to the expectation that around 28 % of FORUM observations will be cloud free, inhomogeneous fields of view owing to fractional cloud cover will affect 9 % of observations and the remaining 63 % of cases will be completely cloud covered. Thus, in common with the IASI-NG near-nadir observations, the FORUM 15 km FOV will enable good sampling of both cloudy and clear sky conditions with less than one in ten observations affected by partial cloud cover.

4.4.3 Mission Duration and Orbit

To enable robust climatological averages, observations need to sufficiently sample inter-annual variability of Earth's outgoing radiation, thus an operational lifetime of at least four years after the commissioning phase is required. This will enable major modes of climate variability such as the quasi-biennial oscillation to be sampled, and should be sufficient to sample at least one El Niño Southern Oscillation. A fixed overpass time provided by a Sun-synchronous orbit (SSO), will provide constant sampling of the diurnal cycle as recommended by the GCOS monitoring principles (GCOS, 2016), and avoid aliasing diurnal variability into the measurements, providing a stable, consistent set of observations suitable to meet the primary science objectives described in Chapter 3. This option also furthers the science aims by allowing FORUM to fly in loose formation with an operational SSO mission, as described in the next Section 4.5.

4.5 Loose Formation Mission Concept with an Operational Mission

As a stand-alone mission, FORUM will provide unique information on the top of the atmosphere FIR spectrum. Flying the FORUM mission in loose formation with the EUMETSAT MetOp-SG(1A) satellite offers many additional benefits. There is a strong synergy between the FORUM FIR spectral measurements and IASI-NG MIR spectral observations. Together the FORUM mission and IASI-NG, will deliver unique hyperspectral observations of Earth's emission spectrum spanning almost five octaves in frequency, from 100 to 2760 cm^{-1} and comprising virtually the whole spectral range of Earth's outgoing energy.

In addition to IASI-NG, the MetOp-SG(1A) satellite will host a range of operational and climate monitoring instruments that will provide complementary information, such as water vapour and temperature profiles, and cloud-field parameters, which will support and enhance the scientific exploitation of the FORUM measurements.

The FORUM coincidence requirement, to fly in loose formation with MetOp-SG(1A) with separation of less than 1 minute will ensure synergistic exploitation of the data from the two platforms. With this time difference, atmospheric fields should be sufficiently stable to enable IASI-NG and FORUM observations to be exploited to provide combined instantaneous retrieval of water vapour and temperature (Section 7). A temporal difference of one minute should also be sufficient to enable synergistic cloud products to be derived, as is done for the A-train satellite constellation. For example, the MODIS and POLDER instruments on Aqua and PARASOL respectively provide observations separated by about three minutes which are used together to derive cloud thermodynamic phase (Riedi et al., 2010). Similarly, the MODIS and IIR instruments, on Aqua and CALIPSO are used to retrieve information on multi-layer clouds using observations separated by up to a minute (Sourdeval et al. 2016).

The Multi-viewing, Multi-channel, Multi-polarization Imaging (3MI) on MetOp-SG(1A) also offers interesting synergy with FORUM FSI measurements. The multi-viewing and polarisation capabilities of 3MI will enable its observations to discriminate between liquid and ice particles and provide the capability to detect super-cooled cloud layers above ice, a frequent occurrence in polar regions. Furthermore, 3MI multi-view observations in the O₂-A band will also provide information on cloud top height and geometrical thickness (Desmons et al., 2013). Given the compatible 4×4 km² pixel size of the 3MI imager, co-registration errors with the FORUM observation should be small enough that this information can be used as a reliable first guess in FORUM cloud property retrievals

MetOp-SG-(1B), flying in an orbit separated by about 30 minutes from MetOp-SG(1A), will host further sensors with the cloud parameters derived from the measurements of the Ice Cloud Imager (ICI) being of most relevance to the FORUM products. Although the 30 minute time difference between the FORUM and MetOp-SG(1B) overpasses will limit direct synergistic exploitation, comparison of spatial and temporal averages of data products from the two missions, such as zonal and monthly means of climate variables should still prove informative.

4.5.1 Advantages of Flying in Loose-Formation with IASI-NG

While the success of the FORUM mission does not depend on IASI-NG, the availability of IASI-NG measurements matching those of the FORUM FSI will enable the following additional activities, contributing to the consolidation, validation and scientific exploitation of FORUM measurements.

- FORUM FSI and IASI-NG spectral radiance comparison verifying the radiometric and frequency intercalibration of the sensors across their overlapping wavenumber range (see Section 6.2).
- Opportunity to verify the spectral consistency of spectroscopic models across the full infrared range. This is particularly relevant for the water vapour continuum

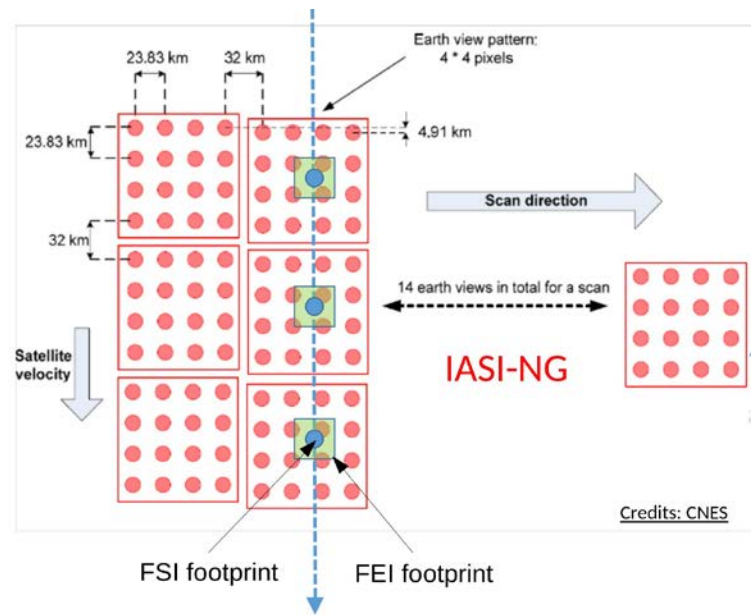


Figure 4.16 Sketch of FORUM and IASI-NG ground sampling patterns. (L. Palchetti, CNR, Italy)

parametrisation and spectroscopic line data such as line positions, intensities, and broadening coefficients relating to molecules that are spectrally active both in the FIR and in the MIR region (up to 2760 cm^{-1}).

- Opportunity to verify spectral consistency of cloud micro-physical models across the FIR and the full MIR regions, from 100 to 2760 cm^{-1} .
- Opportunity for synergistic retrieval schemes to generate improved or more complete Level-2 products, in particular: spectral fluxes, surface spectral emissivity and temperature, cloud parameters, and temperature and water vapour profiles (see Section 7).

4.5.2 Temporal and Spatial Co-registration Requirements with IASI-NG

Fig. 4.16 illustrates the FORUM and IASI-NG ground sampling patterns for the IASI-NG fields of regard either side of the sub-satellite track. For these near nadir observations the distance between the centres of IASI-NG pixels is up to 32 km increasing to about 87 km for the fields of regard at the edges of the IASI-NG swath (not shown). Since the FORUM FSI is nadir-viewing it will only be matched to IASI-NG pixels close to the IASI-NG sub-satellite point and spatial matching with IASI-NG will require the ground tracks of the two satellite orbits to be closely matched. A requirement for the maximum distance between the FORUM and MetOp-SG(1A) ground tracks of $< 100\text{ km}$ as a goal (300 km threshold), guarantees that FORUM FSI and nearest IASI-NG pixel centres will be separated on the ground by less than 23 km (26 km threshold). This distance is the worst case and occurs when the FORUM pixel falls right in-between the fields of regard of IASI-NG. The co-registration requirements corresponds to FORUM viewing the two centre IASI-NG fields of regards for the goal and the centre six for the threshold. This can be considered a very good matching criterion in the light of the results of tests reported in Chapter 7. For an assumed satellite altitude of 800 km the satellite ground tracks will need to be within 7.1° (20.4° threshold). Horizontal smearing of the tropospheric air mass ($< 15\text{ km}$) sounded by the matched IASI-NG measurement will

Level-1 Products	Product Definition and Requirement
FSI Level-1b	Spectrally and radiometrically calibrated spectral radiance in $W/(m^2 sr cm^{-1})$, separated for the two output ports in the 100-1600 cm^{-1} band. Spectral resolution (FWHM): 0.36 cm^{-1} (G) / 0.5 cm^{-1} (T)
FEI Level-1b	Thermal images radiometrically calibrated in $W/(m^2 sr)$ and geolocated with preliminary pixel classification. NeDT: 0.3 K (G) and 0.8 K (T) at 210 K.
FSI Level-1c	Spectrally and radiometrically calibrated spectral radiance, resampled at a specific spectral grid and with the two ports averaged. Radiometric, spectral and geometric errors are appended. Precision(*): Noise-Equivalent Spectral Radiance (NESR) 0.4 $mW/(m^2 sr cm^{-1})$ (G), 0.6 $mW/(m^2 sr cm^{-1})$ (T) in the spectral range 200-800 cm^{-1} 1 $mW/(m^2 sr cm^{-1})$ (G), 2 $mW/(m^2 sr cm^{-1})$ (T) outside the spectral range 200-800 cm^{-1} Accuracy(*): Brightness temperature for all observed scenes in the range of 190-300 K The goal requirement is 0.2 K in 200–300 cm^{-1} 0.1 K in 300–1100 cm^{-1} 0.2K in 1100–1300 cm^{-1} 1 K elsewhere The threshold requirement is 0.25 K from 200 cm^{-1} to 1300 cm^{-1} <1 K elsewhere

(*) Precision is the random error component of each individual measurement. Accuracy is the difference between the true value and the measurement in absence of any random error.

Table 4.1 Level-1 product requirements. (G) and (T), goal and threshold, respectively.

then be less than 2 km (6 km threshold), i.e. significantly smaller than the maximum 23 km (26 km threshold) difference between the FORUM and IASI-NG pixels.

Co-location requires consideration of the temporal difference as well as the spatial match between the FORUM and IASI-NG measurements as temporal evolution of the atmosphere between observations will affect its composition, particularly cloud coverage and properties. Cloud motion into or out of the field of view holds the most potential for producing large effects over a short time period, significantly modifying the measured spectrum and compromising synergist use of data from the two instruments. For this reason, temporal collocation requirements were defined to limit the cloud fraction change in the instrument field of view to less than 2 % over the period between FORUM and IASI-NG measurements. Assuming an average speed of clouds in the troposphere of 20 m/s and a 15 km diameter ground pixel, this translates to limiting the temporal mismatch between FORUM and IASI-NG to less than 1 min.

4.6 FORUM Products

4.6.1 Level-1 Products

Standard Level-1b and Level-1c products are to be delivered (Table 4.1) as the primary FORUM products. They include both the instantaneous spectral radiances of the FSI and the



thermal images of the FEI. Since the FSI has two redundant channels that provide the same spectral information, Level-1c is the average of the two output channels including the errors associated with the instantaneous single measurement. The Level-1c products are the standard radiance products delivered to users for assimilation and will be the basis of analysis and averaging for climate studies. They are also the starting point for the derivation of the Level-2 described in Chapter 6.

4.6.2 Level-2 Products and Potential Higher-Level Products

More information about the retrieval of the products shown in Table 4.2 will be provided in Chapter 6, where also other geophysical quantities, such as temperature vertical profiles, spectral fluxes and surface temperature, will be discussed in details. Additional information such as scene identification from the thermal imager will also be discussed. The Level-2 products (see Table 4.2) include the main parameters to characterise the observed atmospheric state: vertical profiles of water vapour, surface emissivity, and cloud parameters. Since the FIR is expected to realise its major scientific benefit in the study of ice-cloud, the parameters that are required at Level-2 are the column ice water path, the cloud top height and effective particle diameter.

Potential higher-level products could be provided by FORUM through dedicated science centres and other data-processing infrastructures. Examples include Level-3 zonal, monthly averages of Level-2 products and Level-1c radiances suitable for climate detection and attribution studies and facilitating model evaluation.

4.6.3 Data Latency

Timeliness is the period of time from data acquisition to the delivery of the relevant products to the users. Operational global data assimilation requires data in less than 3 hours to be used for forecast applications. Many scientific applications, including climate model evaluation have much longer latencies. For example, 24 hours is sufficient for real time daily monitoring in conjunction with field study execution, and monthly resolution data is preferred for many climate monitoring applications such that latency of a month or more is sufficient.

Level-2 Products	Products Definition and Uncertainty (+) Requirement
All-sky broadband spectral flux	FORUM Level-1c FIR OLR extended to broadband with the Level-1c from IASI-NG, consistent with independent broadband flux observations to within the radiance to flux uncertainty, with minimal bias averaged over all scenes.
Water vapour profile	Vertical profiles of water vapour concentration with 15 % uncertainty at 2-km vertical resolution
Surface emissivity	0.01 in the 300–600 cm ⁻¹ spectral range for polar region on 50 cm ⁻¹ spectral grid
Ice water path (IWP)	20 %
Cloud Top Height (CTH)	1 km
Particle size diameter	20 %

(+) uncertainty is the total error, including both the random and accuracy components.

Table 4.2 Level-2 product requirements.



Therefore, for the objectives of FORUM, a data latency of 24 hours to generate Level-1 products is requested. Similar latency would also be appropriate for temperature and water vapour products and ice cloud properties. Longer latency periods can be afforded for quantities most likely to be employed as averages and for climate applications such as surface emissivity and spectral fluxes.

Near-real-time delivery (i.e. within three hours from acquisition) of radiances and temperature and water vapour profiles after the commissioning phase could support their assimilation in operational Numerical Weather Prediction applications or possible new applications in the context of MetOp-SG if studies showed that FORUM data would be beneficial to model analyses and forecasts.

5 MISSION ELEMENTS

This chapter provides the technical description of the FORUM mission, as derived from the preparatory activities in Phase A. Two technical baseline concepts are described that respond to the mission requirements defined in previous chapters. The concepts were developed in two parallel Phase A system studies by two industrial consortia led by Airbus Defence and Space Limited and Thales Alenia Space UK with Airbus Defence and Space GmbH and OHB Systems AG as instrument subcontractors respectively. Whenever relevant, two implementation concepts (concepts A and B) are described to present the different implementation options capable of meeting the mission requirements. The figures below are courtesy of the respective industrial consortia.

After an overview of the mission architecture and the orbit characteristics (Section 5.1 and Section 5.2), the space segment is described in detail (Section 5.3) followed by the launcher, ground segment and operations concept (Section 5.4, Section 5.5 and Section 5.6). The overall mission performance is summarised in Chapter 7.

5.1 Mission Architecture Overview

Fig. 5.1 depicts the main architectural elements of the FORUM mission. The space segment consists of a single satellite carrying two optical instruments: the FORUM Sounding Instrument (FSI) and the FORUM Embedded Imager (FEI). The satellite flies in a loose formation with MetOp-SG(1A) enabling the fulfilment of the required temporal and spatial co-registration between the FSI and the IASI-NG instrument on MetOp-SG(1A). The formation strategy ensures no risk of collision by allocating sufficient reaction time or by being in a passively safe configuration during safe mode of either satellite.

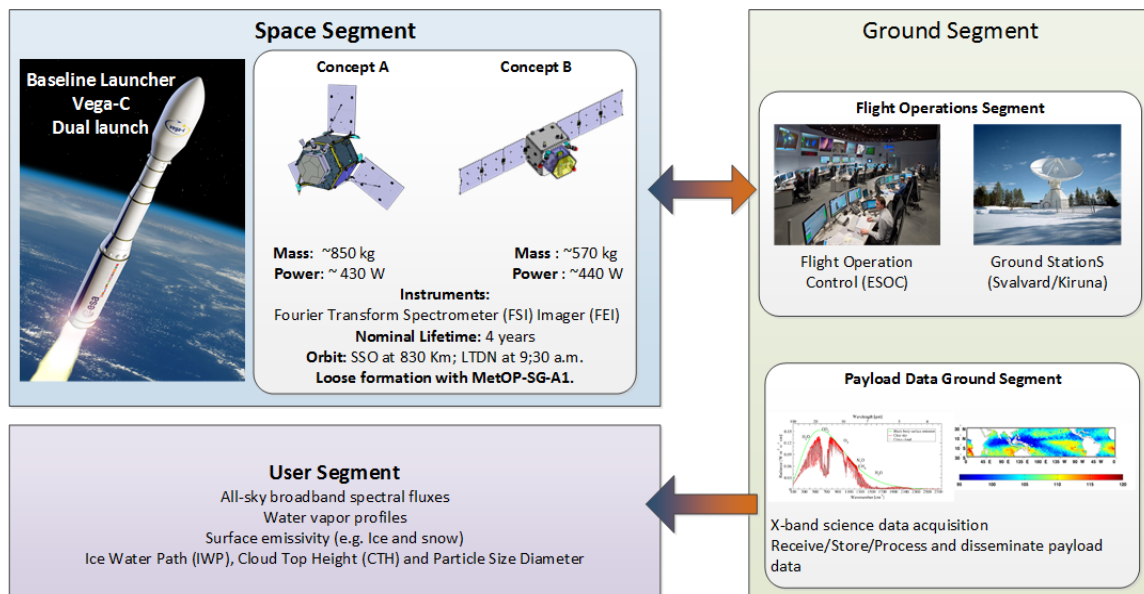


Figure 5.1 FORUM mission architecture for Concept A and B.



Vega-C is the baseline launcher in a dual configuration. It launches FORUM into a phasing orbit, from which FORUM manoeuvres into its nominal orbit, i.e. the one of MetOp-SG(1A).

FORUM performs continuous step-and-stare nadir-looking observations of spectrally-resolved top of atmosphere (TOA) radiances in the mid-infrared (MIR) and far-infrared (FIR) regions of the spectrum. The primary instrument is the FSI, a single-pixel infrared-atmospheric-sounder Fourier Transform Spectrometer (FTS) sampling the electromagnetic spectrum from 100 cm^{-1} to 1600 cm^{-1} ($100\text{ }\mu\text{m}$ to $6.25\text{ }\mu\text{m}$) with a spectral resolution better than 0.5 cm^{-1} . The FSI single pixel is colocated with the footprint of the FEI, a single-band-infrared-imager centred at $10.5\text{ }\mu\text{m}$ with a bandwidth of $1.5\text{ }\mu\text{m}$ and used for scene heterogeneity determination. Both instruments share many common units, such as the entrance aperture, the pointing mechanism, the thermal and mechanical framework and the radiometric calibration devices.

The ground segment uses the generic Earth Explorer ground segment infrastructure, comprising:

- The Flight Operations Segment (FOS), responsible for operations and safety of the spacecraft during all mission phases. It includes the Telemetry, Tracking and Command (TT&C) ground station and the Flight Operations Control Centre (FOCC).
- The Payload Data Ground Segment (PDGS), which includes the Science Data Acquisition Station, the Processing and Archiving Element and the Mission Planning and Monitoring Element.

The FORUM FOS receives orbit and mission planning data from the MetOp-SG's FOS to ensure consistent formation-flying operations. A single high-latitude ground station (e.g. Svalbard, Kiruna) delivers the FORUM scientific data via X-band. The PDGS delivers and distributes science data, processed up to Level-2 to the users within 24 hours or within three hours under request.

5.2 Mission Analysis

5.2.1 Orbit Selection

The spatial and temporal co-registration between the FORUM and IASI-NG observations drive the orbit selection and the need to fly in loose formation with MetOp-SG(1A). FORUM's orbit is the same orbit as MetOp-SG(1A), a 29-days repeat-cycle Sun-Synchronous Orbit (SSO), with a Mean Local Solar Time (MLST) at the descending node of 09:30 and an average orbit altitude of 830 km, as detailed in Table 5.1

For both concepts, the along-track temporal co-registration between the FSI and the IASI-NG nadir observations remains, under nominal operations, below 1 minute. The across-track spatial co-registration remains below 100 km during nominal operation during the mission lifetime, as shown in Fig. 5.2 (bottom) and Fig. 5.3. (left), guaranteeing that the FSI observations are always contained within the IASI-NG field of view (FOV) 1 to 3 during nominal operations, as shown in Fig. 5.9.

Orbit Mean Elements*		Orbit Characteristics	
Semi-major axis	7195.605	Repeat cycle/orbits per day	14+6/29
Eccentricity	0.001165	Repeat cycle length	29 days
Inclination	98.701°	Orbits/cycle	412
LTDN	09:30 a.m.	Min. time FORUM/MetOp-SG(1A) (Concept A)	21.29 s
Arg. Perigee	90°	Min. time FORUM/MetOp-SG(1A) (Concept B)	20 s
*Mean Keplerian Elements (ToD reference system)		Max. distance FORUM/MetOp-SG(1A)	< 1 minute

Table 5.1 FORUM orbit characteristics and mean orbit elements.

5.2.2 Loose Formation Flying and Orbit Maintenance

The FORUM–MetOp-SG(1A) formation is based on a non-cooperative concept that guarantees the fulfilment of the FORUM spatial and temporal co-registration requirements (see Section 7.2), the safety of the satellites and the undisturbed operations of MetOp-SG(1A).

The FORUM station-keeping strategy drives the selection of its position in the formation. Concept A station-keeping strategy is similar to the A-train constellation and is based on coordinated control boxes (Fig. 5.3., right), which guarantee a safe formation with either FORUM flying ahead or behind MetOp-SG(1A). Furthermore, flying ahead ensures no disruption of MetOp-SG(1A) operations in case of FORUM failure.

Concept B, maintains the formation by applying a master (MetOp-SG(1A)) slave (FORUM) strategy, mimicking MetOp-SG(1A) in- and out-of plane manoeuvres. In addition, FORUM also performs any other manoeuvre required to keep the spacecraft a safe distance apart and to fulfil the spatial and temporal co-registration requirements with MetOp-SG(1A)/IASI-NG. This strategy results in a safer scenario when FORUM flies ahead if the relative ballistic coefficient between FORUM and MetOp-SG(1A) is larger than 1, and behind if lower than 1.

The minimum time separation (see Table 5.1) between the two satellites is driven by the requirement from the FOS to have a minimum reaction time of three days before a potential encounter could occur. The distance kept between satellites and the use of different communication frequencies for TT&C and science data downlink prevent any interferences with Met-Op-SG(1A).

Concept B proposes to inject the spacecraft on a phasing orbit similar to the operational orbit, but with an offset of 15 km on the Semi Major Axis (SMA). This offset will result in a slow relative drift, allowing the nominal phasing between the two satellites to be reached in about 67 days in the worst case. Once the target relative position between the two satellites is reached, an in-plane manoeuvre is performed to modify the semi-major axis of the orbit and achieve the reference mission orbit altitude.

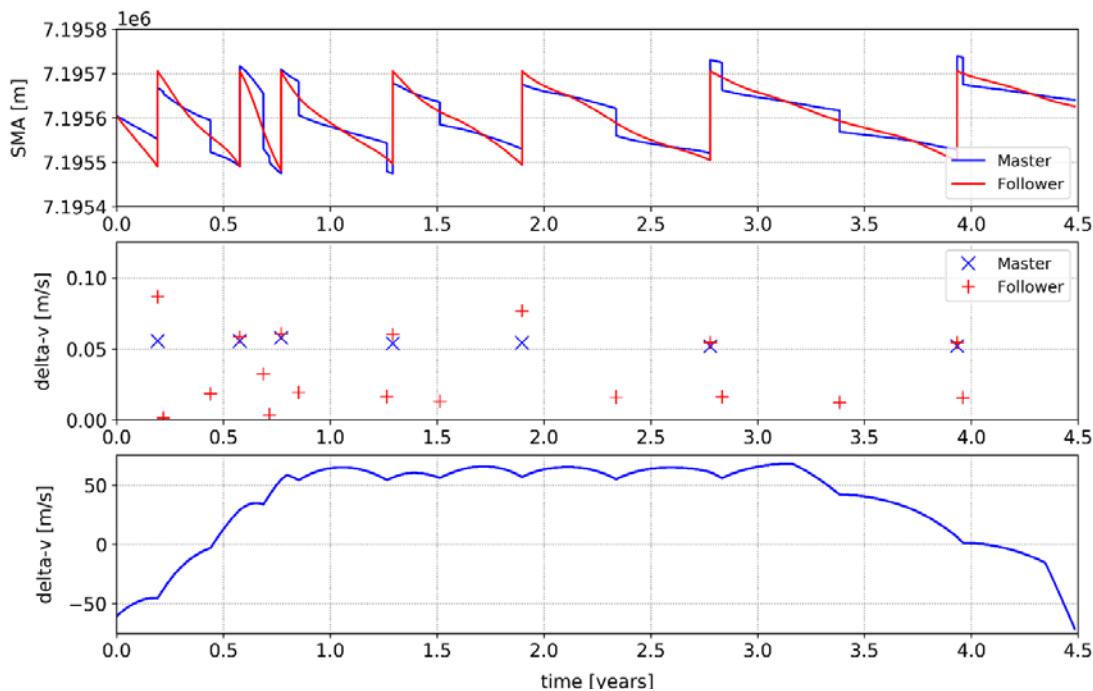


Figure 5.3 Concept B. Top: SMA variation for the master–slave formation concept. Middle: distribution of in-plane manoeuvres and required delta-V. Bottom: cross-track motion of FORUM ground track with respect to MetOp-SG(1A).

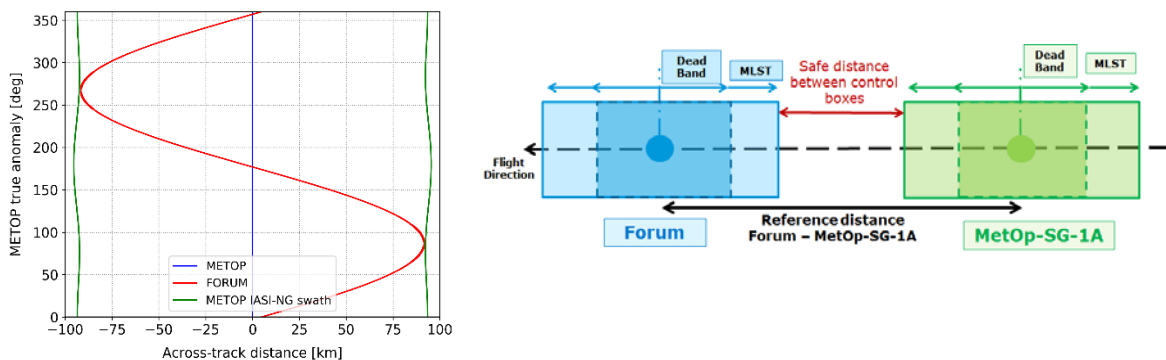


Figure 5.2 Concept A: Across-track motion of FORUM ground track with respect to MetOp-SG(1A) for the worst-case orbit during the mission lifetime (Left). Coordinated control box concept (Right)

Concept A proposes to launch FORUM directly into its nominal orbit, followed by correction of the injection and the formation phasing error by performing in- and out-of-plane manoeuvres. This solution requires specific launch windows.

Both Concepts carry sufficient fuel to fulfil the nominal mission lifetime of 4 years, excluding commissioning, have tank capacity to carry fuel beyond the needs of the mission life and extend their operation for more than two years.

In order to comply with the Space Debris Mitigation Policy and Guidelines, FORUM will perform an end-of-life disposal maneuver to lower the orbit perigee to an altitude that guarantees safe uncontrolled decay within 25 years (See Section 5.6.5).

5.3 Space Segment

5.3.1 Overview

The FORUM space segment consists of a satellite carrying the FSI and the FEI instruments and flying in loose formation with MetOp-SG(1A). Both concepts are based on largely recurrent platforms with mission specific adaptations, which ensures the satellite development to approach the industrial cost target of an Earth Explorer fast track mission while minimising the development risks.

The accommodation of the payload drives the physical satellite configuration, which is based on a classical platform and payload module design. Both concepts, as shown in Fig. 5.4 and Fig. 5.5, foresee the payload to be mounted on top of the platform in launch configuration. In orbit, the satellite flies, in nominal mode, with the launch interface ring panel facing the Sun. Such configuration guarantees the payload an unobstructed view of Earth, keeps the payload shaded from direct Sun illumination and maximises the power generated along the orbit. The required performances are met, for both concepts, with comfortable margins in terms of mass, power, mass memory and consumables sufficient to sustain the 4 years nominal mission lifetime.

The satellite configuration is described in Section 5.3.2 followed by the payload concept in Section 5.3.3, and complemented by the description of the overall satellite subsystems and budgets in Section 5.3.4 and 5.3.5, respectively.

5.3.2 Satellite Configuration

The FORUM configuration design is based on careful consideration of:

- Accommodation of the payload so that the FSI and the FEI have unobstructed nadir view of Earth.
- Direct access to cold space for instrument calibration and thermal control purposes, which requires the accommodation of both instruments on the cold-sky-facing panel of the satellite.
- Pointing and co-registration requirements, which favour the isostatic mounting of the instruments on a specific payload support panel.
- Line-of-sight (LoS) stability during the 14 seconds FSI dwell time, to minimise micro-vibrations and LoS pointing drifts.
- The need to have a thermally stable payload owing to the stringent FSI Absolute Radiometric Accuracy (ARA).
- Accommodation in the Vega-C fairing envelope under a dual launch configuration.
- Assembly, Integration and Testing (AIT), to ensure that the instrument and payload development and integration are decoupled, for optimum schedule and cost efficiency.

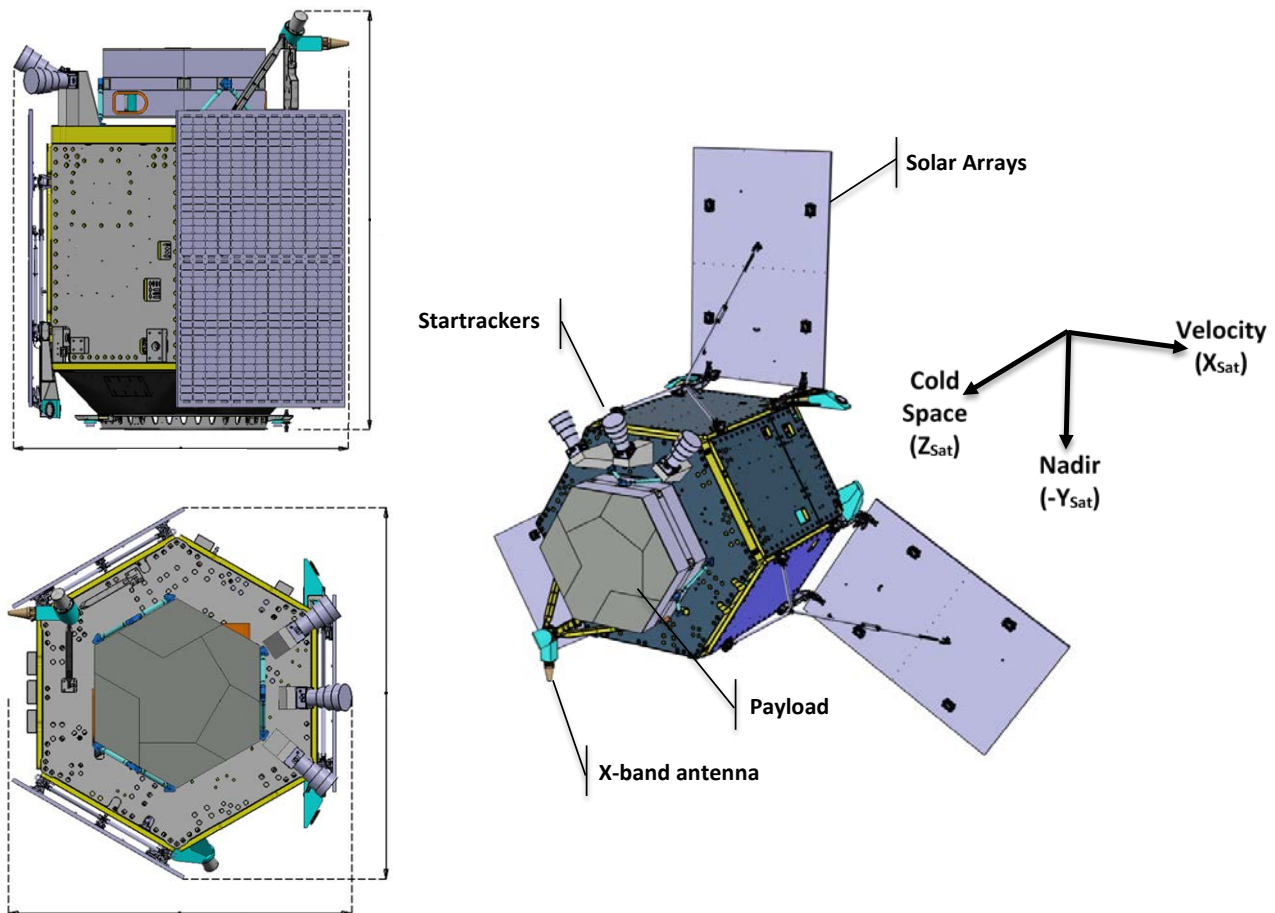


Figure 5.4 Satellite configuration for Concept A.

Concept A, shown in Fig. 5.4., is a 2.370 m high, 1.888 m wide and 2.058 m deep satellite based on the full reuse of the Copernicus Sentinel-5P platform and the Astrobus-M equipment. It provides large margins in terms of payload accommodation (mass and volume), power availability and fuel, at the expenses of a non-optimised platform in terms of mass and volume, but still compatible with a dual launch on Vega-C. The platform has a hexagonal-prism shape, which hosts the avionics equipment, the batteries, several instrument and platform electronics units and the propulsion module. Three fixed deployable solar array assemblies, for power generation, are mounted to the outside of three of the six panels of the structure. The 10 cm-thick top panel of the platform hosts three startrackers, the payload, the X-band downlink antenna and one of the two S-band antennas. The GNSS antenna and another S-band antenna used for up- and downlink TT&C are located at the bottom of the spacecraft, close to the interface ring with the launcher adapter.

The payload is placed in the cold-space side of the satellite, thermally decoupled from the platform and its temperature is kept stable by active and passive means. The startrackers and the payload are mounted on the top panel, the latter isostatically, to minimise thermo-elastic distortions induced by the platform. The platform communicates with the payload for command and control purposes through MIL-1553B interfaces, while the payload data communication is provided through a Spacewire link.

Concept B, shown in Fig. 5.5, has a quasi-cubic shape of 1.666 m high, 1.665 m wide and 1.663 m deep, based on the adaptation of the Proteus 150/300 standard platform and the Copernicus Sentinel-3 and Earth Explorer FLEX equipment. Concept B provides an optimised solution with enough margins in terms of accommodation, power and fuel availability at the expenses of a non-fully-recurrent concept. The platform hosts the avionics equipment, the batteries, several instrument electronics units and the propulsion module. Two fixed and deployable solar arrays made of 3 panels each are mounted on two of the four sides of the outer structure. A 6 cm-thick panel hosts three startrackers and the payload.

The X-band downlink antenna and the S-band antenna are mounted on the nadir-looking panel while the zenith-looking panel hosts the redundant S-band antenna and the GNSS receiver. Two Sun sensors are placed at the tip of the solar arrays. Both concepts use hydrazine-based chemical propulsion, embarking four 1N thrusters located within the launch interface ring, hence perpendicular to the flight direction. Therefore, attitude slew manoeuvres are needed to perform the orbit maintenance.

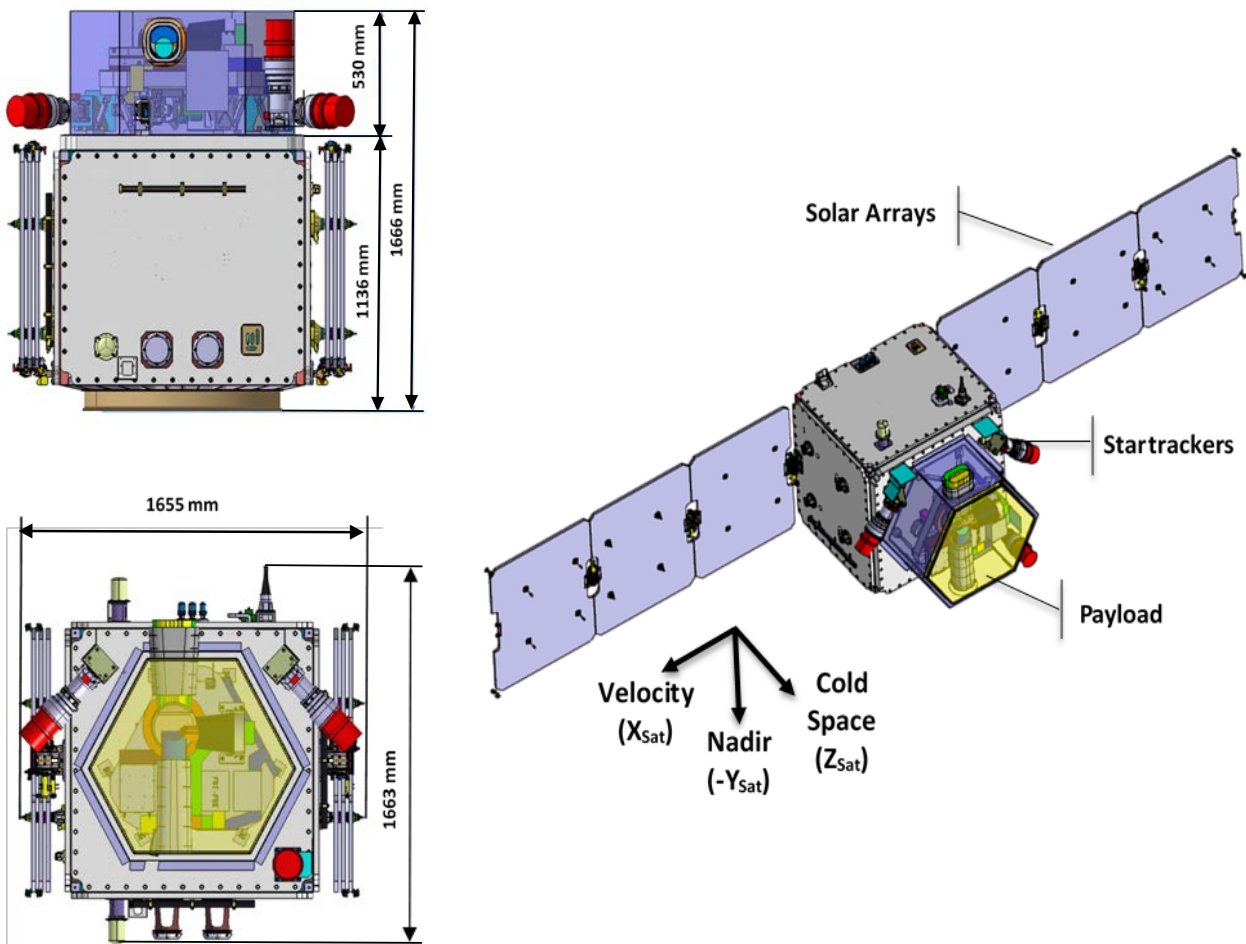


Figure 5.5 Satellite configuration for Concept B.

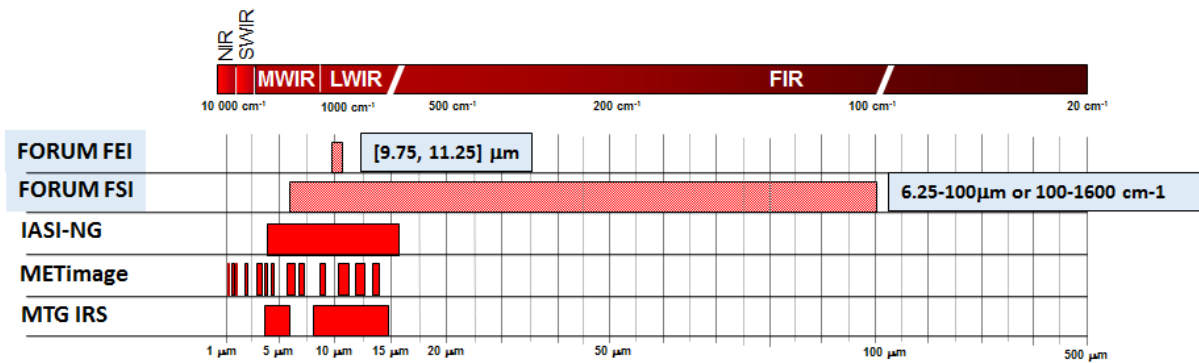


Figure 5.6 FORUM FSI and FEI spectral coverage in comparison with other infrared instruments. (ESA)

5.3.3 Payload

5.3.3.1 Overview

The FORUM payload consists of two optical instruments observing Earth in nadir-viewing mode:

- The FORUM FSI is a Fourier Transform Spectrometer measuring Earth’s TOA emission spectrum from 100 to 1600 cm^{-1} .
- The FORUM FEI is a thermal infrared imager centred at 10.5 micron with a bandwidth of 1.5 micron looking at the same scene as the FSI to acquire co-located images during the FSI dwell time for detection of scene inhomogeneities.

Fig. 5.6. illustrates the spectral coverage of the FORUM FSI and FEI instruments in comparison with other Earth observation infrared instruments. **The FSI acquires spectrally resolved data in a spectral range that no other Earth Observation infrared instrument has ever measured.**

5.3.3.2 Observation Principles

The FORUM payload consists of a single-pixel infrared-atmospheric-sounder FTS, named FSI, providing MIR and FIR spectrally-resolved data of the atmosphere and Earth’s surface. The FSI is complemented by a single-band-infrared-imager, named FEI, used to determine heterogeneity within the scenes observed by the FSI.

The FSI samples the atmosphere and Earth’s surface in a ‘step-and-stare’ mode acquiring emitted TOA MIR and FIR radiances, as illustrated in Fig. 5.7. The sampling starts with the ‘step’ phase by directing, by means of a pointing mechanism, the FSI LoS to the centre of a ground sample located ahead of the sub-satellite point. Once the ground target is fixed, the ‘stare’ phase starts by keeping the FSI LoS fixed on the desired ground target during all the instrument dwell time. The stare is achieved by LOS compensation of the inherent relative

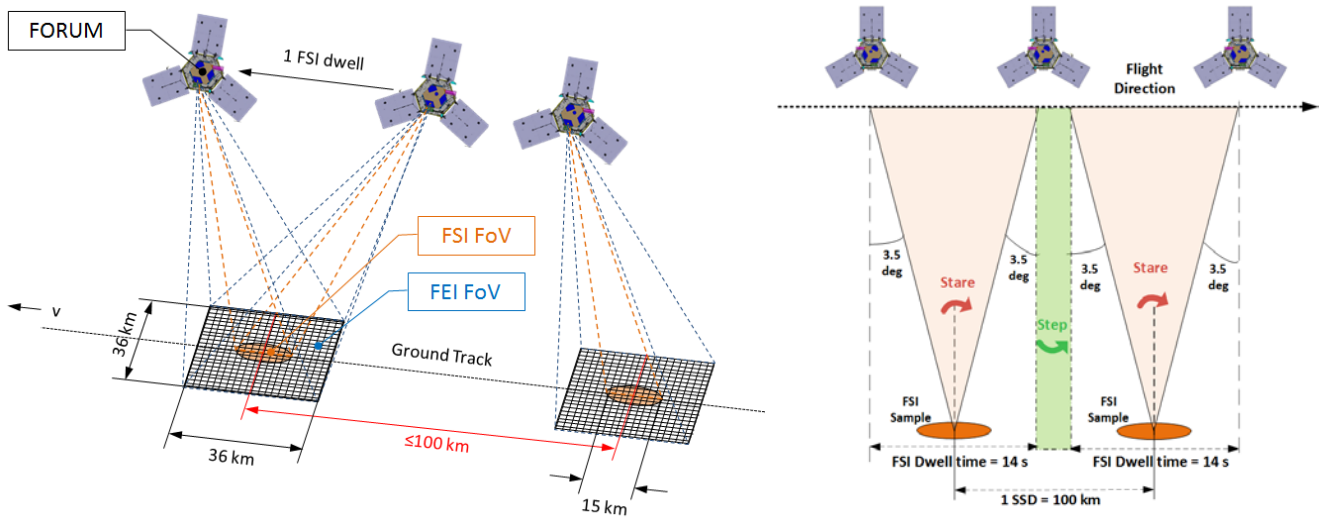


Figure 5.7 FORUM step-and-stare acquisition principle for Concepts A and B.

motion between the satellite and the ground target, whereby the payload compensates for the relative along-track motion by a LOS pointing mechanism and the platform compensates for the relative across-track motion (and partially the along-track motion) induced by Earth’s rotation by means of a yaw steering platform attitude-control law. Once the dwell time is completed, the step phase starts again, hence completing a single data acquisition. The FSI generates an interferogram per stare phase, which requires the synchronisation of the interferogram mechanism and the pointing mechanism (See Section 5.3.3.5.3. and Section 5.3.3.5.4 for more details).

The LoS stability of the 15 km diameter FSI pixel, colocated with the FEI nadir pixel, remains within $\pm 100\text{ m}$ during the 14s FSI dwell time. To achieve this, both instruments share common elements such as the entrance aperture, the pointing mechanism, the thermal and mechanical framework and the radiometric calibration devices.

The FEI acquires at least five images during each FSI dwell time, distributed symmetrically with respect to an acquisition at the middle of the FSI dwell time, where satellite nadir coincides with the FSI LoS. Each FEI image has a footprint of at least $36 \times 36\text{ km}^2$ and it is sampled with a $0.6\text{ km} \times 0.6\text{ km}$, along- and across-track respectively, Ground Sampling Distance (GSD) at the nadir image. The SSD between the centre of the footprint of two consecutive set of 5 FSI images is less than 100 km.

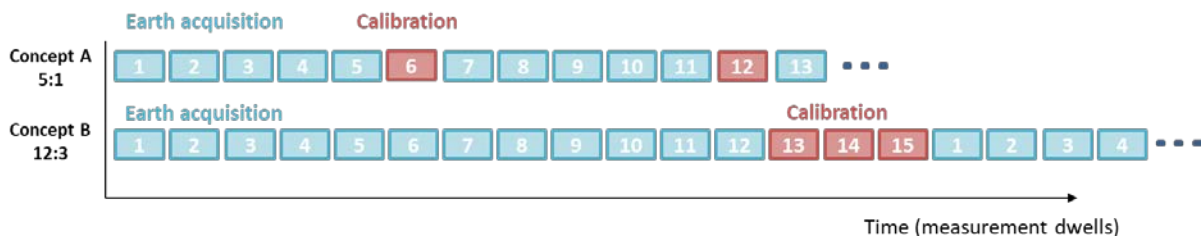


Figure 5.8 FORUM instrument calibration strategy for Concepts A and B.

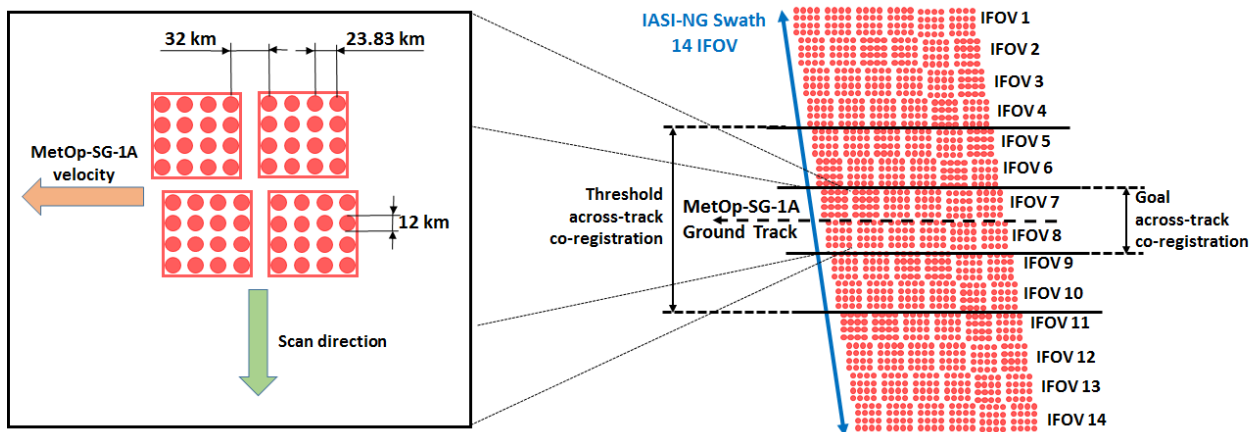


Figure 5.9 IASI-NG and FORUM instruments co-registration.

The FSI acquisitions are split between science observation and radiometric calibration. When in radiometric calibration, the FSI looks into either a hot onboard blackbody or deep space. Both concepts perform autonomous radiometric calibrations in a regular sequence illustrated in Figure 5.8. Concept A sampling strategy is based on a 5 to 1 Earth observation-calibration sequence while concept B baselines a 12 to 3 sequence. Both strategies provide a homogeneously distributed worldwide sampling of Earth's atmosphere and surface. The loss of science acquisitions owing to radiometric calibrations is less than 20% of the total samples without any systematic loss of science acquisitions at any particular Earth location, while meeting the demanding absolute radiometric accuracy mission needs.

The FSI and the FEI instruments perform synergic observations with the IASI-NG instrument on MetOp-SG(1A) with an along-track temporal co-registration of less than one minute. The half-span swath of IASI-NG is made by an array of seven instantaneous FOVs. FORUM's observation is constrained to be co-registered with only the three innermost FOVs on each side (threshold) or the one innermost FOV on each side (goal). This is illustrated in Fig. 5.9. To achieve the temporal and spatial co-registration between the FORUM instrument and IASI-NG acquisitions, FORUM flies in loose formation with MetOp-SG(1A).

The FSI samples the spectrum from $6.25 \mu\text{m}$ to $100 \mu\text{m}$ (1600 cm^{-1} to 100 cm^{-1}) with a spectral resolution better than 0.5 cm^{-1} and a spectral sampling of about 0.36 cm^{-1} . As shown in Fig. 5.6, no other ESA Earth observation mission provides spectrally resolve radiances either the atmosphere or the surface of Earth beyond $16 \mu\text{m}$. FEI features a single IR $1.5 \mu\text{m}$ width band centred around $10.5 \mu\text{m}$.

5.3.3.3 Level-1 Observation Requirements

This section provides an overview of the key Level-1 observation requirements driving the design of the FSI and the FEI instruments. In case threshold and goal values are specified, the threshold value is reported together with the goal value in brackets and identified by G. Details on the performance achieved by both concepts can be found in Section 7.2.

Observation Requirements	Specification	Drivers/Impacts
Calibration coverage loss	< 20%	Calibration strategy
FSI and FEI observation modes	Earth Observation and calibration modes	Calibration strategy, calibration unit design
Maximum LoS depointing angle	< ± 3.5 deg	Calibration strategy, dwell time, NESR
FSI/FEI LoS stability over FSI dwell time	< 100 m (G: 50 m)	AOCS design and equipment, micro-vibrations, thermo-elastic

Table 5.2. FORUM FSI and FEI common observation requirements.

5.3.3.3.1 Observation Requirements Common to FSI and FEI

Table 5.2 summarises the main FSI and FEI common observation requirements.

The FSI and FEI will perform co-aligned and co-registered ground sample measurements in step-and-stare mode, stable within the FSI dwell time, and with an accuracy defined in Table 5.2. This is achieved by an oversized FEI FOV, a common pointing mirror to compensate the satellite ground speed, minimising thermal distortion sharing the same mechanical and thermal configuration, and by on-ground and in-flight calibration.

The FSI and FEI LOS stability during the FSI dwell time is achieved by:

- A thermal control which minimises the instrument thermo-elastic distortions
- An accurate platform attitude control and the minimisation of micro-vibrations
- Implementing a satellite yaw steering attitude control to compensate on-ground LOS drifts due to Earth's rotation velocity

FSI and FEI will have two observation modes: acquisition and calibration. For calibration purposes a calibration blackbody (traceable to SI units) and a deep-space view have been included in the payload and are frequently viewed by both instruments.

5.3.3.3.2 FSI Observation Requirements

Table 5.3 lists the main FSI instrument observation requirements.

Observation Requirement	Specification	Drives/Impact
Geometric requirements		
Along-track spatial sampling distance	< 100km (G: <70 km)	Maximum dwell time, acquisition principle
System integrated energy	> 90% over 15 km area	Geometrical field of view, spatial resolution, image quality
System Energy Distribution Function (SEDF) non-uniformity within one spectral sample	Variation <15% \times SEDF _{MAX} over 90% of Full Width Half Maximum (FWHM) (G: <10% \times SEDF _{MAX} over 80% of FWHM)	Optical design, field stop, detector performance angular dependence
SEDF non-uniformity knowledge	Knowledge error < $\pm 5\%$ over 80% of FWHM	On-ground calibration

SEDF non-uniformity between spectral samples	Difference between 2 spectral samples < $\pm 5\%$ over 80% of FWHM (G: < $\pm 5\%$ over 90% of FWHM)	Detector performance angular dependence, optical design
Spectral requirements		
Spectral range	100 to 1600 cm^{-1}	Product coverage, optics material, coatings, detector type, delta OPD, Optical Ground Support Equipment (OGSE)
Spectral resolution	<0.5 cm^{-1} (G: <0.36 cm^{-1})	FTS MOPD, retrieval accuracy, interferometer field of view
Spectral knowledge	<2 ppm (G: <1 ppm)	Spectral calibration strategy, retrieval accuracy, metrology laser choice and stability
Instrument Spectral Response Function (ISRF) knowledge error	Resulting radiometric error: < 0.06 $\text{mW}/\text{m}^2/\text{sr}/\text{cm}^{-1}$ (G: < 0.02 $\text{mW}/\text{m}^2/\text{sr}/\text{cm}^{-1}$)	Retrieval accuracy, on-ground calibration, instrument stability over time
Radiometric requirements		
Signal dynamic range	Spectral radiances with equivalent blackbody brightness temperature in the range 190 K to 300 K	Detection chain
Noise Equivalent Spectral Radiance (NESR)	<0.6 $\text{mW}/(\text{m}^2\cdot\text{sr}\cdot\text{cm}^{-1})$ (G: < 0.4 $\text{mW}/(\text{m}^2\cdot\text{sr}\cdot\text{cm}^{-1})$) within [200-800 cm^{-1}] < 2.0 $\text{mW}/(\text{m}^2\cdot\text{sr}\cdot\text{cm}^{-1})$ (G: <1.0 $\text{mW}/(\text{m}^2\cdot\text{sr}\cdot\text{cm}^{-1})$) outside [200-800 cm^{-1}]	Instrument throughput (étendue)
Absolute Radiometric Accuracy (ARA)	Goal: <0.2 K from 200 cm^{-1} to 300 cm^{-1} <0.1 K from 300 cm^{-1} to 1100 cm^{-1} <0.2K from 1100 cm^{-1} to 1300 cm^{-1} <1 K elsewhere Threshold: <0.25 K over [200-1300 cm^{-1}] <1 K elsewhere	Retrieval accuracy, on-ground and in-flight radiometric calibration, onboard blackbody design

Table 5.3 FORUM FSI instrument main observation requirements.

Geometric requirements:

FORUM requires a maximum **Along-Track Spatial Sampling Distance (SSD)** of 100 km (goal 70 km) along the orbit while keeping the observation angle below 3.5 degree. This means that the on-ground distance between two consecutive 15 km diameter samples will always be smaller than 100 km (see Section 7.2.1). This requirement drives the maximum FSI dwell time, the detector choice and the acquisition principle.

The spatial performance of the FORUM FSI instrument is fully described by the **System Energy Distribution Function (SEDF)**. It can be seen as the spatial response function, and is defined on the Earth ellipsoid as the spatial distribution of the energy collected by the instrument for an acquired spatial sample. The SEDF reflects the detection sensitivity of the instrument in the spatial domain, in a similar way as the ISRF in the spectral domain. Its integral over the FOV projection defines the System Integrated Energy (SIE). Since the spatial requirements of the FSI define a circular instantaneous FOV of the spatial samples

with stabilised LOS during integration time, the SEDF resembles a circular top-hat function. Its spatial extent is constrained by requirement to 15 km diameter, and primarily depends on interferometer (or telescope) FOV, and orbit altitude (the latter being fixed by the MetOp-SG orbit). The shape is determined by the angular sensitivity of the instrument from various instrument effects, such as optical aberrations and coating performance. Diffraction effects are also significant in the low wavenumber range ($<200 \text{ cm}^{-1}$). The system requirements demand flatness within the inner circle of the SEDF (80% of the diameter), as well as equality in shape for all spectral channels. This will ensure uniform spatial sensitivity across the spectral range.

The **System Integrated Energy (SIE)** describes the imaging quality of the system in terms of spatial resolution. It is the ratio of the energy measured over a specific area (FSI spatial sample of 15 km in diameter) to the energy measured from the entire scene. It is obtained by integrating the system energy distribution over a specified surface area. The SIE is required to be larger than 90% over a 15 km circular area. This requirement defines the geometrical instrument FOV, hence the spatial sampling and resolution of the instrument.

Spectral requirements:

The **Spectral Range** from $100\text{--}1600 \text{ cm}^{-1}$ is one of the core requirements and drives significantly the design of the instrument in terms of detector technology, delta Optical Path Difference (OPD), data rate, optical coatings and optics materials and OGSEs. It poses challenges in terms of the selection of material and coatings, especially for the interferometer beamsplitter and the onboard blackbody (see results of pre-development activities on beamsplitter and on blackbody coating emissivity in Section 5.3.3.5.4.).

The **Spectral Sampling Interval** is the spectral distance between adjacent spectral samples within a spectral band. It is defined as the inverse of twice the Maximum Optical Path Difference (MOPD) between the two split beams: FSI spectral sampling interval = $1/(2 \cdot \text{MOPD})$. This mainly drives the interferometer mechanism design.

The **Spectral Resolution** is the Full Width Half Maximum (FWHM) of the unapodised instrument spectral sampling function, which is typically a cardinal sine (sinc) function whose main lobe is broadened by the instrument self-apodisation. For an FTS, the spectral resolution drives the MOPD and the acceptable instrument self-apodisation. Major contributor to the broadening of the FWHM is the beam divergence, especially if a telescope is used to reduce the beam dimensions inside the interferometer as in the case of FORUM.

The **Instrument Spectral Response Function (ISRF)** describes the spectral response of the whole instrument chain including the transmittance of optical components and the detector response. It relates the radiance $L'(\sigma)$, derived from the acquired interferogram, with the monochromatic TOA spectral radiance $L(\sigma)$ incident on the instrument, see Equation 5.1:

$$L(\sigma_0) = \int_0^{\infty} ISRF(\sigma, \sigma_0) L'(\sigma) d\sigma$$

The system requirements demand an accurate knowledge of the ISRF, as discrepancies between the actual spectral response and the ISRF assumed in Level-2 processing give rise to equivalent radiometric errors, which in turn map into systematic retrieval errors. In order to keep this error source negligible, the ISRF knowledge requirement is formulated in terms of the equivalent radiometric error on Level-1b spectral radiance: the radiometric error from ISRF uncertainty shall be less than 10% of the NESR in the most demanding wavenumber interval (200–800 cm⁻¹). This stringent requirement demands an extensive on-ground calibration of the instrument line shape, as well as accurate characterisation of the transmission properties, including absorption features of the beam-splitter material. It also requires precise characterisation of the self-apodisation effect, resulting from beam divergence in the interferometer, as well as the modulation efficiency.

The **Spectral Knowledge** defines the accuracy of the position of each spectral channel centre within the spectral range. It will be known with an absolute accuracy better than 2 ppm (goal: 1ppm). The spectral axis of a spectrum measured with an interferometer is generated by the laser metrology system. The uncertainty of the apparent laser wavelength creates a scaling error of the spectral axis. This requirement therefore drives the metrology laser choice and the spectral calibration strategy.

Radiometric requirements

The **Dynamic Range** represents the range of brightness temperatures within which requirements are to be met. The brightness temperature is the temperature of a blackbody that would emit the same amount of radiation as the targeted scene/body for a given spectral channel. FORUM requires a dynamic range spanning 190 K to 300 K in equivalent brightness temperature units. It drives mainly the detection chain.

The **Noise Equivalent Spectral Radiance (NESR)** is the standard deviation of a time series of radiance measurements in a given spectral channel. It describes the radiometric resolution of the instrument and is related to the signal-to-noise ratio (SNR) of the measured radiance L by Equation 5.2:

$$NESR = \frac{L}{SNR}$$

The NESR is a key specification for the instrument sizing and retrieval precision (see Chapter 4). Therefore, the NESR is specified over the full applicable dynamic range of the instrument. The NESR values required for the FSI instrument are reported in Table 5.3. The main contributor is the detector noise. The NESR requirement drives the étendue of the instrument leading to a pupil size in the range of around 70–80 mm equivalent diameter.

The **Absolute Radiometric Accuracy (ARA)** is the unknown systematic error of Level-1b measurement. It is specified as an equivalent brightness temperature error over the full dynamic range. The ARA budget combines two main error sources: (1) uncertainties linked to the knowledge of the reference blackbody radiance (2) uncertainty in the measured signal (e.g. NESR of calibration spectra, temperature). The absolute accuracy required for the FORUM FSI instrument reported in Table 5.3 is very demanding, particularly in the spectral region between 300 cm⁻¹ and 1100 cm⁻¹ and at the low end of the dynamic range (i.e. 190 K),

Observation Requirement	Specification	Drives/Impact
Geometric requirements		
Temporal Sampling	>5 acquisitions per dwell time	Acquisition principle, NEdT, data downlink capacity, FEI read out
Field of View (FOV)	>36 x 36 km ²	Detector choice
Spatial Sampling Distance (SSD)	<0.6 km	Detector choice, focal length
Modulation Transfer Function (MTF)	MTF >0.3 at Nyquist frequency	Optical design (aberrations), image quality, detector performance
Spectral requirements		
Spectral Range	10.5 μm ±0.75 μm	Optical design, detector
Instrument Spectral Response Function (ISRF) Knowledge	<5% of the peak value	On-ground calibration, instrument stability
Out-of-band signal	< 2% (G: <1 %) at 210 K	Requirement limiting the out-of-band straylight of the observed scene
Radiometric requirements		
Signal dynamic range	From 190 K to 300 K	FEI detection chain choice
Noise Equivalent delta Temperature (NedT)	< 0.7 K (G: <0.3 K) at 210 K	Etendue of the instrument and optical design
Relative spatial radiometric accuracy (RXRA)	<0.2 K at 210 K	Calibration approach and angular uniformity of the blackbody
Absolute Radiometric Accuracy (ARA)	<3 K (G: < 1 K) at 210 K	Detector surroundings thermal stability
Straylight	≤1.5 K at a distance of 5 SSD (G: <0.8 K at a distance of 3 SSD)	Optical design, coatings reflectivities

Table 5.4 FORUM FEI instrument main observation requirements.

where a goal accuracy of 0.1 K is specified. This requirement drives the calibration strategy, the maximum tolerable noise in the calibration measurements, the blackbody emissivity, the frequency bandwidth to avoid aliasing of the out-of-band signal, the thermal stability and thermal design of the instrument and the blackbody design. Out-of-band straylight is also not detected because filtered by the Germanium coating (VIS) or the gold mirrors (UV), and filtered by the frequency response of detection electronics.

5.3.3.3.3 FEI Observation Requirements

Table 5.4 summarises the main FEI observation requirements while the main requirements are further explained hereafter.

The FEI instrument FOV will **cover an area** on Earth of minimum 36×36 km². The **Along-Track and Across-Track Spatial Sampling Distance** of the FEI will be smaller than 0.6 km. This drives the optical design and the detector choice.

The **Modulation Transfer Function (MTF)** defines the image quality of the FEI and it will be larger than 0.3 at Nyquist frequency. Major contributions to the MTF are the optics diffraction and aberrations and the detector spatial sampling. This requirement drives the detector performance and limits the optical aberrations of the FEI optical design.

Spectral requirements

The FEI measures the scene radiance in a **Spectral Range** defined by one spectral channel centered at 10.5 μm with a 1.5 μm spectral width. This drives the selection of coatings, bandpass filters, optics materials and detector type.

The **ISRF knowledge** is specified as a template (see Chapter 7). This requirement together with the **Spectral Range template** drives the optical filter design and contributes in the NEdT budget. The ISRF will be characterised on ground. Since the requirement is applicable in flight it drives both the on-ground calibration accuracy and the instrument stability.

The FEI **Out-of-Band Rejection** defines the required signal attenuation of the bandpass filter outside of the needed spectral band. It shall be smaller than 2% (goal 1%) for a blackbody of equivalent brightness temperature of 210 K. This requirement addresses the quality of the optical filter.

Radiometric requirements

The **Noise Equivalent delta Temperature (NEdT)** defines the minimum measurable temperature change with respect to a reference temperature level. The required NEdT is reported in Table 5.4 and specified for each FEI image taken during the interferogram dwell time. The maximum image acquisition time is 2.8 s, which allows for a series of temporal samples and co-adding to enhance the ratio between signal and noise. The NEdT drives the instrument throughput (étendue) and therefore the FEI instrument optical design.

The **Relative Spatial Radiometric Accuracy (RXRA)** is the relative variation of the unknown systematic error of the spatial samples acquired in an image while imaging a stable, spatially uniform and Lambertian scene, but with spectrally varying content. It is of key importance as the objective of the FEI is to determine the scene heterogeneity to discriminate scene/cloud information within the FSI spatial sample. The FEI requires an RXRA lower than 0.2 K for a reference scene at 210 K. This requirement drives the calibration approach and the angular uniformity of the blackbody radiance.

The driver for the **Absolute Radiometric Accuracy (ARA)** is the variation of the FEI detector environment temperature between calibrations, which will be in the order a few mK to reach the goal reported in Table 5.4.

Straylight is light generated by unwanted imaging (ghost) and scattering on the elements of an instrument (optical surfaces, contaminants, mounts, internal baffles, higher-order diffraction, etc.). It drives the optical design and the coatings performance of the FEI to limit the straylight generated by ghost images and scattering on mechanical and optical surfaces. The requirement assumes a non-uniform scene having two different levels of radiances. The straylight generated by the higher radiance level part into the lower radiance part has to be lower than 1.5 K (0.8 K goal) at a distance of 5 SSD (3 SSD goal) from the transition.

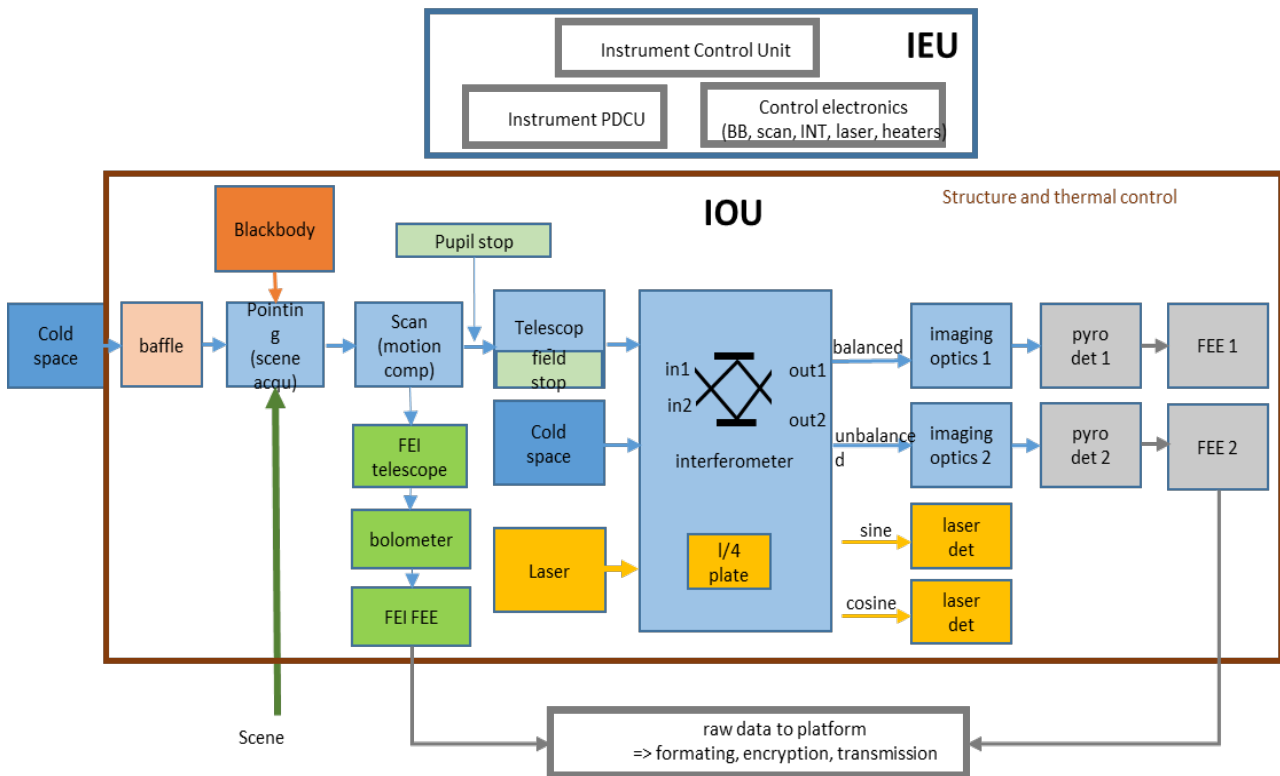


Figure 5.10 Payload functional diagram for Concept B – similar for Concept A.

5.3.3.4 Overview

The payload comprises two instruments: the FSI, which is an infrared four-port, double pendulum-type FTS, and the FEI, which is a single-spectral-band thermal infrared imager. The two industrial consortia each derived very similar payload concepts.

Fig. 5.10 shows the payload functional block diagram (Concept A block diagram not shown but similar). The main subsystems are: deep space/blackbody and Earth ports, pointing unit allowing to select the different ports, FSI instrument (front telescope, four-port interferometer, focusing optics, pyroelectric detectors and associated electronics), FEI instrument (optics, microbolometer detector and associated electronics).

An Instrument Control Unit (ICU) provides control and monitoring of the FSI, the FEI and the pointing mechanism. It interfaces to the Front End Electronic (FEE) on one side and to the platform for power and data on the other side. The interferometer has its dedicated Interferometer Control Electronics (ICE), which also includes the laser metrology system. The metrology system interfaces to the interferometer mechanism via optical fibres. The ICU and the ICE are both mounted inside the platform and connected to the instrument modules via harnesses and optical fibres.

5.3.3.5 Payload Subsystems and Instruments

5.3.3.5.1 Mechanical Accommodation and Analysis

The payload mechanical accommodation is outlined in Fig. 5.11 for Concept A and in Fig. 5.12 for Concept B. The accommodation is driven by the geometrical and thermal stability needed to meet the pointing knowledge requirement and the radiometric requirements (see Section 5.3.3.3.2). For both concepts, the payload includes:

- A very stable optical bench to minimise thermoelastic distortions. It supports all the optical elements, the pointing mechanism, the interferometer, the calibration units and the detection chains. The optical bench is isostatically mounted on the platform. The optical bench together with the optical units is kept at around 293 K for both Concepts A and B.
- A nadir and deep-space baffles minimise undesired radiation inside the instruments from the Earth and Sun, respectively.
- A calibration blackbody accommodated at the entrance of the instruments. The blackbody view is selected by a rotation of the pointing unit.

The optical bench is made of an all-aluminium sandwich for Concept A and a monolithic aluminium panel for Concept B. It supports all the optical elements, mechanisms, interferometer, calibration units and detection chains. The optical bench is isostatically mounted on the platform with three bipods. In order to guarantee the structural performance and thermal isolation from the platform, the bipods are made of Glass Fibre Reinforced Polymer (GFRP) tubes with titanium fittings for Concept A and of titanium for both tubes and fittings for Concept B.

In Concept A, the interferometer, the reference blackbody, the FEE for FEI and FSI, the FSI detectors, the pointing mechanism, the telescope and the FSI focusing optics are mounted on the top side of the optical bench. On the bottom side of the optical bench, only non-dissipating units are accommodated: nadir and deep-space baffles, pointing mirror, blackbody, FEI optics and detector.

In Concept B, all FSI and FEI units (except metrology system and FEEs) are accommodated on the bottom part of the optical bench to guarantee a protected thermal environment. The top part of the optical bench contains the calibration blackbody, the scanning and pointing unit, the nadir and deep-space baffles and the metrology system. The accommodation concepts are sound and provide adequate margins to accommodate changes in later phases, given the existing volume and mass margins at platform and system level.

Mechanical analysis

Both concepts have built up detailed FEM of the instrument representing all structural elements. These models have been used to perform all relevant mechanical analyses (modal, strength, acoustic/random, thermo-elastic and micro-vibrations). For Concept B coupled loads analyses with the platform have been performed while for Concept A, the interface loads derived from the Copernicus Sentinel-5P platform have been deemed representative enough.

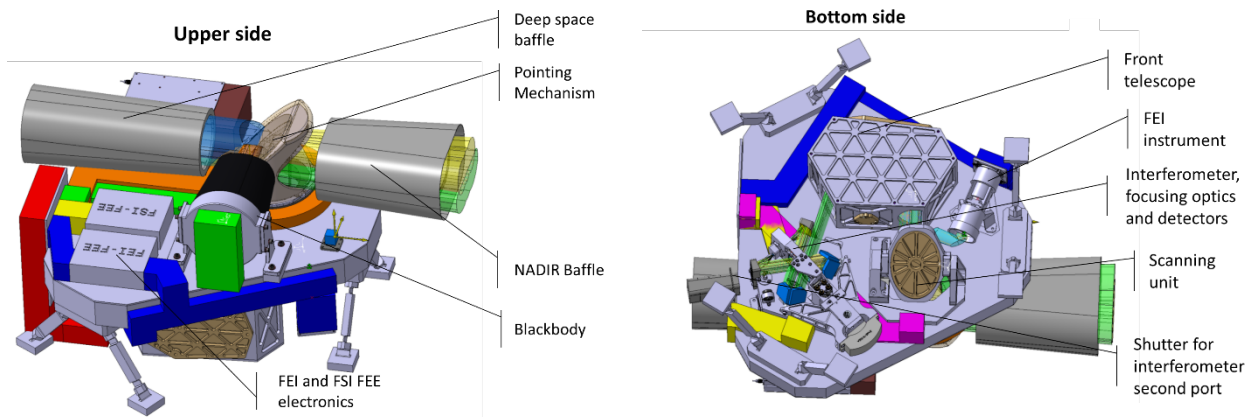


Figure 5.12 FORUM Payload accommodation – Concept B

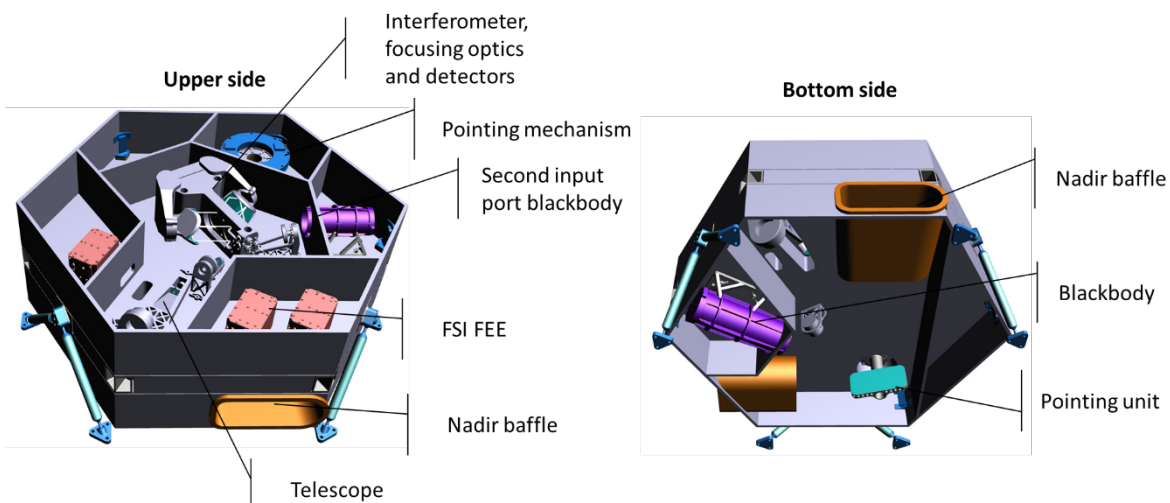


Figure 5.11 FORUM Payload accommodation – Concept A

For both concepts, the natural frequencies of the instrument and platform exceed the required limits and the dynamic coupling between them results in benign loads to the instrument. Sine and random spectra have been notched to acceptable levels, and the analysed stresses for quasi-static loads are low. All margins of safety are positive with a few exceptions, which can be improved easily by increasing the strength of these elements, without any cascade effect at system level thanks to the available volume and mass margins. The thermo-elastic and micro-vibration analyses demonstrated in both concepts that sufficient LOS stability and reduced acceleration levels at sensitive units occur under operational conditions.

As a result, for both concepts, the structure proposed is feasible, stable and robust enough to cope with potential updates of the instrument design.

5.3.3.5.2 Thermal Architecture

Both concepts present different thermal architecture designs. For Concept A, a heater-controlled shroud encloses the whole instrument. Its external sides are covered with Multi-Layer Insulation (MLI) with the exception of radiators and the Earth and deep-space

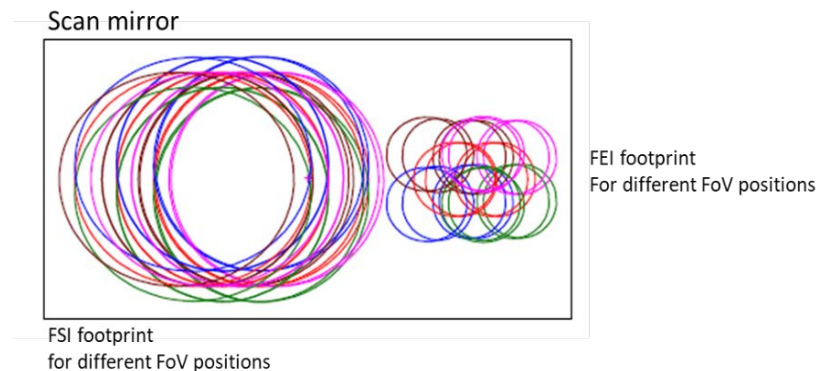


Figure 5.13 FSI (left) and FEI (right) beam footprints on pointing mirror for Concept A.

calibration apertures. The internal sides are black painted to facilitate the radiative coupling with the units. The optical bench and all optical subsystems are in radiative heat exchange with the shroud, like in an oven, imposing a uniform and stable temperature of +20 °C on all non-dissipating units within its cavity. Heat dissipating units are accommodated inside dedicated compartments, whose inner lateral walls are covered in highly reflective MLI and whose top panel is equipped with Second Surface Mirror (SSM) radiators. The radiators are thermally decoupled from the rest of the structure by means of thermal washers. The temperature will be controlled to a lower set point in order to maintain the dissipating units at +20 °C. Although the instrument is in the shade, Earth IR and albedo is a major source of thermal disturbance. Therefore, the instrument apertures are equipped with thermal baffles to reduce the influence of Earthshine and stray light. In order to conductively decouple the instrument from the platform, the former is mounted using GFRP kinematic bipods with Ti6Al4V fittings.

For Concept B, the payload lateral sides are surrounded by a MLI sunshield, with cutouts for both entrances, nadir and zenith. The instrument itself is also covered with MLI with the exception of radiators and apertures. Both passive and active thermal control are present to maintain the payload at the required temperature and within the required stability. Active control of the heaters on the optical bench top sheet ensure that the units are maintained at a stable temperature of +21 °C. The FEE (FEI, FSI and laser system) are conductively decoupled from the optical bench using flexures and radiative insulated with MLI. The radiators are directly attached to the unit upper face. The thermal baffles, which have direct heat flux from the Sun during the orbit, are insulated with MLI. The heater-controlled optical bench, which accommodates all the optical subsystems, is supported by titanium bipods to reduce the conductive coupling between instrument and platform. Both concepts achieve very high temperature stability for the optical subsystems and the optical bench. The orbital temperature stability of the optical bench is better than 0.2 K (peak to valley). The optical units are even more stable (<0.02 K, typically). Preliminary STOP analyses demonstrate that the optical performance degradations caused by thermo-elastic distortions are well below the allocated limits.

5.3.3.5.3 Entrance Aperture and Pointing Mechanism

The entrance aperture of both instruments is defined by the aperture stop, which is located in front of the first telescope mirror for the FSI and in front of the first lens for the imager

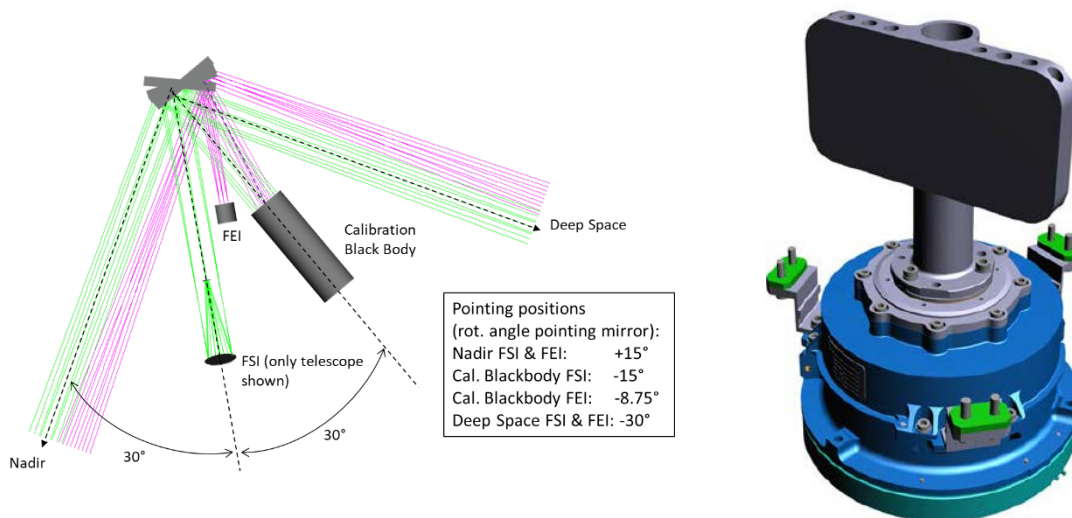


Figure 5.14 FORUM Pointing mirror unit – Concept A

FEI. The entrance pupil circular equivalent diameter is 72 mm for Concept A and 80.2 mm for Concept B. The FEI entrance pupil diameter is equal to 25 mm in the case of Concept A and 29.4 mm in the case of Concept B. The FEI and FSI optical beams are separated using a pupil offset as shown in Fig. 5.13.

The first optical element after the entrance aperture is a pointing unit. Concept A proposes to reuse the MetOp-SG scan mechanism (used for MWI, MWS, ICI and METImage instruments) replacing its mirror and the pointing mechanism control electronics. This concept is a single-axis scanning and pointing mirror unit, which ensures both the Earth, calibration blackbody and deep-space viewing selection by rotation of the mirror. It also performs the scanning function required to maintain a stable ground pointing coordinated with the interferometer mechanism during the simultaneous acquisitions of the FSI interferogram and the FEI images.

Concept B uses two mirrors, each ensuring one function of the above-mentioned functions. In both concepts, the FSI and the FEI share the same Earth view through the pointing/scanning unit. The deep-space view and the onboard calibration blackbody are also common for FEI and FSI for both concepts. Concept B design is based on the IRS scanning mechanism.

The pointing mirror of Concept A is shown in Fig. 5.14 while the pointing and scanning unit of Concept B is shown in Fig. 5.15.

For Concept A, the pointing mirror has to be in a defined position during launch and early orbit (LEOP) to prevent sunlight entering the optical system during any non-nominal pointing of the platform. Additionally, a launch lock is needed because the friction moment will be eliminated during launch by random loads. As the nominal mechanism, outside the nominal operating range. The permanent magnet keeps the mechanism at a fixed position during launch. Once in orbit, the mechanism is rotated by approximately 180° into the nominal operation range, where the permanent magnet does not have an impact.

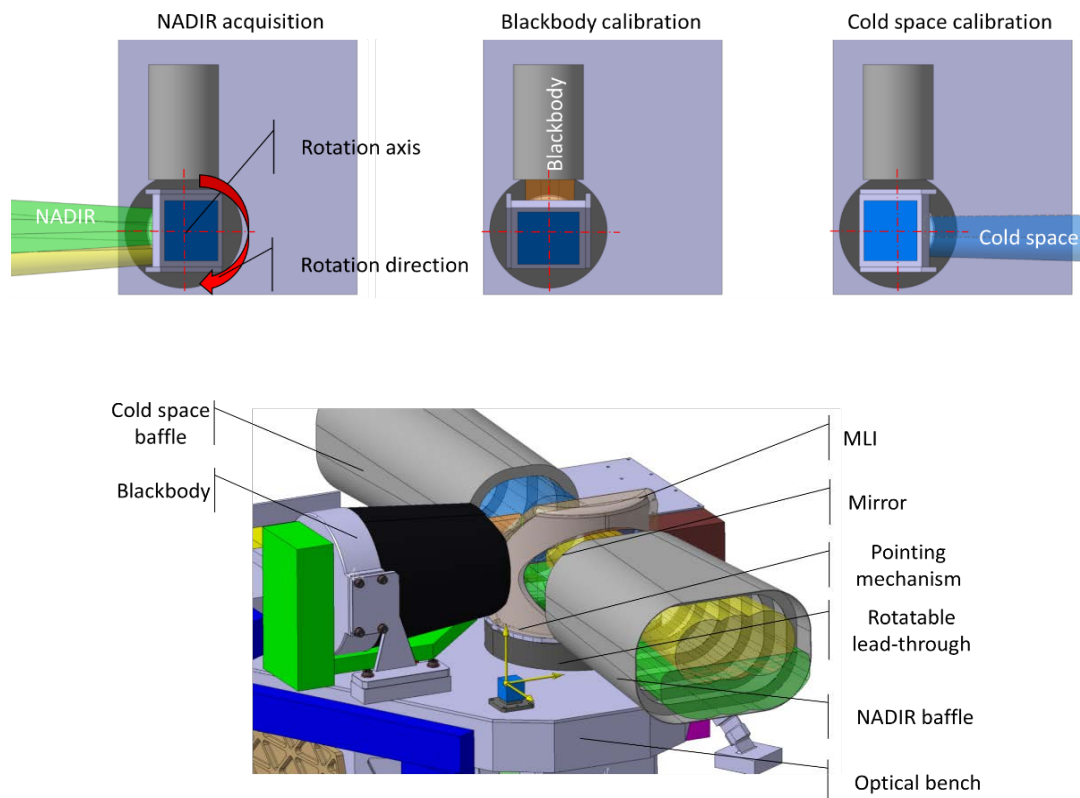


Figure 5.15 FORUM pointing mechanism sketch. It enables the selection of the different views: deep space, calibration blackbody and earth view – Concept B

For Concept B, when rotating the pointing mechanism to one of the selected targets, the other openings will be closed by a co-rotating cylinder. During launch the pointing operation of the FORUM mechanism is limited to a small angular range, a pair of permanent magnets can be placed on the rotating and stationary parts of the mirror and it will point towards the blackbody and both nadir and cold-space baffles will be closed to protect against contamination.

To compensate the satellite along-track motion, the pointing mirror speed will be selected for the individual dwells depending on the current satellite latitude, requiring an update of the commanded rotation speed of the mechanism. This is achieved by using the Position Velocity and Time (PVT) data provided by the Onboard Computer (OBC) to the ICU and extracting the appropriate rotation speed from a stored table.

5.3.3.5.4 FORUM Sounding Instrument (FSI)

Optical concept

The optical design of the FSI for Concepts A and B is very similar. It implements a compact optical instrument keeping, thanks to the front telescope, the interferometer pupil compatible with the manufacturability of corner cubes and beamsplitters. The optical design allows the complete FORUM spectral range with the required spectral resolution to be

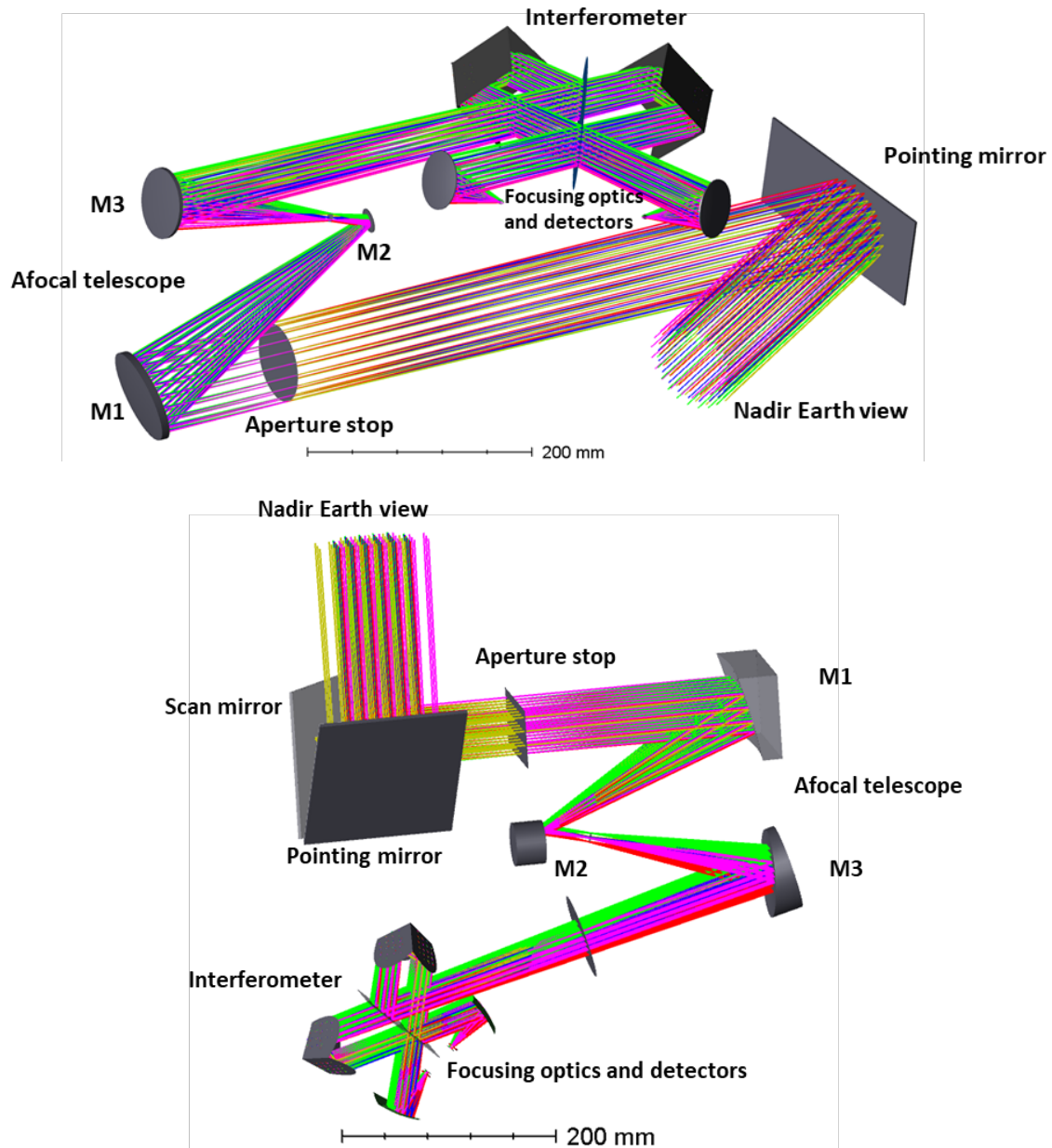


Figure 5.16 FSI optical layout for Concept A (top) and Concept B (bottom).

covered, keeping the beam divergence small for performance optimisation. The optical layout of Concepts A and B is shown in Fig. 5.16.

The system uses a three-mirror fully reflective telescope, a four-port double pendulum interferometer and two focusing optics to direct the light onto the two FSI detectors.

The front telescope optics has three main functions:

- To reduce the beam diameter to keep the beamsplitter and the cube corners in the interferometer at a manufacturable size. The telescope has a magnification of 2.4 (of the field angle) meaning that it allows a compression of the pupil by the same factor. The exit pupil diameter is therefore equal to around 30 mm.

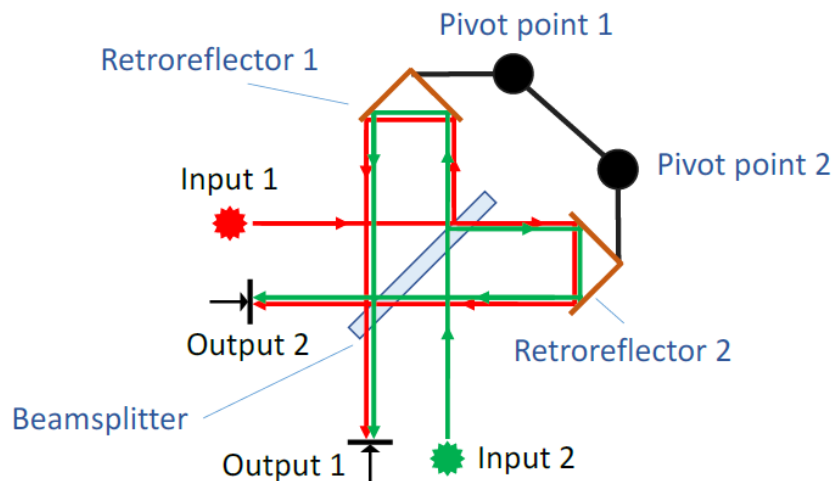


Figure 5.17 Four-ports double pendulum interferometer concept.

- To relay the aperture stop onto the entrance pupil of the interferometer on the cube corners.
- To provide a well-corrected intermediate image plane where the field stop is placed. The spot size at the field stop determines the System Integrated Energy (SIE).

The front telescope optical design consists in a three-mirror afocal telescope. The mirrors are made of aluminium and will be gold coated.

The interferometer is a four-port double pendulum type interferometer. One input port of the interferometer is fed with the light coming from the front telescope optics. The second input port is fed by a reference blackbody source for Concept A and by deep-space view for Concept B. A layout of the interferometer for Concept A is presented in Fig. 5.17. Concept A implements a double pivot mechanism for compactness reasons while Concept B uses a single pivot point preferring a less compact but simpler design. Both concepts have selected a double-sided interferogram acquisition meaning that the interferogram is sampled from $-MOPD$ to $+MOPD$ in a symmetrical way around ZPD. Regarding the trade-off on sampling directions, Concept A has selected a unidirectional sampling meaning that the interferogram sample points are acquired from $-MOPD$ to $+MOPD$ and then there is a return without data acquisition back to $-MOPD$ to restart a new acquisition. Concept B has selected a bidirectional sampling for better efficiency, the interferogram sample points are acquired from $-MPD$ to $+MPD$ and then from $+MPD$ to $-MPD$ and so on.

The interferometer entrance pupil is located at the cube corners apex. The interferometer opto-mechanical design is such that it can accommodate, without any modification, any selected beamsplitter solution from those studied within the Phase A pre-development activities. The interferometer optical design parameters are summarised in the Table 5.5

Parameters	Concept A	Concept B
Interferometer entrance pupil equivalent diameter (nominal)	30.5 mm	33 mm
Beam divergence (nominal, full angle)	43 mrad	44 mrad
Used MOPD	1.4 cm	1.35 cm
Spectral resolution	0.46 cm ⁻¹ at 1600 cm ⁻¹	0.48 cm ⁻¹ at 1600 cm ⁻¹
Beamsplitter options	Diamond Plate (baseline)	Diamond plate (baseline)
	Polypropylene membrane	Polypropylene membrane
	Mylar membrane	Mylar membrane
Cube corners	Monolithic	Monolithic
	Bare gold coated	Bare gold coated

Table 5.5. FORUM FSI interferometer main parameter for Concept A and B.

Beamsplitter

In early Phase A, the beamsplitter was identified as a critical component owing to the need to demonstrate transmission and reflection properties in the FORUM spectral range compatible with the requirements (Section 5.3.3.3.2). This necessitated a dedicated pre-development activity. Both industrial consortia chose an interferometer design that can accommodate different beamsplitter solutions (see Table 5.6) without having to modify its design.

The beamsplitter solutions studied within the frame of the pre-developments by both industrial consortia are: diamond beamsplitter plate, polypropylene membrane and Mylar membrane.

The selected **baseline beamsplitter** is a dual-wedged diamond plate. Diamond is a good candidate material showing a quite high and flat transmission over the full FORUM spectral range. The splitting interface (named front face) between the two arms is enhanced by applying a germanium coating on the beamsplitter diamond substrate. The rear face of the beamsplitter is either bare diamond (fresnel losses in the order of 15% in transmission due to diamond high-optical refractive index) or an antireflective coating improving the overall transmission. As the FORUM spectral range is very wide, it was difficult to find a classic dielectric antireflective coating. Therefore, the implementation of microstructures have been studied as a means to enhance the transmission. Such beamsplitter (diamond substrate germanium coated on one side and microstructuring on the other side) feasibility has already been demonstrated in the frame of NASA's OSIRIS-REX mission. The beamsplitter was however smaller (38 mm in diameter versus around 60–70 mm for FORUM FSI). For more details, refer to "The OSIRIS-REx Thermal Emission Spectrometer (OTES) Instrument (Christensen, et al., 2018)". Within the pre-development activities in Phase A, germanium-coated diamond samples, microstructured diamond samples and full-size wedged and coated-diamond beamsplitters were manufactured and tested for both consortia. The different steps that the samples underwent during the Phase A pre-development activities are summarised in Table 5.7.



Beamsplitter parameters	Concept A	Concept B
Baseline	Dual-wedged diamond plate Germanium coating on one side Anti-Reflection coating on side two	Dual-wedged diamond plate Germanium coating on one side Bare diamond on side two Option: Dual-wedge diamond plate Germanium coated on one side and AR coating on side two
Back-ups	Dual polypropylene membrane Dual Mylar membrane	Single polypropylene membrane Single Mylar membrane

Table 5.6. FSI interferometer beamsplitter solutions both baseline and back-ups (Concepts A and B).

Diamond samples were coated with germanium and the performance was tested (transmission, reflection) before environmental tests (see 4RT performance in Fig. 5.20 left). The diamond samples TVAC test is ongoing at the time of writing this report, results will be reported at UCM presentation. Diamond samples were also manufactured with microstructures and the transmission improvement, with respect to bare diamond interface, was characterised over the full FORUM spectral range, see Fig. 5.18. The improvement is in the range of 5–15%, depending on the wavenumbers which improve the overall NESR performance.

On top of the diamond samples, full-scale wedged-diamond beamsplitters have been manufactured, coated and tested by Concept B (planned for Concept A in Phase A). Fig. 5.19 shows a full-sized wedged diamond beamsplitter manufactured during the pre-development activities. It demonstrates the feasibility of manufacturing and coating a wedged-diamond substrate of size needed for FORUM (70–80 mm in diameter). Fig. 5.20 right reports the compliant WFE performance measured on the full-scale diamond plate after coating and the beamsplitter efficiency based on measured reflection and transmission data.

	Germanium-coated diamond samples	Microstructured diamond samples	Full-size wedged diamond plate
Manufacturing	✓	✓	✓
Coating	✓	✓	✓
Performance testing			
Transmission/Reflection over full FSI spectral range [100–1600 cm ⁻¹]	✓	✓	Ongoing
WFE measurement (before and after coating)	NA	NA	✓
Environmental testing			
Adhesion test	✓	NA	NA
TVAC test	Ongoing	NA	Phase B1

Table 5.7. Beamsplitter baseline phase A pre-development activities summary table – Concept A and B.

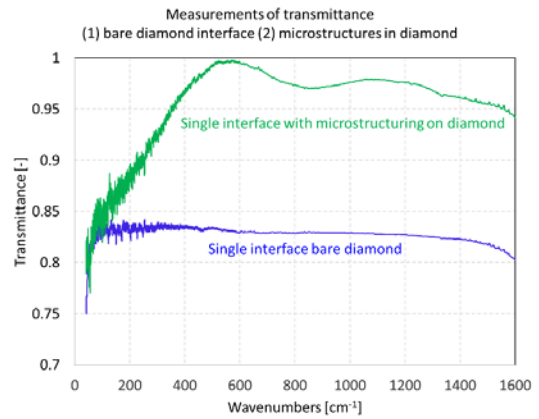


Figure 5.18 (Left) Uncoated diamond sample, (Right) Transmittance of single interface bare diamond compared to bare diamond including microstructuring versus wavenumber – Concept A

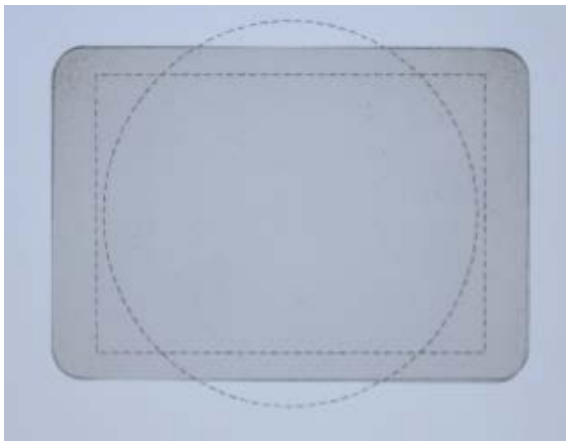


Figure 5.19 FSI interferometer full size wedged diamond beamsplitter breadboard uncoated (Left) and after Germanium coating (Right) - Concept B

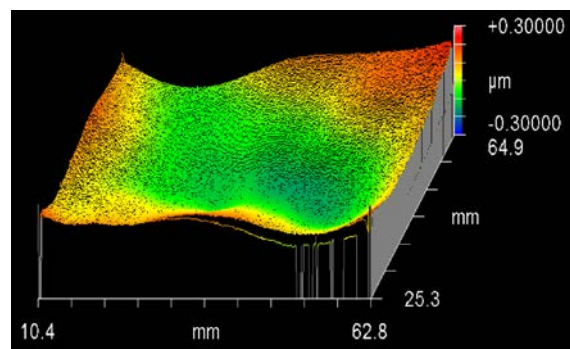
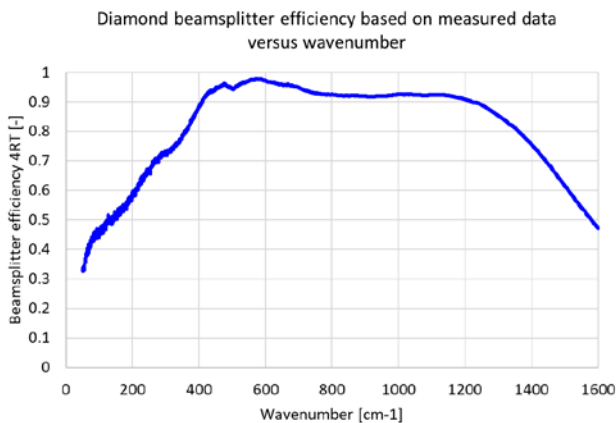


Figure 5.20 (Left) FSI diamond beamsplitter Efficiency based on measurement (Concept A), (Right) Ge-coated diamond WFE measurement in transmission (full scale sample) – WFE measured <100 nm rms (Concept B)



Figure 5.21 FSI Beamsplitter back-up solutions: Concept A Polypropylene beamsplitter (Left), Concept B Mylar beamsplitter (Right). (Courtesy of Cardiff University)

Alternative material beamsplitters pre-developed. Membranes beamsplitters made of Polypropylene or Mylar (see Fig.5.21) have been studied as back up solutions for the FSI. Compared to diamond, the Mylar and polypropylene exhibit absorption features in the FORUM spectral range which would lead to non-compliance to the NESR performance in the absorption bands. Mylar membranes used as beamsplitter in the FORUM spectral range have flight heritage (for example the polarising beamsplitter used on Cassini Composite InfraRed Spectrometer (CIRS) and ground heritage (REFIR-PAD) Moreover, the membranes are sensitive to mechanical and thermal stresses which would require attention. The membranes have a splitting coating in Germanium. The Polypropylene and Mylar beamsplitters have been manufactured and coated with Germanium within the phase A pre-development activities. They have been mechanically mounted in design-representative stainless steel or aluminum mounts. Transmission and reflection measurements over the full FORUM spectral range have been performed. WFE measurements have also been performed. The polypropylene substrate and the germanium coating deposition were not successful presenting significantly lower 4RT performance compared to the predictions and a much higher WFE which is not acceptable for the required modulation efficiency. Investigation to improve the manufacturing process continue however at the time of writing this report. However, with current performance, Polypropylene is not considered a viable solution for FORUM. Mylar shows reasonable WFE, however the germanium deposition present non-homogeneities, which worsen with time, degrading the expected 4RT and the WFE. Further investigations on the germanium deposition process are on-going at the time of writing the report.

Corner cubes.

As retro-reflecting elements of the interferometer, monolithic corner cubes are employed to ensure against angular distortions. Corner cubes less than 90 mm in diameter are standard Commercial Off-The-Shelf (COTS) products. They are aluminum elements coated with a bare gold coating. A photo of the corner cubes integrated in the interferometer breadboard is presented in Fig. 5.22.

Interferometer mechanism

A double pendulum mechanism was selected for the interferometer for both concepts. This choice reliably provides sufficient stroke and beam diameter, with a simple configuration and is robust to environmental loads. In the pendulum mode of operation, the corner cubes



Figure 5.22 Monolithic cube corners made of Aluminum, gold coated – Concept A

located at the tip of both arms move in opposite directions and the resulting OPD between them produces the interferogram.

Concept A uses a double pivot point mechanism, see Fig. 5.23., while concept B uses a single pivot one, see Fig. 5.24. Concept A has heritage from commercial ground-based interferometers, thousands of units are operational with the same double pivot mechanism as the ones proposed for FORUM. Moreover, a prototype of the double pivot mechanism, smaller in size but representative of FORUM’s is currently undergoing space qualification campaign in the frame of the Large Aperture Dual Pivot (LADP) development, with the aim to reach TRL6+ by the end of 2019. Concept B proposes to use a single pivot mechanism, smaller in size but fully representative of the one on the Atmospheric Chemistry Experiment (ACE)-FTS instrument onboard Science Satellite (SciSat) and TANSO-FTS instrument on board GOSAT. These FTS include a double pendulum interferometer based on a single pivot point mechanism. Both interferometer mechanisms are considered feasible and with proved heritage. However, pre-development activities are on-going (and will continue in Phase B1)

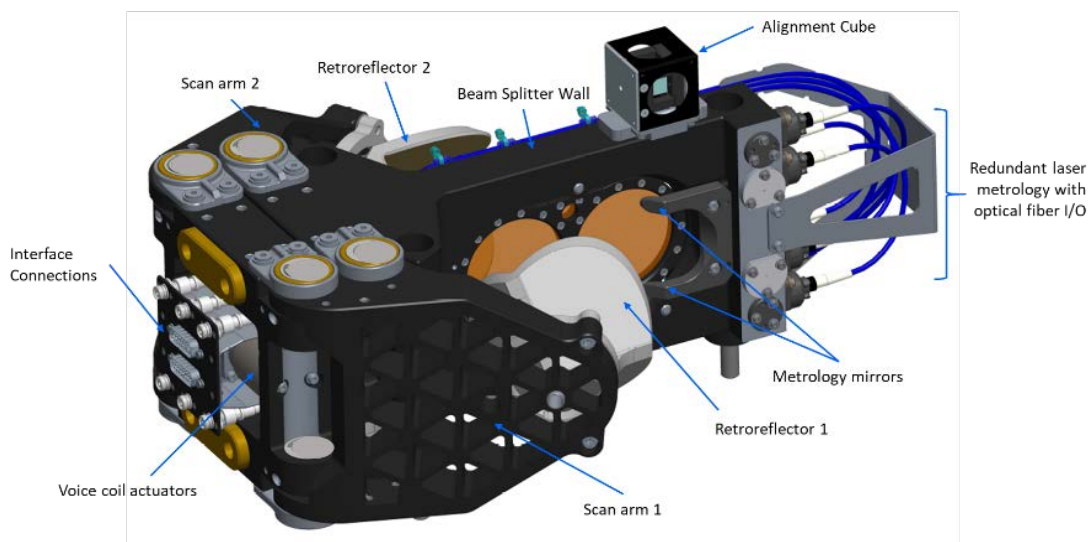


Figure 5.23 FORUM FSI Interferometer breadboard sketch – Concept A. (Courtesy ABB).

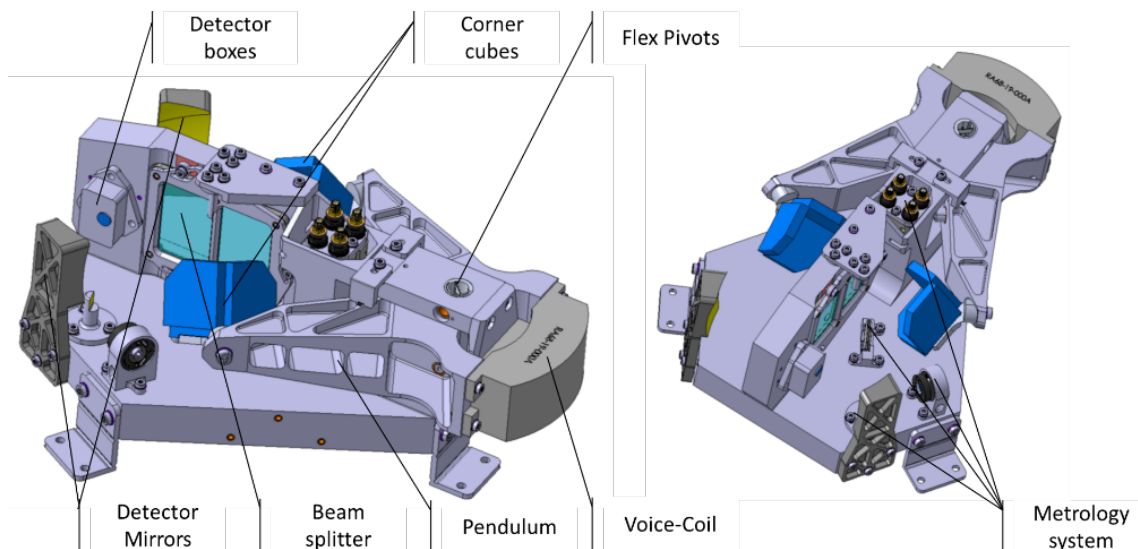


Figure 5.24 FORUM FSI interferometer sketch – Concept B. (Courtesy OHB)

to demonstrate the required performance for the specific FORUM design in the relevant environment.

The actuation principle involves a voice-coil, (in fact a double-coil for redundancy), which imposes the rotation of the two arms with relation to flexible pivot hinges - one single hinge in the case of Concept B. This configuration provides large rotations around a fixed determined axis, showing high stiffness and virtually no friction even without lubrication. The launch loads are resisted by the constrained degrees-of-freedom of the flexible hinges as well as by a pin-puller, which generates low shock upon release.

Fig. 5.25 shows an interferometer breadboard developed by the Canadian Space Agency, which includes the same mechanism as the one proposed for FORUM Concept A.

It has been specified that sampling speed instabilities shall remain lower than 1% during science acquisition. While analysis have confirmed that the interferometer design meets this requirement for both concepts, within the frame of the pre-development activities in phase A, a breadboard for Concept B has been manufactured and aligned – Fig. 5.25. The speed stability and micro-vibrations tests are on-going at the time of writing the report.

During each Earth observation dwell time, the interferometer and the pointing mechanism are aligned such that the acquisition during one dwell is from the same ground sample. The interferometer mechanism movement is synchronised with the pointing mirror movements for high performance LoS compensation. In the short gap between two dwell time windows, the pointing mechanism is set to either back to the new starting angle position, or to the calibration blackbody or towards the deep space view and the interferometer mechanism is reversed for the next interferogram acquisition.

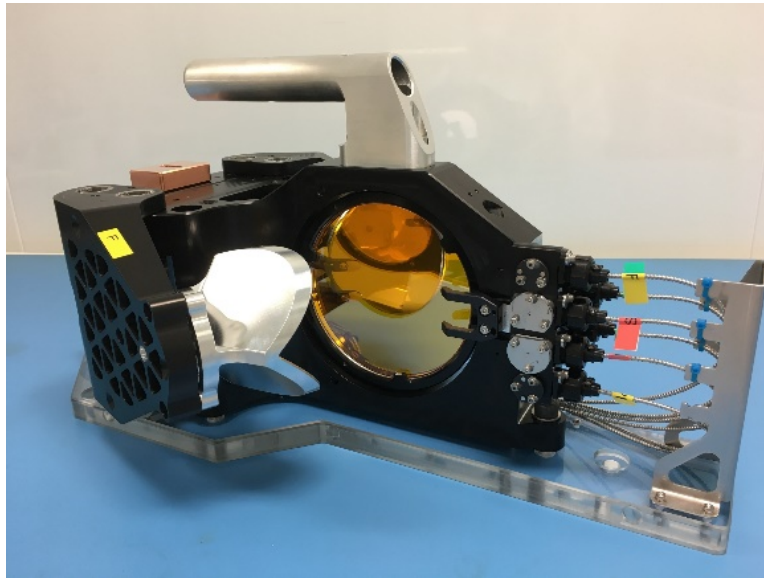


Figure 5.25 Large aperture interferometer breadboard developed by ABB partially funded by the Canadian Space Agency. (Courtesy ABB)

The interferometer runs in a continuous forward/backward motion in a close-loop control using the metrology laser fringe signal. The sampling window signal and the scan direction are sent to the ICU to generate the signal to synchronise the interferometer with the pointing mechanisms. The two synchronisation signals required by the pointing control electronics are one (GSYNC) marking the start of each pointing scan sequence and another (RSYNC) triggering the position/rotation reset.

The GSYNC signal is derived from the ICE Sampling Window Signal and the RSYNC signal is derived from the ICE Scan Direction Signal. The ICE, as well as the ICU operates based upon their internal master clock, but both units receive the pulse-per-second (PPS) signal from the platform.

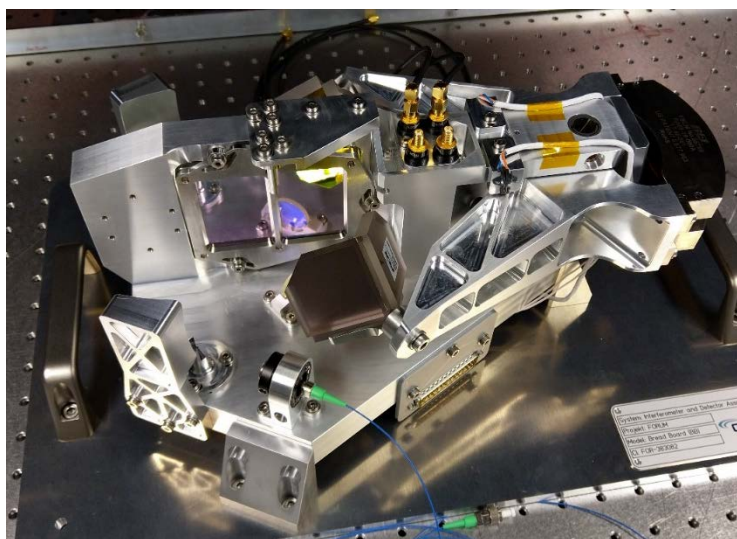


Figure 5.26 FTS Interferometer mechanism breadboard Concept B. (Courtesy of OHB).

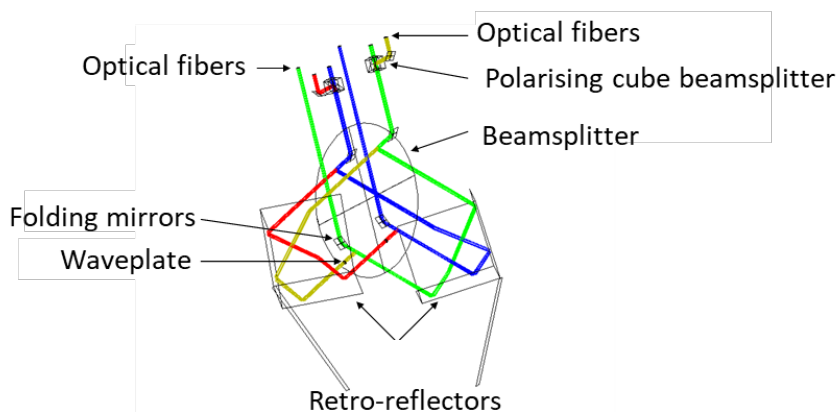


Figure 5.27 Optical layout of the metrology beam in the interferometer.

The interferometer motion is fully periodical and deterministic. Potential timing jitters are well below a μ -second resulting in negligible error contributions compared to the dwell time of 14 seconds. Any long-term drift effects can be compensated for by using a configurable interferometer turn-around time, which allows re-synchronisation (Concept A), or by determining the optical ZPD position (with help of the mechanical ZPD reference) and then symmetrical fringe counts from this position on.

In general, there are four types of disturbances of an interferogram due to **micro-vibrations**. All result in spectral artefacts (ghosts) and cause spectral/radiometric errors. The design of the FSI for both concepts is such that only one exists. FORUM has a single pixel; therefore no shear ghosts are created. FORUM has no integrating detector; therefore no integration ghosts are created. FORUM is not a limb-sounder; therefore, pointing variations do not result in amplitude ghosts. The remaining ghost type to analyse is phase ghosts due to the electrical delays. The electrical delay of the science and the metrology system may be different and would create ghosts in the presence of micro-vibrations. As the delays are stable, they will be characterised and taken into account in the interferogram resampling. The residual ghost is small enough to be neglected, compared to NESR.

Metrology system

The main function of the metrology is to measure the OPD in real time for triggering the science acquisition on known OPD position and to control the motion of the mechanism of the interferometer. The metrology systems for both concepts has heritage from the metrology systems, including the lasers, of IASI, GAIA, MIPAS, TANSO-FTS, IASI-NG and IRS.

The metrology is based on a linearly-polarised laser signal at 1550 nm. Fig. 5.27 shows the optical lay-out of the metrology beam. The laser signal is injected into the interferometer via an optical fibre. The laser beam travels into the interferometer. At the output, a polarisation beamsplitter separates the beam into its two orthogonal polarisation components and each beam is injected into the returning optical fibre and sent to the ICE. The returning signals are captured by photodiodes in the ICE.

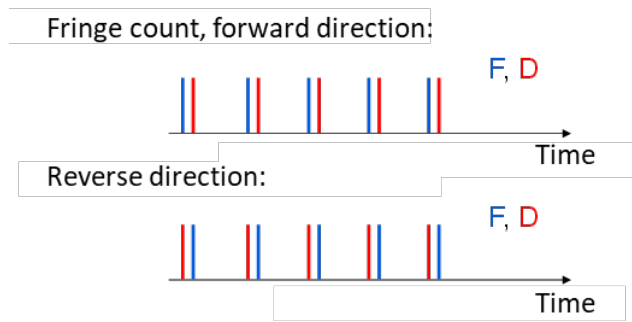


Figure 5.28 Scan arm direction determination with the two metrology signals.

As shown in Fig. 5.28, one signal, called the ‘F’ signal, serves to count the laser fringes and generate the science sampling trigger at equal OPD values. One pulse is sent every X laser fringes. The F signal is also used to feed the servo control of the scan arm and ensure a uniform speed over the sampling window. The second signal is called ‘D’. There is delay introduced between F and D which means that it is possible to distinguish between forward and reverse scans, and determine the direction of the scan arm.

The fringe counting pulses can be generated at every zero crossings of the metrology signal (half wave) or every one out of two zero crossings (once per wave). Alternatively, it is also possible to emit more dense pulses (e.g. every quarter wave) by interpolation. The metrology layout is fully redundant. There is a total of two injection fibres, two polarising beamsplitters and four collection optical fibres.

Focal plane/detection chain.

The FORUM FSI detection chain is located at each of the two outputs of the interferometer, after the FSI focusing optics, and it comprises the FSI detectors and the FSI FEE. The FSI detectors convert the optical interferograms into an electrical signal, which is then sampled by the FEE and formatted into digital data to be sent to the ICU. The two detection chains are electrically and functionally independent.

The selected detectors for the FSI are based on pyroelectric crystal technology. A pyroelectric crystal exhibits a temperature dependent spontaneous electrical polarisation. Thanks to this property, temperature changes result in a change in the electric field at the two faces of the crystal that can be measured allowing the detection of thermal infrared signals, like in the case of the FSI interferograms. The pyroelectric crystal used for FORUM detectors is Deuterated L-alanine Dopped Triglycine Sulphate (DLaTGS) a material offering very high

	Concept A	Concept B
Baseline detector	LEONARDO’s DLaTGS pyroelectric detector 99 series standard	LEONARDO’s DLaTGS pyroelectric detector 106 series standard
Window/lens material	Diamond	Diamond
Detector sensitive area	2 mm	2 mm
Operation mode	Voltage mode	Voltage mode

Table 5.8. Pyroelectric detectors used in the detection chain for the FSI - Concepts A and B.

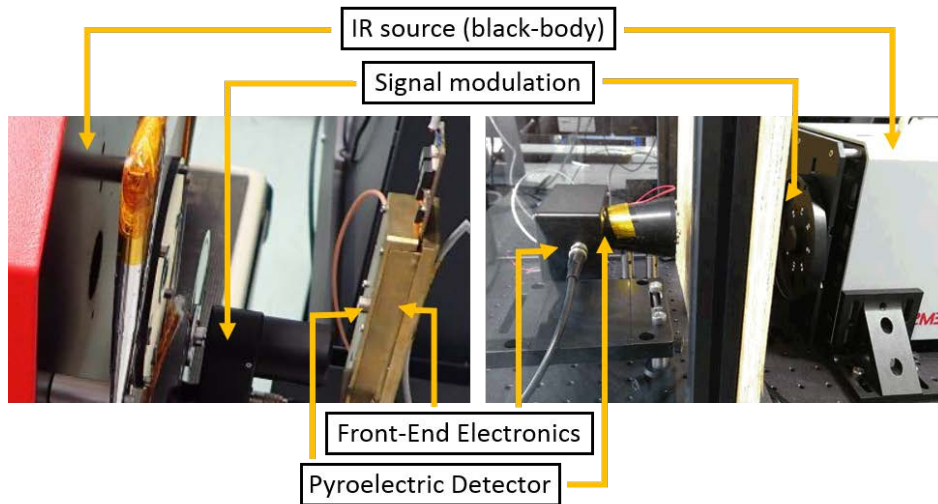


Figure 5.29 The setups built for the detection chain pre-developments activities for responsivity and noise characterisation of the pyroelectric detectors, for Concept A (left) and B (right).

sensitivity in the IR spectral range. The crystal is grown as a wafer and polished into a thin element, with electrodes deposited on the opposite faces. The surface of the crystal exposed to infrared light is blackened to enhance its absorption, and the element is mounted in a hermetically sealed industry-standard electronic package, with a diamond window to admit radiation. The baseline detectors for both concepts are provided in Table 5.8.

The noise and the responsivity properties of several DLaTGS detectors were characterised in laboratory environment within the frame of the Phase A pre-developments activities. In the study for Concept A, the measurements were compared to the datasheet from manufacturers, while the pre-development for Concept B provided a relative comparison of the performances of different detectors. The setup built for the detection chain pre-developments in both studies are shown in Fig. 5.29, where the radiation source (blackbody), the detector and the FEE can be identified easily. Some results for the responsivity of the two

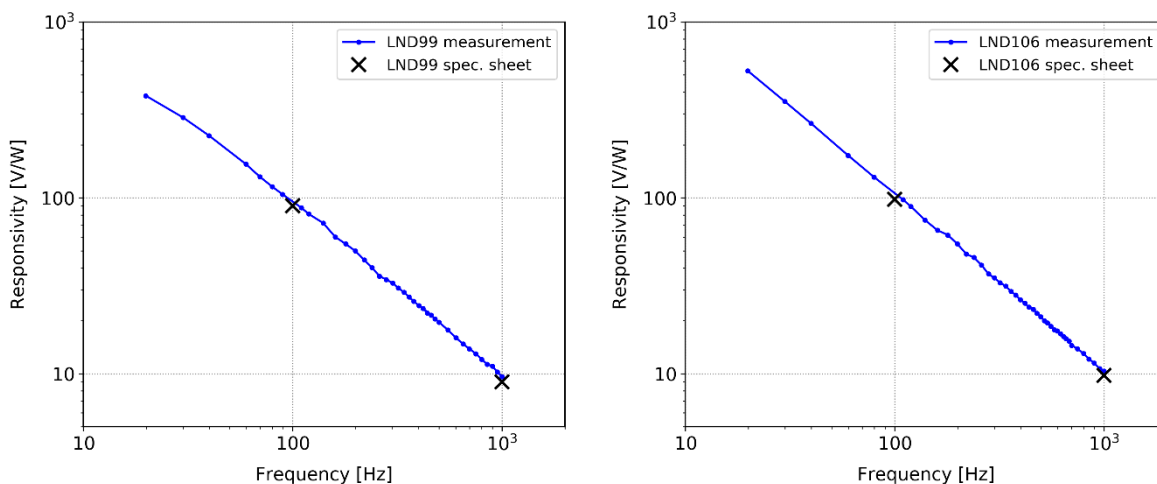


Figure 5.30 Results from the detection chain pre-development for the detectors considered as baseline in Concept A (left) and B (right).

baseline detectors are shown in Fig. 5.30. The results for responsivity and noise are in line with the expected values (coming from detector suppliers datasheet) for both baseline detectors.

The pre-development activities also focused on comparing and providing quantitative data from two different operation modes of the detector, voltage-mode and current-mode. The voltage-mode is the standard mode of operation, and the measurements within the pre-development activities confirmed the manufacturers experience and model. For the current mode, the investigation of detector's performance did not give conclusive results for the correlation between measurements and model.

The dependence of the detector with temperature was also investigated in both pre-developments, but the characterisation could not provide consolidated conclusions on the ideal detector temperature for best performances. A tuning of the detector nominal operational temperature is still considered as a viable strategy for optimising the detector performances, but needs to be confirmed as part of the pre-development activities foreseen in Phase B1.

Black body/calibration devices.

FORUM embarks blackbody sources to perform in-flight radiometric calibration. FSI is calibrated in flight using a deep-space view and a blackbody maintained at instrument temperature (e.g. 293 K), and temperature monitored to provide a known reference radiance.

The calibration blackbody is implemented at the entrance of the instrument. The pointing mirror is used to point to Earth, and to deep space for radiometric calibration, including offset determination and blackbody for radiometric calibration. The calibration blackbody and the deep-space view port are both used for the FSI and the FEI radiometric calibration in flight.

The calibration blackbody baseline for both concepts is based on well-proven black-coated cavity geometries, the design of which allows the emissivity requirement to be reached (>0.99 for most of the FORUM spectral range).

The **black coating baseline** has been selected based on performance, stability and heritage. The outcome of the trade-off and pre-developments of Phase A converged towards the selection of the well-characterised high emissivity paint Mankiewicz Nextel 811-21. The emissivity of several samples of Nextel 811-21 (Fig. 5.31 left) in the FORUM spectral range up to 100 μm have been tested in ambient at the Physikalisch-Technische Bundesanstalt (PTB) facilities in Berlin (Fig. 5.31. center). In addition, PTB has long standing records for on-ground performance stability of this coating. This paint has also flight heritage as it was used, for example, for the blackbody cavity of the High Resolution Dynamics Limb Sounder (HIRDLS) instrument on the NASA EOS Chem satellite. Other potential candidates (Fig. 5.31 right), with better performance but less heritage, such as Vanta S-VIS, S-IR from Surrey

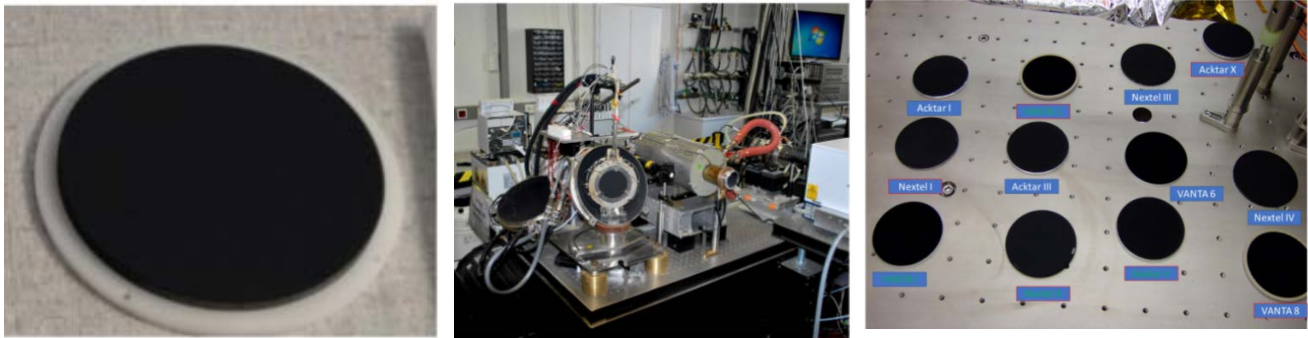


Figure 5.31 From left to right: (1) Black-coated sample for emissivity measurement Nextel 811-21, (2) emissivity measurement set-up in air at PTB, (3) black-coated samples prepared for environmental tests.

Nanosystems and Deep Sky Black from Equinox have been considered as options. The emissivity of all the above mentioned black coating options has been characterised (at the time of writing this report) in air over the complete FORUM spectral range $6\mu\text{m}$ to $100\mu\text{m}$ during and will be characterised in a vacuum by the end of Phase A. The baseline and promising black-coated samples also underwent environmental testing: adhesion test, thermal vacuum cycling and humidity. The deposition process repeatability for the Nextel black coating has also been assessed within the pre-development activity as two samples manufactured from two different batches have been tested. (see Fig. 5.32 showing a stable performance).

The blackbody geometry has been iterated based on some **blackbody performance simulations** using the STEEP software. Several trials of geometry, black coating types have been performed in order to identify the best compromise. Nextel together with well-known cylindrical cavity geometry has been selected as baseline allowing to reach the emissivity requirement. The model has then been refined: a thermal model has been developed and thermal environment simulations were carried out to assess the gradient over the cavity in order to evaluate the impact on radiometric performance. This analysis confirmed the

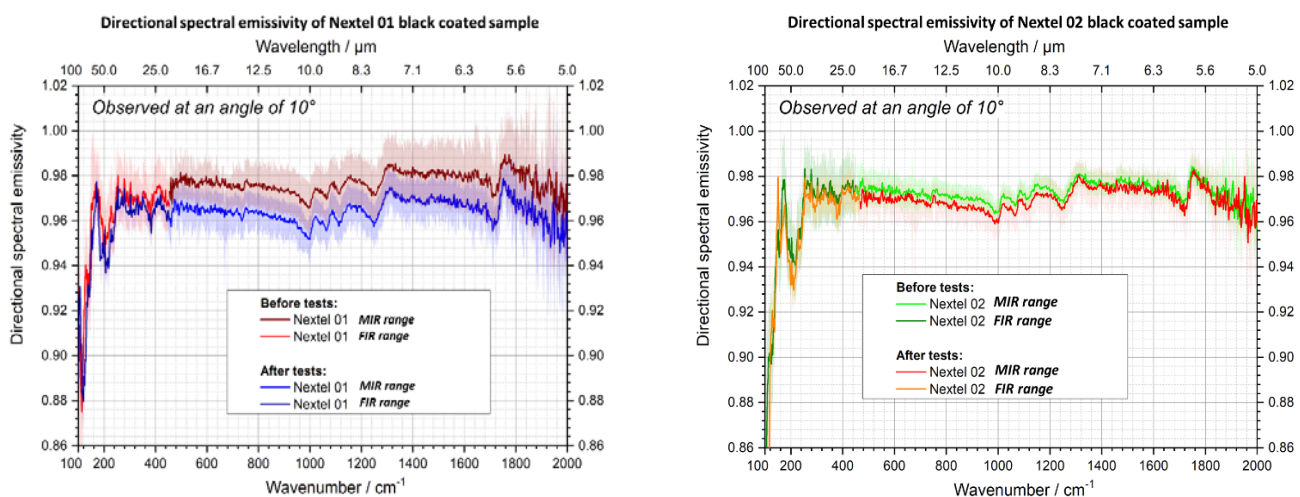


Figure 5.32 Nextel 811-21 black coated sample emissivity measurement results before and after environmental testing for 2 different samples manufactured from 2 batches – Concept A and B. (Courtesy of PTB).

compliance of the blackbody design to the requirements. Further pre-development activities regarding the cavity geometry will be performed during the Phase B1.

Concept A includes a phase changing cell device in order to absolutely calibrate in orbit the thermal sensors and hence reduce some errors due to the **thermal sensors temporal drift** in the overall Absolute Radiometric Accuracy budget. A pre-development activity has been done in phase A to build a representative mock up and test the repeatability of the melting point. The results conclude that the repeatability is well within the requirement of 10 mK, as shown in Fig. 5.33.

The blackbody is maintained at floating temperature (temperature of the instrument) and temporarily increased to around 30deg for the calibration of the thermal sensors thanks to the phase changing cell (once per month).

Concept B does not include an on-board phase change cell device for recalibrating the temperature sensor of the blackbody in-flight. Platinum Resistance Thermometer (PRT) sensors are known for being sensitive to vibrations and thermal cycling, additional errors in ARA budget are accounted for and some measures have to be taken to limit the contribution:

- Temperature variations to be tracked to estimate the range of the PRT hysteresis
- Possible use of on-ground reference PRTs that would experience the same temperature variations
- Maintain the temperature in a small range during MAIT, delivery, pre-flight to minimize the thermo-elastic effects

Concept A also includes a reference blackbody at the second input port of the interferometer. This blackbody is maintained at the instrument temperature. Concept B views deep space in the second input port of the interferometer.

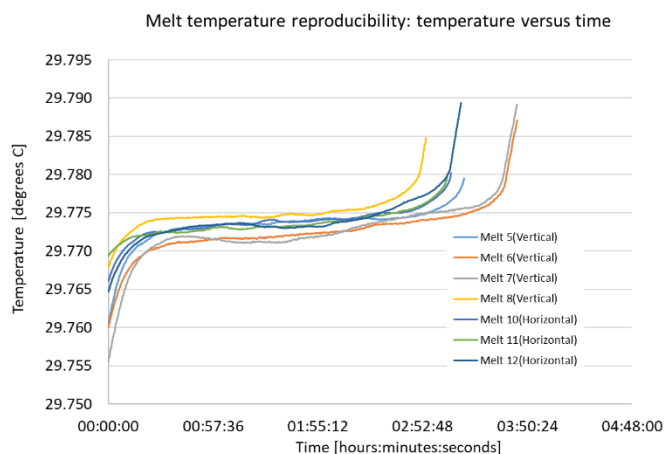
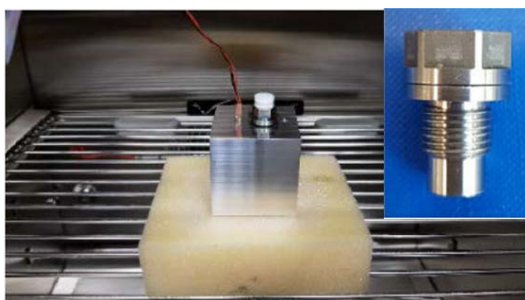


Figure 5.33 (Left) Phase change cell mock-up for plateau repeatability measurement, (Right) Melt temperature reproducibility within 10 mK measurement results – Concept A

5.3.3.5.5 FORUM Embedded Imager (FEI)

Optical concept

Parameters	Concept A	Concept B
Effective focal length	25 mm	48.2 mm
Entrance pupil diameter	25 mm	30 mm
Field of view	41km x 41km	38.4 km x 38.4 km
F/number	1.0	1.6
Spectral range	[9.75;11.25] μm	[9.75;11.25] μm
Pixel size	17 μm	34 μm (spatial binning of 2x2 pixels)

Table 5.9. FORUM FEI optical design main parameters for Concepts A and B.

The FORUM Embedded Imager opto-mechanical design is presented in Fig. 5.35 for Concept B. It is a fully refractive design for both concepts. The optical design for Concept A consists of spherical lenses made of germanium and a flat silicon window part of the detector package. Concept B's optical design is an objective made of spherical and slightly aspherical germanium lenses.

The FEI is equipped with a bandpass filter centred at 10.5 μm and with a bandwidth of 1.5 μm . The bandpass filter is located either as a flat add-on near the aperture stop or on the front surface of the first lens for Concept A. For Concept B, the bandpass filter is applied as an add-on element between the first and second lens. The main optical parameters of both concepts are summarised in Table 5.9.

The **focal plane** unit of the FEI comprises:

- a micro-bolometer array detector and its proximity electronics
- FEE
- a mechanical supporting structure allowing thermal control and mechanical alignment of the detector

A micro-bolometer array is built from a 2D pixel matrix, where each pixel consists of a black, IR absorbing surface. Incident IR radiation heats the pixel surface and changes its resistance, which is sensed by a highly sensitive electric circuitry placed directly under the pixel absorber surface. The temperature reading, which is proportional to the incident IR power, is sampled, amplified, and multiplexed into a clocked analogue video output. The advantage of micro-bolometers, in contrast with IR matrix sensors, is that they can be operated uncooled, and they are smaller, lighter and consume less power. The disadvantage is a lower IR sensitivity, expressed as NEDT and high noise sensitivity to package temperature variations. In addition, micro-bolometers are commonly operated with F/1 optics, whereas photodiode matrix detectors are optimised for slower F/2-F/4 optics. These consideration drives the design, which has led to a relatively simple, cost-efficient and small design while still fully compliant with the FEI requirements.

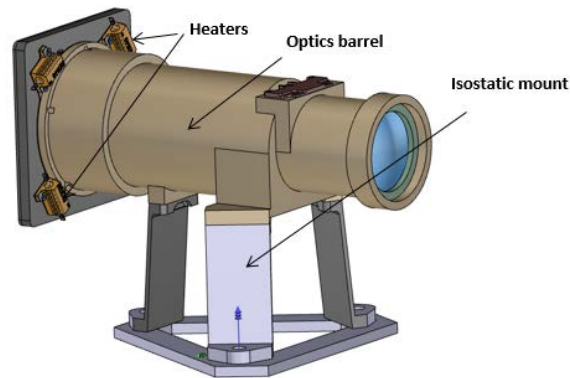


Figure 5.34 FORUM FEI instrument and opto-mechanical design - Concept B

Concept A implements as baseline detector for the imager an ULIS PCIO640 Gen2 microbolometer array.

Concept B implements ULIS PICO 1024-048 off-the-shelf microbolometer detector. ULIS PICO 1024-048 has an NEDT of about 50 mK (@ scene temperature of 300 K, frame rate of 30 Hz and F#1 illumination) and typical thermal time constant of 12 ms in 17 μm pixel size. Both detectors are COTS components and the ULIS PICO 1024-048 has followed a qualification programme funded by ESA.

The **mechanical and thermal accommodation** of Concept A baseline consists of lens housing, spacers and FPA made of the same material. Titanium was selected for the mechanical properties and the CTE very close to the optical elements' materials.

The preliminary structural design for the FEI Concept B is displayed in Fig. 5.34. The germanium lenses are mounted in a single titanium barrel, which is fixed to the optical bench by means of aluminium blades. Thermal conductivity through the blades is required to evacuate the heat dissipated by the detector and rely on the optical bench active thermal control to minimise the FEI displacement variation. The optical bench orbital thermal stability is sufficient to meet the radiometric accuracy requirement. The overall size is about 186×133×146 mm.

The FEI uses the same **calibration devices** as the FSI for the calibration blackbody and deep space view.

5.3.3.5.6 Payload Control Electronics

The electrical architecture includes all required elements and functionalities to support a self-contained design of the instrument. This means that no external control, external to the payload, is required, except for the activation of the payload and the surveillance of essential ICU parameters during the nominal and survival modes. The main building blocks of the FORUM payload architecture are:

- Instrument Control Unit (ICU), which provides the central hardware and software functions to interface with the platform, command and control the instruments and collect and transmit science data to the PDHU in the platform.



- Pointing Control Electronics (PCE), which operates the pointing and scan mechanism. Both functionalities are merged into a single device, for Concept A, and no dedicated control box is foreseen, hence it will be integrated into the ICU. For Concept B, the pointing and scan functions are implemented in two mechanisms. The electronics controlling the scan mechanism will be implanted in a dedicated box while the pointing mechanism is commanded and control by the dedicated module in the ICU.
- Interferometer Control Electronics (ICE), which operates the interferometer mechanism and the metrology equipment. A dedicated electronic box is foreseen in both concepts.
- Two FEE units operating the two FSI detectors.
- One FEE operating the FEI detectors.
- Electrical/electronic equipment, which includes the pointing mechanism actuator and position sensors, the interferometer actuator and metrology equipment, the calibration blackbody and the reference blackbody.
- Thermal control hardware including thermistors and heater of the autonomous operational thermal control system and the survival thermal control system, which is operated directly by the platform.
- Instrument harness, including connector brackets at instrument level and all supporting hardware.

The ICU, ICE and the PCE for Concept B are units exported into the platform and, hence, thermally controlled by the platform. All electronic units implement full redundancy except for the FEE's, where only interface redundancy is baselined.

The ICU implements a LEON2 core based processor. It interfaces the platform to exchange telemetry, command and control, and science data via Spacewire link for Concept A while for Concept B TT&TC is transferred via a MIL-1553 bus while science data is exchanged via Spacewire. The ICU also implements dedicated interfaces for discrete commands (e.g. switch on/off) or discrete signals such as the Pulse Per Second (PPS) for time correlation with the platform. Redundant power lines supporting unregulated voltage are protected via LCL at platform side. The ICU is also capable of receiving EQSOL status signal for the platform to warn the payload of any platform anomaly, that power may be removed from the instrument in few seconds, and that the payload will be entering safe mode. The electrical architecture proposed by for consortia is sound and suitable for the FORUM payload.

5.3.3.5.7 FSI On-Ground Characterisation and In-Flight Calibration

FSI on-ground characterisation

Spectral characterisation: On-ground spectral characterisation involves the characterisation of the metrology system and the determination of the Instrument Line Shape (ILS) and a spectral scaling factor. ILS and spectral scaling factor are characterised using the monochromatic signal of a tuneable laser in the thermal infrared – injected into the instrument using an integrating sphere – and a parametrised mathematical model of the instrument line shape.

The shape of the ILS is scanned by tuning the laser frequency in steps smaller than the spectral resolution of the instrument. The measurements, together with a parametrised mathematical model of the ILS give access to the ILS at every wavenumber in the FORUM spectral range.

The spectral scale factor is determined by comparing the central wavenumber of the measured ILS with the wavenumber of the monochromatic input signal. The difference in wavenumber represents a spectral scale shift over the full spectral range. Spectral shifts arise from a change in angle between the science beam or the metrology laser beam and the interferometric axis, spatial sensitivity of the detector or drifts in wavelength of the metrology laser.

The characterisation of the metrology laser system includes the determination of the metrology laser wavelength as a function of temperature and driving current. The laser wavelength is determined using a calibrated wavemeter. SNR and phase shifts are characterised as a function of interferometer temperature.

Radiometric characterisation: The radiometric response is determined by using an on-ground reference blackbody, SI traceable over the full FORUM spectral range. The blackbody will cover the full FOV. The radiometric characterisation is conducted in vacuum with the use of liquid nitrogen to mimic the deep-space view and, if necessary, the second input port. The internal calibration blackbody and the instrument will have reached their nominal temperature within the expected stability before performing the tests.

Geometric characterisation: The spatial response of the detector is determined using small instantaneous FOV scans over the full instrument FOV, called the knife-edge method. For small wavenumbers, blackbody sources at different temperatures are used and for high wavenumbers, a laser source in the TIR is used.

FSI in-flight calibration

Radiometric calibration: The in-flight radiometric calibration is based on a hot and a cold reference measurement to determine radiometric gain and offset correction factors. A hot cavity blackbody and a deep-space view measured with a pre-defined sequence, serve as a hot and cold reference scene. Earth measurements $S_S(\sigma)$ are calibrated using a gain $\mathbb{G}(\sigma)$ and an offset $\mathbb{L}_{offset}(\sigma)$ correction factor such that:

$$L_S(\sigma) = \text{Re}\left(\frac{S_S(\sigma)}{\mathbb{G}(\sigma)} - \mathbb{L}_{offset}(\sigma)\right)$$

With Equation 5.3

$$\mathbb{G}(\sigma) = \frac{S_H(\sigma) - S_C(\sigma)}{L_H(\sigma) - L_C(\sigma)}$$

$$\mathbb{L}_{offset}(\sigma) = \frac{S_C(\sigma)}{\mathbb{G}(\sigma)} - L_C(\sigma)$$



$L_S(\sigma)$ is the calibrated radiance at wavenumber σ ; $S_S(\sigma), S_H(\sigma), S_C(\sigma)$ are the complex measured spectra for the scene, hot reference and cold reference views respectively. $L_H(\sigma), L_C(\sigma)$ are the calculated radiances for the respective hot and cold reference views.

The challenging requirement on absolute radiometric accuracy requires an elaborated processing of calibration measurements to minimise the radiometric noise residual on the derived correction factors. Efficient ways to reduce noise have been identified, based on a statistical treatment of a series of calibration acquisitions over a specific period of time.

Spectral calibration: Spectral calibration is necessary to retrieve spectral correction factors to determine the spectral scale within the desired accuracy. The accuracy of the spectral scale depends on:

- Alignment of the optical axis of the science beam with the interferometric axis
- Alignment of the interferometric axis and the optical axis of the metrology laser beam
- Spatial sensitivity variation of the detector
- Short term laser wavelength stability

These contributors are characterised on ground and the impact of a possible degradation in-flight over the mission lifetime is computed by opto-thermo-mechanical analysis.

Furthermore, the accuracy of the spectral scale depends on the drift of the metrology laser wavelength due to thermo-elastic effects and aging. This contributor results in a slow varying, long-term spectral scale shift and requires in-flight calibration either by using atmospheric spectral invariant features (baseline approach), as developed for the Infrared Sounder on the Meteosat Third Generation satellite, or by using a gas cell as reference source (back-up approach)

Pointing calibration: The FSI pointing calibration and the co-registration with the FEI is performed to calibrate pointing bias errors, which occur due to launch loads, zero- g effects and ageing effects. Bias errors can be calibrated by using the Moon as pointing target, letting the Moon transit across the FOV. This would require the platform to manoeuvre accordingly.

FSI and FEI in-flight co-registration can be done with in-orbit data of the footprint of the sounder on the imager array at $10.5 \mu\text{m}$ over several orbits, which would give the offset with respect to an arbitrary coordinate origin in the FEI array.

5.3.3.5.8 FEI On-Ground Characterisation and In-Flight Calibration

FEI on-ground characterisation

The FEI is characterised on-ground using the same procedures as foreseen for the FSI:

- Radiometric characterisation is done with the internal and external blackbodies
- Spectral characterisation of implemented filters is done at component level
- Geometric characterisation is done using small instantaneous FOV scans over the full instrument field of view, called knife-edge method. Straylight will be tested together with the FSI SEDF, using a point source at infinity. This test will also allow to determine the co-registration with the FSI.

- The spectral performance will be characterised at filter supplier level.

FEI in-flight calibration

Radiometric calibration: Radiometric calibration is performed thanks to a two-point calibration using a hot and a cold reference scenes. The hot reference scene is a hot blackbody cavity on board while the cold reference scene is a deep-space view. Just like the radiometric calibration for the sounder, a radiometric gain and offset correction factors are derived and used to calibrate Earth measurements.

Spectral and geometric calibration: No in-flight spectral characterisation is deemed necessary because of the temperature stability during the lifetime and because the filter substrate and coating will be radiation-hardened. In-flight LOS calibration may be done using the same methods as described by the FSI.

5.3.4 Platform

5.3.4.1 Overview

Concept A relies on use of the flight-proven Copernicus Sentinel-5P platform while Concept B relies on the use of an existing flight-proven spacecraft design from the Proteus 150/300 generic product line, with extensive reuse of off-the-shelf components (e.g. Copernicus Sentinel-3). This section describes each platform subsystem and provides the rationale for its architecture and the selection of components.

5.3.4.2 Structure

The mechanical design of both platform concepts is driven by:

- The need to accommodate the FORUM payload within the volume available under the Vega-C fairing considering a dual launch
- The compatibility with the launcher mechanical environment
- Simplicity and reuse of flight-proven design to reduce cost and schedule

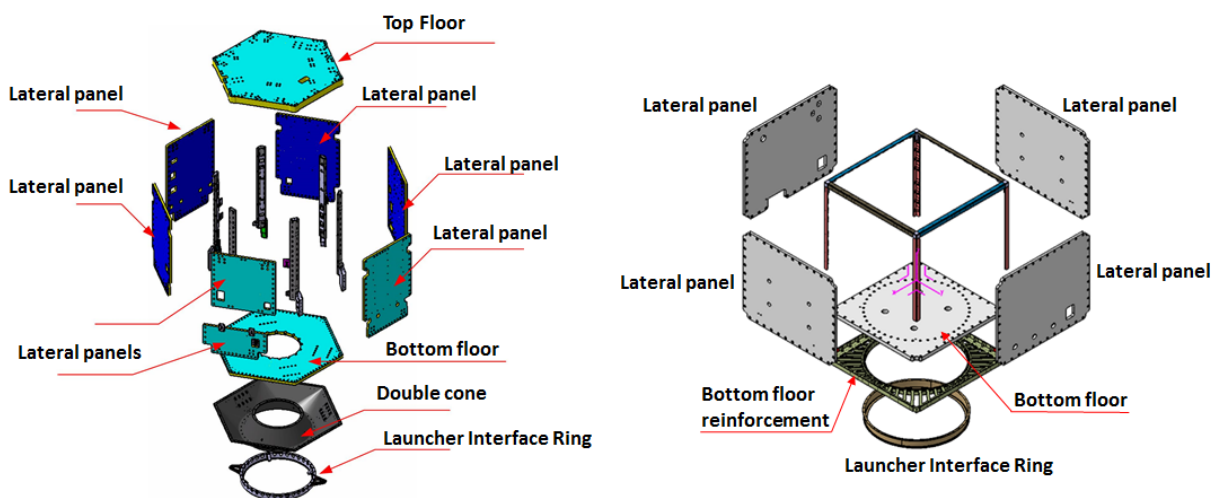


Figure 5.35 FORUM structural concepts, Concept A (left) and Concept B (right).

Fig. 5.35 shows the two structural concepts proposed for FORUM. They are both designed to sustain the launch loads by providing a direct load path to the launcher adapter through the interface ring.

The structure of Concept A is based on an integrated solution that supports both platform and the payload. The structure is a hexagonal prism, 1.7 m high and 1.6 m diameter at the base. A double-cone structure provides the transition between the launch vehicle interface and the hexagonal body. The inner cone provides support to the propulsion module, while the reaction wheels, the solar-array deployment mechanism are mounted on the bottom floor. Six aluminium-alloy machined frame beams connect the bottom floor to the top floor, which serves as the payload interface structure. The six lateral panels, made of aluminium honeycomb, act as thermal radiators and support the main avionics equipment, which are mounted on the panel inner faces and can be accessed during AIT by folding the panels downwards.

Concept B is based on a squared box (1.1 m high, 1.2 m wide, 1.2 m long) of aluminium sandwich panels, assembled on a bar frame with an L-shaped section to facilitate integration operations. The main load path is provided by the primary structure, which is made of six sandwich panels with aluminium skins and honeycomb core (four lateral panels, a top panel and a base panel), a bottom aluminium machined frame and a launcher interface ring.

In both concepts, a standard 937 mm diameter interface ring provides the interface to the launcher adapter to be used in Vega-C dual configuration.

The structure compatibility with the launcher environment has been assessed for both concepts through dedicated mechanical analysis with Finite Element Models (FEM). For concept A the detailed Copernicus Sentinel-5P platform FEM has been used while the Sentinel-5P payload FEM has been replaced with a lump-mass and the FORUM-specific bipods. For Concept B, a coupled (payload and platform) FEM model has been used.

For both Concepts, the quasi-static and dynamic analysis has been performed considering the Vega-C mechanical environment, with the spacecraft located in the upper position of the VESPA-C long adaptor. The results of the dynamic analysis showed that the fundamental axial and longitudinal frequencies of both concepts are compliant with the Vega-C requirements. Quasi-static analysis confirmed the adequacy of the proposed design for Concept A and identified optimisation solutions for Concept B.

The results of the thermo-elastic analysis show that thermo-elastic deformation between the instrument LOS and the startracker optical heads stay within the allocated budget so that the overall system pointing budget can be met with margins.

Both concepts have been designed to minimise the effect of micro-vibrations. By embarking fixed deployable solar arrays, the reaction wheels remain the only source of micro-vibrations. These effects can be mitigated by appropriate accommodation.

5.3.4.3 Mechanisms

Solar arrays are first kept attached to the platform structure during launch and, then, release after launch by means of hold-down and release mechanisms. Both concepts use standard solutions, foreseeing the presence of hinges, a stiffener and a hold-down release mechanism based on thermal knives or non-explosive actuator, depending on the solar array supplier.

5.3.4.4 Thermal Control

The thermal control subsystem maintains all units located in the platform within their specific temperature ranges during all during the full mission lifetime.

For both concepts, the thermal control is based on both passive (filler, doubler, washer, paint, radiators and MLI blankets) and active (heaters and thermistors) hardware and relies on well-proven design concepts based on Copernicus Sentinel-5P, for Concept A, and on Proteus, for Concept B. The platform heat rejection is achieved by optimising the radiators size (1.7 m²) inherited from Sentinel-5P, in Concept A, and by accommodating about 3.3 m² of Second Surface Mirrors (SSM) on the four lateral panels, in Concept B. In Concept A, 26 heater lines are used on the platform and nine heater lines on the propulsion. For both Concepts, the satellite platform can provide the necessary heating power ranging from about 10 W, during nominal observation mode in hot case, to about 100 W, during the worst cold case scenario represented by the safe mode.

5.3.4.5 Electrical Architecture

The electrical architecture integrates the relevant platform and payload subsystems by distributing energy, signals, data and commands, enabling:

- The commanding and control of the satellite in all relevant operation modes
- The acquisition, storage and transmission to ground of payload, auxiliary and HKTM data
- The distribution of power from the generation and storage to all units.

The two concepts make use of similar well-proven architecture solutions and equipment based on Copernicus Sentinel-5P and Astrobus-M for Concept A (see Fig. 5.37), and Copernicus Sentinel-3 and Proteus for Concept B (see Fig. 5.38).

The command and control functions, executed by the OBC (Concept A) or the SMU (Concept B), are transferred to the platform and payload units via Spacewire for Concept A and via redundant MIL-1553B buses for Concept B.

The science data communication link from the payload to the PDHU is accomplished by a cross-trapped cold redundant Spacewire interface to allow high data transmission.

Power lines are designed for power bus voltages between 22 V and 37 V. Power lines distributing power from the solar arrays, PCDU and batteries are protected by controlled double insulation.

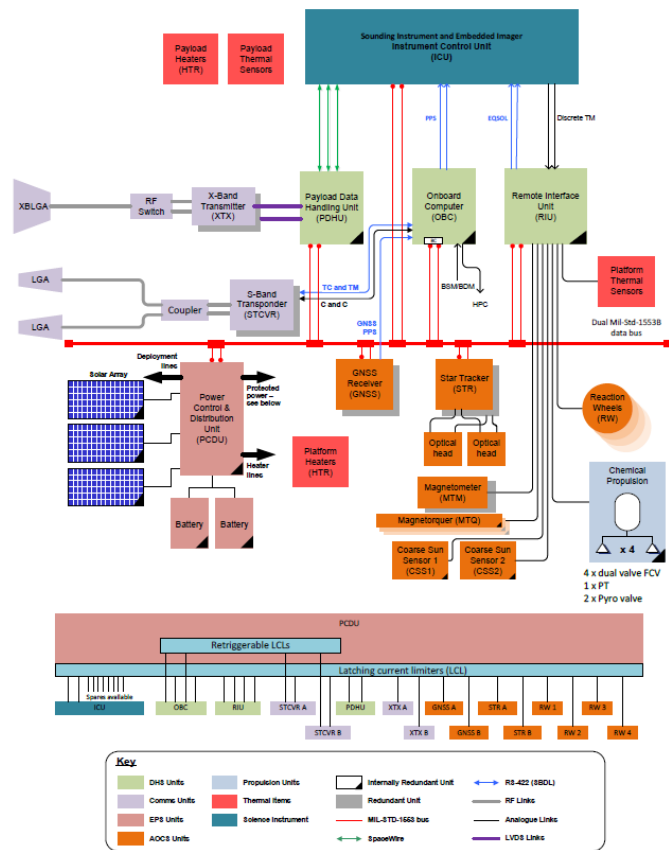


Figure 5.37 Top level electrical and avionic architecture for Concept A.

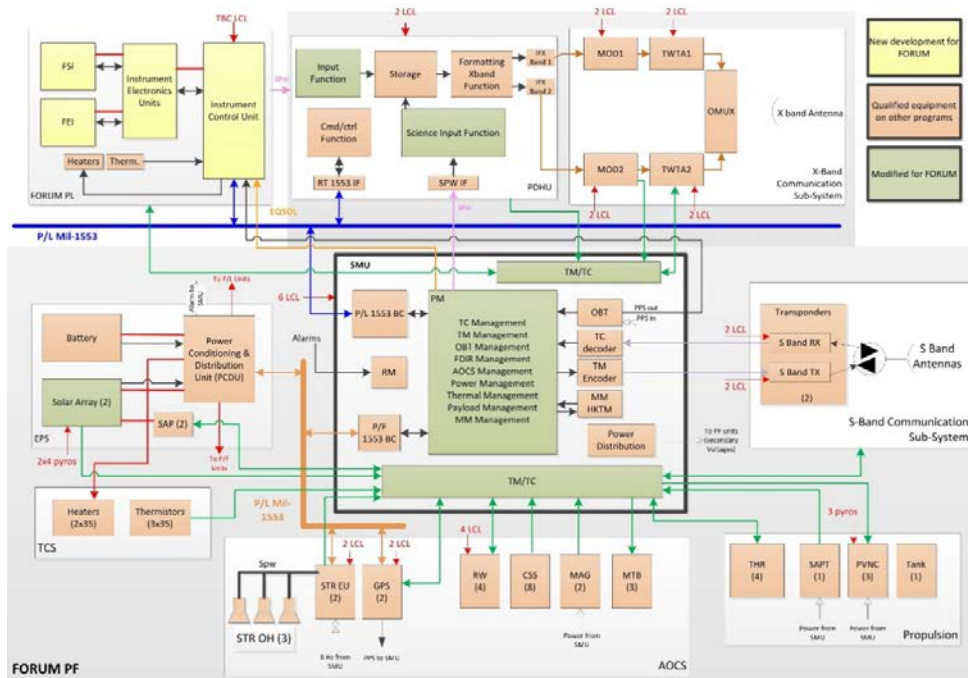


Figure 5.36 Top level electrical and avionic architecture for Concept B.

5.3.4.6 Command, Control and Data Handling

The Command, control and data handling subsystem, together with the electrical architecture, provides the following functions:

- Overall satellite command and control including AOCS algorithms in all relevant operation modes
- Running the onboard autonomy and FDIR
- Provision and distribution of ground- and software-issued commands to the satellite
- Collection and storage of satellite HKTM

For Concept A, the command and control architecture is based on two physical units: The OBC and the Remote Interface Unit (RIU). The OBC is a two-board fully-redundant computer based on a recurrent OSCAT Mk3 unit, which has evolved from the well-proven OSCAR 2 Mk2 on Sentinel-5P and Spot 6/7. One board implements the processor module (PM) and its input/output interfaces, the TM/TC and the reconfiguration unit (RU). The other generates all the power rails. Each PM is based on a LEON 3FT processor providing 256 MB CPU RAM and 512 MB exchange memory/mass memory RAM dimensioned to store HK data for up to 72 hours.

The RIU consists of two cold redundant units that augment the OBC interfaces providing, among others, the commanding of the three magnetorquers and the four reaction wheels and the thruster flow control valves.

The OBC and RIU combination provides the commanding and HK telemetry acquisition for both the platform and the payload.

For Concept B, the command, control and data handling subsystem re-uses the Sentinel-3 Satellite Management Unit (SMU), which provides the processing resources, the TMTC interfaces and the platform busses controller. The SMU manages the satellite operations, performs low-rate data handling, attitude and orbital control tasks. It is also responsible to manage the flow of housekeeping telemetry to the ground via the S-band transmitter. The SMU also provides the PPS time-code signals to all time-sensitive units in the satellite. It also provides dedicated discrete I/O interfaces for control and monitoring of the propulsion, power, thermal, mechanisms and instrument systems and provide standard interface sets, such as high power commands or thermistor monitoring. Finally, startrackers are managed by dedicated electronics units.

5.3.4.7 Payload Data Handling and Transmission

The payload Data Handling and Transmission (PDHT) subsystem, together with the electrical architecture, acquire, store and transmit to ground the scientific data generated by the payload. It consists of the Payload Data Handling Unit (PDHU), which includes one or more redundant Mass Memory Units (MMU), and the X-band downlink chain.

The payload data flow starts from the ICU, which ensures the transfer of data to the PDHU for storage until the next scheduled pass over the ground station. The MMU's inside the

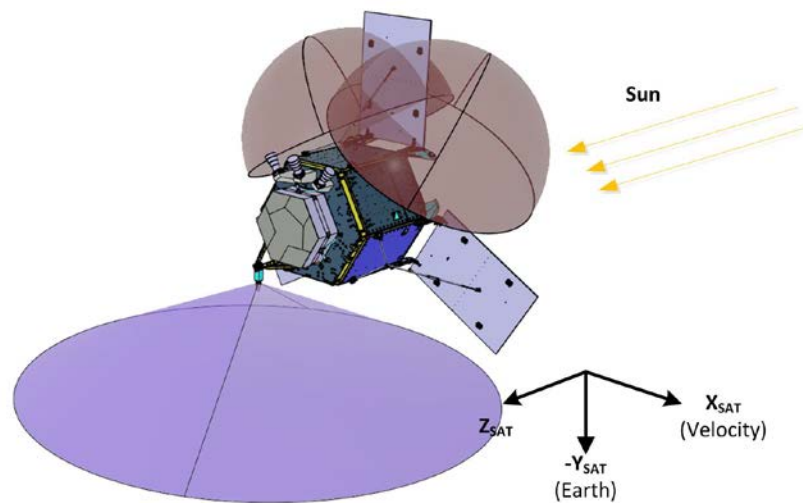


Figure 5.38 X-band antenna and GNSS antenna FOV for Concept A.

PDHU store the payload data, auxiliary data required for data processing (e.g. position, velocity and attitude data) as well as relevant platform and payload HKTM.

For both concepts, the architecture includes a redundant mass memory array and a simple, cold-redundant X-band downlink chain, featuring a modulator, amplifier, Travelling Wave Tube Amplifier (TWTA) a Radio Frequency (RF) switch and an isoflux fixed antenna (see Fig. 5.38) with an RF power of 4 W (Concept B) and 1 W (Concept A). The PDHU is cross-trapped in cold-redundancy with the ICU and the X-band downlink chain.

Both concepts generate onboard scientific data with an average rate of 1.82 Mbs^{-1} for Concept A, and 0.97 Mbs^{-1} , for Concept B, and then transmitted from the ICU to the PDHU where they are stored. According to these rates, Concept A will produce about 10 Gbit per orbit and about 150 Gbit in 24 hours, while Concept B will generate about 5.5 Gbit per orbit and about 84 Gbit per 24 hours. Concept A reuses the PDHT from Astrobus-M AS250 avionics (Sentinel-5P) while Concept B uses the baseline for the FLEX PDHT architecture. Both PCDU have a mass memory of about 2 Tbit which give to the satellite the capability to store more than one week of scientific data.

The payload data downlink speed to ground is 120 Mbs^{-1} for Concept A, which assumes QPSK modulation, and 270 Mbs^{-1} for Concept B, which assumes a 8PSK modulation. This architecture is compatible with two downlinks per day (24 h data aging) or one downlink per orbit (3 h data aging).

In Concept B, the HKTM generated and stored on board is downloaded within the X-band data stream, while in Concept A this function is not provided and only a subset of platform telemetry useful for data processing is included in the scientific data stream.

5.3.4.8 Electrical Power

The electrical power subsystem, together with the electrical architecture, supports the following functions:

- Generation of power



- Energy storage
- Power regulation and distribution to all equipment

The average power consumption is about 432 W for Concept A and 439 W for Concept B. Both concepts present classic and flight-proven power architectures with classic design solutions.

An internally redundant Power Conditioning and Distribution Unit (PCDU) is responsible for distributing power from the solar arrays and the battery to the platform and to the relevant payload equipment, providing power and battery charge control and monitoring. Both concepts implement a Direct-Energy-Transfer (DET) power-conditioning scheme comprising a classic architecture based on Sentinel-5P (Concept A) and FLEX and Sentinel-3 (Concept B). The PCDU distributes power via single power lines that are protected by Latching Current Limiters (LCL). Critical components, namely OBC and S-band transponder, are connected through resettable current limits, which maintain power to the protected unit even after an anomaly. Both concepts use a non-regulated 28 V power bus based on direct connection to the batteries and ranging in voltage between 22 V and 34 V for the operation mode for Concept A and between 24 V and 37 V for Concept B, hence compatible with the power needs.

Power is generated by body-mounted deployable solar arrays. In Concept A, the solar array has three wings distributed in a petal configuration, each with an available area of 5.6 m². In Concept B, there are two 3.25 m² wings with three panels each. Both cases use triple-junction gallium-arsenide cells with efficiency of 29.5% at the beginning of life. The maximum power generated at End of Life (EOL) is about 760 W for both concepts. The solar panels are stowed against the panels of the structure during launch, and release autonomously by the onboard software after separation from the launcher. Concept A will use recurring units with additional power margin in excess of 15%, while Concept B will use an up-scaled version of the FLEX solar arrays.

Both concepts have baselined off-the-shelf batteries with heritage from previous missions. The batteries are charged during daylight operations thanks to the excess power generated by the solar array while they are used in eclipse and during contingency operations. The battery consists of two modules of lithium-ion stackable decks in a 8s104p configuration with a capacity of 4500 Wh (BOL) for Concept A, and one module of 216 NL cells in a configuration of 9s24pa and a capacity of 57.6 Ah for Concept B. During nominal operation battery Depth of Discharge (DoD) is on average 16% for Concept A while it is slightly above 20% for Concept B.

A complete passivation of the power subsystem is performed once the satellite reaches the end of its operational life. All the energy stored in the battery will be depleted and the solar array will be prevented from recharging. This prevents any potential explosion, minimising impact on space debris.

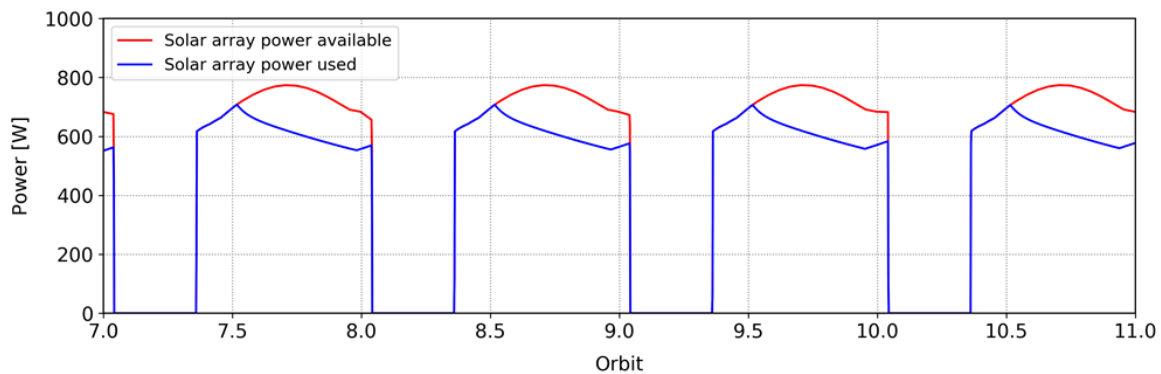


Figure 5.39 Power consumption and generation profile for Concept A.

5.3.4.9 TT&C

The TT&C subsystem provides S-band communication capabilities between the satellite and the ground stations and support the following functions:

- Command reception, for reception and demodulation of commands sent from the ground station
- Telemetry transmission, for modulation and transmission of HK data to the ground
- Ranging and Doppler tracking providing range and range-rate determination as back-up of the onboard GNSS receiver data for orbit determination in the event of an emergency and during LEOP

The TT&C functions are implement for both concepts via a traditional and flight proven architecture (Concept A based on Astrobus AS250 avionics inherited from Sentinel-5p and Concept B based on Sentinel-3 inherited avionics) using a functional chain consisting of two S-band transponders connected to two S-band low-gain hemispherical omnidirectional antennas via a 3 dB hybrid splitter/coupler. The receivers work in hot redundancy while the transmitters function using cold redundancy. Fig. 5.40 shows the configuration of the S-band antennas and their unobstructed field of view.

Two omnidirectional antenna ensures a communication link for all possible attitude of the satellite in nominal and non-nominal conditions.

Concept A is designed to download to ground all the realtime and the recorded HKTM via the S-band link. Operationally, the satellite is expected to perform parallel dumping of HKTM data through two different channels towards the TT&C ground station at least twice per day.

On the other hand, Concept B TT&C design expects only transmission of realtime HKTM during nominal operations because recorded HKTM are dumped via the X-band link and the ground station dedicated to scientific data acquisition. Playback recorded telemetry can be downloaded also through the S-band link in case of contingency operation (e.g. failure of the X-band link).

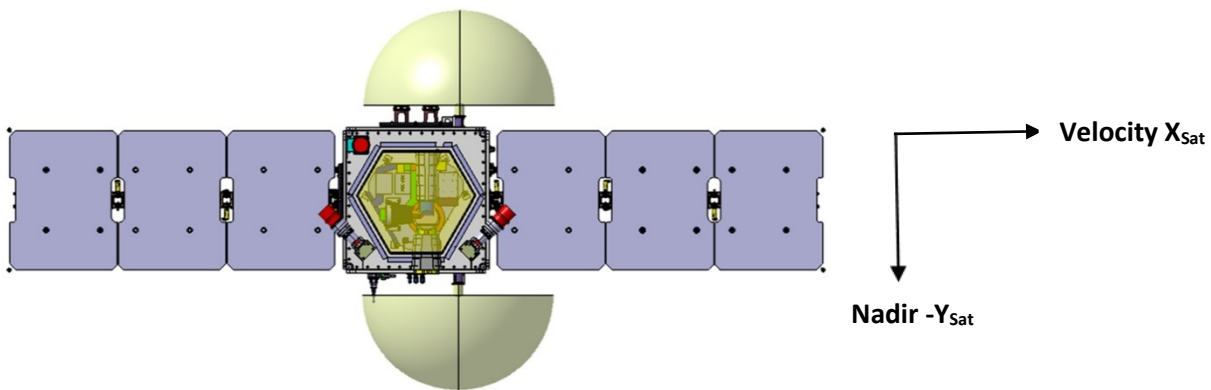


Figure 5.40 S-band antenna FOV for Concept B.

Telecommands are uplinked at a rate of 64 kb s^{-1} through the TT&C ground station, while two operational modes are used to downlink the telemetry data. A low data-rate link transmitting at 124 kb s^{-1} and using a SP-L/PM modulation scheme is available when ranging function is activated (LEOP and contingency operations due to GNSS failure). During nominal download operations, a high telemetry transmission data rate is available at 2 Mb s^{-1} for both concepts. By accounting for an onboard telemetry data generation of 8 kb s^{-1} for Concept A and of 14 kb s^{-1} for Concept B, S-band download performances allows for the transmission of 72 hours of recorded HKTМ to TT&C ground station in few consecutive orbits (4 to 6). When required by a contingency event, this will allow ground operators to acquire onboard telemetry data useful to identify and analyse anomalies.

5.3.4.10 AOCS

5.3.4.10.1 AOCS Architecture

Both concepts baseline a three-axis stabilised spacecraft with an attitude and AOCS based on a gyro-less architecture constituted (see 5.4.2) by flight-proven sensors, to determine attitude and orbit position, and actuators to control attitude and perform orbit manoeuvres.

The AOCS software implements several modes of operations, which are similar for both concepts. Each mode relays on a specific set of sensors and actuators (see Table 5.10), which allow the implementation of the necessary actions throughout the mission life, from launch and separation to decommissioning, including, nominal, contingency and manoeuvring operations. Main modes mostly comprise several sub-modes. Shifts from one mode to another is done via telecommand or automatically, except for recovery from safe mode and initiation of control mode, for which a ground control intervention is mandatory for safety reasons.

5.3.4.10.2 Initial Acquisition and Safe Mode

This mode is active as of satellite separation from the launcher or triggered by the FDIR after detection of a critical failure. It aims to reduce the residual angular momentum and acquire an attitude necessary for starting solar power generation. Starting from any arbitrary

Equipment	Redundancy	Modes		
		SAFE	NOM	OCM
Sun sensors (CSS)	1 internally redundant (Concept A) 2 branches of 4 in hot redundancy (Concept B)	X		
GNSS receiver	2 units in cold redundancy		X	X
Startracker (STR)	2 electronics in cold redundancy + 3 optical heads in hot redundancy		X	X
Magnetometer (MAG)	2 units in cold redundancy	X		
Magnetorquer (MTQ)	3 units internally redundant	X	X	X
Reaction wheels (RW)	4 units in hot redundancy	X	X	X
Propulsion system	4x1N thrusters			X

Table 5.10 AOCs equipment vs. AOCs modes for FORUM Concepts A and B.

orientation and angular rate, the satellite is driven and maintained in a Sun-pointing attitude. In this mode, only vital satellite functions are maintained and the satellite is put into safe conditions where it is able to survive for the time necessary to solve the contingency. Coarse Sun sensors and magnetometers provide the satellite attitude estimation while magnetotorquers and reaction wheels perform the necessary control functions.

This mode has no provision to avoid Sun intrusion within the payload FOV, since both concepts implement measures to prevent Sun intrusion in the optical path. Concept A implements a shutter mechanism and Concept B positions the mirror of the pointing mechanism in a safe configuration.

5.3.4.10.3 Nominal Operation Mode

The nominal mode ensures the accurate three-axis stabilisation of the satellite during scientific observations and instrument calibration. Attitude estimation is achieved through startracker measurements, orbit navigation through GNSS and attitude actuation using reaction wheels. Angular momentum accumulation is off-loaded by magnetotorquer bars using an onboard magnetic field model. The platform also performs a sinusoidal yaw steering manoeuvre to compensate for the rotation of Earth, while the instrument scanning mirror compensates for the relative motion the satellite with respect to ground during the 14 seconds FSI dwell time. These relative motion compensation strategies remove the largest components of the FSI LOS drift, however small drifts in the order of meters, peaking to tens of meters at the poles, still remain, but allowing to meet the requirements.

5.3.4.10.4 Orbit Control Mode

This mode is in charge of performing any in-plane and out-of-plane orbit manoeuvres during the commissioning, nominal and EOL phases, as well as controlling the formation and any collision avoidance manoeuvre. All manoeuvres are performed using thrusters. Reaction wheels, in-orbit control mode for Concept A and in nominal mode for Concept B, are used to perform slew manoeuvres before and after the thrust to properly orient the satellite. Concept A implements non-tilted thrusters, two axes are controlled through off modulation of the

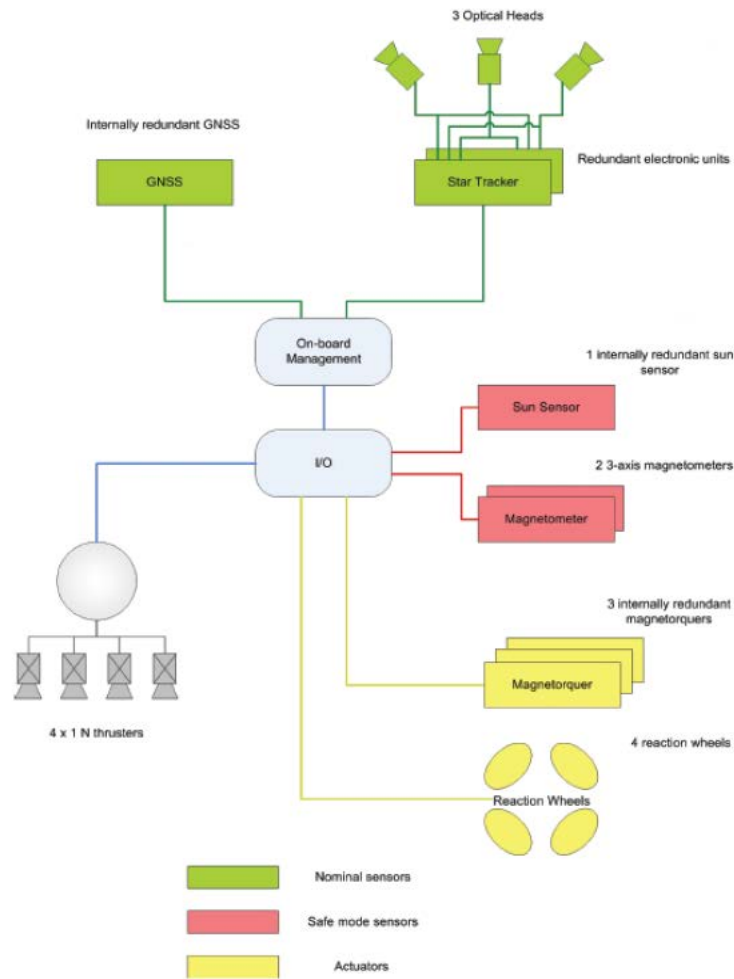


Figure 5.41 Concept A AOCs Architecture.

thrusters, whilst the third axis is controlled with the reaction wheels. Concept B accommodates tilted thrusters (see Fig. 5.42 left) and can use pulse off modulation to unload wheel angular momentum. Attitude estimation during orbit control mode is achieved through startracker measurements, and orbit navigation through GNSS.

5.3.4.10.5 Other Modes

Concept B implements a transition mode that manages the transition from the Sun pointing to nominal mission pointing attitude. This mode uses startracker and GNSS measurements and manages autonomously the attitude slew to avoid any Earth or Sun blinding of the startracker.

5.3.4.10.6 Pointing Budgets

The instrument and platform attitude errors contribute to the pointing and geolocation performances, which can be budgeted in terms on Absolute Pointing Error (APE), Relative Pointing Error (RPE) and Absolute Knowledge Error (AKE), shown in Table 5.11.

Error Contributors	Concept A						Concept B					
	AKE		APE		RPE		AKE		APE		RPE	
	AT	ACT	AT	ACT	AT	ACT	AT	ACT	AT	ACT	AT	ACT
Bias AT/ACT [μ rad]	591	565	591	565	0	0	306	295	877	885	12	13
Bias [μ rad]	817		817		0		425		1246		18	
Harmonic AT/ACT [μ rad]	7	44	12	78	12	40	278	293	278	295	0	2
Harmonic [μ rad]	45		79		42		404		405		2	
Random AT/ACT [μ rad]	31	11	36	13	38	16	12	13	44	45	44	46
Random [μ rad]	33		39		41		18		62		63	
Total [μrad]	895		935		83		847		1713		82	
Total (computed @ altitude 830km) [m]	743		776		69		703		1423		68	

Table 5.11. Pointing budget summary for both concepts.

The pointing error budget takes into consideration the following errors:

- Time-Constant Errors (or Bias) contributing linearly to the budget:
 - AIV (e.g. Startracker integration and Payload Integration)
 - In-orbit Factor: E.g. 1–10 g offload, Flight temperature distortion.
 - AOCS Accuracy, Startracker bias and aging effects for electronics and AOCS
 - FSI and FEI Alignment
 - Mechanism Accuracy for the Pointing unit and Scan unit
- Time-Variable Harmonic Errors, contributing linearly to the budget:
 - Platform and instrument Thermo-Elastic Distortion and errors
 - Orbit Error from Line of Sight (e.g. yaw steering law error)
 - Scanning Velocity error
- Time-Variable Random Errors contributed RSS to the budget:
 - Platform and payload Random Environment including micro-vibration
 - Orbit Model Error. e.g. geoid model errors
 - AOCS Stability and control rate, startracker noise, AOCS controller error
 - Scanning mechanism control errors

5.3.4.11 Navigation and Time Generation and Distribution

The navigation subsystem is in charge of generating a reference time signal, which is distributed to other units for direct use or for co-relation with other time references generated by other clocks. The GNSS also provides autonomous in-orbit navigation and determination for normal operations, including orbit corrections. PVT (Position, Velocity and time) is calculated and transmitted by the OBC as required for use in the AOCS and TT&C subsystem. At 1 Hz a PVT message and attitude quaternions is sent to the instrument control unit which embeds this information within the science data downlinked each orbit. This signal is also used to co-related the interferometer sweeps and the pointing mechanism with a reference onboard time.

Both Concepts implement TT&C ranging function to support LEOP operations and GNSS failures. Furthermore, for Concept A, an accurate onboard orbit propagator is proposed too in order to propagate the orbit in case of transit GNSS system outage.

For both concepts the baseline consists of two GNSS units, with two antenna operated in cold redundancy.

5.3.4.12 Propulsion

The FORUM propulsion subsystem provides the necessary thrust for correction of launcher injection errors, for orbit control manoeuvres and for the EOL de-orbiting manoeuvres. Both concepts use standard and well-proven solutions based on a mono-propellant hydrazine system, pressurized with helium for Concept A (see Fig 5.42 right) and nitrogen for Concept B and operated in blow-down mode.

Concept A baselined propulsion system is the recurrent PM-22 module developed by Arianespace which has already flown on Sentinel-5P, SPOT 6/7. It offers a maximum fuel storage capacity of 82 kg, giving about 6 kg more fuel than the mission needs. Concept B propulsion subsystem reuses flight proven units, such as Sentinel-3 or Exomars, and equipment for which the qualification is in progress in the frame of FLEX. The tank offers a maximum fuel capacity of 45 kg, offering about 3.5 kg margin with respect to the mission needs.

Four 1N thrusters are accommodated on the bottom panel. This means, before any manoeuvre, the satellite will be reoriented with a slew manoeuvre through the activation of the AOCS actuators. In Concept A the thrusters are parallel and aligned with the Z axis of the satellite. In Concept B, the thrusters are slightly tilted to provide capability of generating torque and support for the attitude control if necessary (see Fig. 5.42 left). For both concepts, the thrusters are configured in two pairs providing the means to comply with all thrust needs for every manoeuvre during the mission lifetime. Actually, the propulsion subsystems are

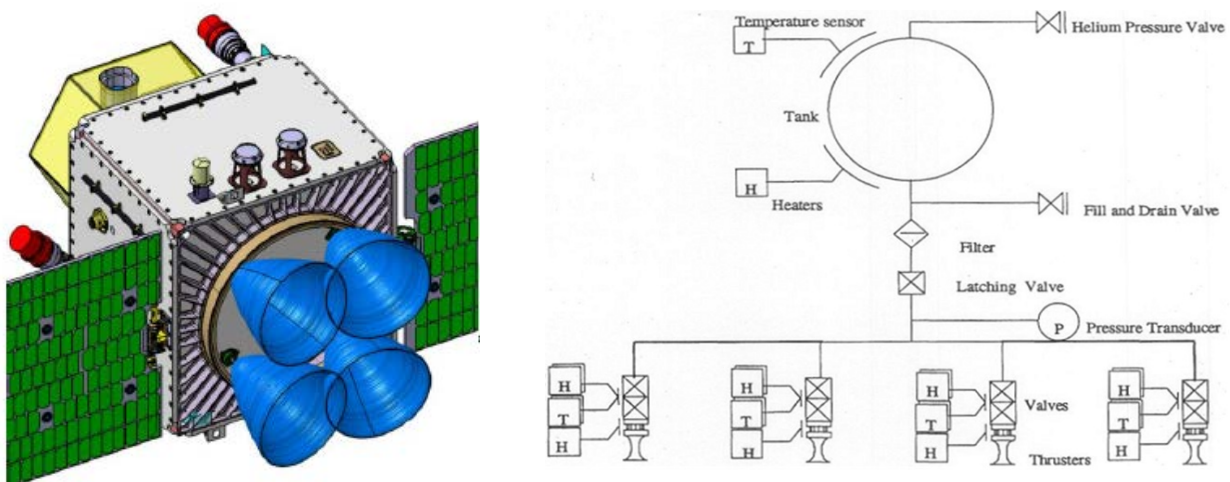


Figure 5.42 Orientation of the thruster plumes for Concept B (left) and propulsion subsystem schematic for Concept A (right).



able to generate sustained 4N thrust for large manoeuvres as well as minimum impulse of less than 0.3 mm/s in Concept A and less than 0.5 mm/s in Concept B, in line with the manoeuvring accuracy required to ensure orbit maintenance and formation flight control. The thrusters operate in cold redundancy allowing for the isolation of a failure thruster and the operation of the second set of thrusters to ensure the continuation of the mission.

In order to comply with the ESA requirements on debris mitigation, which impose the complete depletion of all the energy sources stored on board after the operation phase, the propellant tank will be completely emptied when the deorbiting manoeuvre has been completed. The use of pyro-valves, which when opened, allows complete depletion of all the propellant residuals is considered in both concepts either as baseline (Concept B) or as an option (Concept A).

5.3.4.13 Software

The FORUM software architecture is based on standard modular architectural design principles inherited from AstroBus Earth observation missions, the PUS product and the OSCAR OBC, for Concept A and for Proteus based projects and Sentinel for Concept B.

For Concept A, this modular architecture allows flight-proven solutions to be combined with mission adaptation and features two main layers:

- A standardised execution platform software: providing all services to implement the application processes including realtime kernel, input/output System, PUS Services and finally the application interface and framework.
- Application process software: implementing the functional of the software (e.g. satellite initialisation, AOCS functions, payload management, FDIR) based on the application interface and framework provided by the execution platform software.
- In addition to the OBC hosting the CSW, payload, the startracker, the GNSS receiver and the PDHU contain flight software that may need to be adapted.

For Concept B, the following software components will be adapted:

- OBSW – application: platform onboard application software fully FORUM specific
- OBSW – boot: platform onboard boot software
- STR SW: startracker software
- GNSS SW: GNSS software
- Instrument SW: ICU software

5.3.5 Budgets

5.3.5.1 Mass and Power Margin Philosophy

Table 5.12 shows the mass and power margins applied to any unit. An additional 15% margin at system level has been applied to the mass and power budget against unpredictable mass and power evolutions.

5.3.5.2 Power Budget

FORUM power consumption will vary according to the operational modes. Observation and downlink mode is expected to be the most power demanding because payload instrument and electronics operate together with the PDHT. The safe mode is characterised by the minimum power consumption. Table 5.13 reports the power budgets for the two concepts, focusing on the total power consumption needs for the various operational modes.

5.3.5.3 Mass Budget

Table 5.14 reports the mass budgets for both concepts studied. Concept A is heavier than Concept B. Concept A is based on a medium class type of platform, while, Concept B takes advantage of a small class bus. This is true, in particular, for structure and propulsion module masses, as well as for the available onboard propellant. Nevertheless, for both concepts, it will be possible to accommodate the satellite in Vega-C dual launch configuration by ensuring a sufficient mass allocation for a secondary passenger.

5.3.5.4 Delta-V and Propellant Budget

The delta-V budgets and the related propellant needs are summarised in Table 5.16. Slight differences between concepts appears due to the solutions applied to reach the operational orbit and because of different formation flight acquisition and maintenance strategies. Furthermore, Concept B propellant needs are relatively low thanks to the lighter design than Concept A. Propellant margin would allow an extension of the lifetime of more than 2 years for both concepts.

Type of unit/ Equipment	Mass and power budget Unit margins
Harness	30 %
New units/equipment	20%
Modified units/equipment	10%
Recurrent units/equipment	5%

Table 5.12: Mass and power unit margin.

Operating Mode	Concept A	Concept B
Safe Mode [W]	349	404
Orbit Control Mode [W]	292	466
Observation [W]	426	436
Observation and Downlink [W]	485	561
Observation in eclipse [W]	426	445
Observation and Downlink in eclipse [W]	485	570
Nominal (orbit average) [W]	432	439

Table 5.13: Power budget for Concept A and B.

	Concept A	Concept B
Data Handling [kg]	17	21
Electrical Power S/S [kg]	96	79
Harness [kg]	63	27
X-band comm S/S [kg]	14	14
S-band comm S/S [kg]	7	4
AOCS [kg]	63	48
Structure [kg]	223	109
Thermal S/S [kg]	34	10
Propulsion [kg]	29	15
Platform Total [kg]	547	327
Payload Total [kg]	107	124
Dry Mass Total [kg]	654	451
System mass margin (15%) [kg]	98	68
Balance Mass [kg]	15	4
Dry Mass with margin [kg]	767	523
Propellant [kg]	82	45
Wet Mass [kg]	850	568
Launcher performance [kg]	2020	2020
Launcher adapter [kg] (Vespa long)	575	575
Launch margin (mass available for secondary passenger) [kg]	595	877
Launch margin w.r.t. LV performance [%]	29%	43%

Table 5.14: Mass budget for Concept A and B.

	Concept A	Concept B
Instrument data rate [Mbs ⁻¹]	1.82	0.46
Downlink rate [Mbs ⁻¹]	120	270
Average instrument duty cycle [%]	100%	100%
Mass memory requirement [GB]	138	35
Mass memory size EOL [GB]	250	230
Mass memory margin [%]	45%	85%

Table 5.15: Data rate and volume budgets for Concept A and B.

Delta-v [m/s]	Concept A	Concept B
Orbit injection correction and formation acquisition	32.5	26.1
Orbit maintenance	39.8	24
Collision avoidance	2.0	4.3
Deorbit manoeuvre	105.6	83.7
Total	179.9	138.1
Propellant mass incl. residuals [kg]	71.9	39.16
Total (incl. 15% margin)	76.2	41.35
Tank capacity [kg]	82.3	45
Propellant margin [kg]	6.13	3.65
Propellant margin [%]	7%	8%

Table 5.16: Delta-V and propellant mass budget for Concept A and B.

Elements	Concept A	Concept B
	Mass [Kg]	Mass [Kg]
S/C	850	568
VESPA-C (LONG)	455	455
PLA 937	120	120
Total	1425	1143
Launcher performance	2020	2020
Mass margin (mass available for secondary passenger)	595 (29%)	877 (43%)

Table 5.17: Vega-C performance and mass allowance for the second passenger.

5.4 Launcher

Vega-C is the baseline launch vehicle, used in dual launch configuration. The spacecraft can be accommodated on top or inside the Vega Secondary Payload Adapter (VESPA) structure, as shown in Fig. 5.43 and Fig. 5.44. Two versions of VESPA will be available: a long version, which enhances the allocated volume for the lower satellite, and a short version, which give more space to the upper satellite. The FORUM satellite is compatible with the upper position of both versions of VESPA, with large volume margins. In the lower position, however, FORUM is only compatible with the long version of VESPA for both concepts. Concept A with no margin due to the position of the S-band antenna and Concept B with more than 20% volume margin.

Both concepts accommodate a 937-mm standard launcher interface ring with clamp-band and push springs as release mechanisms from the launcher vehicle. The backup launcher is Ariane 6.2, which will replace Arianespace Soyuz in the 2025 timeframe. It represents a European backup that comfortably envelopes the size and performance of Vega-C providing

equivalent or even improved dual launch capability. Furthermore, selection of a Kourou-based alternative adheres to the ESA launch policy and offers the benefit that launch range requirements, procedures and safety requirements are broadly similar to those of the nominal option. A first assessment has confirmed the compatibility of the mechanical design with the backup launcher.



Figure 5.43 Concept A accommodation in the Vega-C fairing, inside (left) and on top (right) of the VESPA-long.

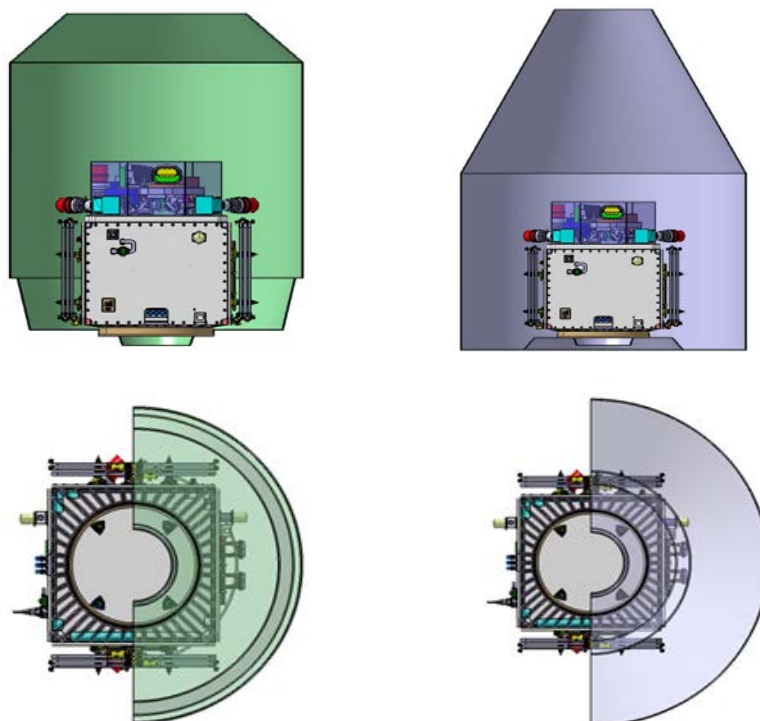


Figure 5.44 Concept B accommodation in Vega-C fairing, inside (left) and on top (right) of the VESPA-long.

5.5 Ground Segment and Data Processing

5.5.1 Overview of Ground Segment Elements

The current generation of Earth Explorers ground segments uses generic components configured or adapted to each satellite. In line with this approach, the FORUM ground segment comprises two main components: the FOS and the PDGS as shown in Fig. 5.45. The FOS includes the TT&C ground station and the FOCC. The TT&C ground station provides the following main functions:

- HKTМ acquisition and telecommand uplink
- Satellite tracking
- Data connection to the FOCC

During LEOP, a dedicated ground station network supports the operations. This network uses Estrack core and enhanced stations where possible. The FOCC is based at ESOC and will provide the following main functions:

- Satellite monitoring and control
- Flight dynamics and manoeuvre planning
- TT&C ground station network control
- Overall software maintenance
- Mission simulation
- FOS supervision
- Spacecraft system data distribution
- Interface with the launch site for LEOP

The PDGS is responsible primarily for receiving the science data from the satellite, applying the appropriate processing algorithms and delivering the data products to the users. It comprises the following functions:

- Payload data acquisition and ingestion for downlink of science data telemetry
- Processing, archiving and dissemination
- Mission planning
- Monitoring, quality control and calibration/validation
- User segment/service
- The FOS and PDGS are design as independent as possible. Existing interface formats and specifications supported by the ESA infrastructure software are used wherever applicable.

5.5.2 Flight Operation Segment

The FOS is responsible for the spacecraft operations control and monitoring during all mission phases. Operations control and monitoring activities include housekeeping telemetry, performance monitoring, telecommanding of all activities, orbit control, constellation monitoring and control, reaction to space debris conjunction warnings, on board software maintenance and mission planning. The FORUM FOS is based on existing ESA hardware and software adapted to the FORUM mission where necessary.

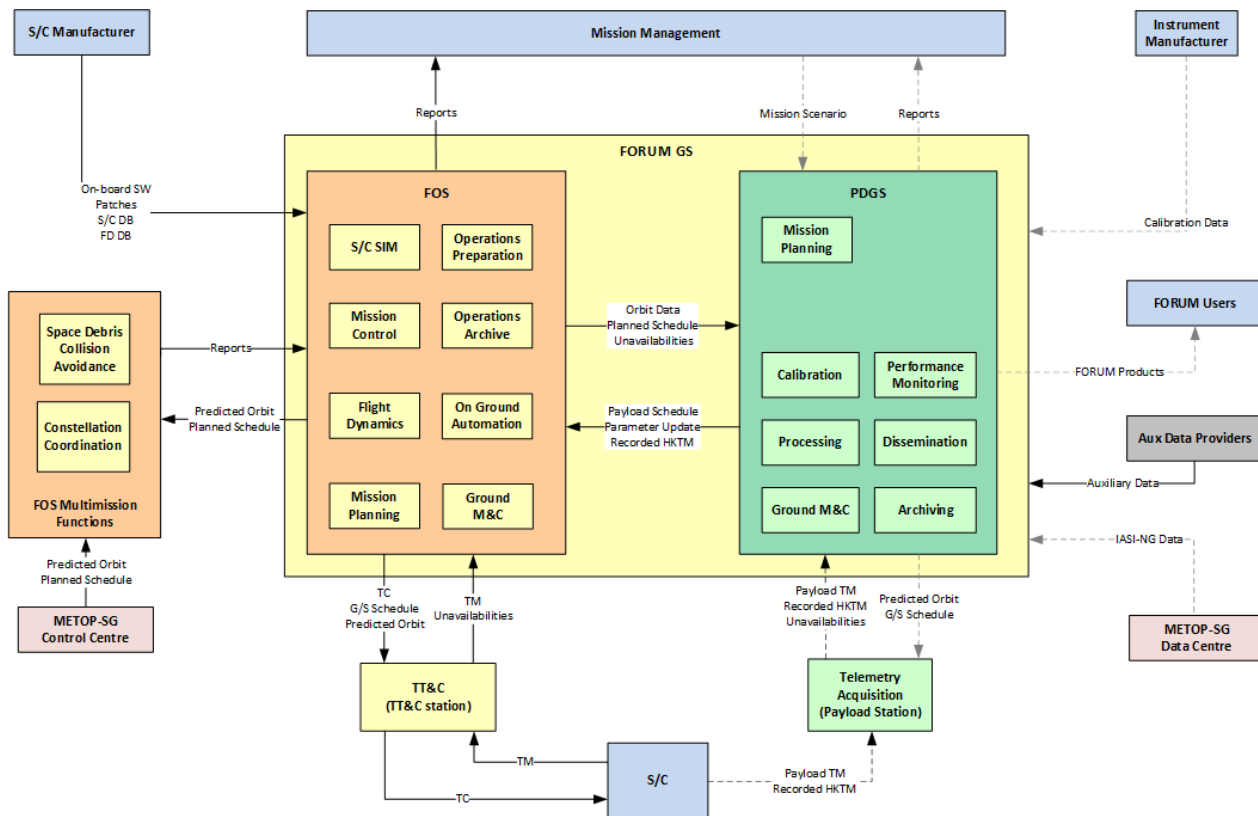


Figure 5.45 Ground segment architecture for both Concept A and B.

5.5.2.1 Telemetry, Tracking and Command (TT&C)

The FORUM spacecraft provides S-band for TT&C capability and X-band for high speed downlink of stored scientific data.

The operations concept for the FORUM mission routine phase foresees two TT&C passes per day during nominal working hours and additional TT&C passes under request after orbit control manoeuvres, to confirm successful manoeuvres execution. Either the Kiruna or Svalbard ground stations are foreseen as the baseline TT&C ground station making use of the combined S- and X-band capability. Additional TT&C stations will be available during LEOP. No specific modifications/upgrades of the proposed S- and X-band ground station network are needed in support of FORUM operations.

GNSS data is used as input to the orbit determination process, although tracking data collected during S-band passes can also be used for orbit determination, if required. Planning of the TT&C ground station passes can either be based on pre-agreed standing order requests or, if combined S- and X-band, in combination with PDGS activities.

FORUM TT&C passes will be scheduled independently from MetOp-SG(1A) TT&C in a different or the same ground station site. The ESTRACK Management and Scheduling System (EMS) will execute all scheduling of the FORUM ground station TT&C passes.

5.5.2.2 Mission Control System (MCS)

The main functions of the MCS are to manage all flight operations of the spacecraft, during both real-time activities when in TT&C contact with a ground station and all non-real time operational activities. The MCS is based on the Earth Explorer MCS, which is an extension of SCOS-2000, or its successor EGOS-CC. Customisation of the MCS to support the FORUM specific mission databases, ground interface specifications, the final operations concept, will be carried out using the existing capabilities of the MCS.

There are no requirements to coordinate the MCS with the MetOp-SG MCS.

5.5.2.3 Flight Dynamics (FD)

FD service delivers orbit information and orbit related event files to the various planning entities and ground stations. FD supports the generation of the parameters needed as input to manoeuvres telecommand sequences and to execute monitoring of the spacecraft. The FD service will receive regular updates of the MetOp-SG(1A) orbit to plan and co-ordinate the associated FORUM orbit and formation flying manoeuvres.

The ESOC Earth observation FDS infrastructures will be re-used for FORUM. Mission specific customization will be carried out to support the external interfaces i.e. orbit and status data exchange with MetOp-SG(1A) MCS, FORUM ground station network, format specific updates e.g. GNSS receiver data formats, satellite telecommand parameters for orbit manoeuvres, etc.

The monitoring of the loose formation flying with MetOp-SG(1A) shall be performed by the Constellation Coordination System (ESA-CCS). Which is a centralised multimission tool for monitoring satellite constellation configurations enabling information exchange between geographically distributed mission operations centres.

The ESOC Space Debris Office (SDO) provides the space debris monitoring and collision avoidance service. In the event of conjunction warnings the SDO provides the related data allowing the SDO, FCT, FD teams to assess the risk and establish the needs for executing collision avoidance manoeuvres. All conjunction data will be shared with MetOp-SG(1A) MCC and any collision avoidance manoeuvres coordinated with MetOp-SG(1A).

5.5.2.4 Mission Planning System (MPS)

The MPS is provided as part of the MCS and will be tailored for FORUM to receive input files from PDGS (science, payload, operations), FD, ESTRACK scheduling and FCTs. The output of the ESOC mission planning are conflict-free schedules to drive the automated pass activities of the MCS and ground stations, and the mission timeline command sequences (in UTC or orbit position) for loading into the satellite mission timelines.

The MPS will require configuration in accordance with the mission constraints laid down in the Flight Operations Procedures.

5.5.2.5 FOS Operational Approach and Implementation

During routine phase, operations are automated as far as possible to reduce manpower requirements. The FOS is nominally manned during working hours, five days per week. In case of critical events/ anomalies outside of these working hours, the on-call engineer is alerted. Immediate response to failures out of working hours is not required. Assessment of the impact of any anomalies, safe-modes, conjunction warnings and ESA-CCS generated alerts will be carried out by the FORUM and the SDO /FD on call service, as required. Any anomaly responses shall be coordinated as necessary with the MetOp-SG(1A) MCC. The FORUM orbit is such that the formation flying strategy provides a passive-safe scenario in which no immediate reaction is needed to avoid a collision event between the MetOp-SG(1A) and FORUM satellites.

During LEOP, operations are supported by a network of LEOP dedicated ground stations using both ESTRACK Core (i.e. Kiruna) and Augmented stations (i.e. Svalbard or Troll), see Fig. 5.46. The specific ground stations to be used during FORUM LEOP will be driven by the launcher selection and launch orbit characteristics.

The FOS operational approach for LEOP is to have a full FCT available for the LEOP activities covering the foreseen LEOP period (nominally 3 days), 24 hours a day split into two shifts. The autonomous initialization sequence that will handle the Solar Arrays deployment, the AOCs activities and the S-band TM activation.

For routine phase a team within the ESOC Earth observation division will be available maximizing shared resources with operational activities coordinated through the Satellite Operations Manager (SOM). Contact with the pre-defined set of ground stations is automated driven by the ESOC scheduling and planning service and monitored by ESTRACK (24/7 availability). Execution of the ground station passes is automated to allow both manned and unmanned passes to be taken from the MCS. Depending on the specific implementation for FORUM two TT&C passes are foreseen to be executed per day, which can be selected to occur during working hours.

Daily operations will be characterised by the use of automated timelines both on board and ground supported by weekly FOS mission planning. There is no requirement for realtime re-

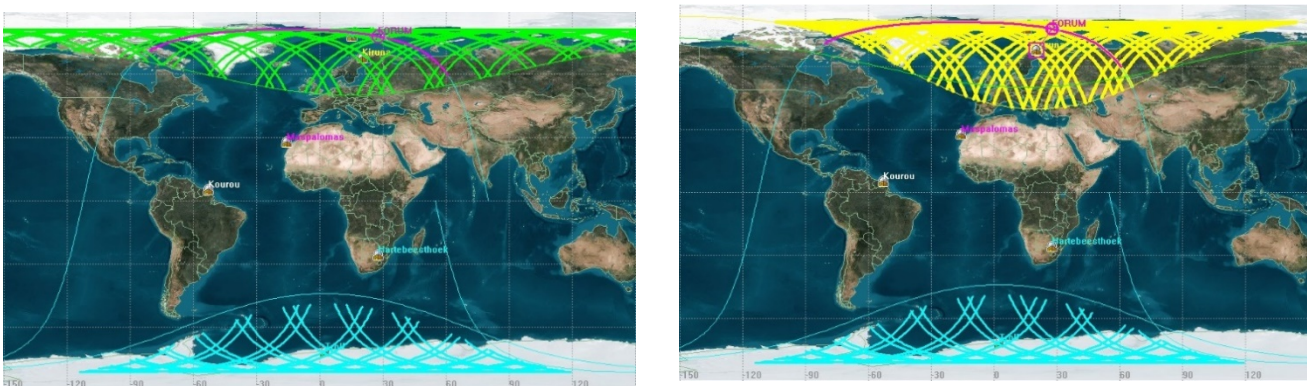


Figure 5.46 Ground station contact areas Svalbard and Troll (left) and ground station contact areas Kiruna and Troll (right)



planning of schedules nor out-of-hours mission planning support. Telemetry monitoring is autonomously executed by the MCS taking the housekeeping TM received in real time and playback data dumped during ground station passes. All alerts, out of limits, or non-nominal events are reported and analysed by the FCT engineers.

The external inputs to the FORUM FOS are orbit and manoeuvre data from MetOp-SG(1A) provided by MetOp-SG MCC. This information is required to monitor the loose flying formation between FORUM and MetOp-SG(1A) and to plan the FORUM orbit control manoeuvres to maintain this formation.

5.5.3 Payload Data Ground Segment

FORUM uses the generic, but satellite configurable, PDGS components developed for previous Earth Explorers. Thus, a standardised PDGS provides the following functions:

- Payload data acquisition and ingestion for downlink of science data telemetry
- Processing and reprocessing
- Archiving, user services and dissemination
- Mission planning
- Calibration and Validation
- Instrument performance and monitoring

5.5.3.1 Payload Data Acquisition and Ingestion

Science data along with recorded HKTM downlink will be performed via X-band. The choice of the acquisition station is mainly driven by the data latency. For the threshold latency of 24 hours, it is sufficient to download data twice per day. Such a service can be provided by a single station like Kiruna and possibly a lower latitude station. On the other hand, a data latency of three hours requires one downlink per orbit. A single high-latitude station such as Svalbard or a combination of stations is required in this case.

MetOp-SG(1A) does not impose specific constraints on the selection of FORUM X-band stations. The risk of interferences in case of using the same station is removed by the fact that both satellites are always distant by at least 0.1 deg and the additional possibility to use different X-band frequency ranges for FORUM versus the ones used by MetOp-SG(1A) (7750-7900 MHz). The absence of potential conflicts also simplifies the task of the PDGS mission planning facility in charge of planning X-band downlinks.

5.5.3.2 Processing and Reprocessing

The PDGS processing function is in charge of generating Level-0, -1b and -1c products for the two instruments. The PDGS is also expected to generate Level-2 products. Higher-level synergistic products between FORUM and IASI-NG may also be produced.

The processing function operates systematically and in a data-driven manner using as main input the science raw data generated by the telemetry acquisition function as well as auxiliary data as secondary inputs.

The update of ground processors occurring during Phase E require reprocessing of historical data to maintain consistent product quality. While reprocessing of limited datasets is

Product	Data/Orbit [MB]	Data/day [GB]	Data/year [TB]	Mission Data [TB]
L0	1378.7 – 348	19.7 – 5.0	7.2 – 1.8	35.9 – 9.1
L1a	66.8 – 135.5	1.0 – 1.9	0.3 – 0.7	1.7 – 3.5
L1b	66.8 – 135.5	1.0 – 1.9	0.3 – 0.7	1.7 – 3.5
L1c	19 – 17.8	0.3 – 0.3	0.1 – 0.1	0.5 – 0.5
Total	2910 - 966.9	41.5 – 13.8	15.2 – 5.0	75.8 – 25.2

Table 5.18. Product data volume (left Concept A; right Concept B).

expected to be managed by the main processing function, systematic reprocessing of past data require important computing resources over a limited time and the current trend is to rely on resources shared with other missions.

5.5.3.3 Archiving and Dissemination

Level-0 and Level-1 products will be systematically generated and archived. Table 5.18 summarises the volumes of generated products as estimated by the two different concepts.

The archiving will interface with the user and re-processing service to routinely deliver the Level-1b and Level-1c data products to the FORUM users.

5.5.3.4 Mission Planning

This function is in charge of defining the plan of activities for the instruments and to update onboard settings for both instruments as an outcome of calibration activities, trend analysis and specific request. This function is also in charge of planning X-band downlink activities over acquisition stations.

Both instruments operate in a systematic way. The FSI performs autonomously radiometric calibration by regularly pointing deep space and an onboard hot blackbody. Only few other calibration activities (e.g. FEI blackbody calibration performed once per orbit) are explicitly controlled by the Mission Planning function.

The planning of X-band downlink will grant sufficient flexibility to support a single or multiple ground stations as well as several latency objectives including the 3 hours goal and the 24 hours threshold. Plans generated by the mission planning will typically cover a week of operation and will be sent to FOS two weeks in advance. This function will also support re-planning to cope with contingencies.

5.5.3.5 Calibration/Validation

The main functions of the calibration/validation facility are:

- Processing of in-flight calibrations measurements and update of onboard instrument settings or calibration parameters used by the ground processors as required
- Identification and characterisation of deviation based on the processing of in-flight calibrations or vicarious measurements that may trigger payload planning requests (e.g. additional in-flight calibrations) or possibly processors evolutions



- Support to Cal/Val users (provision of special calibration products...)
- Configuration control of the instruments calibration databases.

5.5.3.6 Instruments Performance & Monitoring and Control

This function performs the systematic extraction of key parameters at all product levels starting from source packets. Those parameters are used to generate various instrument monitoring reports, products quality reports and perform trend analysis.

The main objective of the monitoring and control function is to ensure that the PDGS fulfils its objectives in particular in terms of performances and availability so that the mission requirements can be met. This task is fulfilled by compiling status information and reports generated by all the PDGS in order to detect possible anomalies and deviation from expectations as predicted by models.

The list of parameters to be monitored will typically include instrument temperatures of sensors distributed over the instrument, black body temperatures, other instrument HKTM parameters such as voltages and currents, product quality related parameters such as spectra quality level, and life-limited items such as number of scans, scan mirror and pointing mirror movements.

5.5.3.7 User Services and Dissemination

ESA pursues a policy of developing a multi-mission infrastructure for the distribution of data products to end-users. It is assumed that such multi-mission User Services will be upgraded to handle FORUM data products for end users. The user services will support data product discovery, access and visualisation, as well as provide general information on the FORUM mission status and help desk.

Access to FORUM products will be free and open following ESA policy for Earth observation Level-1b and Level-1c data. Access to Level-0 and calibration data products will be available for selected users, e.g. calibration and validation teams and instrument specialists. The users will be able to access systematically specific products levels (e.g. for assimilation purposes) or selected specific products based on specific criteria including at least product type, time windows and geographic area.

5.5.4 Level-0 to Level-1 Data Processing

The main task of the Level-0 to level 1 on-ground processor is to process all the received interferograms from the satellite. The FORUM processing chain follows a rather usual sequence of events for an FTS (See Fig. 5.47)

5.5.4.1 FSI Processing

The low amount of data production and the available downlink is sufficient to allow the full transmission after only application of bit trimming and the corresponding data formatting for download. Downloading the full bandwidth will be advantageous to remove efficiently the large part of errors created by speed variations and part of the microvibration effects.



The on-ground processing of the FSI data starts by checking the overall integrity of the received data. Afterwards the atmospheric data and the calibration data is process in parallel:

- Science measurements processing, consisting on the following main steps:
 - Determine OPD grid and correct temporal delays in the reference signals
 - Interferogram pre-processing
 - Spikes detection and correction.
 - Non-linearity correction: The pyro-detectors show a high non-linearity. Therefore the interferogram values must be corrected before any other processing
 - Gain equalisation: Both interferograms, measured by the two detectors for the same spatial sample, shall be added. Therefore the gain of the two detectors should be equal
 - Interferogram resampling: resamples the interferogram samples, which are equidistant in time, to a grid equidistant in space.
 - Spectral and phase correction.
 - Retrieve radiometric and spectral correction factors
 - Radiometric calibration: Assignment of radiance levels to the measured signal
 - Spectral calibration: Assignment of wavenumbers to each spectral sample
 - Geometric calibration: Assignment of the position on the Earth and the co-registration with the imager pixel grid.
 - Provide the output spectra in the pre-defined spectral grid
 - Determine spectra quality level
 - Determine the ISRF to be delivered with the obtained spectra or (TBC) perform an ISRF normalization to a pre-defined ISRF choice
- Deep-space and internal blackbody calibration measurements processing, consisting on the following steps:
 - Determine OPD grid and correct temporal delays in the reference signals
 - Correct the non-linearity, spikes and electronics delays and filtering
 - Determine spectra quality level
 - Determine the radiance based on the blackbody model and the measured blackbody temperature and instrument temperature
 - Store complex spectra based on the measurement case, time and orbit part ID to be used in the radiometric calibration of the science data.

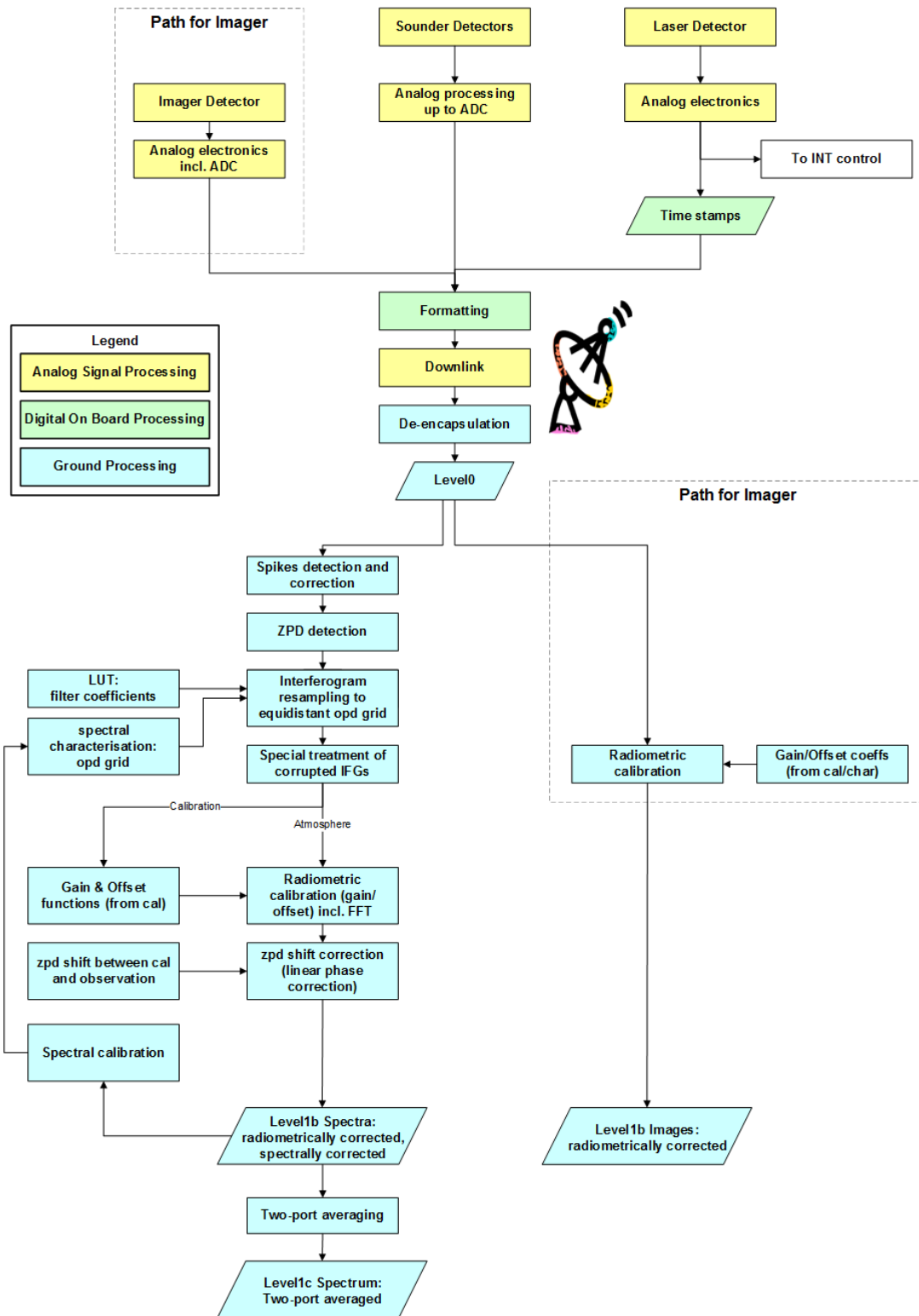


Figure 5.47 Processing chain for Concept A and similar for Concept B.

5.6 Operations, Utilisation and Disposal Concept

5.6.1 Overview

The FORUM operation concept is standard for a SSO mission with need to maintain the formation with MetOp-SG(1A) as the only operational constraints. During the 4 years of nominal operations (excluding commissioning), the observations occur continuously over the entire orbit. Table 5.19 summarises the main mission phases and Fig. 5.48 shows, as illustration, the mission operation reference timeline for Concept B.

5.6.2 LEOP and Commissioning

The LEOP covers the period from switch-over to internal power on the launch pad until the satellite is in its deployed configuration in orbit and the AOCS is operating in Normal Mode. The nominal duration of the LEOP is three days. The correction of any orbit injection errors and orbit acquisition to MetOp-SG(1A) will be combined and performed outside of the LEOP phase.

FORUM will be launched with Vega-C from the Europe's Spaceport in Kourou, French Guiana. After separation from the launcher, an autonomous sequence initiates the solar array deployment, the S-band transmitter switch-on and the AOCS initialisation, attitude rate reduction and acquisition of sun pointing. The automated LEOP sequence includes autonomous re-attempts to deploy solar arrays in case of failures.

Upon completion of the LEOP sequence, initial satellite checkout is executed from ground using the S-band communication opportunities from the LEOP ground segment network of ground stations. The subsequent steps prepare the satellite to transition from Initial Acquisition mode into the normal three axis stabilized Normal Mode. The LEOP sequence is such that the ground shall not need to intervene in less than 6 hours from launch and that execution of an orbit control manoeuvres shall be possible 24 hours after separation (in the event of debris conjunction). After confirmation of the health of the satellite and acquisition of the Normal Mode, LEOP can be declared complete.

Operational Phase	Duration
LEOP	3 days
Commissioning Phase	No longer than 6 months
Formation acquisition	Approx. 60 days (in parallel with commissioning)
Nominal operation phase	4 years
End of Life phase	Up to 1 month
Disposal	Within 25 years

Table 5.19. Main FORUM mission phases and their duration.



The commissioning and loose formation acquisition phase begins after the end of the LEO phase. The loose formation acquisition may take up to 67 days depending on the injection orbit and any launcher dispersion errors which allows for commissioning activities to be run in parallel with the orbit correction and formation acquisition. The platform commissioning involves the switch on and check out for health and performance of all nominal platform units. Redundant units will only be commissioned if it does not impact the nominal operational configuration i.e. they can be operated off-line. The payload (FSI and FEI) commissioning will occur over a longer period starting with functional check out followed by the performance and calibration of the payloads. In addition to the satellite in-orbit verification and adjustment, the whole FORUM system including FOS and PDGS up to Level-2 processing will be checked out, including the coordination with the MetOp-SG(1A) FOS and PDGS.

5.6.3 Nominal Operations and Calibrations

After completion of commissioning phase and acquisition of the loose formation with MetOp-SG(1A), FORUM will commence with nominal operational activities.

The FORUM mission is designed for maximum autonomy of operation driven from on board mission timelines uplinked from ground (two-week mission plan) on a weekly basis. Two TT&C passes per day are baselined for routine operations. The stored housekeeping telemetry is either received via S-band or via the X-band link depending on the mission specific implementation. Science data can either be downlinked once per orbit to achieve a data latency off three hours or twice per day to achieve 24 hours data aging. The operational concepts proposed have considered combining the S- and X-band activities into a single ground station antenna offering the dual downlink capability and using the two pass per day approach for both TT&C and science data downlink.

The formation shall be maintained, mainly, through in plane manoeuvres that aim at controlling the co-registration between the two satellites in the defined operational range. The frequency of these manoeuvres will be below eight per year and will be grouped with standard in-plane maintenance manoeuvres when feasible. Orbit control manoeuvres are expected to be one month apart at solar maximum and up to six months apart at solar minimum.

Even though FORUM may use the same ground stations as MetOp-SG(1A), it will not interfere with its communications nor constrain MetOp-SG(1A) operations in any way. This interference management is performed using two techniques: different communications frequency bands (S- and X-bands) and limiting the minimum distance between spacecraft to geometrically avoid any interference, achieved with more than 15 seconds difference.

The nadir facing observation attitude is maintained throughout the orbit and science data acquisition is continuous, also during TT&C and science downlink. Instrument calibrations are thus part of the payload normal operations with the exception of potential LOS calibration using the Moon.

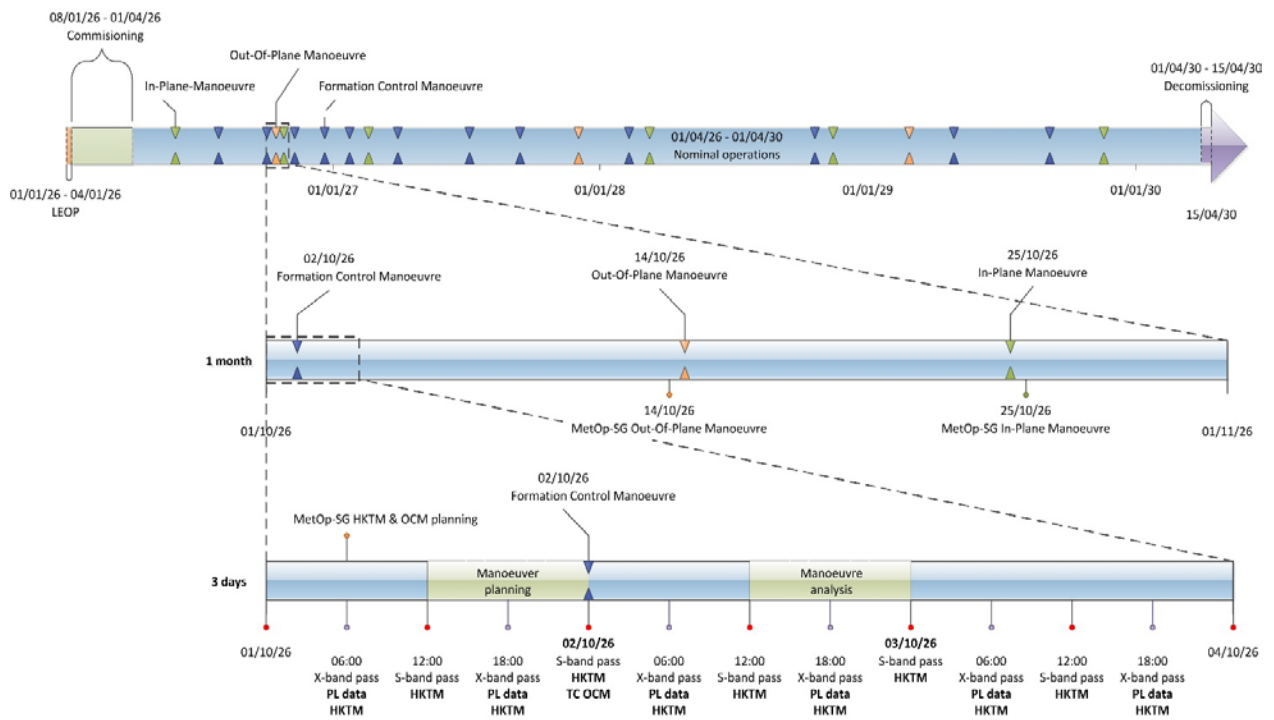


Figure 5.48 Mission Operations reference timeline (Concept B)

5.6.4 Contingency Operations

5.6.4.1 Description of FDIR Concept

The FDIR strategy is based on a categorization of the onboard failures into several failure levels having each of them a specific detection mechanism and resolution. As an example, Concept B FDIR strategy is based on the following levels:

Level-0: Failures with no impact on the mission. Example: Single bit memory errors corrected by EDAC.

Level-1: Failures of a unit or function managed by a local reconfiguration without impact on the current mode. Example: AOCS sensor failure.

Level-2: failures affecting a functional chain. Example: Attitude control error, abnormal estimation of total angular momentum. .

Level-3: failures related to the Satellite Data Processing function. Example: Persistent OBSW overrun.

Level-4: failures are spacecraft critical failures. Example: Power bus under-voltage, thruster ON time.

The PUS FDIR monitoring service are implemented utilizing the Service 12 for monitoring and Service 19 for event-action triggering.

5.6.4.2 Approach to Formation Safety

The approach for the MetOp–FORUM formation safety has been discussed in Section 5.3. The orbit maintenance strategies ensure a safe formation under nominal and safe mode conditions with minimum or no disturbance in the MetOp-SG(1A) nominal operations

In the scenario where a contingency situation has generated a parasitic delta-V (i.e. manoeuvre incorrectly planned or executed, thruster failure), equal to or smaller than of the maximum in-plane orbit control manoeuvre of FORUM, the FOS team have a minimum of 3 days to investigate and react, from receiving the TM notifying the contingency situation to executing the contingency response. Instead of the nominal 8 days if no parasitic delta-V has been generated.

The use of the ESA-CCS tool facilitates the monitoring and information transfer between the two Mission control centre FCTs of the orbit evolution especially around orbit maintenance manoeuvres (in-plane, out-of-plane), any individual debris avoidance manoeuvres, safe mode orbit evolution, and associated mission status information.

The MCC at ESOC will be set up with a multi-mission FD and SDO team available 24/7 to support monitoring and response to collision avoidance manoeuvres and any emergency manoeuvres including orbit manoeuvres impacting the safety of the loose formation flight with MetOp-SG(1A). The on-call FCT engineers for FORUM would support the resulting conjunction analysis and any contingency response activities to be executed on FORUM.

5.6.4.3 Overview of Contingency Operations

In response to any on board monitoring triggered by the onboard FDIR or alerts raised by the Space Debris office, ESA-CCS or MetOp-SG(1A) MCC, various levels of response and resulting contingency operations would be put in place.

The ESOC FOS provides a 24/7 service on-call, out-of-hours service in support of:

- Collision Avoidance Manoeuvres
- Emergency Manoeuvres (including orbit manoeuvres impacting the safety of the loose formation).
- The ESOC FOS provides working hours, 5 days/week service in support of:
 - Contingency Recovery Actions,
 - Responses to anomalies reported by MetOp-SG(1A) FOS,

For new anomalies, FOS would get the support from Industry/Project/Mission Manager as required depending on the anomaly characteristics. For reoccurring anomalies, FOS can execute pre-defined contingency recovery actions to recover and return to nominal operations as soon as possible.

5.6.5 Disposal

After FORUM reaches the end of operational lifetime, or in the event of a critical situation that would induce the need to terminate the mission, it enters a decommissioning phase. This phase will ensure that the space segment does not present a casualty risk and does not remain in the LEO protected region more than 25 years after end of the mission. The disposal manoeuvres will be performed over several successive orbits to lower the perigee. At present, the expectation is that the casualty risk will be below the required 1 in 10000 for an uncontrolled re-entry.

FORUM will decrease the orbit perigee down to an altitude of between 530 to 490 km depending on an aero stable or tumbling approach and in a way to prevent any risk of



collision between FORUM and MetOp-SG(1A). These manoeuvres require a Delta-V of 106 m/s (Concept A) to 84 m/s (Concept B). Simulations performed to assess the survivability and associated casualty risk of re-entry show that for an uncontrolled re-entry in the year 2054 (see Fig. 5.49), the long-term casualty risk assessment is compliant with the risk threshold of 10⁻⁴. After the last manoeuvres, thruster valves are kept open until all the hydrazine has been released. The satellite can be oriented in the maximum drag attitude. Solar arrays are passivated to prevent battery recharge. The satellite will then be inoperable.

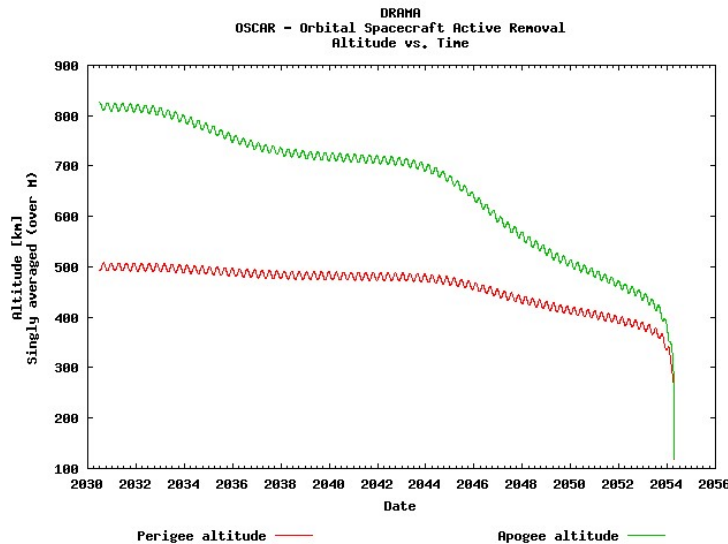


Figure 5.49 Perigee and apogee altitude evolution for EOL disposal for uncontrolled re-entry.

6 SCIENTIFIC DATA PROCESSING AND VALIDATION CONCEPT

Far-infrared-Outgoing-Radiation Understanding and Monitoring (FORUM) will uniquely provide top-of-the-atmosphere spectrally-resolved far-infrared (FIR) radiances. The methods and tools for the data processing are based on experience with mid-infrared (MIR) sensors. Though methods such as inversion techniques to obtain atmospheric profiles from radiances are well-understood and transferrable, the underlying models such as the spectroscopy for water vapour, surface emissivity, or parameterisation of the optical properties of ice cloud have only been tested in a very limited number of field and laboratory experiments. These assessments have shown notable inconsistencies: a) airborne measurements indicate that microphysical models of ice cloud properties that are valid in the MIR cannot explain observations in the FIR. This is due primarily to assumptions regarding crystal habit (Section 7.4.2.1); b) measurements from balloons and from the ground have led to updates in the underlying FIR water vapour spectroscopy, however uncertainties are still significant (Mlawer et al., 2019); c) FIR emissivity models urgently need to be evaluated (Sections 2.2.4/7.4.2.2). As shown in Chapter 2, uncertainties in these parameters can have far-reaching impact.

FORUM radiances will be routinely analysed to obtain the vertical distribution of water vapour, surface temperature and emissivity and cloud properties. The obtained Level-2 products will undergo a validation process to evaluate the quality of the data and to highlight possible problems in both the analysis method and in the auxiliary data used to perform the analysis. This implies the use of FORUM radiances to evaluate and improve the quality of the existing spectroscopy and available ice cloud optical property parameterisations. For spectroscopy this will be done comparing the differences between observed and simulated radiances using different spectroscopic data. Improving the representation of cloud optical properties is more challenging but will be informed by the ability of both forward and inverse modelling to capture the observed behaviour over a wide range of ice cloud scenarios. For example, existing retrieval approaches (Section 6.1.2.2) can be extended to consider the full range of crystal shapes and potentially include the impact of shape combinations. Again, planned validation activities will contribute to this effort by providing in-situ microphysical information collocated with FORUM radiance observations.

More generally, rigorous testing of the FORUM retrieval tools and methods in the run-up to launch, coupled with continuous evaluation of the underlying models will allow the scientific community to maximise the potential of FORUM.

6.1 Retrieval Approach

This Section outlines the main principles that form the basis of the FORUM data processing. The FORUM embedded imager (FEI) images acquired during the FORUM sounding instrument (FSI) dwell time will be used to quantify the sub-pixel inhomogeneity and the temporal variability of the scene observed by the FSI. These data will be used for diagnosis and characterisation of the FSI response and will ultimately improve the accuracy of the

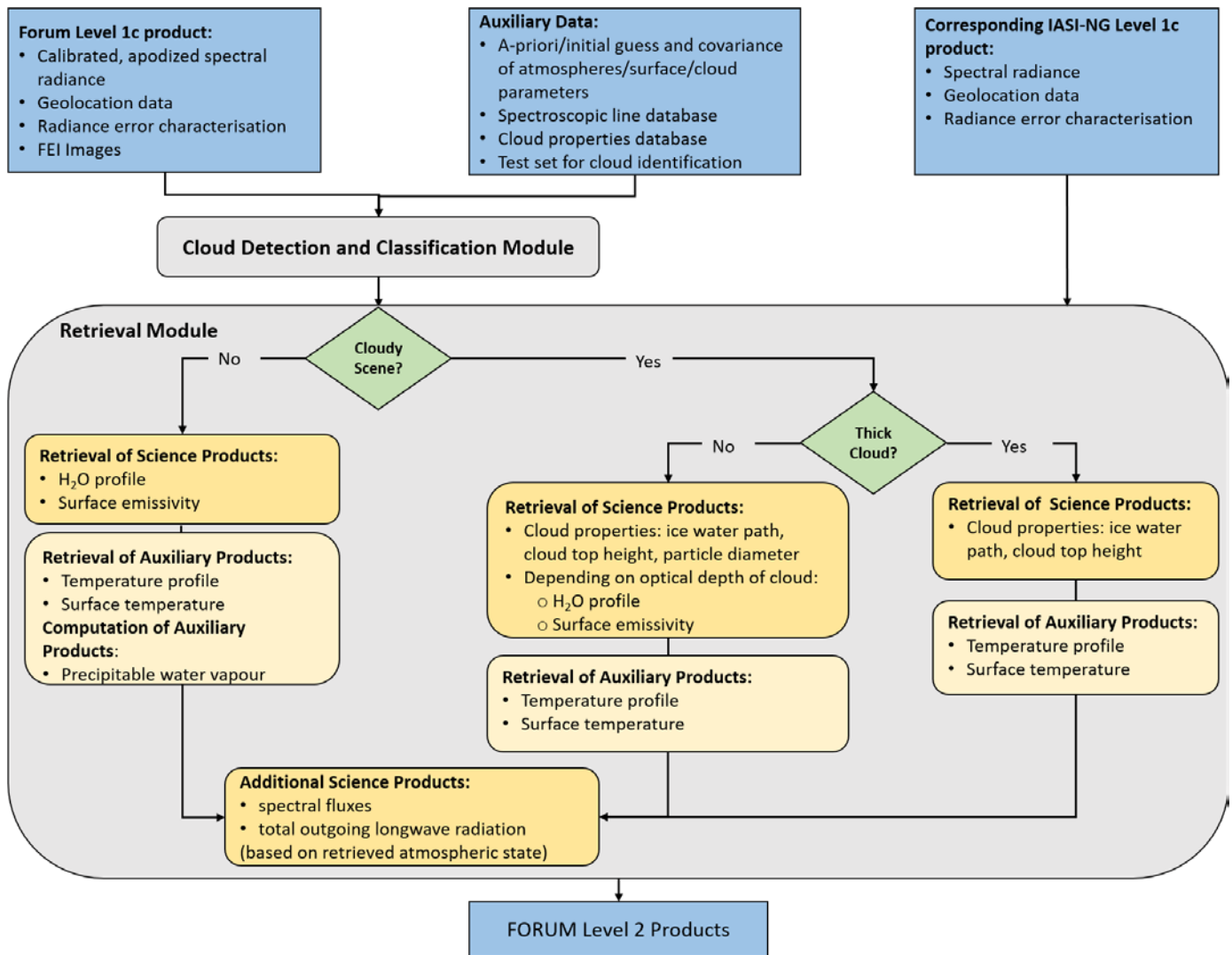


Figure 6.1. FORUM FSI data processing chain. (ESA)

processing chain applied to the measured FSI spectra. Here the focus is on the general principles driving the analysis of the FSI-measured radiances.

First, a pre-processing algorithm, referred to as *cloud detection and classification module*, will discriminate if the observed radiance refers to clear or cloudy sky. In the latter case, the cloud will be classified in terms of phase (liquid/solid) and in terms of opacity. The spectral radiance will then be processed by the *retrieval module* that, on the basis of the results of the cloud detection and classification, will choose the set of parameters to be retrieved. In clear sky, atmospheric state parameters such as temperature and water vapour volume mixing ratio profiles, and surface properties such as the emissivity spectrum and temperature will be retrieved. In the presence of an ice cloud (alone or in multilayer conditions), the total amount of ice in the cloudy column, called Ice Water Path (IWP in g/m^2), ice cloud top height (CTH in km) and ice cloud bottom height (CBH in km) will be retrieved by assuming fixed temperature and water vapour profiles as well as surface properties from ECMWF reanalysis. The posterior error estimation of the retrieved

quantities will take into account the contribution of these non-retrieved parameters as well as measurements errors. For optically thin ice cloud, the retrieval module will be flexible enough to enable simultaneous retrieval of cloud parameters and atmospheric state parameters, which should increase the number of atmospheric state retrievals (usually non-treated in the presence of cloud) and give more accurate or unbiased results by taking into account the ice cloud contribution. In the presence of optically thick ice cloud only the CTH will be retrieved with an estimate of the IWP. An estimation of the water vapour above the ice cloud will also be considered. After retrieval of the atmospheric, surface and cloud parameters, spectral and total fluxes will be computed, exploiting both the retrieved atmospheric state and the spectral radiances. Fig. 6.1 shows a scheme summarising the FORUM FSI data processing chain.

6.1.1 Cloud Detection and Classification

Before undergoing Level-2 processing, the measured FORUM spectral radiance will be pre-processed by a Cloud Identification and Classification (CIC) module. The algorithm planned for implementation in the CIC module of the FORUM Level-2 processor is based on one recently developed by Maestri et al., (2019). This algorithm was also implemented and tested in the FORUM end-to-end simulator (see Section. 7.1). CIC is a machine-learning algorithm based on principal component analysis. A database of simulated spectral radiances is first established. The database contains synthetic observations relating to a variety of atmospheric conditions, cloud and surface types. In this database, the radiances are grouped into different classes depending on latitude and on whether they refer to clear or cloudy sky. In case of cloudy sky, the radiances are classified according to the cloud phase (solid, liquid or mixed) and type (optically thin or thick). A covariance matrix is then built for each class of radiances and its eigenvectors are computed. When a new observed spectrum becomes available, it is added to each of the classes of spectra of the pre-computed database. For each of these *extended* classes, the covariance matrix and its eigenvectors are computed. A predefined similarity index is then evaluated to establish whether the eigenvectors related to the *extended* class differ significantly from those of the *original* class. If the eigenvectors of the extended class are sufficiently similar (within a certain threshold of the similarity index) to those of the original class, then the measured spectrum is considered to belong to that class.

This cloud detection and classification algorithm is partially based on past works of Malinowski (2002) and Turner et al., (2005). However, compared to the existing algorithms it is easy to implement, user-friendly, fast and efficient. In Maestri et al., (2019), this algorithm was also used to demonstrate that exploiting FIR spectral channels in addition to the MIR channels greatly improves the capability to identify and classify clouds.

After the cloud detection and classification, the scene homogeneity will be examined. The five FEI images acquired during dwell time of the FSI will be investigated. From each, only the pixels relative to the surface observed by the FSI pixel will be extracted. The comparison of the extracted pixels belonging to different images will be used to assess the scene variation in time. Then the selected pixels of each FEI image will be classified according to their brightness temperature (BT) and the frequency distribution of the BTs will be computed. If all the FEI pixels fall within a limited range of BT, the scene will be considered homogeneous,

otherwise a degree of inhomogeneity will be reported according to the distribution of BT within the FSI pixel.

6.1.2 Retrieval Method

Retrieving the atmospheric, cloud and/or surface state from the measured upwelling spectral radiances \mathbf{y} is generally referred to as an *inverse problem* (Rodgers, 2000). The solution to this is usually referred to as *optimal estimation*. The problem is solved by fitting a physical model of the observed radiances to the actual measurement. The *physical model* is referred to as the forward model. The forward model simulates the observed radiances on the basis of an assumed atmospheric, cloud and surface state and on a set of ancillary data, including spectroscopic line database, cloud microphysical properties database and instrument response functions. The atmospheric, cloud and surface state parameters to be retrieved are represented by the unknown state vector \mathbf{x} . All the other quantities that are assumed as *known* in the forward model, are represented by the vector \mathbf{p} . Thus, the forward model is a function of both \mathbf{x} and \mathbf{p} and is indicated as $\mathbf{f}(\mathbf{x}, \mathbf{p})$. Further details about the forward model are provided in Section 6.1.2.1. Starting from an *a priori* estimate \mathbf{x}_a of the atmospheric state, cloud and surface properties, the forward model is able to simulate the spectral radiance reaching the instrument. In the maximum *a posteriori* probability method (Rodgers, 2000), the best estimate of the state vector \mathbf{x} is obtained with the vector \mathbf{x}_f corresponding to the minimum of a scalar cost function defined as:

$$\chi^2(\mathbf{x}) = (\mathbf{y} - \mathbf{f}(\mathbf{x}, \mathbf{p}))^T \mathbf{S}_y^{-1} (\mathbf{y} - \mathbf{f}(\mathbf{x}, \mathbf{p})) + ((\mathbf{x}_a - \mathbf{x})^T \mathbf{S}_a^{-1} (\mathbf{x}_a - \mathbf{x})) \quad (6.1)$$

In this expression \mathbf{S}_y and \mathbf{S}_a are the covariance matrices describing the error that affects respectively the measured/forward modelled radiances $\mathbf{y}/\mathbf{f}(\mathbf{x}, \mathbf{p})$ and the *a priori* estimate \mathbf{x}_a . In the χ^2 (chi-square) function, the first term represents the error-weighted summation of the squared differences between the observed spectral data points y_i and the corresponding simulations $f_i(\mathbf{x}, \mathbf{p})$. The second term of Eq. 6.1 is the error-weighted summation of the squared differences between the state vector elements x_i and their corresponding a priori estimates x_{ai} . This second term is introduced to penalise the solutions that differ significantly from the a-priori estimate \mathbf{x}_a . The smaller the diagonal elements of the a priori error covariance \mathbf{S}_a , the stronger the penalisation. The penalisation term is used because, on its own, the first term of Eq. 6.1 often shows a degenerate minimum, i.e. the minimum may be a kind of a *canyon* or a *flat valley* instead of a single point. In this case, the inversion is said to be *ill-posed* and has infinite solutions. Among the possible solutions minimising the first term, the second term of Eq. 6.1 selects the solution closest to the a priori estimate \mathbf{x}_a .

Several numerical methods can be adopted to find the minimum of Eq. 6.1. One of the most popular methods is the Gauss-Newton method, eventually modified according to the Levenberg-Marquardt (LM) recipe to cope with possible strong non-linearities in $\mathbf{f}(\mathbf{x}, \mathbf{p})$ (Rodgers, 2000). The covariance matrix mapping the errors \mathbf{S}_y and \mathbf{S}_a into the solution \mathbf{x}_f is given by:

$$\mathbf{S}_x = (\mathbf{K}^T \mathbf{S}_y^{-1} \mathbf{K} + \mathbf{S}_a^{-1})^{-1} \quad (6.2)$$



where \mathbf{K} is the Jacobian matrix, containing the derivatives of $f(\mathbf{x}, \mathbf{p})$ with respect to the state vector \mathbf{x} . Fig. 6.2 illustrates the behaviour of the retrieval procedure in clear-sky both in the spectral (left panel) and in the state vector (right panel) domains. In this case the retrieval is based on a synthetic FORUM FSI observed spectral radiance obtained from a forward model simulated spectrum to which measurement pseudo-random noise has been added according to the goal noise equivalent spectral radiance (NESR) requirement. In the left panel of Fig. 6.2, the black curve represents the observed (synthetic) spectrum \mathbf{y} and the red curve the simulated spectrum $f(\mathbf{x}_f, \mathbf{p})$ at the end of the retrieval. It is interesting to inspect the differences between observed and simulated radiances, the so called *residuals* of the fit, that is the vector $\mathbf{y} - f(\mathbf{x}_f, \mathbf{p})$. In Fig. 6.2, left panel, the elements of this vector are represented by the blue line. If the retrieval converges properly and the measurement and forward model errors are well accounted for in the matrix \mathbf{S}_y , then the residuals are randomly distributed around zero, with standard deviations equal to the square roots of the diagonal elements of \mathbf{S}_y (the magenta lines). The orange curve shows the forward model $f(\mathbf{x}_0, \mathbf{p})$ at the first iteration, pointing out the inadequacy of the initial-guess atmospheric state.

The right panel in Fig. 6.2 shows the behaviour of the components of the state vector \mathbf{x} referring to the temperature profile. In this plot the orange line represents the initial guess profile and the dark-green line the a priori profile \mathbf{x}_a . The error bars of the a priori profile are not shown as in this illustrative case they are all assumed equal to 10 K. The blue circles represent the retrieved values \mathbf{x}_f , with their error bars given by the square roots of the diagonal elements of \mathbf{S}_x . Finally, the black line represents the true value of \mathbf{x} used to generate the synthetic observed spectrum. Considering that the error bars represent 1σ statistical errors, the retrieval procedure is able to recover the true state vector within the error margins. Note that for illustrative purposes in this test retrieval, the a priori error of temperature was artificially set to 10 K (a huge value), therefore also the errors of the retrieved profile are very large. Realistic retrieval error estimates are shown in Chapter 7.

The above χ^2 function (Eq. 6.1) is by design well-suited to introducing any climatological constraint by means of its second term. For a cloudy case, it is known that the information concerning the bottom height will be much smaller than for top layer and total water content. Therefore, the algorithm uses climatological constraints to help the convergence especially for the CBH. This climatological constraint comes from auxiliary data like the radar/lidar (DARDAR) project (Delanoe and Hogan, 2008), which provides an unprecedented global database of the ice water content profile over more than 10 years. This product was obtained by using the combination of the two active sensors, the cloud-aerosol lidar with orthogonal polarization (CALIOP) and the radar CloudSat. This climatological database together with the penalising term of the above χ^2 function will therefore constrain the CBH corresponding to a given IWP and CTH to stay within the limits given by the DARDAR observations.

6.1.2.1 Forward Model

The forward models used to simulate clear and cloudy sky radiances are different because of the added complexity to treat multiple scattering within the cloud. The task of the forward model is the simulation of the spectral radiance $f(\mathbf{x}, \mathbf{p})$ measured by the FSI. This is achieved in two steps:

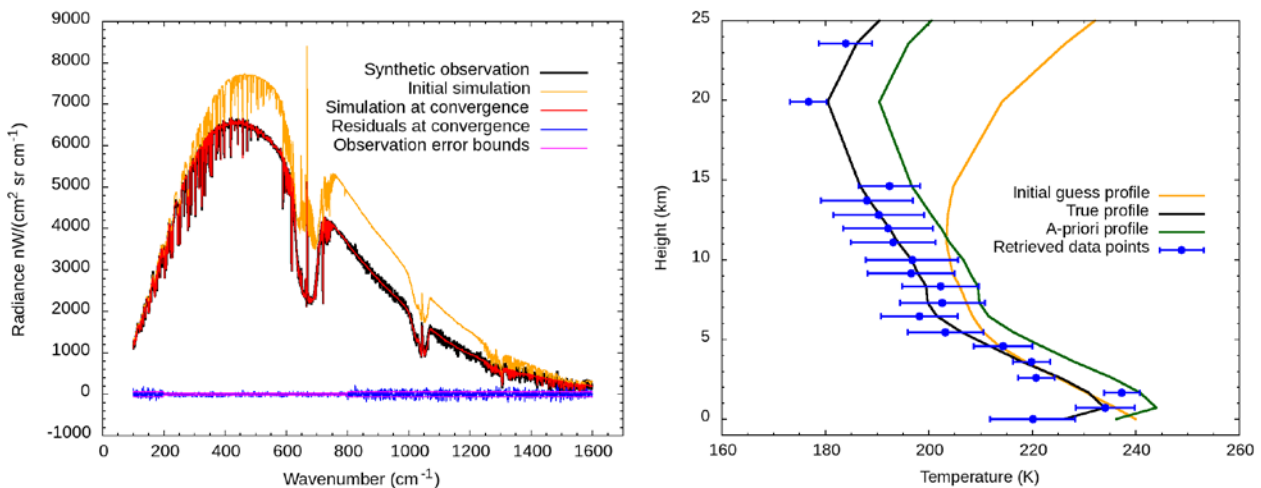


Figure 6.2. Illustration of the retrieval procedure in the spectral domain (left) and in the state vector domain (right). The plotted elements of the state vector refer to the retrieved temperature profile. Note that for illustrative purposes in this test retrieval, the a priori error of temperature was artificially set to 10 K (a huge value), therefore also the errors of the retrieved profile are very large. (M. Ridolfi, University of Bologna, Italy)

1. For each relevant frequency σ_i , the radiance $S(\sigma_i)$ reaching the FSI is simulated by solving the radiative transfer equation (Eq. 6.3) with an integral along the FSI's line of sight to Earth's surface.
2. The distortions introduced by the measuring instrument are simulated by convolving the radiance $S(\sigma_i)$ with the instrument response functions both in the spectral and spatial domain.

The radiative transfer equation to be solved for the calculation of the spectral radiance $S(\sigma_i)$ reaching the FSI at altitude z_1 can be written as:

$$S(\sigma_i) = S_{\text{surface}} + \int_{z_0}^{z_1} J(\sigma_i, T(z)) \frac{\partial \tau(\sigma_i, x(z))}{\partial z} dz \quad (6.3)$$

In this expression the second term on the right represents the radiance contribution from each overlying atmospheric layer that reaches the FSI. z is the altitude coordinate, z_0 is the altitude of Earth's surface, and x is the coordinate along the line of sight of the instrument. $T(z)$ is the temperature at height z . $\tau(\sigma_i, x(z))$ is the atmospheric transmission between the point x along the line of sight and the observer. It depends on the atmospheric pressure, temperature and composition via the coordinate x . It also depends on the spectroscopy of the atmospheric gases. $J(\sigma_i, T)$ is the source function that, in clear-sky conditions, and assuming local thermodynamic equilibrium is the Planck function. In cloudy conditions, or in the presence of aerosols, the source function also includes the scattering source function that is the contribution due to the scattering of the radiation by the cloud/aerosol particles. The optical properties of the cloud or aerosol, which determine the scattering contribution, are evaluated knowing the cloud phase or aerosol composition, the size distribution of the particles and their shape or shapes (see Section 6.1.2.2).

The first term on the right of Eq. 6.3, $S_{surface}$, is the contribution of Earth's surface emission to the radiation measured by the FSI, and may be written as:

$$S_{surface} = [L_d(\sigma_i)(1 - \epsilon_{surf}(\sigma_i)) + \epsilon_{surf}(\sigma_i)B(\sigma_i, T_{surf})]\tau_0(\sigma_i) \quad (6.4)$$

where L_d is the downwelling radiance at the surface, ϵ_{surf} is the surface emissivity, T_{surf} is the surface temperature and τ_0 is the transmissivity between the surface and the FSI. The first term on the right is hence the downwelling atmospheric radiance reflected back towards the instrument by the surface. The second term is the thermal emission of Earth's surface, both of which are modulated by the atmospheric transmission. Equation 6.3 is usually solved numerically, by dividing the atmosphere vertically into thin layers, evaluating the radiation emitted and absorbed in each layer, and, in presence of cloud/aerosol, scattered along the line-of-sight of the instrument.

Cloudy-sky approach

Conventional radiative transfer (RT) codes that accurately reproduce the scattering effects are very time consuming and cannot be reasonably used in real-time in any retrieval scheme. This limitation explains why there are so few cloud products from high spectral resolution measurements (beside the altitude of the cloud top layer). The Radiative Transfer for TOVS (RTTOV) model (Saunders et al., 1999; Saunders et al., 2018) is a fast RT model originally developed to simulate Tiros-N Operational Vertical Sounder (TOVS) measurements in clear-sky conditions, for assimilation of large band spectral radiances into NWP model analyses. RTTOV is also widely used in satellite retrieval, simulation of imagery and data assimilation communities. The core of RTTOV is a fast parameterisation of layer optical depths due to gas absorption. It has been extended to simulate a variety of different instruments from passive visible, infrared and microwave downward-viewing satellite radiometers. Recently, to account for scattering effects in the IR, a method based on Chou et al. (1999) was introduced into RTTOV. The performance of the updated model has been assessed via comparison with more accurate RT code, which treats the scattering contribution exactly, and shows that RTTOV can now reproduce radiances with an error less than 0.2 K in the MIR in cloudy conditions (Vidot et al., 2019), and is currently being tested in the FIR. In addition to radiances, RTTOV also provides layer transmittances, a Jacobian matrix and is therefore perfectly suited for use in a retrieval module. During Phase A studies, RTTOV has been updated to simulate the FSI measurements by taking into account the spectral resolution and ISRF requirements. RTTOV can also handle a cloud fraction profile to enable simulations for atmospheres partially covered by cloud (use of maximum overlap method), and it can also handle any mixture between liquid and ice phase in the same layer.

6.1.2.2 Clouds Microphysical Model

Ice clouds

As described in Section 6.1.2.1, the cloud properties enter into the forward model through the scattering source function that is a function of both the macro-physical properties of the clouds (CTH, CBH) and of their micro-physical properties. As outlined in Section 2.1.3, one of FORUM's main targets is the study of ice clouds. Therefore, in the Phase A studies, two approaches have been explored as representative of ice cloud models currently used within

the scientific community. The first, referred to as the *conventional approach*, is currently implemented in the FORUM end-to-end-simulator (see Section 7.1). It is based on the microphysical representation of the bulk ice properties developed by Yang et al. (2013), who have produced an optical properties database for different particle shapes and effective sizes. This database covers a wide range of ice particle dimensions (between 2 and 10 000 μm), shapes (up to 11) and wavelengths (between 0.2 to 100 μm). In the FORUM end-to-end-simulator approach, a particle shape is pre-assigned and the retrieved cloud parameters are the particle effective size, cloud optical depth at 900 cm^{-1} and CTH.

The second approach, labelled as the *explorative approach*, makes use of an original representation of bulk ice optical properties from the knowledge of ice water content (IWC which is the amount of ice per volume in g/m^3) and temperature (Baran et al., 2014, Vidot et al., 2015). The optical properties have been linked to the amount of ice and cloud temperature by evaluating more than 20000 *in situ* samples of IWC and temperature. For each sample, a size distribution was first computed following the method of Field et al. (2007), which makes use of the measured IWC and temperature to obtain a universal size distribution. The bulk ice optical properties are then computed given the size distribution and by using the ensemble model of Baran and Labonnote (2007), which considers six different ice crystal shapes representative of the observed cloud ice particle shape complexity. The particle shape is attributed depending on the particle size (simple shape for small particles to complex shape for large particles). A parameterisation of these optical properties has been developed afterwards as a function of IWC and temperature (Vidot et al., 2015), allowing the ice bulk microphysical properties to be represented by these two parameters only, with no need of choosing a particle shape and size distribution. During Phase A studies, this parameterisation was extended to the FIR and now covers the spectral interval between 0.2 to 100 μm and is included in the RTTOV model. In this *explorative* approach, the retrieved cloud parameters are therefore: the total amount of ice (the IWP in g/m^2), CTH and CBH. The cloud optical depth at any wavenumber can also be computed directly from the relation, provided by the microphysical model, between the extinction coefficient and the couple (IWC, temperature).

Liquid clouds

In case of multilayer scene, it is important to take into account the liquid cloud contribution under the ice cloud in the forward model. RTTOV model can handle these multilayer configurations and even mix layers (liquid + ice) by attributing to each layer an amount of ice and/or liquid content. This water content (and temperature for the ice phase) is then converted into optical properties for each phase by means of a microphysical model. Concerning the liquid phase, five different types of clouds are considered that correspond to five different microphysical models. For each cloud type, a gamma standard size distribution is assumed and is given by Equation 6.5.

$$n(r) = Cr^\alpha e^{-br^\gamma} \quad (6.5)$$

Table 6.1 gives the coefficients (α , b and γ) of the size distribution for each cloud type and have been taken from the OPAC database (Hess et al., 1998). The last coefficient, S , is also provided by the OPAC database and allows the translation of the liquid water content (LWC)

in a particle number concentration ($N_{\text{liq}} = \text{LWC}/S$ in cm^{-3}) which is then used to compute the liquid cloud optical properties needed in the forward model. To summarise, when the CIC module detects a multilayer cloud, a liquid cloud type, both a geometrical extension and an amount of water has to be established either from climatology or ECMWF reanalysis. The forward model is then run with this liquid cloud contribution to retrieve the ice-cloud layer properties. Any misrepresentation of this liquid cloud water content and geometrical extension will map an error into the retrieval process. This error will be estimated *a posteriori* to derive a realistic ice-cloud parameter error.

Cloud type	α	\mathbf{b}	γ	\mathbf{S} [$\text{gm}^{-3}/\text{cm}^{-3}$]
Stratus continental	5	0.938	1.05	0.00112
Stratus maritime	3	0.193	1.30	0.00375
Cumulus continental clean	5	0.0782	2.16	0.00065
Cumulus continental polluted	8	0.247	2.15	0.00023
Cumulus maritime	4	0.00713	2.34	0.00677

Table 6.1 Coefficients of the gamma size distribution (see Eq. 6.5) for the five different liquid cloud types provided by the OPAC database.

6.1.3 Calculation of Spectrally-Resolved and Total OLR Fluxes

Fig. 6.3 provides a schematic of the relationship between radiance and flux. Assuming azimuthal independence, the upwelling flux of energy at a wavenumber σ , F_{σ} , at the top of the atmosphere is defined by:

$$F_{\sigma} = 2\pi \int_0^{\frac{\pi}{2}} S(\sigma, \theta, \mathbf{x}) \sin \theta \cos \theta d\theta \quad (6.6)$$

where θ is the zenith angle and $S(\sigma, \theta, \mathbf{x})$ is the upwelling spectral radiance, which varies with viewing angle and is dependent on the underlying atmospheric state, \mathbf{x} , as discussed in Section 6.1.2.1.

Since FORUM measures only at nadir the contribution of the radiances from other angles to the upwelling flux has to be inferred. This is a common problem for satellite-derived fluxes and is tackled by using knowledge of geophysical properties of the scene to determine the conversion between radiance and flux. For deriving broadband OLR there are two well-established options for doing this. The first involves the direct computation of OLR using a suitable forward model fed with the best estimates of the atmospheric and surface state (e.g. Zhang et al., 2004, Susskind et al., 2012). The second makes use of scene dependent observation geometry dependent anisotropy models known as angular distribution models (ADMs) which describe the angular variation of the radiance. Scenes are typically categorised according to variables such as surface type and temperature, water-vapour content, temperature-lapse rate, cloud fraction and optical depth, which must be determined for each radiance observation. These ADMs can be generated using radiative transfer modelling or can be built up over time from many prior observations if an instrument samples all the relevant directions. This latter approach is the one taken for the CERES

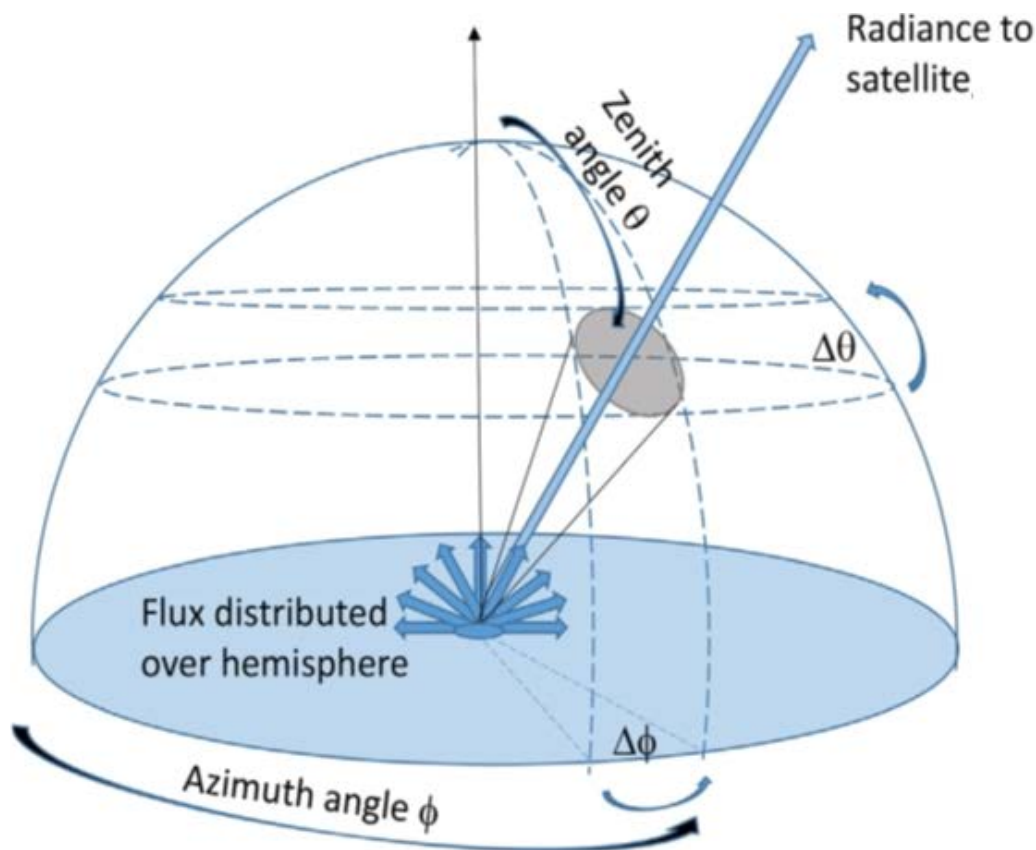


Figure 6.1. Relationship between radiance and flux. (Adapted from Brindley and Russell, 2018)

broadband instrument, based on scene identification from the Moderate Imaging Spectroradiometer flying on the same platform and ancillary meteorological information (Su et al., 2015). Historically, the ADM approach has been applied to broadband radiance measurements, but work by Huang et al. (2008, 2010) has seen the development of spectral ADMs (with 10 cm^{-1} resolution) using a combination of RT modelling and reanalyses.

The initial approach for FORUM, is based on the first method. Using the best estimate of the underlying state from the measured nadir radiances, a forward model of the spectral angular radiance distribution will be performed. Spectral top of atmosphere fluxes will be generated by integrating over the upward hemisphere (Eq. 6.6). The main assumption here is of horizontal homogeneity of the atmosphere below the sensor, but this is implicit in all similar approaches and in the calculations of current climate models.

Using this approach will ensure that the fluxes are spectrally consistent to the limit of the accuracy of the forward model and the FORUM measurements. As discussed, the spectral consistency of the forward model is limited by the uncertainties in the spectroscopic and cloud models, especially in the FIR. Iterative forward model improvements achieved by comparison with FORUM measured radiances (Section 6.1), mean that, in principle, it will be possible to reduce these forward model errors to the absolute radiometric accuracy level of FORUM measurements. With this method it will be possible to evaluate fluxes over any



spectral interval, including the total OLR and to consistently link variability and changes in the derived fluxes to the underlying causes.

6.2 Validation Concept

Following best practice guidelines (e.g. Bates and Privette, 2012; Bojinski, 2014; Su et al., 2018) the FORUM validation strategy will:

- cover the full range of conditions
- account for uncertainties in the validation methodology and comparison data.
- establish the International System of Units (SI) traceability of the measurements
- provide quantitative uncertainty estimates and temporal and spatial error covariance.
- incorporate strategies to detect systematic biases and changes to the error characteristics
- define and establish automated monitoring of data quality
- formally report methods and results in the peer review literature.
- ensure up to date information is available to users.

6.2.1 Validation Organisation

Pre-launch activities will focus on the development and validation of processing systems and retrieval tools. They will also establish the instrument characteristics and provide an assessment of the expected accuracy of the radiances and derived products. Activities to refine the processing and retrieval methods, including the underlying RT codes and cloud models will also be carried out during this phase. After launch, comparison with ground based, *in situ* and remotely-sensed data and products and NWP models will be employed to quantify the accuracy of all the products and compare the result against the expected accuracies. The methods and models will be confirmed and refined as necessary during initial in-orbit validation.

In-orbit validation will be broken into three stages, designed to move from the simplest conditions to more complex cases, culminating in the release of validated products with associated uncertainties. Validating the radiances and temperature and water vapour profile products will be the focus of the first two stages, with the aim to have these products ready for wide scale release at the end of the second stage.

Stage 1 will focus on simple cases of clear-sky spatially homogeneous scenes over ocean. These initial studies will establish broad confidence in the data and algorithms under operational conditions and, if necessary, enable iterative improvement of the instrument model, the forward modelling and the profile retrievals. A clear-sky field campaign deploying an instrument capable of resolving the infrared spectrum from 100–1600 cm^{-1} should be part of this stage, allowing direct comparison with FORUM across the full spectral range.

Stage 2 activities will extend the evaluation of the radiances and temperature and water-vapour profiles and characterise their uncertainties globally over the full range of conditions. It will evaluate the ability to correctly detect cloud and to identify ice cloud for subsequent



derivation of properties, validating the ability of CIC module of the Level-2 processor to classify spectra for appropriate Level-2 retrieval treatment.

Stage 3 activities will validate Level-2, ice cloud properties, surface emissivity and spectral fluxes. Field campaign focusing on ice cloud retrievals and others providing surface emissivity observations will be required for these comparisons. At the end of stage 3, validation should be sufficient to enable initial release of all the remaining products along with full uncertainty information.

Evaluation of all the products will continue beyond these initial intensive validation activities to provide continuing assessment of product quality and uncertainty. Automated procedures will be put in place to flag low quality data, and large scale retrospective analyses for spurious trends or cycles or other deterioration in the quality of the products will be carried out periodically.

6.2.2 Validation Methods

The complex problem of screening and selecting data and applying the corrections or transformations required to optimise the comparison due to mismatches in the quantities observed will be handled within the framework of a comparison model. Spatio-temporal mismatch and differences arising from discrepancies in the measurement characteristics and retrieval details will be addressed by the model, with the specifics varying with the product being validated, the data used for its evaluation and the detail of the scene. As well as optimising the comparison, the model will provide an estimate of the uncertainty in the comparison result considering both the uncertainty in the input data and the comparison methodology and incorporating supplementary information where needed.

NWP models will allow a comparison of the FORUM-measured radiances globally with those simulated from the model fields of temperature, water vapour, clouds and surface properties. Although the model fields will have some uncertainties the radiance biases should be <1 K for clear-sky scenes and the global coverage allows problems in remote areas to be detected at an early stage. The behaviour of the biases around an orbit and during the day can provide useful information on instrument calibration issues. Combining such evaluation with comparison against other sensors will also help identify NWP model and sensor dependent errors.

Comparison of radiances and retrieved profiles with IASI-NG will be performed globally. Comparison to other polar-orbiting sounders will exploit simultaneous nadir overpass opportunities expected at high latitudes. The comparison model will consider the spatial and temporal variability of each scene to define appropriate coincidence criteria and associated errors and consider the effect of spatial sampling differences. Radiance comparisons will be made in the spectral overlap region by apodising to a common wavelength scale. Retrieved profiles will be compared making allowances for the different spectral ranges and averaging kernels of the instruments and *a priori* assumptions of their retrieval methods. A conversion of retrieved profiles from one sensor to the inferred radiances for the other will complete the sounder intercomparison.



Field campaigns using airborne interferometers covering the FIR will provide radiance comparisons across the full FSI spectral range and enable retrieved profiles to be directly compared to measured quantities. To allow the comparison model to derive the best estimate of the atmospheric profile for the satellite overpass, simultaneous sampling of upper and lower atmosphere from balloon sensors, such as radiosondes and cryogenic hygrometers, launched at intervals and supplementary information on atmospheric variability from well-instrumented ground sites or field campaign data will be used (see Tobin et al., 2006; Chahine et al., 2000). Although subject to significant mis-match errors correlated with environmental state (Sun et al., 2017, Pougatchev, 2008), global comparisons employing established quality radiosonde networks can be used for wider-scale qualitative assessment of the retrieved profiles providing an upper bound on retrieval quality (Divakarla et al., 2006; Trent et al., 2019).

Level-2 spectral flux validation will concentrate on comparisons with other derived flux quantities. Coincident views with Clouds and the Earth's Radiant Energy System (CERES, Wielicki et al., 1996) and Geostationary Earth Radiation Budget (GERB, Harries et al., 2005), both broadband Earth radiation sensors, will be analysed as a function of view angle difference and scene to investigate overall consistency and variations in bias with observation characteristics. Co-locations with satellites carrying CERES-AIRS, CERES-CrIS and the CERES follow-on instrument can also be exploited to make comparisons with spectral fluxes derived by the methods outlined in Huang et al. (2008, 2010) and Han et al. (2013).

Validation of the Level-2 surface emissivity will require surface based and airborne measurements of the upwelling radiance across the FSI spectral range, as well as independent measurements of surface skin temperature and surface characteristics such as snow specific surface area and density. Since the far infrared emissivity is only expected to be retrieved in very dry atmospheres its validation does not need to be global but will need to establish the reliability of identifying such conditions, properly characterising the uncertainty and flagging poor quality retrievals. This can be achieved by longer term ground based deployment at a few well selected sites to sample a range of conditions (e.g. Dome Concordia (Antarctica), Summit (Greenland), Libya, Atacama Desert, Morocco).

Validating the Level-2 ice cloud properties will require field campaigns employing multiple aircraft. These will provide simultaneous above cloud spectral observations across the mid and far-infrared and in-situ cloud microphysical data. Additional measurements from lidar will give cloud vertical information and multiple meteorological balloon launches and dropsondes will sample the atmospheric state. Used together, the data will enable detailed case study validation of the ice cloud properties (e.g. O'Shea et al., 2016, Whiteway et al., 2004). It will also be used to evaluate the cloud microphysical models and test their ability to consistently capture the observed radiances across the MIR and FIR in a tightly constrained environment with observed ice-crystal habits and distributions. Wider-scale qualitative measures of consistency between FORUM ice-cloud properties and those retrieved by other missions will be used to broaden the validation domain and identify problematic regimes and trends in the data (see Hollmann, 2018; Karlsson and Devasthale, 2018). Intercomparison and modelling studies carried out during field campaigns will be used to help interpret differences between cloud datasets, quantifying the impact of the



different spectral ranges and the modelling assumptions employed in the other retrievals, as well as the effect of differences in spatial or temporal sampling.

6.2.3 Quality Monitoring

As well as retrospective analysis to investigate trends in the data, ongoing monitoring of data quality and automated checking to flag poor-quality data and provide real-time alerts, will be implemented. Monitoring the bias between observations and calculations based on near-real-time NWP profiles will provide timely monitoring across a range of spectral regions and identify cloud contamination in observations identified as clear (e.g. Saunders et al., 2013). Well-defined scenes will allow the most sensitive detection and double difference comparison of the bias with other observations will enable screening of NWP model dependent errors. The relative calibration of the FSI radiances can be tracked against other sounders by comparing bias corrections determined from geostationary sounders, and also at selected wavelengths using observations sites such as Dome Concordia, located in Antarctica at an elevation of 3,233 metres (Aumann et al., 2016). Statistics of the IASI-NG and FORUM FSI radiances in their spectral overlap region will be monitored against the baseline established during initial validation to highlight changes. Flagging of individual spectra will employ cross comparison with IASI-NG and expected correlations between FSI wavelengths, following methods employed to monitor noise and identify spurious signals in the infrared spectra observed with the AIRS and IASI instruments (Goldberg et al., 2005; Serio et al., 2018; Tobin et al., 2009) using statistical techniques such as principal component analysis.

7 MISSION PERFORMANCE ESTIMATION

7.1 FORUM End-to-End Mission Performance Simulator

The Far-infrared Outgoing Radiation Understanding and Monitoring (FORUM) end-to-end simulator (FEES) is a tool to predict and assess the Level-1 and Level-2 performances of the mission. The FEES architecture is based on established and well proven end-to-end architectures representative of passive optical remote sensing techniques and instruments (e.g. the Earth Explorer 8 FLEX end-to-end simulator).

The simulator models the elements relevant to the Level-1 and Level-2 mission performance. Each module is chained to others in a logic that follows the observation sequence of events. The modules can be run sequentially, continuously (i.e. end-to-end), or individually; the latter configuration is used for verification and validation purposes or to reduce processing time in parametric analyses. When run in end-to-end mode, the FEES is used to demonstrate the consistency and coherence of the observation concept (including the instrument), the whole processing chain up to Level-2 and the impact of errors in the Level-1 and 2 performance. This is achieved by modelling the main error sources and its propagation through the detection/retrieval chain in a data driven manner where the interfaces between modules are established through output files that act as input files to the next module in the chain.

Fig. 7.1 details the FEES architecture in its individual modules. The different modules model the observed geophysical scene, the propagation of the radiation in the atmosphere until the TOA (forward model), the spacecraft/mission elements relevant for the mission (e.g. orbit, satellite pointing), the instruments, the processing chain and the retrieval algorithms. The

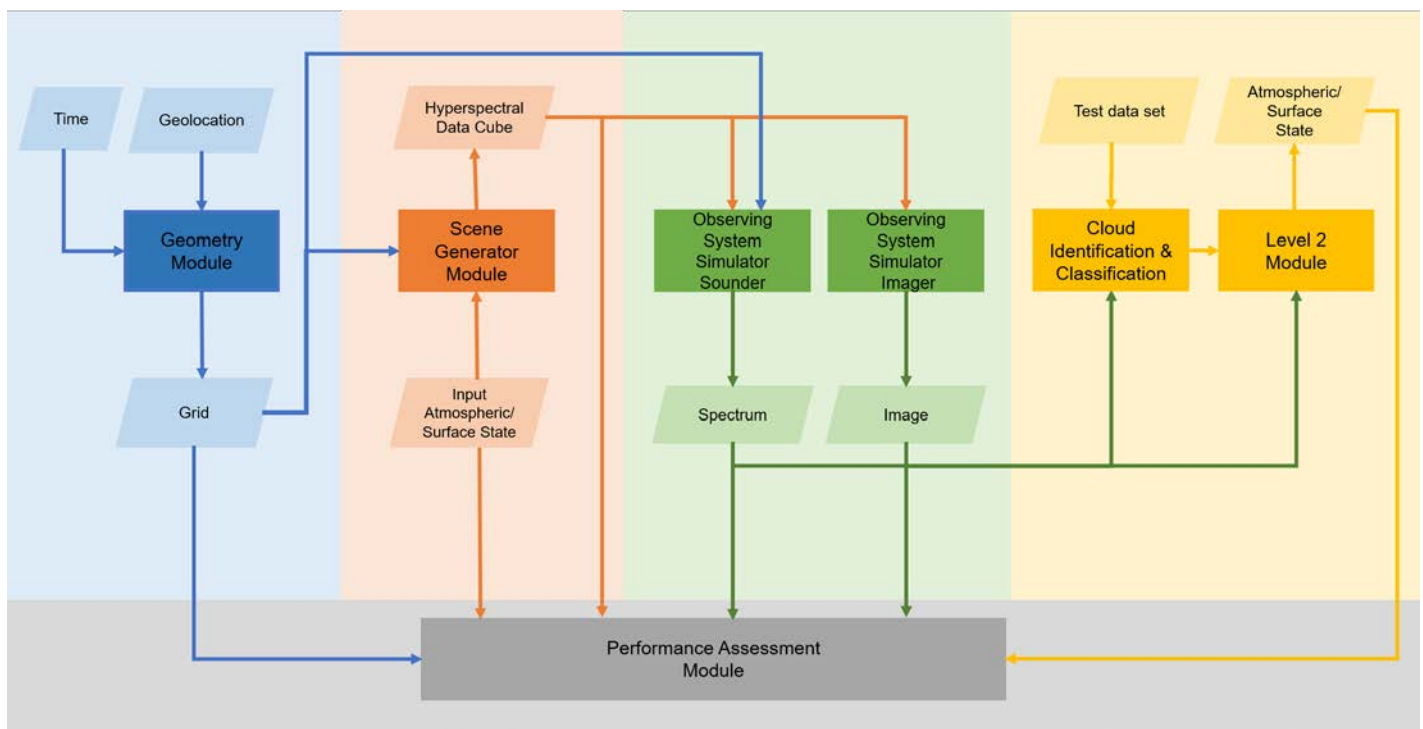


Figure 7.1 High level architecture of the FORUM end-to-end simulator (ESA)



end-to-end chain starts with an input of the orbit time and geolocation. Top of the atmosphere (TOA) radiances are created from the surface properties (surface emissivity and surface temperature) and the atmospheric state (gases, temperature, and clouds), at a spatial resolution suitable to simulate scenarios for the FORUM measurements. The top of the atmosphere radiances are sampled on a spectral grid much finer than the spectral resolution of the two instruments, the FORUM sounding instrument (FSI) and FORUM embedded imager (FEI). Spatial and spectral complexities are required to analyse geometric and radiometric uncertainties. Level-2 products are generated after the instrument simulators and the Level-1 processor. The performance assessment module compares the outputs of the Level-2 processor with the initial inputs. Each individual module, as well as the complete chain have been verified and/or validated using standard methods such as dedicated tests, review of design and code and analysis inspection. In the next sections each component of the FEES will be described in more detail.

7.1.1 FEES Geometry Module

The Geometry Module is executed first in the end-to-end chain. It generates a geometric grid of the input scene by modelling the satellite orbit, the platform attitude, and the viewing geometry based on user input of orbit time and geolocation.

The geometry module provides the real and estimated geolocation information (latitude and longitude) of each pixel in the grid by making use of ESA's Earth Observation Custom Furnished Item (EO-CFI) tools. It also provides information on the angular viewing (e.g. observation zenith angle) of each pixel of the grid and it is user-configurable, allowing to create grids with a spatial sampling up to ten times better than the FEI spatial sampling resolution. Such fine grids can be used to investigate the impact of scene inhomogeneities in both FSI and FEI.

The geometry module can also create a user configurable number of grids during an individual FSI dwell time, which allows modelling the pointing stability of the instrument's line of sight once perturbed with satellite attitude errors. This can be used to determine the impact of such instabilities on Level-1b with the FSI simulator and later, on Level-2 products with the Level-2 module.

The grid generated from the geometry module is combined with the scene generator and the observing system simulator so that the correct geophysical and spectral radiance information is assigned to each pixel of the grid, correlated with the extent and position of the field of view of the FSI and FEI.

The Geometry Module has been verified and validated making use of the well-established and proven routines contained in the EO-CFI tools.

7.1.2 FEES Scene Generator Module

The scene generator module, second to be run in the simulation chain is able to generate user configured scenes based on satellite or climatological data. The scene generator module provides hyperspectral data cubes of top of the atmosphere radiances derived from uniform or heterogeneous surface and atmospheric scenarios.

The scene generator module draws from complex 3-dimensional input scenes for generating realistic, high-spectral resolution top-of-atmosphere radiances. The atmosphere is defined by temperature and pressure profiles, the geometric height, trace gas concentrations of water vapour (H₂O), carbon dioxide (CO₂), ozone (O₃), nitrous oxide (N₂O), carbon monoxide (CO), methane (CH₄), oxygen (O₂), nitric oxide (NO), sulphur dioxide (SO₂), nitrogen dioxide (NO₂), ammonia (NH₃), and nitric acid (HNO₃), and the surface by its temperature, elevation, and emissivity. Clouds are described by cloud top height, geometrical thickness, optical depth at 900cm⁻¹, cloud phase, and cloud effective radius following the *conventional approach* based on Yang et al. (2013) as outlined in Section 6.1.2.2. These are all the parameters determining the top-of-atmosphere radiances in the far and mid-infrared, the relevant spectral range for these simulations. The atmospheric data is created from a combination of ERA-Interim (ERA-I) Reanalysis (Dee et al., 2011) and climatological data from IG2 v5.4 (Remedios et al., 2007) or from moderate-resolution imaging spectroradiometer (MODIS) product data when using the full complex 3-dimensional capabilities. There are several options for selecting the input scenes for initiating this module (see Section 7.1.6).

From the geolocation and time information (latitude, longitude, date and hour), the corresponding data from ERA-Interim and IG2 are picked. ERA-Interim provides data four times a day with a horizontal resolution of 0.75°. The ERA-Interim Reanalysis files account for atmospheric vertical profiles of the temperature, pressure, water vapour and ozone mixing ratios, besides information on the surface temperature and surface altitude. The IG2 data files contain altitude, pressure, temperature and gaseous mixing ratio profiles and the data is stored according to latitudinal belt (0–20°, 20–65°, 65–90°, for both North and South), day period, and season. The data sets are merged using surface temperature, temperature, pressure, water vapour and ozone mixing ratios between the surface and 60 km from ERA-Interim, and above 60 km until 80 km of altitude, as well as for the other trace gases IG2. CO₂ has been linearly corrected to concentration levels representative of 2018. The final number of vertical levels used in the computation is 52 and the vertical atmospheric grid extends from the surface to 80 km. If the surface altitude is higher than the sea level the number of layers might be reduced.

The surface emissivities are taken from the Huang et al. (2016) database containing emissivity values along the extended FORUM spectral range assigned to eleven different surface types. These surface emissivities are assigned according to a database of surface types created from MODIS measurements (Huang et al., 2016) and are chosen according to geolocation and month.

For creating cloudy scenes, the user defines cloud top height, cloud geometrical thickness, cloud optical depth at 900 cm⁻¹ and cloud effective radius. Clouds can be inserted into the full or part of the scene. The auxiliary data for the cloud microphysical properties are derived from the Yang et al. (2013) database for non-spherical particles, and from *Scattnlay* for spherical particles (Peña and Pal, 2009). For ice clouds, the Yang et al. (2013) database is used to construct the auxiliary file that contains the extinction/scattering coefficients and phase matrix of non-spherical particles. The ice crystals are assumed to be aggregates of pristine columns. From the single scattering properties of single particles, cloud bulk



properties are generated assuming that the particle size distributions are a set of gamma type functions with a shape parameter equal to 0.1. The distribution is sampled on the radius of the equivalent spheres. The effective radii of the final particle size distribution for ice clouds spans the 2-100 μm range.

In the case of scenes based on MODIS data, the following data sets were assembled for the simulations:

- The MODIS cloud product (06_L2) for cloud parameters (cloud particle phase, cloud particle effective radius, cloud optical thickness and cloud top height) and the surface temperature, retrieved at a spatial resolution of 1km
- The MODIS Atmospheric Profile product (07_L2) for temperature and water vapour profiles, and the surface height
- The GlobCover 2009, a Global Land Cover Map constructed with global MERIS (Medium Resolution Imaging Spectrometer Instrument) fine resolution mosaics, with about 300 m spatial resolution. The global land cover map counts 22 land cover classes defined with the United Nations Land Cover Classification System (LCCS), and these surface types are associated to one of the eleven surface types from Huang et al. (2016) emissivity database.

All input data, for both MODIS and the ERA-I/IG2 cases, is mapped onto the grids provided by the geometry module. For each grid, the scene generator module will then assign a hyperspectral data cube of top-of-atmosphere radiances. These are calculated by a couple of line-by-line multiple scattering radiative transfer codes at high spectral resolution (i.e. 10^{-2} cm^{-1} or higher) in the 50-1649 cm^{-1} spectral range. This covers the measurement intervals of the FSI and FEI sensors.

The radiative transfer codes are LBLRTM (Line-by-line Radiative Transfer Model – Clough et al. 2005) and LBLDIS (Turner et al., 2005) for clear and cloudy skies. The LBLDIS is a combination of LBLRTM and the DISORT (DIScrete Ordinate Radiative Transfer – Stamnes et al., 1988). The auxiliary database of gas spectroscopy properties is the AER v3.6 that in turn is derived from the high-resolution transmission molecular absorption (HITRAN) database. The water vapour continuum is described by the CKD_MT3.2 parametrisation, used to generate the clear sky radiances for the FEI and FSI. In the case of cloudy sky the LBLRTM calculates the optical depth of each atmospheric layer and vertical profiles, later used as input to LBLDIS. The LBLRTM is one of the most used radiative transfer models. The results have been validated with the observations of many instruments, and its execution time is acceptable, especially when the list of selected gases is kept short. The DISORT algorithm remains the undisputed leader of the full-physics methods for calculating multiple scattering effects. While there are different approaches (doubling and adding, stochastic methods), the DISORT has a very solid mathematical basis.

7.1.3 FEES Instrument and Level-1 Processing Modules

The behaviour of both FSI and FEI is modelled with dedicated modules. These modules introduce the most relevant error sources and uncertainties, and also include the Level-1 processors. Two instantiations of the FSI and FEI, representative of Concept A and Concept B were implemented in the end-to-end performance simulator.

7.1.3.1 FSI Module

This module simulates the behavior of the FSI by modelling a Mach-Zehnder interferometer, the most general design of an FTS, giving access to both input and output ports and allowing the implementation of separate divider/recombiner beamsplitters. The modelling follows a procedure further outlined in Bianchini et al. (2009).

The FSI module works as a chain. The hyperspectral data cube provided by the SGM is converted into an interferogram (Level-0) making use of interferometric coefficients and optical and electronic transfer functions, customised to represent concepts A and B. The interferogram (Level-0) is then transformed into an uncalibrated spectrum (Level-1a) using Fourier transformation with the possibility to compensate for specific instrument characteristics, with a zero path difference detection and a phase correction of the interferogram. In the following step, the radiometric calibration is performed on the uncalibrated spectrum making use of a hot and a cold reference measurement. Furthermore, the a-priori error originating from the calibration procedure (calibration error) and the detector noise (NESR) are estimated. The outputs of this last step are the measured atmospheric spectral radiance as observed on each of the two detectors at the two outputs of the interferometer (Level-1b). As a final step, the calibrated spectra obtained in each output port are averaged and then resampled on a configurable frequency grid (Level-1c), to obtain a single spectrum with the required spectral sampling to be provided as input to the Level 2 module.

A separate module calculates the instrumental line shape (ILS) according to the FSI instrument parameters. In particular, the instrumental line shape is computed considering the effects of the finite maximum optical path difference, and the line broadening and shift due to the finite divergence of the radiation propagating inside the interferometer (self-apodisation effect). The output of the ILS module is a set of tabulated and truncated ILS functions centered at specific, selectable wavenumbers.

Both Level-1c and ILS generated by the FSI are later used as inputs by the Level-2 module to perform the corresponding retrievals.

The following features, error sources, and uncertainties are included and propagated in the interferometer simulation chain in order to model the behaviour of the FSI:

- a model of the blackbody with customisable temperature (cold deep space or a set blackbody temperature) to allow flexibility in the customisation of the simulator
- High spatial resolution input scenes are used to account for the effects of the finite field of view and the consequent beam divergence inside the interferometer, also in case of observing non-homogenous scenes. The beam divergence, together with the finite optical path difference, results in a wavenumber-dependent instrumental line shape that introduces a frequency shift in the corresponding spectral radiance. The high-spatial resolution scene allow to accurately calculate the shape of the instrumental line shape
- Errors induced by line of sight drifts are included by interpolating between a set of interferograms acquired for a set of slightly different input scenes corresponding to different observation angles along the duration of the dwell time

- The beam splitter efficiency is one component of the interferometric efficiency and it is calculated considering the beam splitter's complex amplitude transmission and reflection coefficients
- The modulation efficiency is another component of the interferometric efficiency and is calculated considering contributions from wavefront tilt, wavefront shear and root-mean-square wavefront error
- The optical transfer function, also part of the interferometric efficiency, accounts for absorption and incomplete reflection in the instrument optics that are outside of the interferometric path, for instance, the windows on the detectors or the front telescope mirrors
- Electronics transfer functions modulating the outputs of the interferometer (e.g. detector response and preamplifier response)
- Detector noise, added and propagated through the FSI modules
- Calibration errors due to uncertainties on temperature and emissivity of the blackbody sources, and propagated through the calibration algorithm
- Sampling errors and digitisation noise
- Calibration functions are derived from a combination of the spectra of a hot and cold reference blackbody; these are obtained as an average of a customisable number of hot and cold blackbody measurements

Two sets of calibration measurements (at least) and one scene measurement are necessary to perform the radiometric calibration in the Level-1b module, resulting in at least three iterations of the main functional block. Error propagation is applied to calculate the calibration function and the calibrated measured radiances. The a-priori error on the calibration blackbody source thermometry and on the blackbody emissivity is used to calculate the calibration error, while the detector noise, expressed in terms of noise-equivalent power (NEP), is used to calculate the spectral noise. The two radiometrically calibrated spectra as well as the calibration error and spectral noise of the two detector channels, as a function of the wavenumber, are the output of the Level-1b module. The calibration strategy is fully configurable, and both the spectral noise and radiometric accuracy can be provided as pre-calculated inputs.

Dedicated tests comparing the results against dedicated pass/fail criteria have been carried out. Among others:

- The correct generation of the interferograms (Level-0), the instrument response and the final calibrated spectrum (Level-1b/c) including the calibration function, have been tested using TOA spectra acquired by the REFIR-PAD instrument in 2005 in a stratospheric balloon flight (Brazil) in the required wavenumber range.
- The correct ingestion, generation and propagation of noise errors has been tested by comparing noise error estimation by industry to the computed noise errors.
- The correct generation of the ILS has been evaluated by comparing the calibrated Level-1c spectrum of the FSI module to a radiative transfer model spectrum calculated at high spectral resolution and convolved with the tabulated ILS.

7.1.3.2 FEI Module

The FEI module models the FEI sensor behavior by processing spatially and spectrally oversampled scenes. This module accounts for the main instrument effects and noise error (both systematic and random) influencing the radiance acquisition, its sampling and its transformation into FEI Level-1b products. The features and error sources implemented within the FEI module are:

- Optical point spread function (PSF) for the spatial convolution of the high-resolution input scene.
- Instrument spectral response function (ISRF) for the spectral convolution of the high-resolution input scene
- Radiometric noise, modelled as a random signal with normal distribution with a standard deviation equal to the noise equivalent delta temperature (NE Δ T)
- Calibration bias and calibration gain uncertainty
- Quantisation and saturation errors in the analog-to-digital converter
- Attitude errors for the estimation of each pixel geolocation

The modelling and results of the features and errors listed above have been verified using dedicated tests with pre-determined pass/fail criteria. When relevant, the results were compared with the ones calculated by the dedicated performance models provided within Concept A and B industrial activities.

7.1.4 FEES Level-2 Retrieval Module

From the FSI Level-1c radiances, this module identifies whether the scene is clear or cloudy and then inverts the noisy spectra to extract information about the atmospheric composition. In addition, ancillary information is retrieved from the FEI Level-1b. The Level-2 retrieval module follows the approaches outlined in Section 6.1. Here some more specifics are provided.

A machine-learning algorithm based on principal component analysis, is the first step to assess whether the measured scene is clear or cloudy and what kind of cloud is present. The measured scene here is the Level-1c output of the FSI observing system simulator. The full algorithm is described in Maestri et al. (2019). Four classes of synthetic test sets were extracted from the same data sets as in the scene generator model for the area of interest over Europe and parts of Northern Africa (see Fig. 7.2): clear sky, cirrus cloud, water cloud and ice cloud. It should be noted that this is different from when the same algorithm is applied to the airborne data as described in Section 7.4, where only two classes (clear and cirrus cloud) were encountered during the campaign. Test set matrices are assembled from radiances at high spectral resolution. These test sets were processed with the two instances for the FSI observing system simulator to obtain test sets **TS $_x$** fully compatible with the two mission concepts of the two consortia taking the noise of the measurements into account. X can stand for clear, water, ice, or cirrus.

Eigenvectors ϵ **TS** and eigenvalues λ of the covariance matrices of the four (clear, cirrus, ice, water clouds) test sets are computed. The number of significant principal components that allows removing the part of the signal associated with the noise is defined by Turner et al. (2005) as the number P_0 that minimises the function:

$$ND(p) = \frac{RE(p)}{(P - p)^2} \tag{7.1}$$

where p is the p^{th} principal component, P is the total number of principal components, and

$$RE(p) = \sqrt{\frac{\sum_{i=p+1}^P \lambda_i}{J_X(P - p)}} \tag{7.2}$$

where λ_i is the i^{th} eigenvalue, and J_X is the number of spectra in the test set.

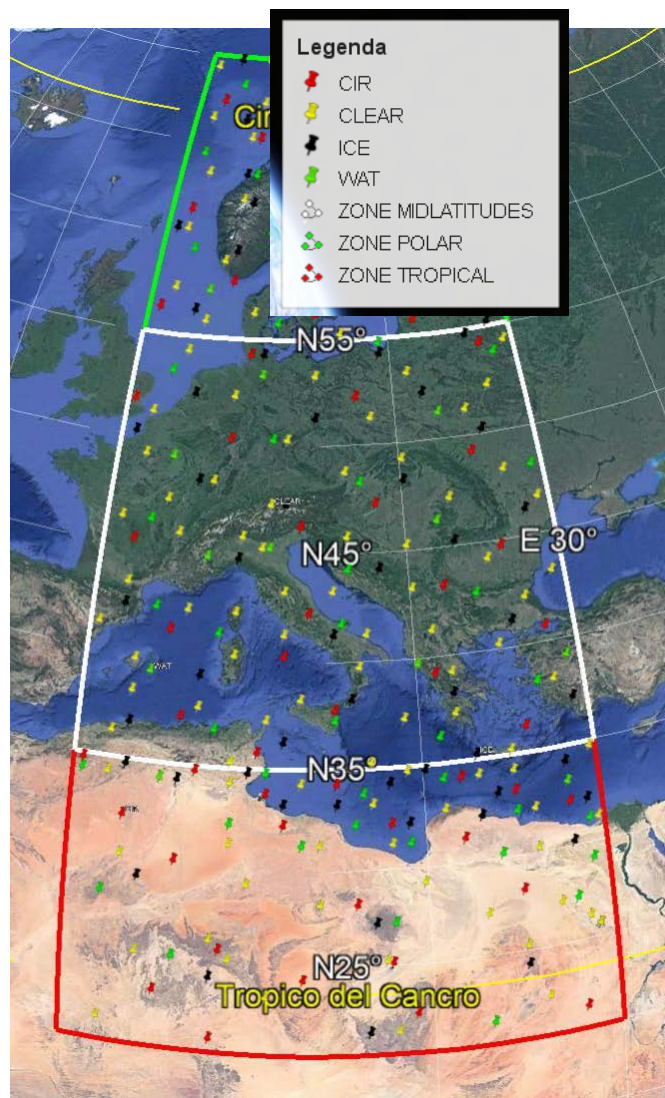


Figure 7.2 Locations of scenes and their classification that were used for creating the test data set for the machine learning cloud identification code (University of Bologna, Italy)

To perform the classification of the radiance produced in the end-to-end simulator chain, extended training sets \mathbf{ETS}_X are defined by adding the *measurement* to the test set matrix. With these similarity indices SI_X are computed:

$$SI_X = 1 - \frac{1}{2P_0} \sum_{p=1}^{P_0} \sum_{v=1}^{v_{tot}} |\epsilon \mathbf{ETS}_X(v, p)^2 - \epsilon \mathbf{TS}_X(v, p)^2| \quad (7.3)$$

where $\epsilon \mathbf{TS}_X$ and $\epsilon \mathbf{ETS}_X$ are the eigenvectors of the four training set and of the four extended training set, and they depend on the wavenumber v . For instance, if the Level-1c radiance is a clear sky case, then the $\mathbf{TS}_{\text{clear}}$ is similar to the original $\mathbf{ETS}_{\text{clear}}$, because no new information was added, whereas the $\mathbf{ETS}_{\text{cirrus}}$ will be different from the original $\mathbf{TS}_{\text{cirrus}}$ because a significantly different element was introduced. The highest SI establishes the class of the scene. This classification undergoes an additional test depending on the highest similarity index. Again, for the clear sky measurement example, the following tests have to fulfill the criteria:

- $SI_{\text{cirrus}} - SI_{\text{clear}} < 0$
- $SI_{\text{water}} - SI_{\text{clear}} < 0$
- $SI_{\text{ice}} - SI_{\text{clear}} < 0$

A successful classification has to pass all three tests and an unclassified scene results from an inconsistent cross test. The performance of the cloud identification and classification module has been thoroughly tested. Details can be found in Maestri et al. (2019).

Depending on the clear or cloudy classification, the Level-2 module will branch either into a clear-sky retrieval or cloudy-sky retrieval. In future updates to the FEES, also clear-sky parameters will be retrieved for cirrus cloud cases.

In the clear-sky case, the retrieval is performed using optimal estimation (Section 6.1.2) with an a priori covariance matrix adapted to the FEES settings, originating from the covariance matrix applied to assimilate IASI radiances into the UK Met Office models. Water vapour, temperature profile, and surface temperature are retrieved simultaneously. The FEES also calculates the total precipitable water vapour. The a priori profiles are given by the true profiles perturbed by a quantity compatible with the covariance matrix of the a priori profile. Surface temperature and water vapour and temperature profiles are given by 10 year climatological averages from ECMWF ERA interim data and are used as first guess in the inversion. In future versions, for cases with precipitable water vapour below a certain threshold value, the emissivity will also be retrieved. This will be possible because the atmosphere will be more transparent, and the observed radiance will contain information about the surface (Fig. 2.6).

In the cloudy-sky case, a priori estimates of surface temperature and atmospheric temperature and water vapour profiles are defined in the same way as for the clear sky case. A priori cloud properties are estimated as follows:

- **Cloud top height:** if the cloud is optically thick the cloud top height is estimated from the FSI brightness temperature at 900cm^{-1} . In the case of cirrus, the cloud top height is set according to latitude based on Veglio and Maestri (2011) as cloud top height = $15 - (\text{latitude}/10)$.
- **Cloud optical depth:** For optically thick clouds, the optical depth is set as the most probable value for that location and pressure level according to the ESA monthly cloud CCI data. For optically thin clouds, a fixed optical depth value is used. This is defined based on Veglio and Maestri (2011) for tropical scenes (latitude $\leq 30^\circ$) as 0.82, and for midlatitude/polar scenes (latitude $> 30^\circ$) as 0.96.
- **Cloud particle effective radius:** The cloud particle effective radius is set to the most probable value for the location according to for each kind of cloud is also read from the ESA monthly cloud CCI datab, with no dependence on the pressure level.
- **Cloud thickness.** The cloud geometrical thickness is set to a standard value according to cloud type.

In the case of missing ESA cloud CCI data, standard values of effective radius and optical depth are used. A priori errors are also fixed: 1 km for cloud top height and cloud geometrical thickness; 2 for cloud optical depth and $10\ \mu\text{m}$ for the cloud effective radius. In the cirrus cloud case, a pre-processor refines the a priori estimates of cloud optical depth, cloud particle effective radius, and cloud top height with a 1-dimensional minimisation based on a bisection method.

The cloud thickness is not included in the retrieval state vector and its value is kept fixed at the standard for that cloud type. The other parameters are retrieved using the a priori values described above as a starting point for the inversion algorithm.

The Level-2 retrieval uses the same radiative transfer codes as the scene generator module, LBLRTM and LBLDIS (Section 7.1.2). This avoids errors being introduced into the chain from phenomena parametrised differently in different radiative transfer codes. The same 52 level vertical grid, as use for the scene generator module is used.

Additional data qualifiers are derived from the FEI Level-1b measurements and the geolocation, e.g. the sea/land fraction is calculated for the field of view of the FSI. The inhomogeneity of the scene is evaluated by analysing the FEI Level-1b radiances within the FSI field of view. Groups of data are defined on the basis of the distribution of FEI brightness

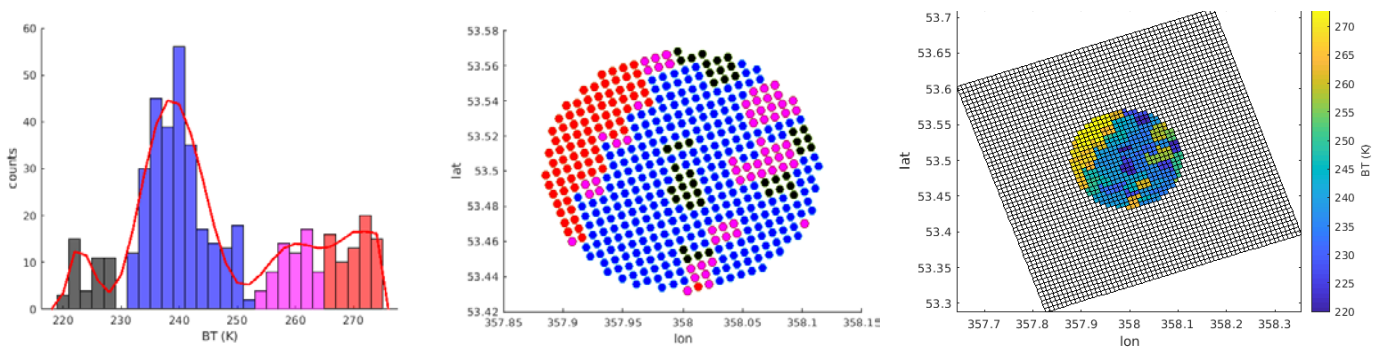


Figure 7.3 Brightness temperature distribution for the FEI for a complex scenes (this is the MODIS 7 case) (right panel), the frequency distribution (left panel) and the fitted 4 levels of heterogeneity (middle panel) (University of Bologna, Italy)



temperatures. This is achieved by fitting a polynomial of variable order to the brightness temperature histogram. The minima of the polynomial are then used to group the data and thus calculate the fraction of the FSI field of view corresponding to each. This process is illustrated in Fig. 7.3 which shows a distribution with four levels of inhomogeneity. The corresponding fractions are: 9 % grey, 60 % blue, 14 % pink, 17 % red.

The performance of the Level-2 module has been assessed and refined during the Phase A study by comparing the output with the truth. In Phase B these efforts will continue and spectral fluxes will also be added as a FEES Level-2 product.

7.1.5 FEES Performance Assessment Module

The performance assessment module is the last module executed in the chain. It produces a series of figures of key performance factors to compare the outputs of the end-to-end chain with the input scenes. It is based on standard plotting routines and functionalities.

7.1.6 FEES Test Scenarios Description

As mentioned in Section 7.1.1, there are several data sets that can be used to initialise the end-to-end simulations; one is based on ERA-I/IG2 data and another one based on MODIS data products. In general, the FEES is able to simulate FORUM measurements all over the globe. But in order to make the FEES a portable tool, input data sets are limited to areas of interest. The chosen region for the ERA-I/IG2 data is shown in Fig. 7.4, left panel, 70°–20°N, and 0°–30°E. The scene is considered for two days, one day in Summer, 15 July 2017, and the other one in Winter, 15 January 2018, both days for 00, 06, 12, and 18 UTC.

This area is chosen to be representative of the most typical atmospheric conditions, including extreme cases, polar, mid-latitudes and equatorial latitudes. The input to the simulator is selected from the area of interest by geolocation and date. Any kind of clouds can be defined in the input files and these will then be added to the scene. Similarly, the surface properties from the databases can be overwritten. From these, uniform or heterogeneous scenes can be created. For the heterogeneous scenes there are two ways: a circle of any diameter can be inserted anywhere into the field of view. Alternatively, a straight-line segment can be added with customisable position. This would be e.g. representative of a coastline scene having two different surface temperatures and emissivities, or in the former case, a cloud. Two instances of heterogeneity can be added simultaneously and those can also overlap enabling the simulator to create multilayer clouds.

Scientific assessment of the FEES is based on 12 scenes outlined in Table 7.1. These 12 key scenes address a wide range of the environments that will be encountered by FORUM. Six of the scenes account for cloud cover and six are in clear sky but with the same surface and atmospheric properties of the corresponding cloudy case. This was done in order to:

- provide a challenging dataset for cloud identification/classification
- allow the evaluation of the errors associated with the retrieved geophysical parameters when misclassification are assumed.

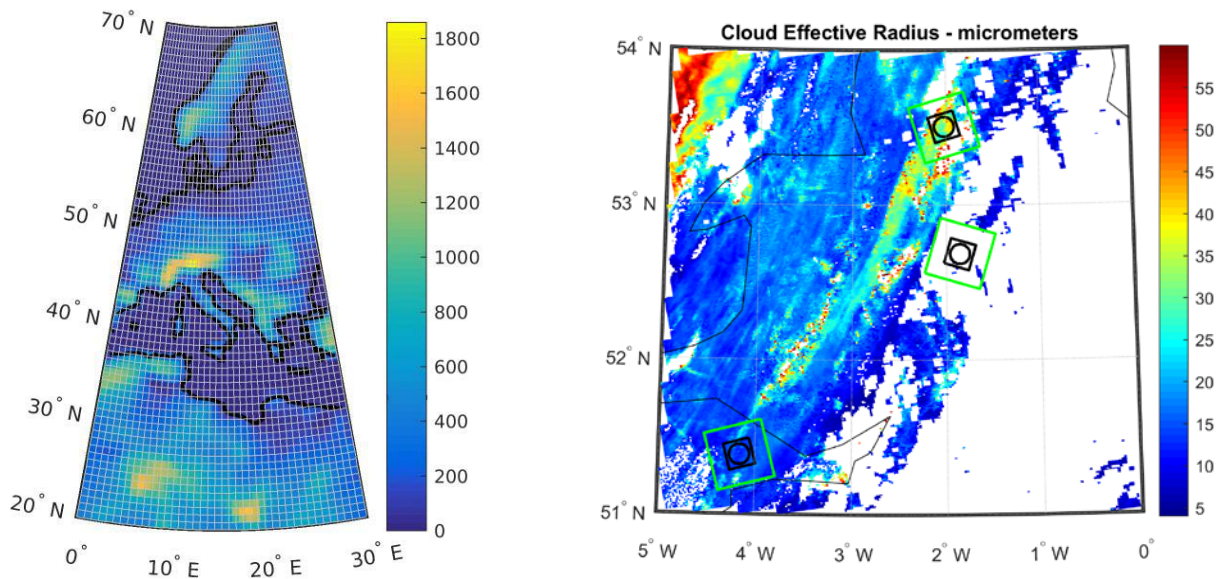


Figure 7.4 Left panel: the study area for which dedicated datasets have been generated, here the surface levels in metres. Right panel, MODIS region of interest from a granule recorded over the United Kingdom on 7 February 2018. From North to South, the three regions are referred to as MODIS 7, 8, and 9 (University of Bologna, Italy)

The simulations of the selected scenarios are based on information derived from ERA-Interim reanalysis and monthly averaged surface properties derived from satellite measurements and thus represent realistic observational conditions. The scenes span observational conditions ranging from Arctic regions to Tropics, and include the following extreme cases:

- a desert case for evaluating the effects on the profile retrievals (temperature and humidity) of a large temperature gradient between surface temperature and atmospheric/cloud layers
- an ocean case is a very common case and is a typical observational condition. When in presence of a very thin cirrus cloud (optical depth is set to 0.3) it represents a scientifically relevant case for cloud identification and properties retrieval.
- an ocean case with stratus is common, but challenging. It is suitable to evaluate the errors in the retrieval of atmospheric properties when the stratus is not identified due to its low altitude and its properties similar to the ocean layer.
- a continental case in clear sky or in presence of an altocumulus cloud, allowing a verification of the clear/cloudy retrieval algorithm over land.
- a snow surface representative of Arctic conditions that are observed every orbit by FORUM. When accounting for an ice cloud with moderately thick opacity (optical depth of 3) it is a very challenging case owing to the similarity of the cloud properties to the atmospheric background.
- a Po valley case with a cumulonimbus is relevant for the study of extremely thick clouds and also archetypal of hurricane conditions.

Scene	Surface	Cloud phase, if cloudy	Cloud top height/ thickness (km)	Optical depth	Effective particle radius (μm)
Cirrus on desert [Tropical – Sahara Desert] Summer	desert	ice	12/2	1	10
Cirrus on ocean [MidLat - Mediterranean] Summer	sea	ice	15/1	0.3	6
Coastal marine stratus [MidLat - Mediterranean] Summer	sea	liquid	1.25/0.5	20	10
Continental 1 altocumulus [MidLat – Black Forest] Winter	vegetation	ice	10/2	6	30
Ice cloud on snow ground [Polar - Finland] Winter	snow	ice	8/2	3	18
Continental 2 cumulonimbus [MidLat – Po Valley] Summer	vegetation	ice	11/6	300	80

Table 7.1 Description of the 12 scientific scenes considered in the FEES

Heterogeneous scenes, are obtained using atmospheric and surface properties as in the uniform scenes. These scenes are applied to evaluate how the quality of retrieved products is degraded by the presence of heterogeneities.

In the case of scenes based on MODIS data, radiances were pre-computed over a region in the United Kingdom (see Fig. 7.4). Three cases have been selected as marked in the figure, a clear sky scene (referred to as MODIS 8), and two cloudy scenes (MODIS 7 and MODIS 9). These are challenging scenes with respect to their heterogeneity.

7.2 Level-1 Mission Performance

This section reports the Level-1 performance achieved by the technical concepts described in Chapter 5, at the time of the Preliminary Requirements Review (PRR) at the end of the Phase A. The performance have been computed by means of dedicated system and instrument performance models using, when available, test data obtained from the technology pre-development activities, also described in Chapter 5. The FORUM End-to-End Performance Simulator (FEES) has been used to model FEI Level-1b and FSI Level-1c data products, as defined in Chapter 4, using geophysical scenes constructed either synthetically or by ingestion of MODIS data. The FEES has been also used to confirm system and instrument performance, when relevant.

7.2.1 Level-1 Mission Performance Summary

Table 7.2 shows that one of the two technical concepts (Concept B) described in Chapter 5 is able to achieve Level-1 performance in line (and sometimes better) with the mission requirements defined in Chapter 4, which were derived from the FORUM scientific mission objectives (Chapter 2 and 3). Full compliance is also expected to be achieved by the other

concept (Concept A) during Phase B1, based on the technical similarities between both concepts.

Mission Requirement	Specification		Performance Achieved			
			Concept A		Concept B	
Mission Lifetime	4 years excluding commissioning		>4 Years	[✓]	>4 Years	[✓]
Latency of level-1 data	24 hour nominal 3 hour under request		< 17 hours	[✓]	<17 hours	[✓]
			< 2 hours	[✓]	< 2 hours	[✓]
Coverage gaps due to calibration	≤ 20% of samplings		18 %	[✓]	20 %	[✓]
Spatial Sampling Distance (SSD)	< 100 km (G: <70 km)		< 100 km	[✓]	< 100 km	[✓]
Temporal co-registration with MetOp-SG(1A)	< 1 minute		< 1 minute	[✓]	< 1 minute	[✓]
Across-track spatial co-registration MetOp-SG(1A)	<300 km (G: < 100km)		< 100 km	[✓]	< 100 km	[✓]
Maximum FSI LoS depointing angle	< ± 3.5 deg		[✓]		[✓]	
Pointing Requirement	Specification	Pointing error	Performance Achieved			
Geolocation accuracy (absolute knowledge)	< 750 m	AKE	743 m	[✓]	703 m	[✓]
Across-track absolute pointing accuracy	< 1250 m	Across track APE	544 m	[✓]	1017 m	[✓]
Line of Sight Stability (diameter)	< 200 m (G: 100 m)	RPE + APE yaw steering error contributor	194 m	[✓]	186 m	[✓]
FSI Observational Requirements and Performance						
Spectral Requirement	Specification		Performance Achieved			
Spectral Range	100 to 1600 cm ⁻¹		[✓]		[✓]	
Spectral Resolution	< 0.5 cm ⁻¹ (G: < 0.36 cm ⁻¹)		< 0.46 cm ⁻¹	[✓]	< 0.48 cm ⁻¹	[✓]
Spectral Knowledge	< 2 ppm (G: < 1 ppm)		1 to 3ppm	[✓]	< 1 ppm	[✓]
			See 7.1.3.4 for more details			
Instrument Spectral Response Function (ISRF) knowledge error	< 0.06 mW/(m ² sr cm ⁻¹) (G: < 0.02 mW/(m ² sr cm ⁻¹))		<0.02 mW/(m ² sr cm ⁻¹)	[✓]	< 0.04 mW/(m ² sr cm ⁻¹)	[✓]
Geometric Requirement	Specification		Performance Achieved			
System Integrated Energy (SIE)	> 90% over 15km area		> 90.8%	[✓]	> 94%	[✓]
System Energy Distribution Function (SEDF) within one spectral sample	Threshold: variation < 15% x SEDF _{MAX} over 90% of Full Width Half Maximum (FWHM) Goal: variation < 10% x SEDF _{MAX} over 80% of Full Width Half Maximum (FWHM)		<15%	[✓]	<15%	[✓]
SEDF between spectral samples	Threshold: difference between 2 spectral samples < ±5% over 80% of FWHM		< ±5%	[✓]	< ±5%	[✓]

	Goal: difference between 2 spectral samples < ±5% over 90% of FWHM		
Radiometric Requirement	Specification	Performance Achieved	
Signal dynamic range	Spectral radiances with equivalent Brightness Temperature from 190 K to 300 K	[✓]	[✓]
Noise Equivalent Spectral Radiance (NESR)	<0.6 mW/(m ² ·sr·cm ⁻¹) (G: < 0.4 mW/(m ² ·sr·cm ⁻¹)) within [200-800 cm ⁻¹] < 2.0 mW/(m ² ·sr·cm ⁻¹) (G: <1.0 mW/(m ² ·sr·cm ⁻¹)) outside [200-800 cm ⁻¹]	[✓]	[✓]
Absolute Radiometric Accuracy (ARA)	Threshold: <0.25 K from 200 to 1300 cm ⁻¹ <1 K elsewhere Goal: <0.2 K from 200 cm ⁻¹ to 300 cm ⁻¹ <0.1 K from 300 cm ⁻¹ to 1100 cm ⁻¹ <0.2K from 1100 cm ⁻¹ to 1300 cm ⁻¹ <1 K elsewhere	[✓] from 200 K to 300 K [✗] from 190 K to 200 k See 7.1.3.2 for more details	[✓]
FEI Observational Requirements and Performance			
Spectral Requirement	Specification	Performance Achieved	
Spectral Range	10.5 μm ±0.75 μm	[✓]	[✓]
ISRF Knowledge	<5% of the peak value	<5% [✓]	<5% [✓]
FEI Out-of-band signal	< 2% (G: 1%) at 210K	<1.3 % [✓]	<0.6% [✓]
Geometric Requirement	Specification	Performance Achieved	
Temporal Sampling	> 5 acquisition per dwell time	28 [✓] (16 images co-added per acquisition)	5 [✓] (84 images co-added per acquisition)
Field of View (FoV)	>36 x 36 km ²	41 x 41 km ² [✓]	38.4 x 38.4 km ² [✓]
Spatial Sampling Distance (SSD)	<0.6 km at half FSI dwell time	0.577 km [✓] (Hmax)	0.599 km [✓] (Hmax)
Modulation Transfer Function (MTF)	MTF > 0.3 at Nyquist frequency	0.32 [✓]	0.32 [✓]
Radiometric Requirement	Specification	Performance Achieved	
Dynamic range	From 190K to 300K	[✓]	[✓]
Noise Equivalent delta Temperature (NEdT)	≤ 0.7 K (G: < 0.3 K) at 210 K	0.7 K [✓]	0.18 K [✓]
Relative spatial radiometric accuracy (RXRA)	<0.2 K at 210K	< 0.2 K [✓] (Linear sum)	<0.13 K [✓] (linear sum)
Absolute Radiometric Accuracy (ARA)	< 3K (G: < 1K) at 210K	< 2K [✓] (linear sum)	<1.1 K [✓] (linear sum)
Straylight	≤1.5 K at a distance of 5 SSD (G: <0.8 K at a distance of 3 SSD)	< 1.5 K at 5 SSD [✓]	< 1.5 K at 5 SSD [✓]

Table 7.2 Main Level-1 mission and instrument requirements and achieved performance for Concept A and B. Compliance is highlighted with [✓] while [✗] is used to highlight non-compliance or partial non-compliance.

7.2.2 Level-1 Mission Performance

Data latency: The data latency, defined as the time interval from acquisition of data by the instrument to the delivery of the product at the user interface, is driven by various factors, e.g. data volume, number and location of downlink Ground Stations (GS), space-to-ground downlink speed, transfer time to PDGS, and processing speed. Both Concepts achieve less than 24 hours of maximum data latency of Level-1 products by downlinking twice per day at Kiruna GS and less than 3 hours when downlinking to Svalbard GS every orbit, as shown in Fig. 7.5. The performance achieved provides more than one hour margin to also process and distribute Level 2 data.

Coverage and sampling: Both FSI concepts sample the Earth continuously with a spatial sampling distance varying from 99 km to 100 km, as shown in Fig. 7.7 (right) along the orbit. FORUM achieves the required sampling by implementing a step-and-stare concept with a dwell time of 14 seconds, constant along the orbit, and a repositioning time of the pointing mirror of less than one second. The calibration strategy defined in Chapter 5 results in about 18% and 20% samples loss during nominal operations for Concept A and B, respectively. Fig. 7.6 (right) shows, for Concept B — similar for Concept A —, that the sampling strategy does not create systematic loss in coverage.

FORUM provides a homogenous worldwide coverage as shown in Fig. 7.6 left, despite the coarse sampling, the small FSI footprint and the missed samples due to calibration. FORUM provides daily revisit of the Polar Regions between 76° and 82° (North and South Hemisphere).

Geolocation, pointing and LoS stability: Table 7.2 summarizes the geolocation and pointing performance (i.e. absolute pointing knowledge, across-track absolute pointing and LoS stability over the FSI dwell time). Both consortia meet all requirements with a gyroless concept. Fig. 7.7 (left) shows the LoS stability during a FSI dwell time — Concept A (top) and Concept B (bottom) —, as modelled by the FEES, using attitude errors as derived from the Phase A activities. The geolocation of the FSI LoS during 5 FEI acquisition, equally distributed during the FSI dwell time, are plotted. All of them remain within a circumference of 200 m, as specified in the requirement.

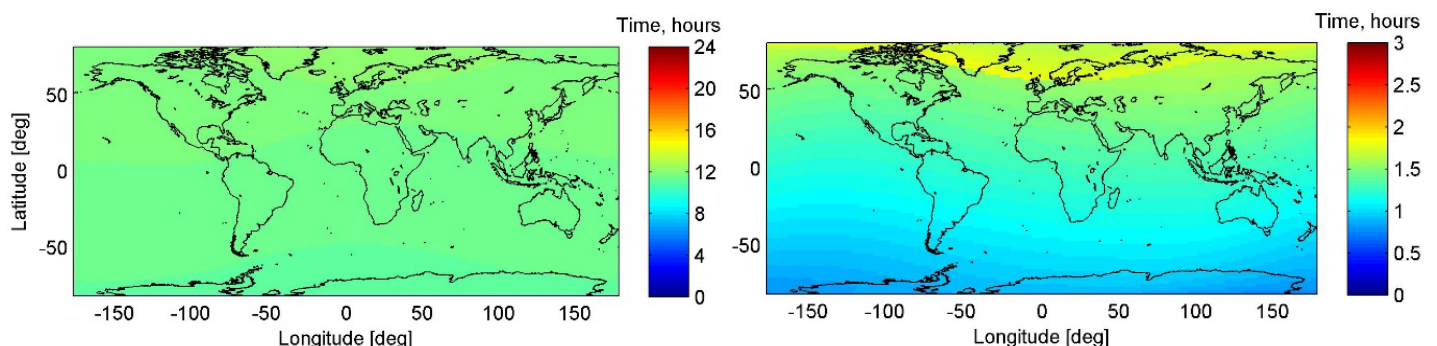


Figure 7.5 Maximum data latency for Level-1 data products when downlinking twice per day using Kiruna GS (Left) or with one downlink per orbit using Svalbard GS (Right). Plots for Concept B, similarly for Concept A

FEI Ground Sampling distance and FSI/FEI footprint co-location Fig. 7.8 (left top and bottom) shows the FEI footprint for a nadir acquisition at about 24 degrees latitude modelled using FEES. The colour map shows the SSD for each of the pixels within the FEI footprint. The variation of the SSD within the pixels of the footprint due to Earth’s curvature is clearly observed. The SSD of all pixels remain below 600 m. Fig. 7.8 (right) shows the spatial co-location of the FSI and FEI footprint for Concept A, as modelled by the FEES.

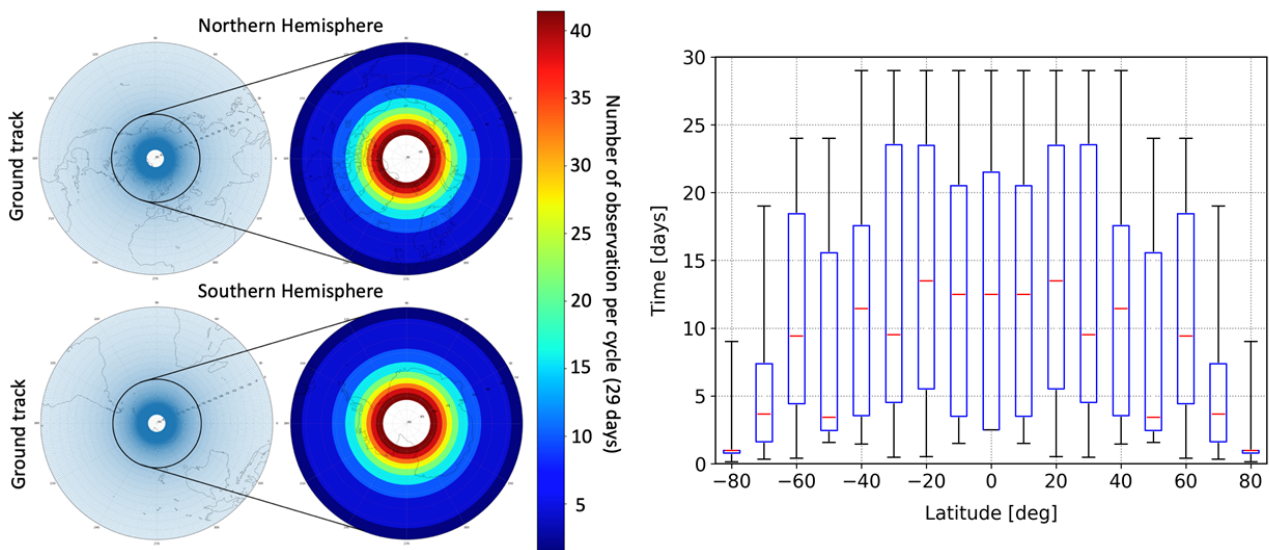


Figure 7.6 : Left: Concept A and similar for Concept B, orbit ground track and coverage in the Northern Hemisphere (top) and in the Southern Hemisphere (bottom), data computed for an orbit repeat cycle. Right: Concept B and similar for Concept A average (red line), 25% and 75% percentiles (blue bars) and minimum and maximum (error bars) revisit time per latitude after a sample is missed due to calibration. Data is computed for a period of 12 repeat cycles.

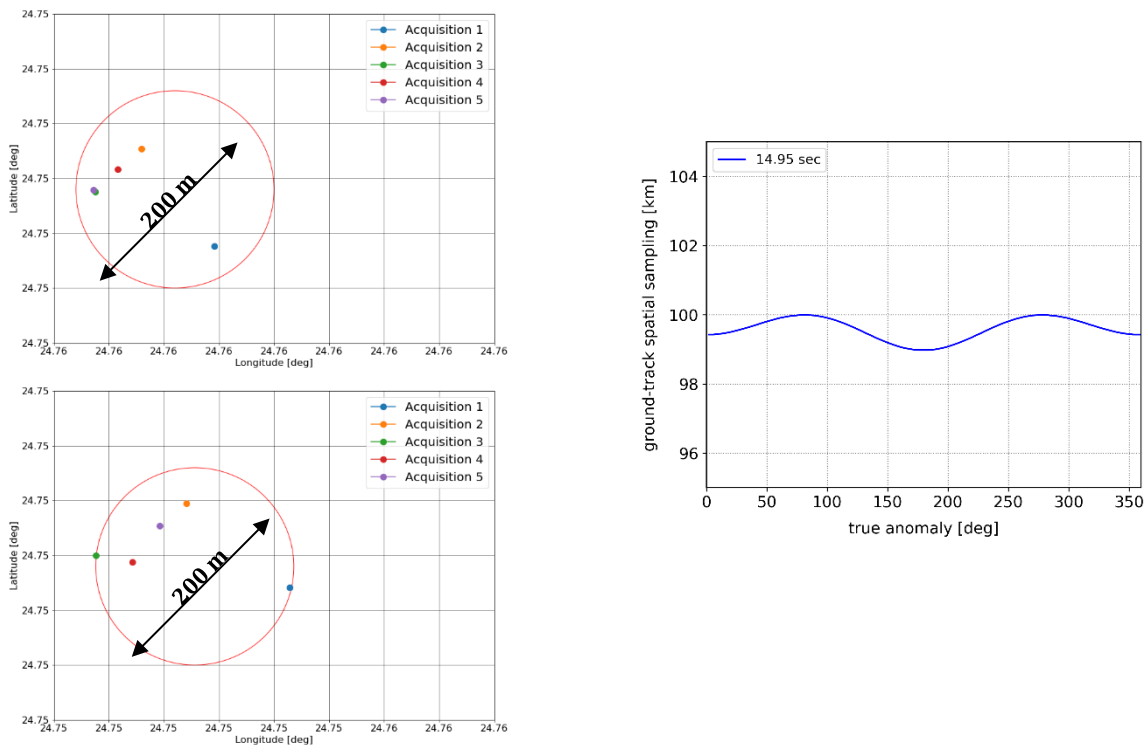


Figure 7.7 Left: LoS stability during the FSI integration time - Concept A (top) and Concept B (bottom) modelled using the FEES and attitude errors as derived from the Phase A baseline concepts. Acquisition 1: beginning FSI dwell time, Acquisition 3: middle FSI dwell time, Acquisition 5: end FSI dwell time. Right: SSD between two consecutive FSI samples plotted along the orbit (true anomaly).

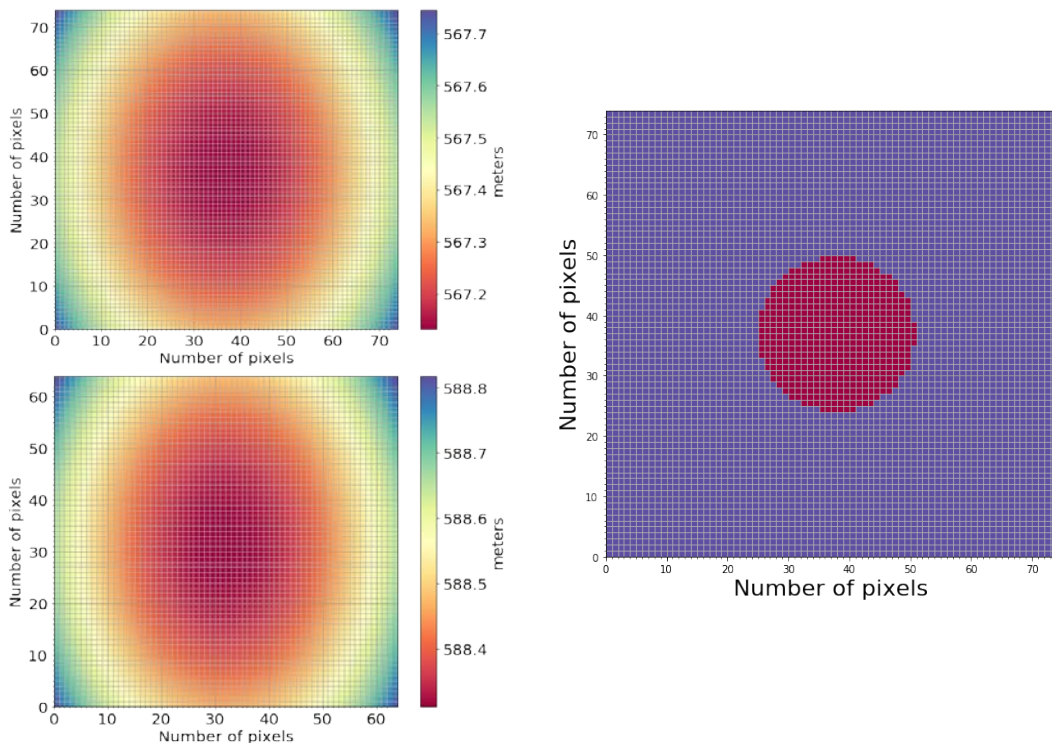


Figure 7.8 Left: FEI footprint for a nadir FEI acquisition at ~24 deg latitude. The plot shows a colour map of the SSD for every pixel in the footprint – Concept A (top) and Concept B (bottom). Right: FSI footprint (red circle) co-located with the 74 x 74 pixel grid of the FEI (purple square) – Concept A and similar for Concept B.

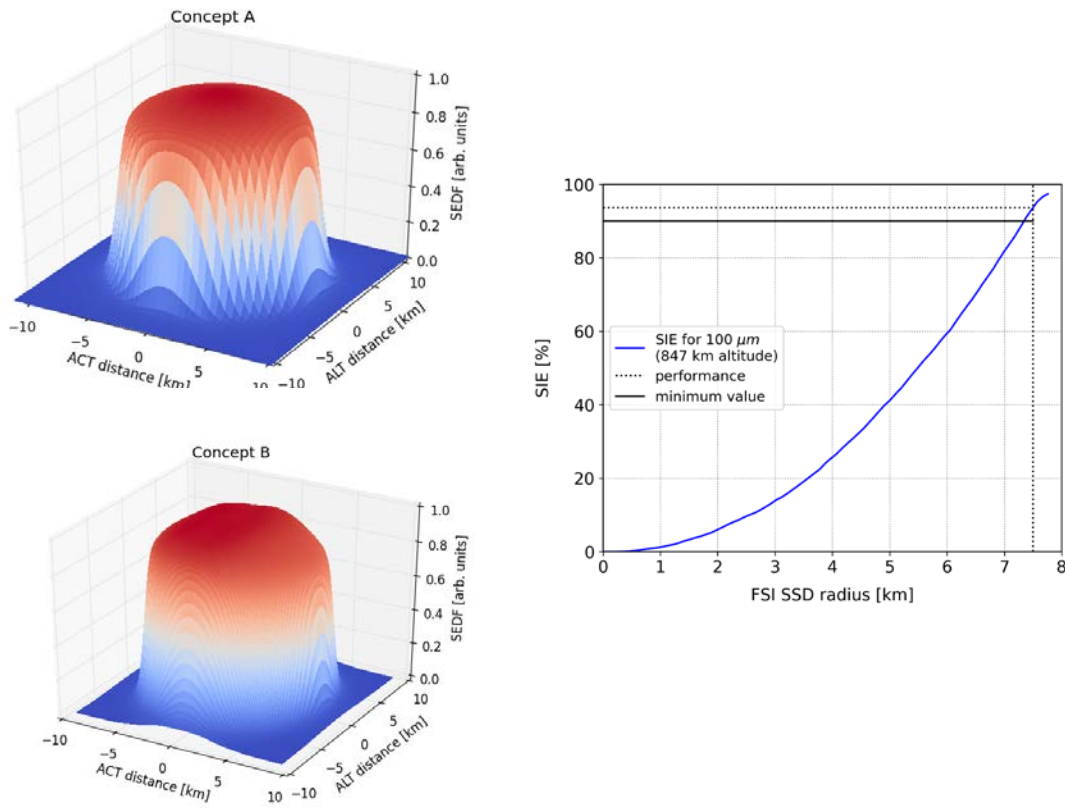


Figure 7.9 Left: SEDF at 100 cm⁻¹ for Concept A (top) and B (bottom). Right: Worst case SIE at 100 cm⁻¹ for half of the spatial sample – Concept B similar for Concept A

7.2.3 FORUM Sounding Instrument (FSI) Level-1 Performance

7.2.3.1 Geometric Performance

System Integrated Energy (SIE) and System Energy Distribution Function (SEDF): Fig. 7.9 shows the SEDF of both instrument concepts (left top: Concept A, left bottom: Concept B) at 100 cm⁻¹. Despite of diffraction effects blurring the SEDF edges significantly at the lowest wavenumber of the spectral range, both concepts offer almost perfect circular spatial sensitivity with flatness in the centre according to the specifications (see Table 7.2). The sharpness at the edges of the SEDF defines the performance in terms of System Integrated Energy (SIE), which is depicted in the right panel of Fig. 7.9, also at the worst-case wavenumber (100 cm⁻¹). As seen in the Fig. 7.9, it complies with the demands that 90% of the total detected energy originates from within a circle of 15 km diameter.

7.2.3.2 Radiometric Performance

Noise Equivalent Spectral Radiance (NESR): The main contributors for the NESR budgets, together with their typical values, are listed in Table 7.3; all contributors are mutually independent and hence summed up in root-sum-squared. The main component of



the NESR budget is the noise created by the pyroelectric detectors (i.e. Detector Noise Equivalent Power). Other relevant noise sources are the front-end electronics (i.e. amplifier and quantisation noise and sampling errors), the speed fluctuations of the scanning mechanism, the sampling errors due to noise in the metrology channel and delays between the science and metrology signal. Shot noise is orders of magnitude smaller than detector noise hence considered negligible.

The NESR performance for the baseline concepts is shown in Fig. 7.10. The green curves shows the NESR calculated using data available from the predevelopment activities (i.e. diamond Beamsplitter: 4RT) and with the detector technical specifications from the vendor, also verified with data measurements in the pre-developments. The blue curves show the expected performance when using screened detector (improvement between 10 and 15 %, see Chapter 5). The red dotted curves show the potential improvement (5 %) of the instrument performance by optimization of the operation temperature of the pyroelectric detector. The red-dotted curve for Concept B also include the anti-reflection treatment on

Contributor to the NESR	Summation rule	Typical value at 800 cm ⁻¹ [mW/sr/m ² /cm ⁻¹]
Detector Noise Equivalent Power (NEP)	rss	0.5
Amplifier noise	rss	0.003
Quantization noise	rss	0.4
Sampling errors	rss	0.002
Speed fluctuations	rss	0.05
Shot-noise (scene/detector)	rss	Negligible

Table 7.3 Contributors to the NESR budget considered in Concept A and B

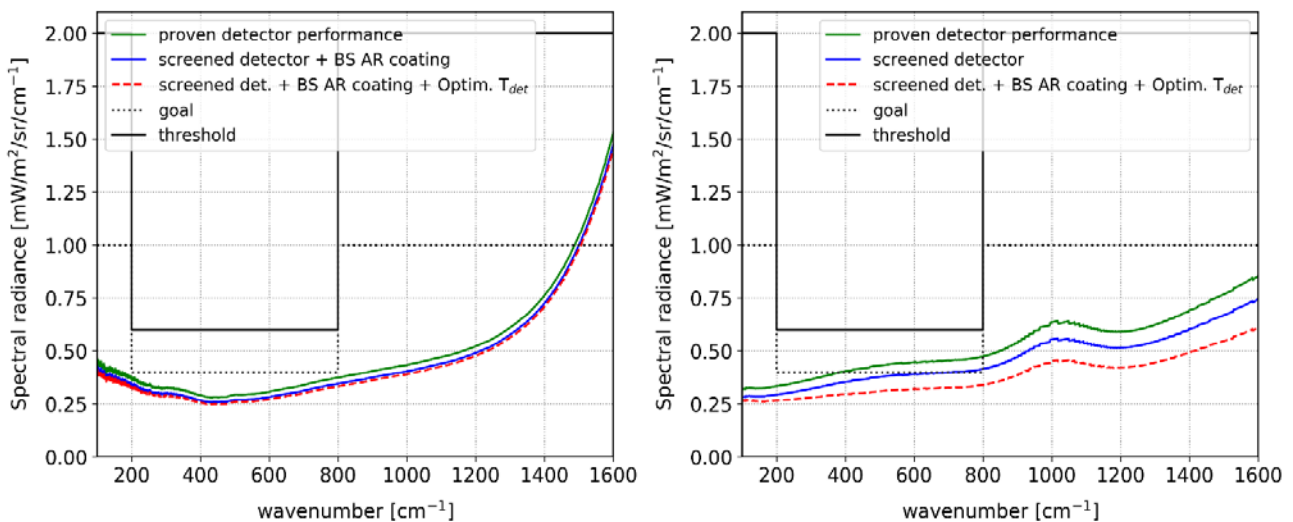


Figure 7.10 Left: NESR for Concept A; baseline beamsplitter and detector performance based on data obtained in the detection chain and beamsplitter predevelopment (green) (see Chapter 5), with screened detectors (blue), with screened detectors and optimum detector temperature (red dotted). Right: NESR for Concept B; based on data obtained from the beamsplitter and detection chain pre-developments (See Chapter 5) (green), screened detector (blue) and screened detector, antireflection coating and optimum detector temperature (Red dotted).

the diamond beam-splitter, considered in the baseline of Concept A, with an expected to improvement of 5 to 15%, depending on the spectral position, should the on-going Phase A pre-developments be successful. The NESR is compliant with the Threshold requirements by an ample margin for both baseline concepts. In case of using optimised detectors and a successful pre-development results in Phase B1, the performance could be better than the goal for both concepts in all the spectral range, especially in the FIR.

Absolute Radiometric Accuracy (ARA): The main contributors to the ARA budget are associated to calibration blackbody temperature and emissivity, instrument background temperature, noise on calibration measurements as well as biases due to scattered solar radiance and different incidence angles on the scanning mirror as detailed in Table 7.4. Calibration of measured Earth radiances relies on the implementation of an on-board blackbody cavity with temperature, emissivity and reflected instrument background knowledge as main uncertainties.

The blackbody temperature is monitored continuously in-flight using a thermistor including a phase change cell (Concept A) or a Platinum Resistance Thermometer (PRT) (Concept B). The emissivity of the blackbody is characterised on ground to an accuracy of 0.001. Depending on the sampling speed of the interferometer, solar radiance scattered by the TOA and Earth surface and not filtered by the Ge coating of the beam splitters (VIS) or the gold-coated mirrors (UV) may result in spectral aliasing in the FORUM wavenumber range of interest. This aliasing can be effectively suppressed by an appropriate detector sampling frequency.

Radiometric noise reduction on acquired calibration measurements is essential to meet the requirement. This is achieved by statistical methods using calibration data acquired continuously during several days/weeks with an improved performance the longer is the calibration data set. The residual creates a systematic radiometric noise accounted for in the budget.

Contributor to ARA	Summation rule	Typical values @ 100 cm ⁻¹	Typical values @ 1600 cm ⁻¹
Calibration blackbody temperature knowledge	rss	0.015K - 0.02K (@190K)	0.01K - 0.02K (@190K)
		0.03K - 0.04K (@300K)	0.03K - 0.05K (@300K)
Calibration blackbody emissivity knowledge	linear	0.006K - 0.02K (@190K)	0.004K - 0.02K (@190K)
		0.01K - 0.04K (@300K)	0.01K - 0.04K (@300K)
Instrument background temperature knowledge	rss	0.05K (@190K)	0.01K (@190K)
		0.09K (@300K)	0.03K (@300K)
Instrument background temperature stability	rss	0.01K (@190K)	0.29K (@190K)
		0.01K (@300K)	0.01K (@300K)
Radiometric noise residual	rss	0.04K - 0.11K (@190K)	0.35K - 0.84K (@190K)
		0.01K - 0.11K (@300K)	0.02K (@300K)
Sun aliasing residual	linear	0.01K (@190K)	0.57K (@190K)
		0.02K (@300K)	0.017K (@300K)
Incidence angle on scanning mirror	linear	0.02K (@190K)	0.11K (@190K)
		0.02K (@300K)	0.003K (@300K)

Table 7.4 Contributors to the Absolute Radiometric Accuracy budget considered in Concept A and B.



Although the instrument background temperature is kept constant, it shows a slow periodic variations along the orbit, which causes a systematic error, also accounted for.

Uncorrelated contributors are summed up as root-sum-squared whereas correlated contributors are summed up linearly. For contributors that are always positive such as the sun aliasing, a linear summation is assumed. A special case is the calibration blackbody emissivity contributor. It is an uncorrelated contributor but since the emissivity has an upper boundary at 1 and the contributor is most likely to be positive, a conservative linear summation approach has been chosen.

Fig. 7.11 shows the total ARA performance for Concept A (Left) and Concept B (Right) summing the contributors as indicated in Table 7.4. Concept B presents a performance better than the goal requirements over the full FORUM spectral range within the full specified dynamic range [190K, 300K].

Concept A ARA is better than the goal specification within a scene temperature interval of [210K, 300K] and compliant to the threshold specification within a scene temperature

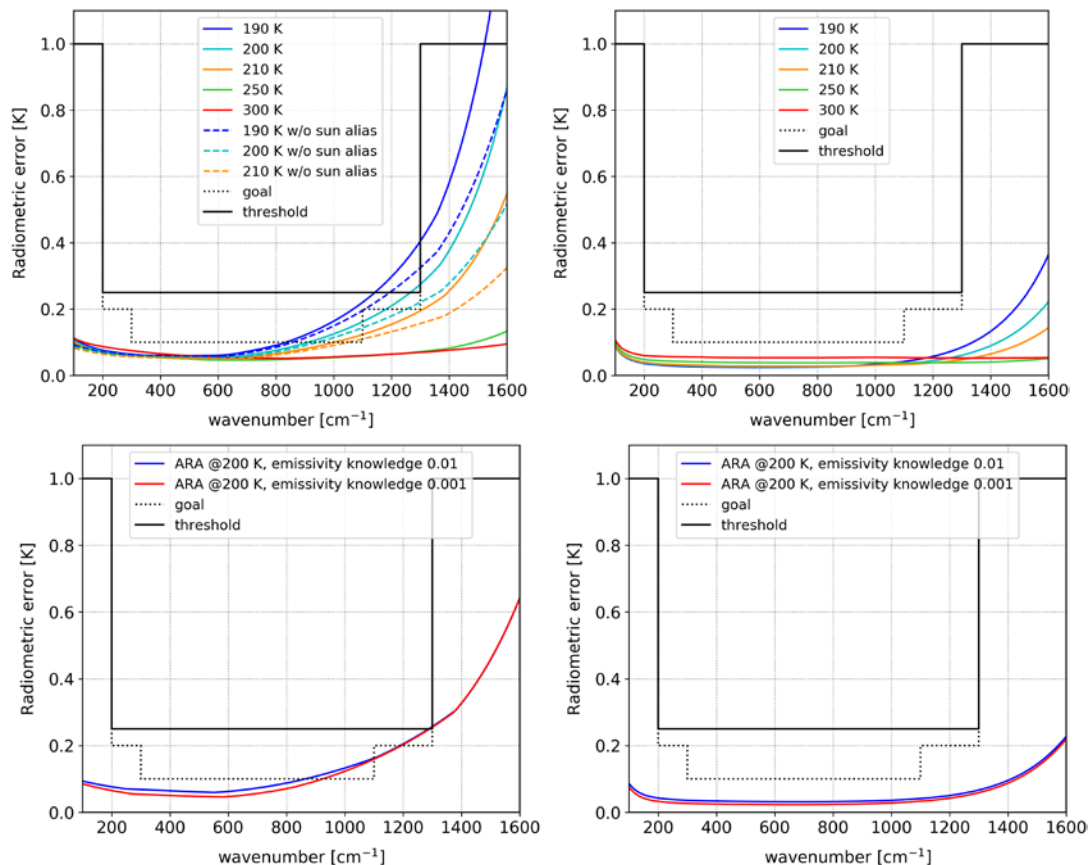


Figure 7.11 Top: ARA performance in equivalent delta temperature – Concept A (left) and Concept B (right). Bottom: ARA in equivalent delta temperature at 200 K without out-of-band signal contribution and for varying the blackbody emissivity knowledge, assuming the same instrument background temperature stabilisation.

interval of [200 K, 300K], if optimisation of the detector sampling frequency and removal of

the sun alias is achieved. For the scene temperature interval between [190 K to 200 K] full compliance is not achieved in the spectral range between 1100 cm^{-1} and 1300 cm^{-1} but is ensured with the goal values in the FIR range [800 cm^{-1} to 100 cm^{-1}]. Differences in performance between concept A and B mainly arise from the different calibration scheme.

The ARA is computed with a 99.7 % confidence Level. Temperature sensors are recalibrated in-flight, with the expected degradation over mission lifetime is included in the ARA budget. The degradation of the blackbody emissivity cannot be calibrated in-flight, although its degradation could be estimated on-ground. A sensitivity analysis on the impact of the degradation of the emissivity of the calibration blackbody has been performed at a scene temperature of 200 K. Fig. 7.11 (bottom) shows the ARA budget for both concepts when neglecting the sun aliasing and increasing the blackbody emissivity knowledge error by factor of 10. Models shows that the main impact of the black body emissivity uncertainty occurs at low wavenumbers, where the available margins would still allow complying with the goal requirements for Concept B in the whole dynamic range and with the threshold requirements for Concept A from $\sim 200\text{ K}$ to 300 K .

7.2.3.3 Spectral Performance

Spectral resolution: The FSI threshold spectral resolution is met with margins for both concepts. The MOPD is chosen as 1.40 cm for Concept A and 1.35 cm for Concept B to comply with the spectral resolution requirement (0.5 cm^{-1}) at 1600 cm^{-1} in the presence of self-apodisation due to the angular span of interfering beams. The impact of self-apodisation on spectral resolution performance depends on wavenumber resulting in a spectral resolution is better than 0.46 cm^{-1} (Concept A) and 0.48 cm^{-1} (Concept B) at wavenumber 1600 cm^{-1} and better than 0.43 cm^{-1} (Concept A) and 0.45 cm^{-1} (Concept B) at 100 cm^{-1} (Fig. 7.12).

Instrument Spectral Response Function (ISRF): Since both concepts baseline diamond beam splitters with relatively constant transmission, there are no spectral regions with elevated radiometric errors associated to beam splitter absorption features. The systematic errors remain below 10% of the noise Level (NESR) across the entire spectral range of the FSI, and full compliance to the ISRF knowledge requirement is achieved by both concepts.

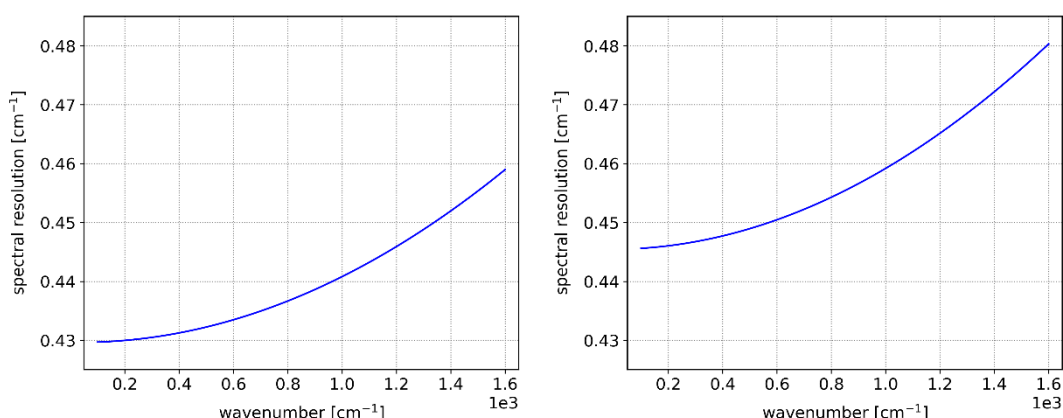


Figure 7.12 Spectral resolution dependence with wavenumber due to self-apodisation (Left: Concept A; Right: Concept B).

Spectral accuracy: The position of the spectral channel centers is measured in flight via the metrology laser system sampling the OPD. As a consequence, the dominant spectral error arises from the limitations of the laser wavelength stability, translating into a scale error of the FSI spectral grid. The requirement is therefore expressed as a fraction of the spectral channel center, and specified to 2 ppm. Such precision requires a highly stable metrology laser, and on-board spectral references (e.g. gas absorption cells), if the requirement is to be met by design. Alternatively, long-term spectral shift errors can be determined by making use of atmospheric spectral features in the acquired Earth radiance spectra. Both concepts target a mixed approach, performing in-flight spectral calibration via stable laser technology, as well as spectral scale correction of radiance spectra in the L1b ground processor. While the metrology laser assures the short-term stability of the spectral scale, the post-processing aims at correcting for long-term drift of the laser frequency

For Concept A, a simulation analysis was performed, resulting in spectral scale correction with an accuracy of about 3 ppm. It is, nevertheless expected that significantly better accuracy of the spectral scale correction can be achieved by improving the algorithms during Phase B1. Alternatively, embarking long-term stable lasers, would guarantee the compliance to the requirement at the expenses of increasing the cost and complexity.

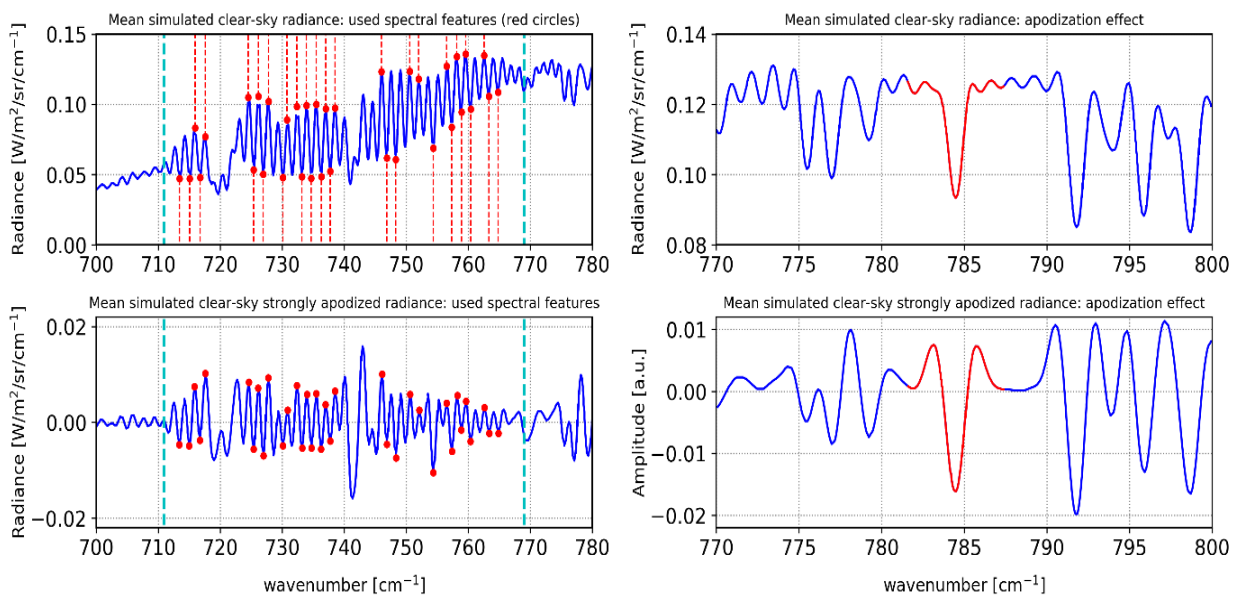


Figure 7.13 Examples for spectral calibration concept for Concept B. The upper panels show a mean of 600 simulated clear-sky radiance spectra representative of the North Atlantic Ocean (IRS LWIR spectral range). The lower panels show the strong apodisation response. The left panels show the selected spectral features for the spectral calibration (long term drift monitoring), the right panels show the effect of the apodisation that removes the blackbody shape and extension of the side-lobes.

Concept B relies on a technique developed for the Infrared Sounder (IRS) instrument on-board the Meteosat Third Generation (MTG) to monitor and correct the long-term drift of the metrology laser system (see Fig. 7.13). It determines the spectral scale factor changes from atmospheric absorption features that are spectrally stable for uniform scenes above the North Atlantic Ocean. The spectral invariance is reached after application of a strong

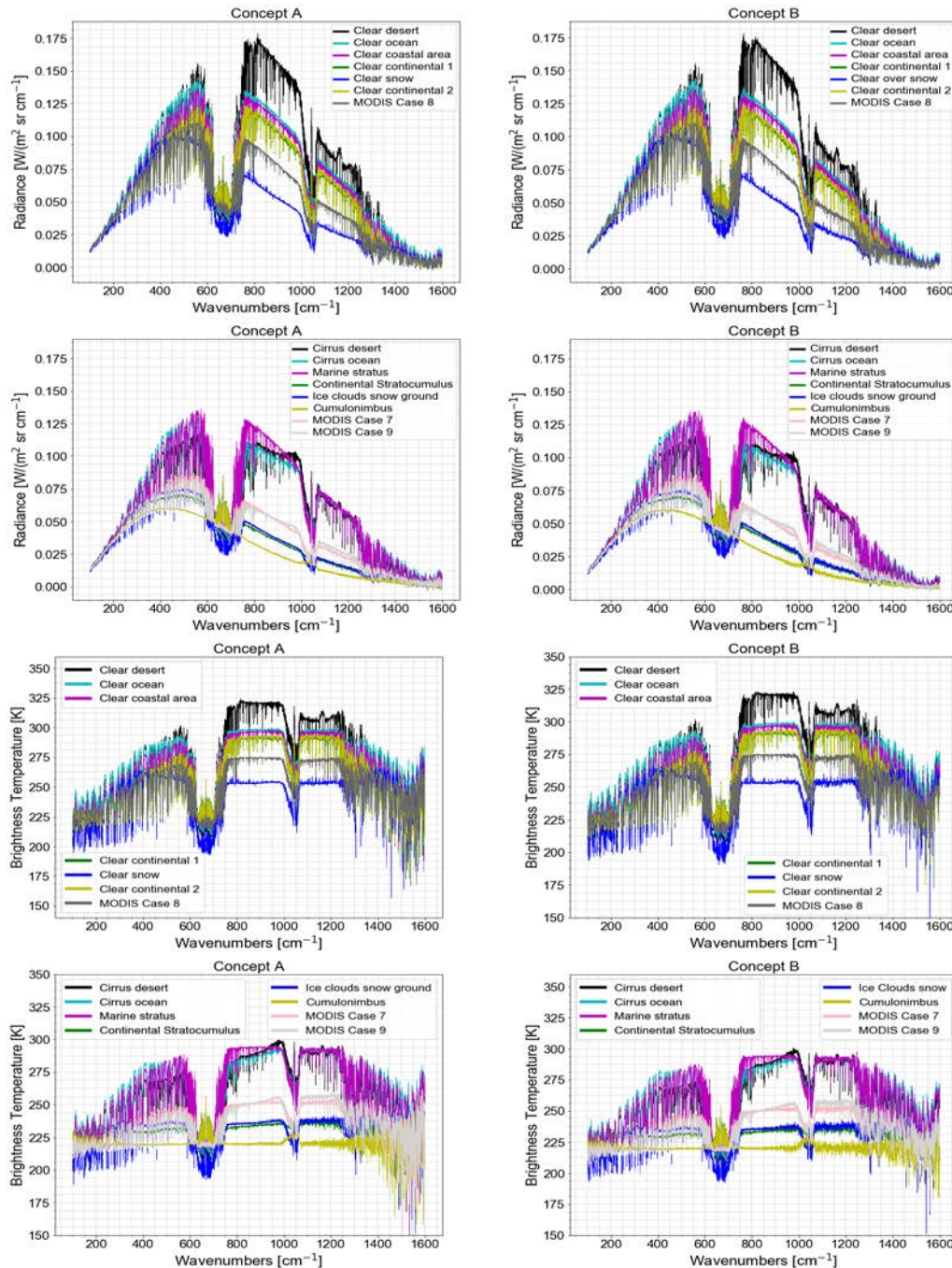


Figure 7.14 FSI Level-1c data product modelled using the FEES. Spectra shown in radiance (Top four figures) and in Brightness Temperature units (Bottom four figures) for 7 clear and cloudy sky scenes, computed with Concept A (Left) and Concept B (Right) baselines instrument performance parameters as described in Chapter 5 and 7.

apodisation, which removes the radiance baseline and efficiently removes most spectral features originating from further side lobes of the ISRF. The measurements acquired over the spectral calibration area are filtered in terms of scene uniformity and strength of the absorption features. The position of the selected spectral features is then determined to high accuracy, and the weighted average over the calibration period is used to calculate the scale error. In this way, a continuous monitoring of the spectral scale shift originating from the long-term wavelength-drift of the metrology laser is achieved. The technique predicted to yield spectral accuracies of better than 0.5 ppm for IRS, is deemed to be fully applicable to the FORUM instrument spectral since the spectrum is measured at highest spectral resolution.

7.2.3.4 FSI Level-1c Performance Modelled with the FEES

Fig. 7.14 shows the FSI Level-1c data product as modelled by the FEES. It shows the spectrum in radiance and brightness temperature units for seven input scenes under clear sky and eight under cloudy sky conditions, as defined in Section 7.1.6. Level-1c has been modelled using the baseline concepts instrument configurations and performance as derived from the results of the PRR of the Phase A activities. Fig. 7.14 shows consistency in the results obtained running the FEES with both concepts, as expected due to the similar technical designs and achieved performance.

7.2.4 FORUM Embedded Imager (FEI) Level-1 Performance

7.2.4.1 Geometric Performance

FEI Temporal Sampling: Both concepts acquire over 400 images per FSI dwell time (14 s). In the case of Concept A, 16 images are averaged per acquisition, meaning that 28 FEI acquisitions per FSI dwell are downlinked while in the case of concept B, 84 images are averaged per acquisition, leading to a downlink of 5 acquisitions per FSI dwell. Both concepts are compliant with the temporal sampling requirements.

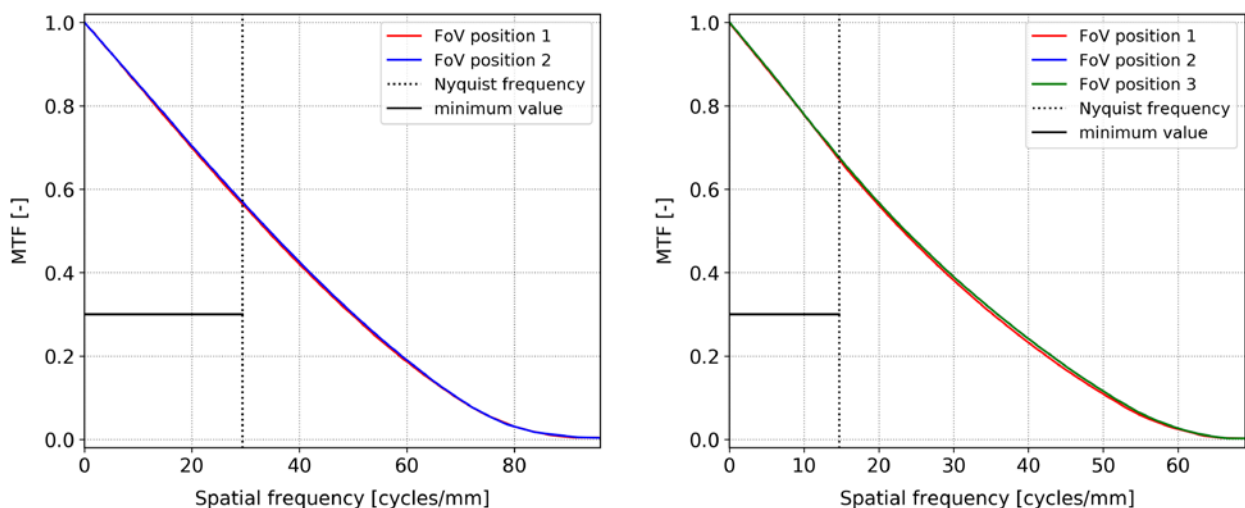


Figure 7.15 FEI optics MTF (Zemax) in the nominal configuration for different field positions as a function of frequency (Nyquist frequency: Concept A=29.4 cycles/mm, Concept B = 14.7 cycles/mm) – Left: Concept A, Right: Concept B.

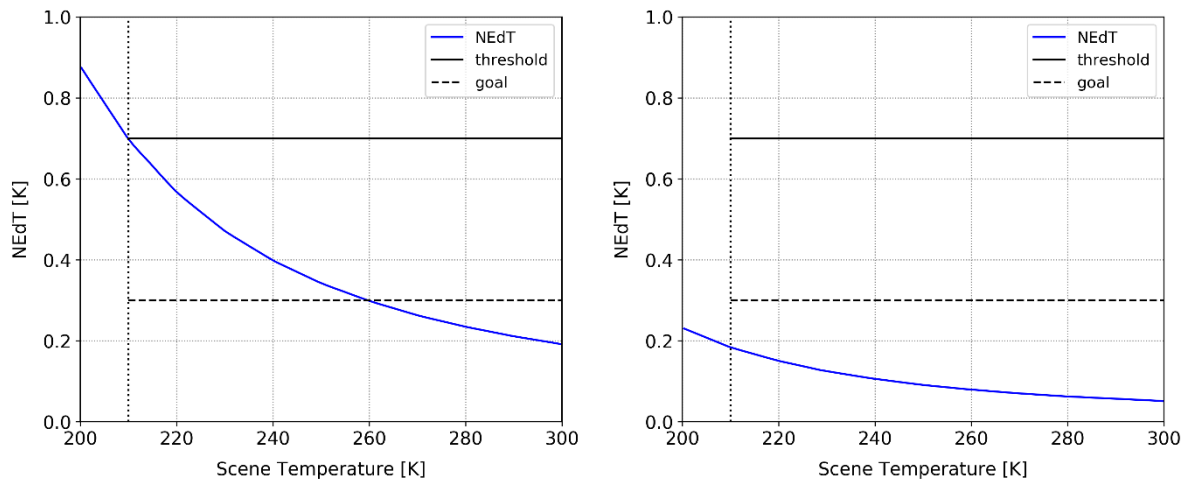


Figure 7.16 FEI NEdT. Left: Concept A; Right: Concept B.

FEI Field-of-view: Both concepts are compliant by implementing microbolometer array detectors able to acquire much larger areas than the required $36\text{km} \times 36\text{km}$. For Concept A, the central 74×74 pixels of the detector lead to a minimum FoV of $41\text{km} \times 41\text{km}$. For Concept B, the central 128×128 pixels of the detector (with 2×2 binning) provides a FoV of $38.4\text{km} \times 38.4\text{km}$.

Modulation Transfer Function: The MTF of the FEI has been assessed at Nyquist frequency for 3×3 field positions over the FEI FoV. The MTF is computed as the product of the detector MTF, the optics MTF (aberrations due to alignment and manufacturing errors) and the diffraction MTF. In addition, the LoS instability during acquisition caused by platform instabilities and scan unit inaccuracies has been considered. The optics and diffraction MTF has been assessed thanks to Zemax tolerancing analysis worst-case output. The worst case MTF at Nyquist frequency (Concept A: 29.4 cycles/mm, Concept B: 14.7 cycles/mm) is for both concepts higher than 0.30 with margins, making the FEI instrument compliant to the MTF requirement. (Fig. 7.15).

7.2.4.2 Radiometric Performance

Noise Equivalent delta-Temperature (NEdT). Fig. 7.16 shows the compliance of both concepts to the NEdT requirement for different scene temperatures. Both concepts acquire images at a much higher rate to perform temporal averaging reducing the noise level of the detectors at the required temperature (210K). Concept B complies with the goal by averaging 84 images while Concept A complies with the threshold performance by averaging 16 images.

Absolute Radiometric Accuracy (ARA): The main contributors to the ARA are the errors introduced by the calibration sources, and the thermal stability of the FEI. The offset is affected by the thermal background, given by the self-emission of the optical and mechanical elements in its field of view, and the temperature of the detector itself. Both concepts are compliant by designing the instrument to limit the temperature fluctuations of the FEI assembly between two calibration events. An improvement of the radiometric

accuracy is possible using blind pixels of the microbolometer (not-illuminated detector pixels) to compensate for temperature variations at detector level between calibrations.

Relative Spatial Radiometric Accuracy (RXRA): This performance is primarily affected by inhomogeneities of the thermal radiation background reaching the detector. In both concepts, the design and the thermal stability between two calibration events enable to reach compliance to RXRA requirement as reported in Table 7.2.

7.2.4.3 Spectral Performance

Spectral range: The FEI covers a single spectral band centered at 10.5 μm with a spectral bandwidth of 1.5 μm . The spectral band is achieved thanks to a bandpass filter.

Out-of-band signal: The FEI out-of-band signal achieved is 1.3% and 0.6% at 210K for Concepts A and B, respectively. The performance has been assessed based on already

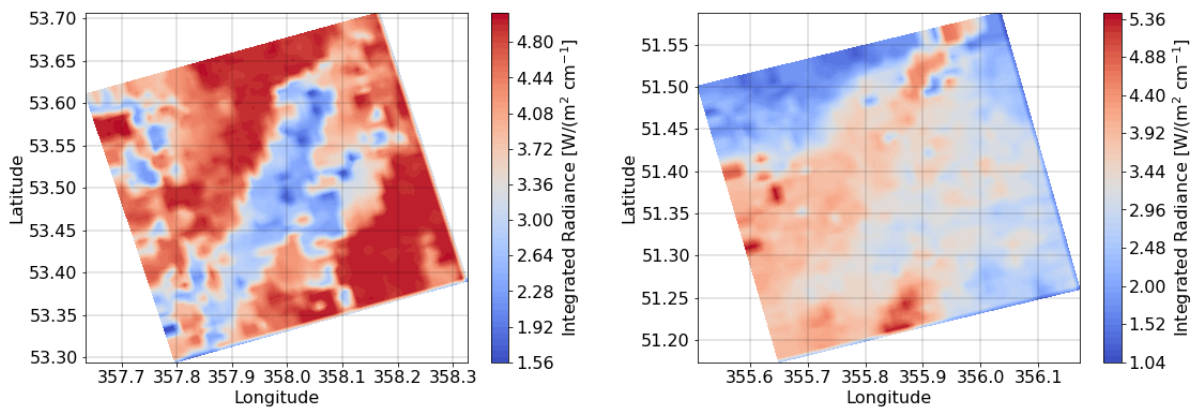


Figure 7.17 FEI Level-1b data products in integrated radiance units modelled with the FEES using MODIS based data (case 7: left and case 9: right as defined in Chapter 7.1.6) as input scenes.

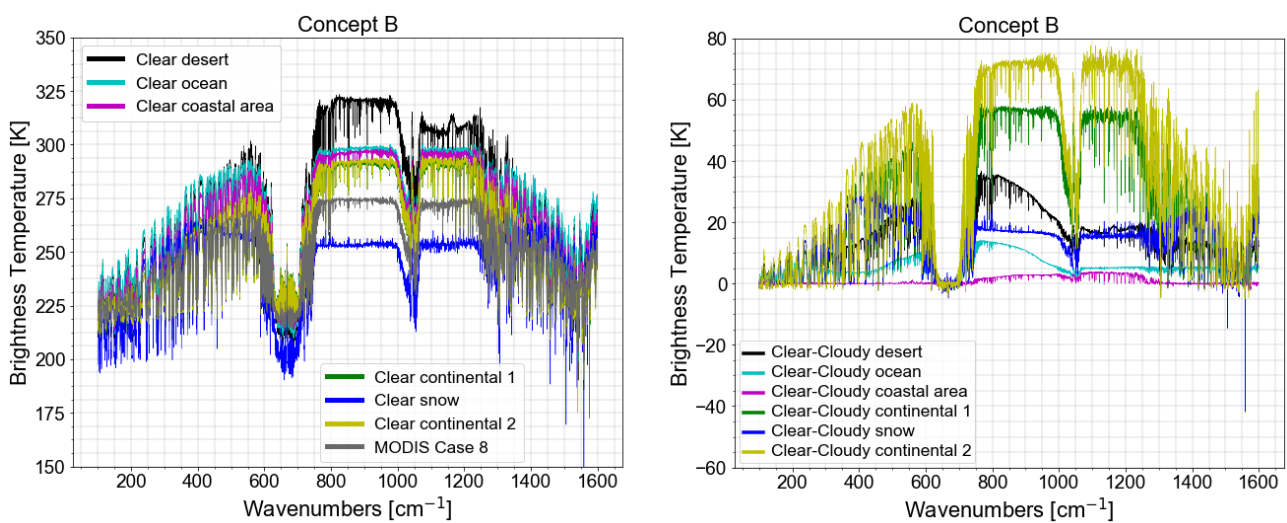


Figure 7.18 Radiances in brightness temperature for the six clear sky scenarios plus MODIS case 8 (left) and the corresponding brightness temperature difference to the six cloudy scenarios (right). (ESA)

Scene (cloudy)	Cloud identification	Scene (clear-sky)	Cloud identification
Cirrus on desert [Tropical – Sahara Desert] Summer	cirrus	desert [Tropical – Sahara Desert] Summer	clear
Cirrus on ocean [MidLat - Mediterranean] Summer	cirrus	ocean [MidLat - Mediterranean] Summer	clear
Coastal marine stratus [MidLat - Mediterranean] Summer	clear (water)	Coastal [MidLat - Mediterranean] Summer	clear
Continental 1 altocumulus [MidLat – Black Forest] Winter	ice	Continental 1 [MidLat – Black Forest] Winter	clear
Ice cloud on snow ground [Polar - Finland] Winter	cirrus	snow ground [Polar - Finland] Winter	clear
Continental 2 cumulonimbus [MidLat – Po Valley] Summer	ice	Continental 2 [MidLat – Po Valley] Summer	clear

Table 7.5 Performance of the cloud detection for the 12 science scenes considered in the FEES. Green indicates a successful detection, red unsuccessful.

existing filters in the frame of EarthCare MSI and S3 SLSTR instruments. Concept A is compliant to the threshold while Concept B is compliant to the goal out-of-band signal.

ISRF and ISRF knowledge: In Concept A, the ISRF includes the spectral responses of anti-reflection coating, Germanium lenses, detector coating and dedicated band-pass filter. The band-pass filter spectral response is taken from the analogous component used in the EarthCARE-MSI instrument. In Concept B, the feasibility is assessed using as a reference the measured data for an already developed band pass filter for Sentinel3-SLSTR (central wavelength of 10.8 μm and a bandwidth of 1.1 μm).

The in-flight ISRF knowledge accounts for the accuracy of the on-ground characterisation and the stability between on-ground and in-flight lifetime. Compliance is achieved based on instrument heritage (e.g. S3 SLSTR and EarthCare MSI).

7.2.4.4 Level-1b Product Modelled with FEES

Fig. 7.17 shows the FEI Level-1b data product as modelled by the FEES. It shows the FEI integrated radiance using as input MODIS data of a realistic cloudy/clear sky heterogeneous input scene. Radiance variation due to input scene heterogeneity due to clouds is clearly captured by the FEI.

7.3 Scientific Performance

In the following sections, the performance relevant to the science goals is evaluated.

7.3.1 FEES Performance

Only results for Concept B are presented from hereon because of the similarities to Concept A. As explained in Section 7.1.6, six cloudy and corresponding clear-sky scenarios were selected to cover the range of expected cloud/ clear contrast in the atmosphere. Results for

these are shown in Fig. 7.18. The largest temperature contrast in the atmospheric window between clear and cloudy conditions occurs for the cumulonimbus case (light green) and the smallest contrast, which exhibits only a few degrees difference between clear and cloudy scenes if for the marine stratus cloud in a coastal area (magenta). Table 7.5 shows this case is challenging for the cloud detection algorithm. All clear, cirrus and ice cloud scenarios were correctly identified. The three MODIS cases were assigned to cirrus and clear cases albeit as heterogeneous scenes (Table 7.6, Fig. 7.4, right).

For the two cirrus cases, cirrus over desert and cirrus over ocean, the cloud optical depth was decreased in steps of 0.01 whilst keeping all other parameters unchanged, to determine the lowest detectable cirrus cloud optical depth. For the desert case, this was 0.05 and for the ocean case, 0.02 (Table 7.7). This is well within the requirements (Chapter 3).

For each case identified as cloud a full retrieval of cloud parameters is performed. Results for the five plus 3 MODIS scenes (the coastal marine case was wrongly attributed to a clear sky retrieval) are summarised in the Tables 7.8 and 7.9. For each parameter the retrieved value and the truth are stated.

Scene	Cloud identification
MODIS 7	cirrus
MODIS 8	clear
MODIS 9	cirrus

Table 7.6 Cloud/clear-sky detection for the three MODIS case.

Scene	Minimum optical depth for successful cloud identification
Cirrus on desert [Tropical – Sahara Desert] Summer	0.05
Cirrus on ocean [MidLat - Mediterranean] Summer	0.02

Table 7.7 Minimum cloud optical depth for cloud identification

Scene	Cloud optical depth		Cloud top height (km)		Effective particle radius (μm)		Chi-square
	Truth	Retrieved	Truth	Retrieved	Truth	Retrieved	
Cirrus on desert	1.0	1.0	12.0	11.8	10.0	9.9	1.003
Cirrus on ocean	0.3	0.3	15.0	15	6.0	5.8	1.115
Continental 1 altocumulus	6.0	6.2	10.0	9.6	30.0	42.5	1.310
Cirrus cloud on snow	3.0	3.0	8.0	8.0	18.0	15.4	2.304
Continental 2 cumulonimbus	300.0	10.0	11.0	10.7	80.0	59.8	1.050
MODIS 7	3.0 \pm 2.2	2.3	5.2 \pm 2.8	5.843	29.6 \pm 9.9	3.4	13.30
MODIS 9	2.5 \pm 2.4	1.4	9.3 \pm 1.6	10.3	14.9 \pm 3.2	14.0	1.650

Table 7.8 Performance of the cloud parameter retrievals.

Scene	Ice water path (g m^{-2})		
	Truth	Retrieval	Difference (%)
Cirrus on desert	3.70	3.64	1.7
Cirrus on ocean	0.79	0.76	3.8
Continental 1 altocumulus	57.88	83.80	-44.8
Cirrus cloud on snow	18.01	15.71	12.8
Continental 2 cumulonimbus	7491.67	187.50	> 100
MODIS 7	28.00 ± 8.10	X	X
MODIS 9	12.62 ± 7.56	6.68	47.1

Table 7.9 Performance for the calculation of the ice water path.

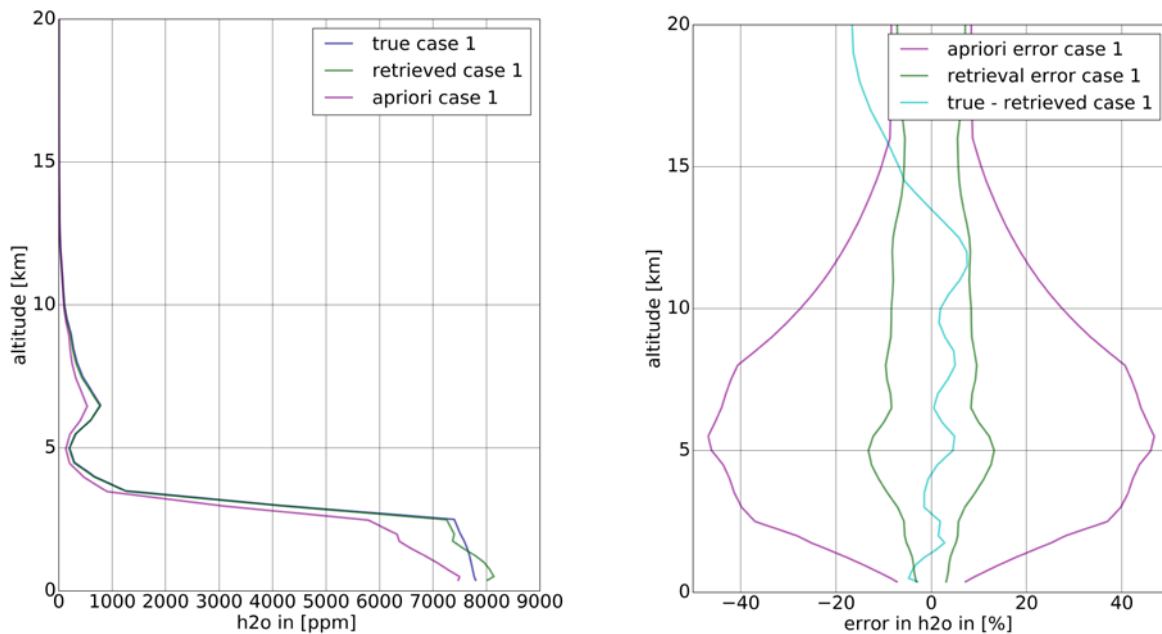


Figure 7.19 Example retrieval for a water vapour profile for the desert case.

The retrieved cloud top height is always within 1 km of the truth, which meets the requirements. For the three cirrus cloud cases the effective particle radius and the ice water path retrieval accuracy is better than the 20 % requirement. For the thicker clouds the results are mixed. The retrieval cannot obtain any information from within the cumulonimbus cloud and it struggles with the altocumulus particle radius though the optical depth retrieved agrees well with the true value. The MODIS 7 case has several cloud types and heights in the FSI pixel as indicated by the large standard deviations and chi-square for these retrievals. This is the case where the analysis of the imager indicated a distribution of four levels of heterogeneity (Fig. 7.3). Given the large range of optical depth encountered for MODIS 9, the results are still considered reasonable.

For the clear-sky retrieval, an example for the water vapour profile retrieval is shown in Fig. 7.19. This is the desert case with low humidity. The right panel shows the uncertainties. There is a significant reduction from the a priori uncertainty to that estimated for the retrieval. However, the true error, obtained from the difference of the true and the retrieved profile is significantly lower than the estimated uncertainty. This result is expected for a model scene and reflects the results from the uncertainties of the cloud property retrievals. In Phase B the performance will be investigated by statistical analysis of results for larger numbers of scenes. The uncertainty budgets will also be rigorously assessed with respect to systematic contributions, e.g. the unknown ice crystal shape.

7.3.2 Complementary Scientific Performance

In this section, further scientific performance is presented. This analysis focusses on cloud properties, water vapour information, and emissivity.

7.3.2.1 Retrieval from Synthetic Observations in Clear Sky

To verify the performance of FORUM Level-2 products in clear-sky, synthetic FSI observations were generated according to both the goal and the threshold requirements on the measured spectral radiance described in Chapter 4. Observations were simulated for 80 clear-sky scenarios, spanning different seasons, latitudes (five polar, 41 mid-latitudes, and 34 tropical latitudes) and surface types (vegetation, snow, ocean, and desert).

Based on each synthetic spectral radiance, simultaneous retrievals for temperature, water vapour and ozone profiles, surface temperature, and emissivity were carried out. The initial guess used for the retrieval is from Liuzzi et al. (2016) and the a priori errors on the target parameters are those used at United Kingdom MetOffice for the assimilation of IASI measurements in their operational numerical weather prediction model. The retrieval is performed on a vertical grid of 2 km steps from 0 to 10 km, 1 km steps from 10 to 20 km, and 5 km steps from 20 to 80 km.

The top panels of Fig. 7.20 show the precision on the water vapour and temperature retrievals for the different latitude bands, for the goal (full line) and threshold (dotted line) radiometric requirements. As one can see, water vapour is retrieved in the upper troposphere with a precision of 10–15% and therefore meets the goal requirements in the tropics and the threshold in polar and mid latitude regions for Level-1 observations meeting either the goal or threshold requirements. The air temperature is retrieved with a precision of 0.2–0.4 K in the troposphere/ lower stratosphere for all latitudinal bands. The precision on the emissivity retrievals is shown in the bottom panel of Fig. 7.20. Since the spectral emissivity change slowly with wavenumber, it is retrieved with a spectral sampling grid of 50 cm⁻¹. As one can see, the threshold emissivity requirement cannot be met in the tropics, but the goal requirement is met (between ~450 and ~600 cm⁻¹) in polar region and the threshold in mid latitude regions, for Level-1 data meeting either the goal or threshold radiometric requirements.

7.3.2.2 Retrieval from Synthetic Observations in Cloudy Sky

To evaluate the quality of the cloud parameter retrieval module presented in Section 6.1, a dataset provided by ECMWF containing a diverse set of atmospheric profiles has been used,

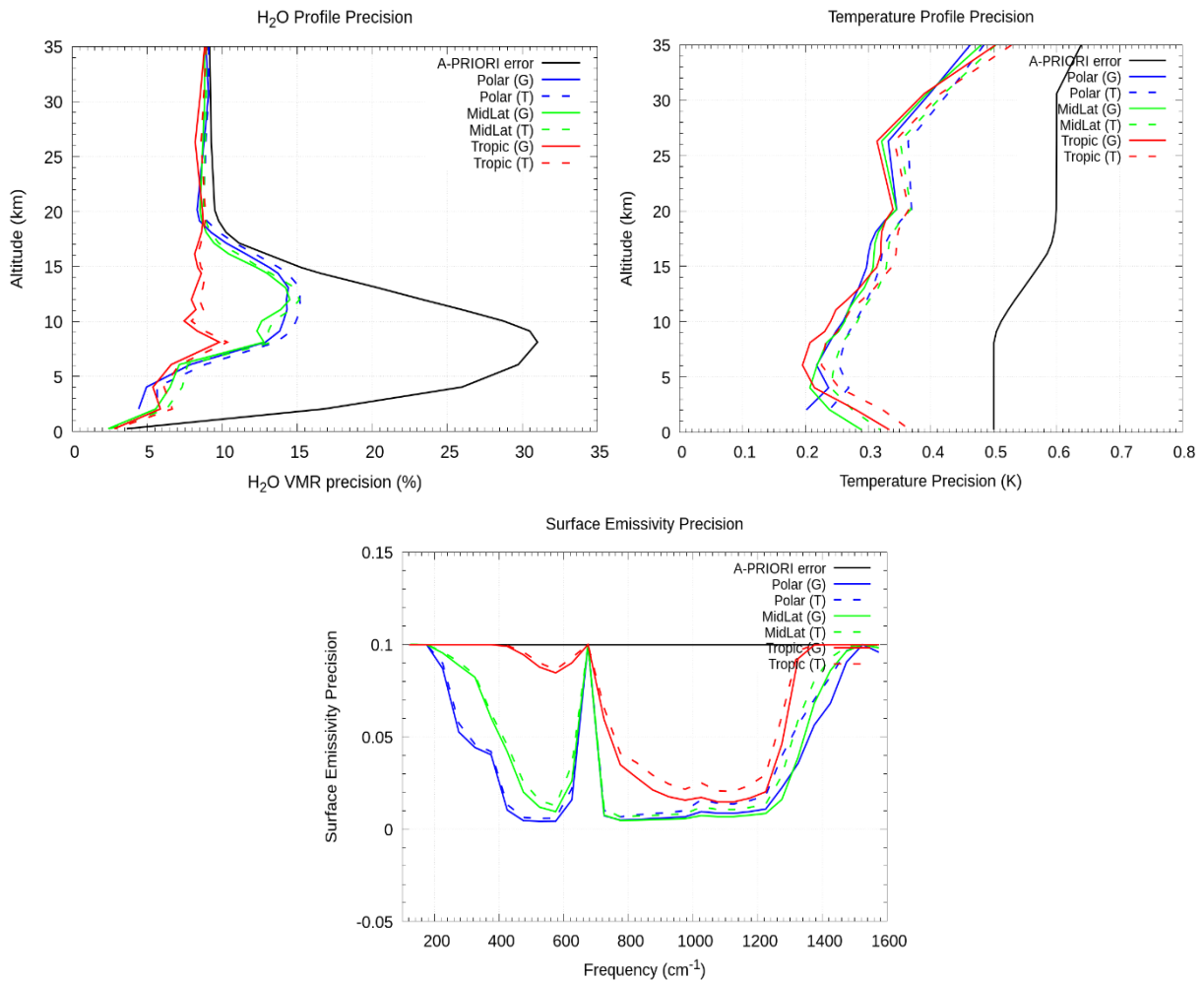


Figure 7.20 Precision on the water vapour retrieved profiles (top left panel) and the temperature (top right panel), Precision of retrieved surface spectral emissivity (bottom panel). (S. Del Bianco, CNR, Italy)

enabling a realistic ice cloud description in terms of ice water content (IWC) profile and atmospheric state. From these realistic profiles and the FSI Level-1 requirements (see Chapter 4), a set of synthetic observed radiances have been computed and fed through the retrieval module to test its performance in terms of the Level-2 requirements (see Chapter 4).

A dataset of 5000 diverse profiles sampled from the ECMWF NWP model fields available from the European Organisation for the Exploitation of Meteorological Satellites (EUMETSAT) NWP Satellite Application Facilities (www.nwpsaf.eu/site/software/atmospheric-profile-data/) has been used to obtain a realistic range of atmospheric profiles. The variables considered from these profiles were temperature, water vapour, ozone and cloud water content (ice and liquid), designed to represent the full range of values encountered in the Earth’s atmosphere. This dataset comprises of 212 single-layer ice cloud cases, and 3151 multi-layer cloud cases. Here, only results from single-layer clouds are considered. Fig. 7.21 shows the geographical location of the single-layer ice cloud cases with the corresponding opacity indicated by the colour scale.

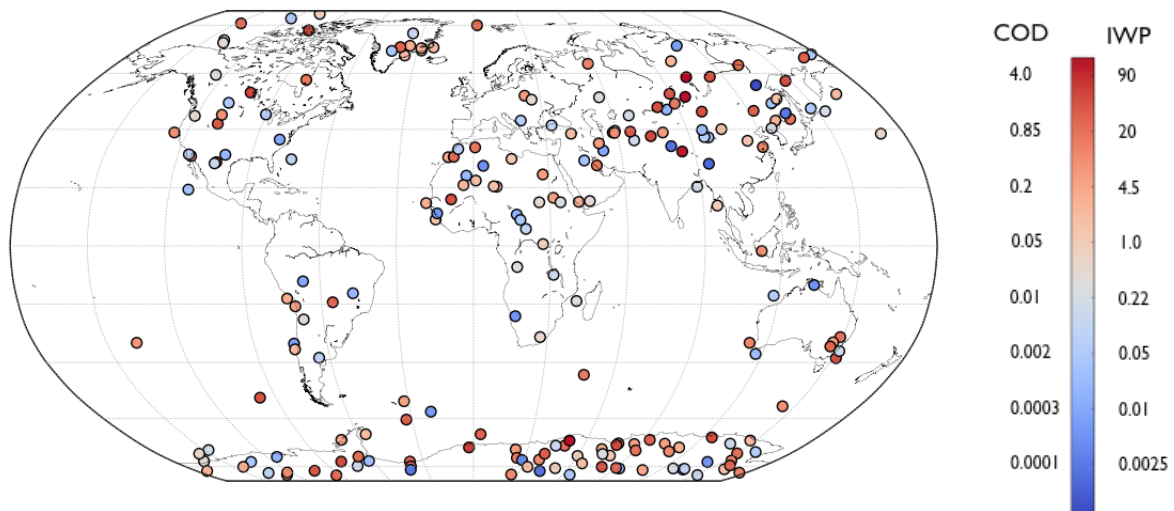


Figure 7.21 geographical location of the single-layer ice cloud cases. The colour scale indicates the opacity of the cloud in terms of the optical depth at $10\ \mu\text{m}$ ($\text{COD}_{10\mu\text{m}}$) and equivalent ice water path (IWP in g/m^2). (L. Labonnote, University of Lille, France)

It is interesting to note that almost 45 % of these ice only cases have a cloud optical depth (COD) at $10\ \mu\text{m}$ ($\text{COD}_{10\mu\text{m}}$) less than 0.05 (equivalent to an ice water path (IWP) $< 1\ \text{g}/\text{m}^2$) corresponding to sub-visible ice cloud

Several previous studies have shown that passive measurements are not very sensitive to thin cloud, for example Ackerman et al. (2008) demonstrated that clouds with a visible optical depth of less than 0.4 cannot be detected using the MODIS instrument. However, the detection of thin clouds can be improved by the use of high spectral resolution measurements that enables the absorption lines that can be used to detect cloud, to be better resolved. Indeed a recent cloud identification and classification (CIC) algorithm (Maestri et al. 2019) has been developed specifically for the FORUM mission (see Sections 6.1.1 and 7.1) which shows that the lower limit of detection, expressed in $\text{COD}_{10\mu\text{m}}$, is reduced to approximately 0.03 for tropical atmospheres and 0.5 in polar regions. These results suggest that the detection of the very thinnest of sub-visible clouds might not be possible from passive measurements, even with high spectral resolution in the FIR. Consequently, the retrieval performance will only be shown for cases that present an $\text{IWP} > 1\ \text{g}/\text{m}^2$ ($\text{COD}_{10\mu\text{m}} > 0.05$), which reduces the number of single-layer ice cloud cases to 120.

Using the ECMWF dataset of single-layer ice cloud cases as input to the RTTOV model, a set of 212 synthetic radiances have been simulated. The surface emissivity values used for these simulations are reported in Feldman et al. (2014), which provides emissivity for four classes (snow, desert, vegetation and ocean) between 10 and $3000\ \text{cm}^{-1}$. Each profile has been assigned an emissivity that depends on its geographical location and season. A realistic random noise, based on the FSI NESR goal requirements, has been added to the synthetic radiances.

Fig. 7.22 presents the retrieved IWP, CTH and CBH as a function of the true value for the single layer ice cloud. A perfect retrieval would yield a scatter plot distributed along the first

diagonal (1:1 line). The figure also indicates the number of cases where convergence is achieved (i.e. a successful retrieval) compared to the total number of 120 single layer ice cloud cases with IWP > 1 g/m². The goal and threshold values (defined in Chapter 4 and provided by the WMO-OSCAR database) are indicated by the orange and green dashed lines respectively. The colour of each dot indicates the temperature contrast between the surface and the top (or bottom) layer of the cloud.

As can be seen from the top panel of Fig. 7.22, the number of successful retrievals is high (> 88 %). The threshold requirement for IWP is achieved for more than 92% of cases, and the goal requirement for 75 % of the cases. Perhaps unsurprisingly, cases where the temperature contrast between the cloud top layer and the surface is low (the darkest red dots) result in larger differences between the retrieved and true values. These cases generally correspond to profiles that have a temperature inversion in the troposphere, which results in multiple potential solutions to the retrieval inversion. The bottom left panel of Fig 7.22 shows that the cloud bottom height (CBH) is more difficult to retrieve, with relatively large

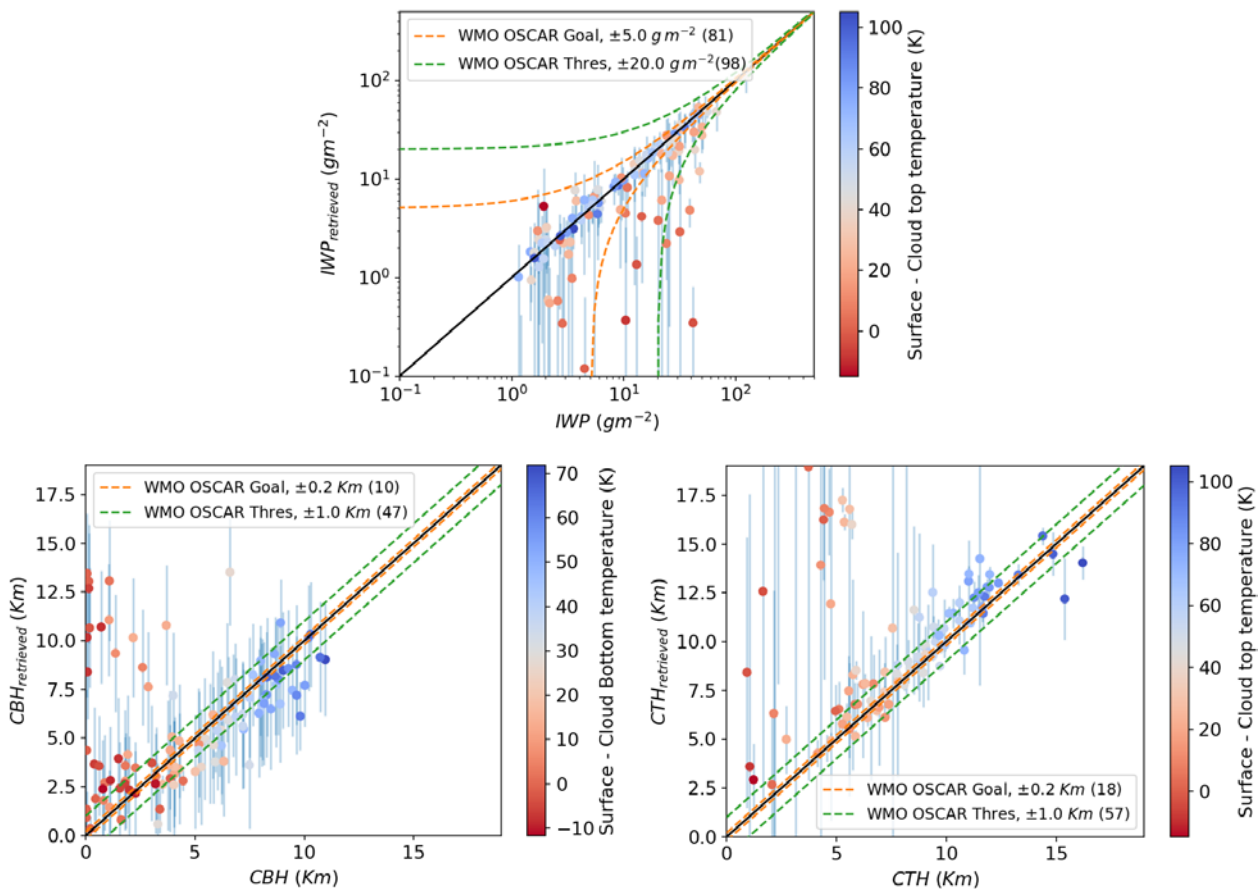


Figure 7.22 Scatter plot of the retrieved IWP (top), CBH (bottom left) and CTH (bottom right) as a function of the truth for the single-layer ice cloud cases (total of 120 cases with IWP > 1 g/m²). Vertical light blue line show the retrieval uncertainties attached to the retrieved parameter. The colour scale indicates the temperature contrast between the surface and the cloud top (or bottom) in degrees K. The orange and green dashed lines show the limits in which the retrieval must fall in order to achieve the Level-2 goal and threshold requirements, respectively. Numbers in bracket indicates the number of retrievals that reach the corresponding requirements. (L. Labonnote, University of Lille, France)

uncertainty ranges, which do however generally encompass the true values. However, the performance in terms of Level-2 requirements is poor compared to the IWP, with only ~8 % (~40 %) of cases achieving the goal (threshold) requirement. The bottom right panel of Fig. 7.22 shows that the cloud top height (CTH) is retrieved well apart from cases suspected to contain temperature inversions. Although the performance in terms of Level-2 requirements is better than for CBH, it remains much lower than the IWP performance with only ~15 % (~50 %) of cases achieving the goal (threshold) requirements.

Numerous passive sensors provide information on cloud top height (or cloud top pressure), however, only a few passive sensors retrieve both the cloud altitude and extent. Ferlay et al. (2010) and Desmons et al. (2013) developed a method to retrieve both the cloud top pressure (CTOP) and the cloud geometrical thickness from the multi-viewing and polarised instrument POLDER3 on board PARASOL. Evaluation of the retrieval performance of POLDER3 and MODIS versus active sensor has been analysed by Desmons et al. (2013) and results are summarised in the left panel of Fig. 7.23 for CTOP.

In order to compare the performance of FORUM with that of Desmons et al. (2013) shown in the left panel of Fig. 7.23, the Level-2 requirements for the CTH and CBH expressed in km were translated into pressure units (Fig. 7.23, right panel).

One can see from this figure that for a cloud top layer at 7.5 km, the goal requirement of 0.2 km would be less than 15 hPa (reduces to ~ 5 hPa at 20 km), and the threshold requirement of 1 km would be lower than 50 hPa (reduces to ~20 hPa at 20 km). If these requirements are applied to the POLDER3 and MODIS CTOP retrieval performance, one can see from the left panel of Fig. 7.23 that for POLDER3 about 17 % of retrievals achieve the goal requirement of 15 hPa, 25 % the threshold requirement of 20 hPa (for CTH=20km) and 55

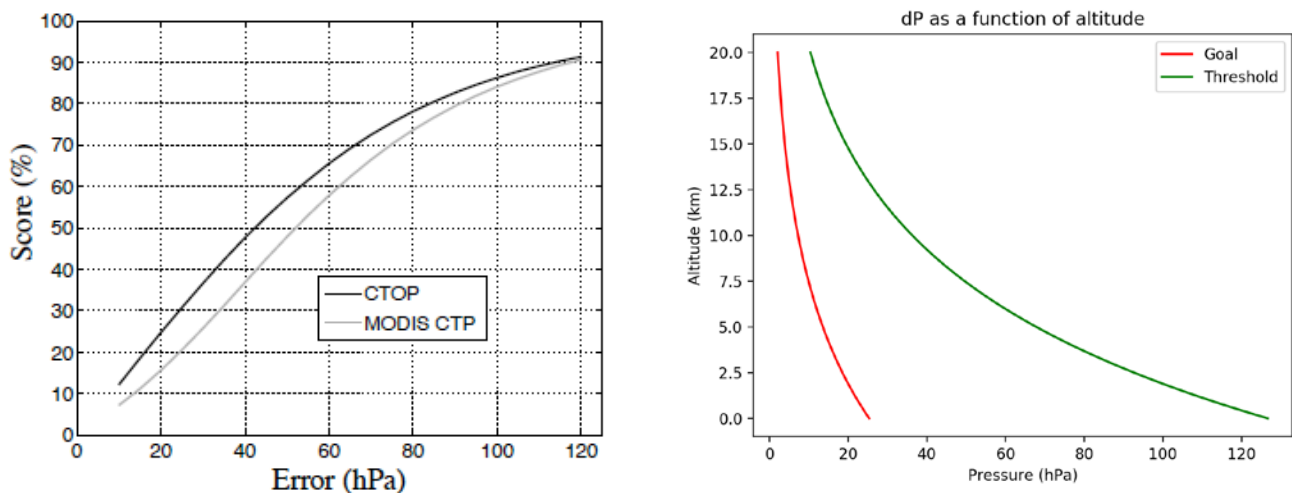


Figure 7.23 Left plot: scores obtained in 2008 by the POLDER3 instrument (black line) and MODIS CTP (grey line) for single layer ice cloud as a function of the error in hPa. The error is the difference between the truth given by the Lidar CALIOP and the retrieved cloud top pressure, and scores are the percentage of cases with a difference (truth-retrieval) smaller than the error. Figure has been obtained from Desmons et al. (2013). Right plot: Translation in pressure unit of the goal (red line) and threshold (green line) L2 requirements for the CTH and CBH. We recall that the goal requirement has been set to 0.2 km and threshold to 1 km for both CTH and CBH. (L. Labonnote, University of Lille, France)



% the threshold requirement of 50 hPa. For MODIS these numbers reduce to 10%, 15% and 45% respectively.

The results of this simple comparison suggest that FORUM will be able to greatly improve upon CTH retrievals from MODIS and POLDER3. Concerning the ice cloud geometrical thickness POLDER3 performance, Desmons et al. (2013) have shown that the mean bias over 2008 was about 1.5 (0.85) km with a standard deviation of 5.8 (4.85) km over ocean (land). Again, these numbers highlight the added potential value of FORUM to retrieve the cloud vertical extent.

Furthermore, since those instruments only use visible wavelengths limiting their capability to daytime retrievals, FORUM will have the additional benefit of being able to perform these retrievals at all times. FORUM could also provide additional benefits to other planned instruments such as 3MI (POLDER next generation), by enabling a more comprehensive sampling of the cloud fields and vice versa.

7.3.2.3 The Synergistic Inversion of FORUM and IASI-NG Measurements

As outlined in Section 4.5, FORUM will fly in loose formation with IASI-NG on the MetOp-SG(1A) satellite. This will enable synergistic, simultaneous inversions of matched FSI and IASI-NG measurements. To assess the advantages of the synergistic retrieval, the retrieval uncertainty relating to the inversion of FORUM only, IASI-NG only, and the synergistic FORUM+IASI-NG measurements were computed. The computation was done for several scenarios: namely, three clear-sky atmospheric scenarios (Antarctic Winter over ice, Mid-Latitude Spring over land, and tropical Summer over ocean) and 21 scenarios with a single layer of ice clouds. For this assessment a joint retrieval of the following target parameters were executed: temperature, water vapour and ozone Volume Mixing Ratio (VMR) profiles with 1 km vertical retrieval grid in the 0 – 50 km range, and surface temperature and spectral emissivity (from 100 to 2700 cm^{-1} with 50 cm^{-1} steps). In the cloudy cases IWP, CTH and CBH are also included in the retrieval vector together with the atmospheric and surface parameters. The total retrieval uncertainty is computed as the mapping onto the solution (see Eq. 6.1), of the following uncertainty components: measurement NESR and ARA compliant with the respective goal requirements for the FSI, spectral interference from non-retrieved CH_4 VMR profile (10% variability) and uncertainty in the CO_2 VMR (0.25%) (see Remedios et al. 2007). IASI-NG measurement characteristics reported in Crevoisier et al. (2014) were applied. In the initial computations, the FSI and IASI-NG measurements were considered as simultaneous and perfectly matching in space. An example result is shown in Fig. 7.24 for water vapour profiles and surface emissivity for two different scenarios: clear-sky Antarctic Winter over ice, and tropical atmosphere over land in the presence of an ice cloud layer between 8.5 km and 15.5 km. The ice cloud is defined with an IWP of 8.899 g/m^2 and optical depth at 1000 cm^{-1} of 0.34.

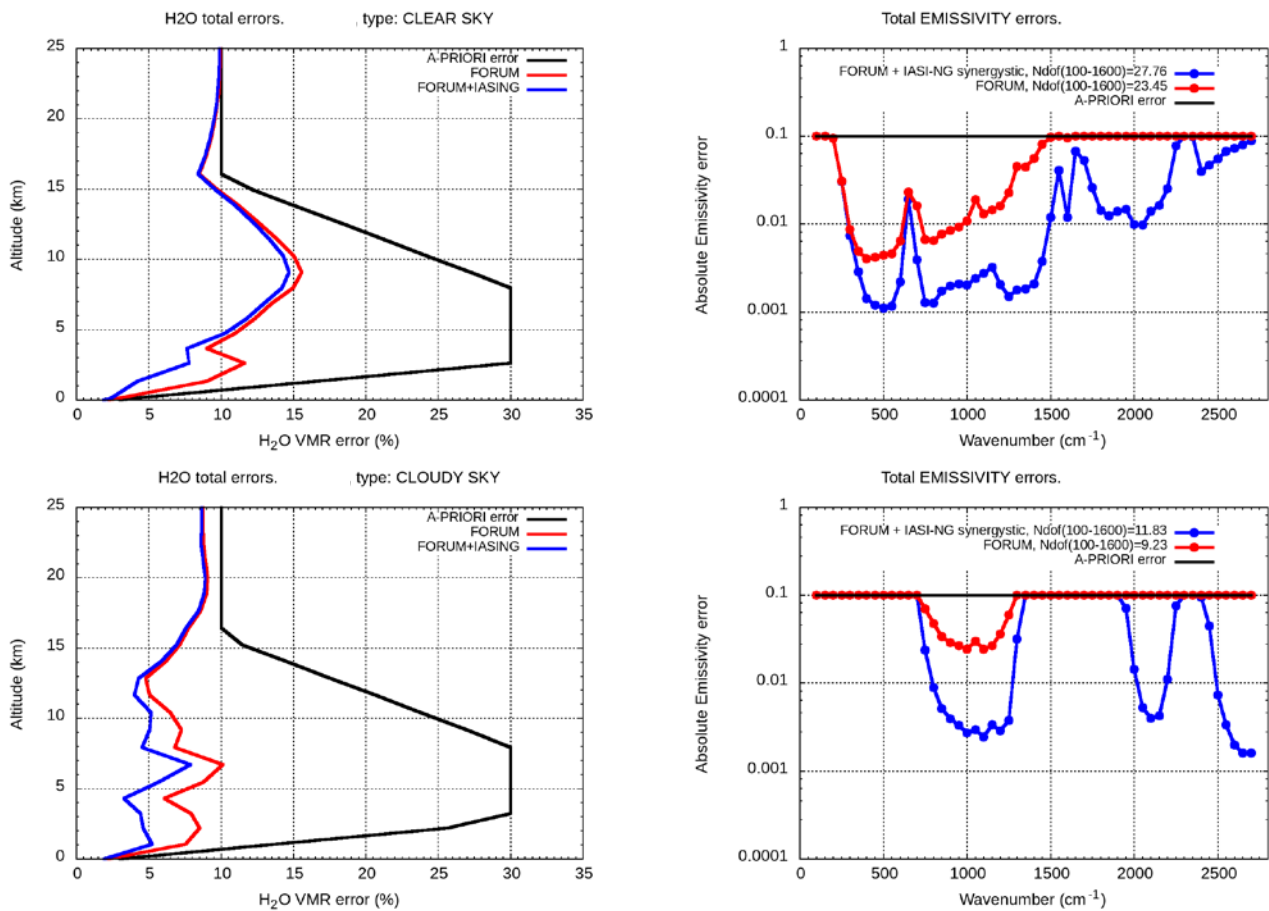


Figure 7.24 Top panels: H₂O VMR (left panel) and surface emissivity (right panel) retrieval uncertainties for a clear sky, Antarctic Winter scenario over ice. Bottom panel: The same as the top panels. But for a tropical atmosphere over land, in the presence of an ice cloud between 8.5 and 15.5 km. Black curves represent the a-priori uncertainty, red curves the FORUM-only retrieval uncertainty and the blue curves the retrieval uncertainty of the synergistic FORUM+IASI-NG retrieval. The differences between red and blue curves highlight the improvements achieved with the synergistic FORUM+IASI-NG retrievals. (M. Ridolfi, University of Bologna, Italy)

In the Antarctic Winter case, the atmosphere is very dry and therefore it is sufficiently transparent in the FIR region to allow surface emissivity to be retrieved with a small uncertainty across the majority of the IR. Due to the relatively small thermal contrast between the surface and the troposphere, water vapour is retrieved with a larger relative uncertainty as compared to tropical cases. The tropical example shows opposing characteristics to the Antarctic winter case: the large amount of water vapour in the lower atmosphere prevents the detection of the surface characteristics in the FIR region. On the other hand, due to the large thermal contrast between the lower and the upper troposphere, water vapour is retrieved with smaller relative uncertainty compared to the polar case. In Fig. 7.24, the differences between red and blue curves highlight the improvements achieved with a synergistic FORUM plus IASI-NG retrieval: The water vapour VMR uncertainty improves slightly. On the other hand, the uncertainty on the retrieved surface emissivity is considerably reduced. Particularly, in the FIR region between 300 and 600 cm⁻¹, a 70% reduction of the uncertainty as compared to the inversion of the FSI measurement alone can



be achieved. Note that this uncertainty reduction occurs despite the fact that IASI-NG measurements do not cover the FIR spectral region. This is a result of the improved temperature profile and surface temperature retrieval achieved when introducing IASI-NG measurements in the inversion. Due to the correlation among retrieval parameters, and especially between surface emissivity, surface temperature and temperature in the lowest atmospheric layers, using IASI-NG measurements results in a significant reduction of the uncertainty on the overall set of retrieved parameters, including surface emissivity in the FIR.

Fig. 7.25 shows the retrieval uncertainties of surface temperature and cloud parameters: IWP, CTH and CBH, for the various atmospheric scenarios considered. Each measurement scenario is characterised by a given value of IWP as reported in the horizontal axis of the plots. In the panel relating to surface temperature, the three clear-sky scenarios (polar winter, mid-latitude spring, and tropical) are artificially associated with IWP values less than 0.01 g/m² to enhance plot clarity (see the grey area in the top left plot of Fig. 7.25). The black lines show the a-priori uncertainty assumed in the retrieval, the red symbols indicate the

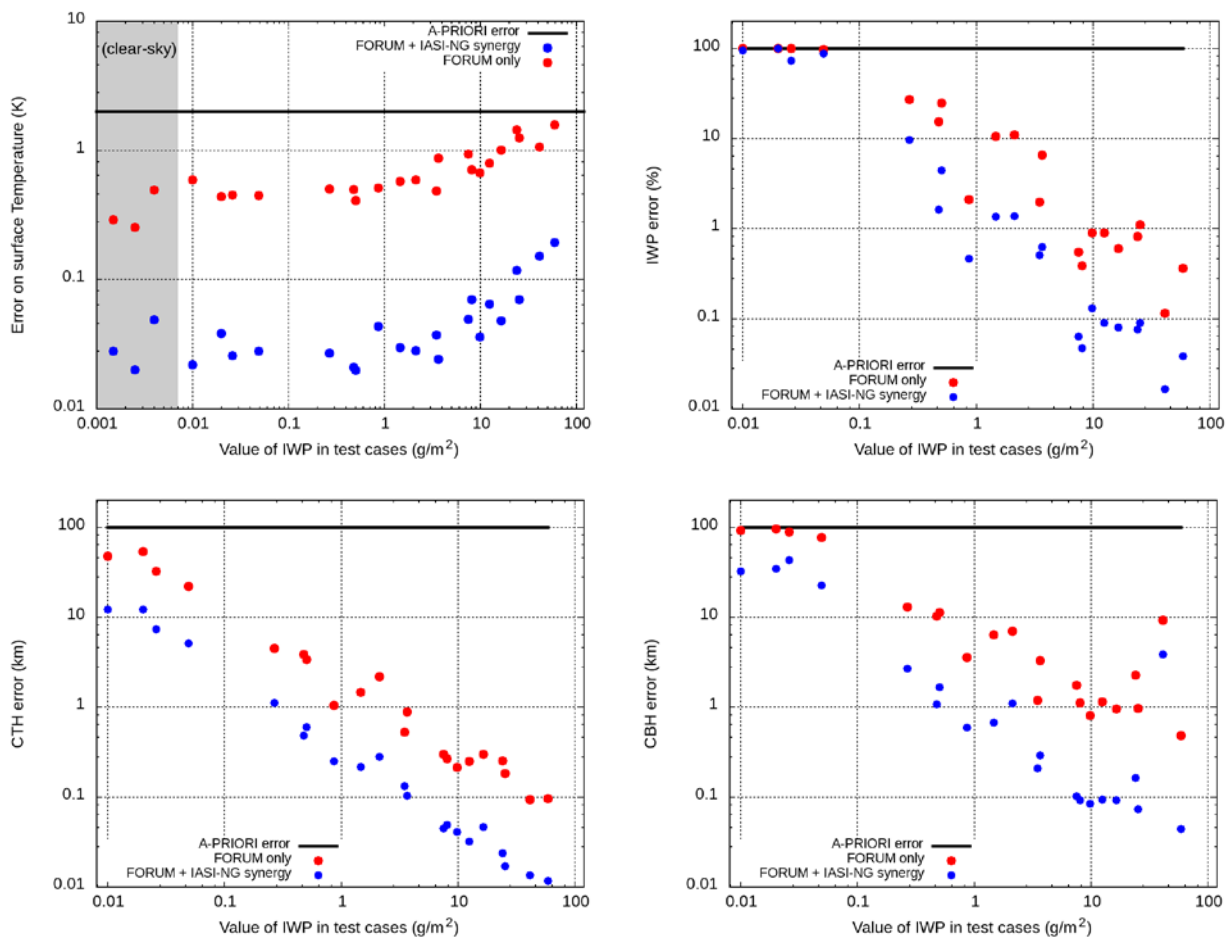


Figure 7.25 Retrieval uncertainties on Surface temperature (top left), IWP (top right), CTH (bottom left) and CBH (bottom right) for the various test atmospheric scenarios considered. Black lines represent the a priori uncertainties, red symbols the FORUM-only retrieval uncertainties and the blue symbols the uncertainty in the synergistic retrieval. Each measurement scenario is characterised by the IWP value in the horizontal axis. (M. Ridolfi, University of Bologna, Italy)



uncertainty achieved with the inversion of only FSI measurements and the blue symbols refer to the uncertainty associated with the synergistic retrieval of FORUM+IASI-NG measurements. The synergistic retrieval with IASI-NG results in marked reductions of the retrieval uncertainty in most of the cases. The synergistic retrieval typically reduces the

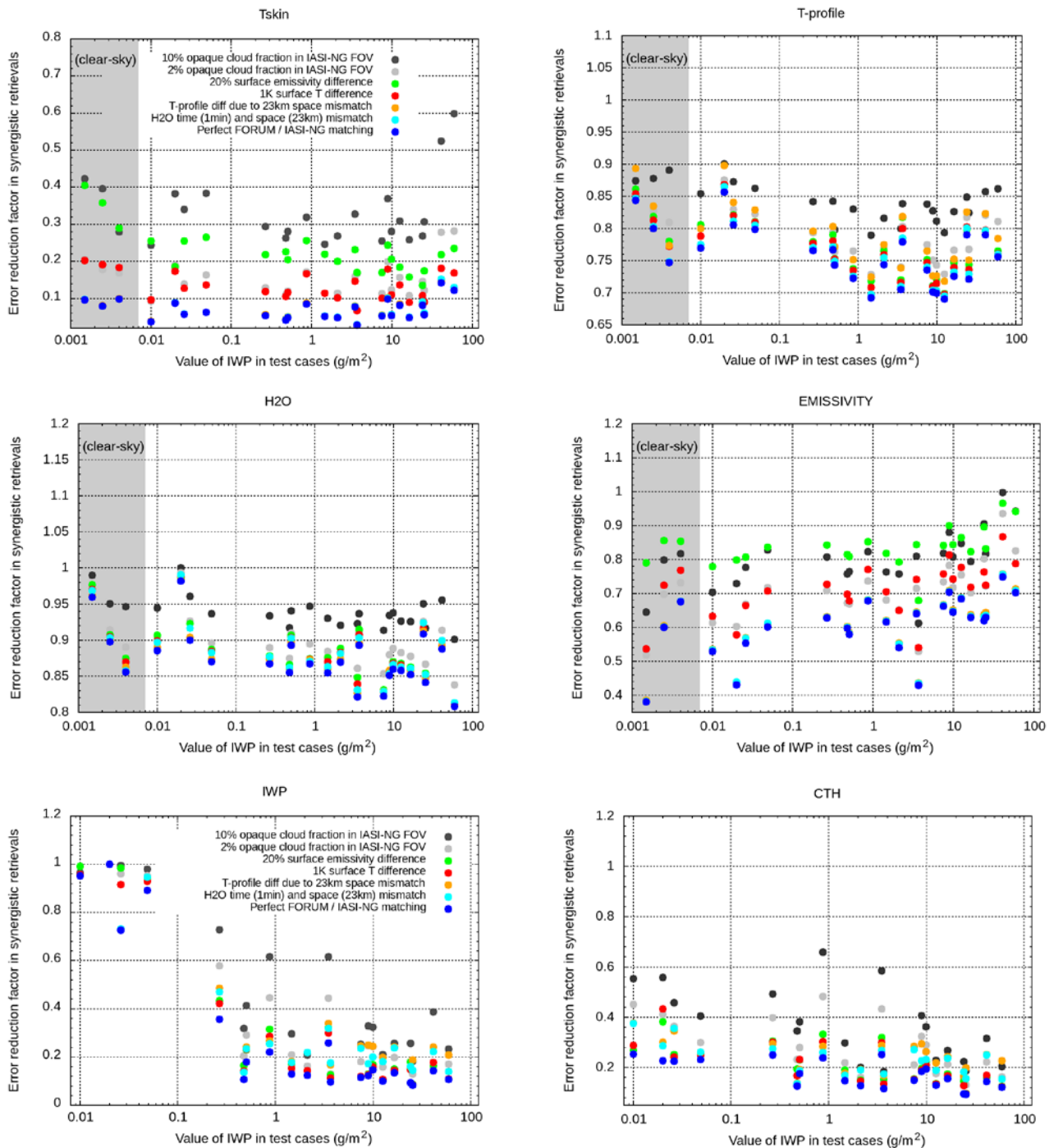


Figure 7.26 Error reduction factors achieved in the synergistic retrieval of FSI and IASI-NG measurements. Each plot refers to a specific retrieval parameter indicated in the plot's title. The coloured symbols refer to the different mismatch error components as indicated in the plot's key. (M. Ridolfi, University of Bologna, Italy)



surface temperature uncertainty by about one order of magnitude. In the case of cloud parameters, the synergistic use of IASI-NG measurements is also effective at reducing the retrieval uncertainties, with the reductions dependent on the value of IWP.

These results do change when the time- and space- mismatch between the FSI and IASI-NG measurements is considered. In phase A studies, the impact of measurement mismatch on the synergistic retrieval has been evaluated by assigning to the IASI-NG measured spectral radiance an additional uncertainty component, the so called *matching uncertainty*, that accounts for the fact that the spectrum itself is not acquired for exactly the same atmospheric and surface conditions as those of the FSI measurement. The following mismatch uncertainty components were considered, with characteristics compliant with the FORUM orbit requirements discussed in Section 4.5:

1. Natural variability of water vapour VMR and temperature profiles in a 23 km radius area. As explained in Section 4.5, based on the FORUM orbit requirements, 23 km is the maximum distance between the centres of FORUM and IASI-NG ground pixels.
2. Variability of water vapour VMR profile within a 1 min time interval.
3. 1 K variability of surface temperature (typical variability in a 23 km radius area).
4. 20 % variability of surface emissivity, to account for the cases in which the surface type is different in the two matching measurements.
5. 2 % and 10 % opaque cloud fraction difference between FSI and IASI-NG FOVs. This mismatch uncertainty component accounts for the cases in which an opaque cloud enters the instruments' FOV in a time lag of 1 min between the two measurements, i.e. only one of the instruments observes this cloud.

Variabilities 1 - 4 were estimated using the high-resolution (1.5 km) atmospheric and surface fields provided by a NWP model run from the UK MetOffice for this purpose, for a limited geographical area over the UK, and for 3 different times of a day (25 January 2018). All the variabilities mentioned above were then transformed into spectral uncertainties attributed to the IASI-NG spectrum using the Jacobian of the forward model (see eq. 6.1). The uncertainty of the synergistic retrieval was then re-computed and compared to that obtained for perfect matching of the measurements. To illustrate how the performances of the synergistic retrievals degrade with mismatch uncertainties present, the ratio between the synergistic retrieval uncertainty and the FORUM-only retrieval uncertainty were computed for the various retrieval parameters. In case of vector retrieval parameters, i.e. in the cases of water vapour and temperature profiles and in the case of the surface emissivity spectrum, the average of this ratio over the vector elements was computed. Values much smaller than 1 indicate that a marked reduction of the uncertainty is achieved using the synergistic retrieval relative to the FORUM-only retrieval. Values of the ratio close to unity indicate that a negligible uncertainty reduction is obtained using the synergistic retrieval.

Fig. 7.26 shows, for each retrieved parameter, the uncertainty reduction factor as a function of the IWP for the various measurement scenarios considered. The blue symbols refer to the case of perfect matching (both in time and space) of FSI and IASI-NG measurements. The other coloured symbols refer to the uncertainty reduction factors achieved in presence of mismatch uncertainties as indicated in the plots' key. In general, the mismatch uncertainties due to variations of water and temperature profiles cause only a marginal loss of the

improvements obtained in the synergistic retrievals. The effect for the case in which an opaque cloud enters the field of view of one of the instruments, is most pronounced. In this case, the improvements achieved with the synergistic retrieval are partially or significantly lost depending on the retrieval variable. Significant differences in the emissivity and the temperature of the ground surfaces sounded by the two instruments also result in a reduction of the improvement obtained in the synergistic retrieval of surface emissivity. However, these critical cases can be detected and effectively mitigated in operational conditions. For example, differences in cloud fraction between FSI and IASI-NG FOVs can be detected via MetOp-A METImage measurements. Similarly, geolocation data and maps of surface type can be used to check if the ground pixels of the two instruments are sounding surfaces with significantly different spectral emissivity. In these cases, a correction scheme can be implemented in the synergistic retrieval: the IASI-NG measurement will only be included when the joint retrieval provides an improvement to the FORUM-only retrievals.

7.3.2.4 Performance of FORUM for Detecting Inter-Annual Variability

In this section, the performance of FORUM with respect to inter-annual variability of water vapour will be investigated. Due to the nominal FORUM mission lifetime of 4 years, the focus here is on variations mainly caused by El Niño-Southern Oscillation (ENSO), which represents an important inter-annual (short-term) climate variability. Recently, the 2015–2016 El Niño exhibited a strong influence on upper tropospheric and lower stratospheric temperature and H₂O as indicated in ERA-Interim data and Aura Microwave Limb Sounder (MLS) satellite observations (Diallo et al., 2018). This can even be seen in zonally averaged temperatures, which increased by about 5K in the upper tropical troposphere (50°S – 50°N) from January 2015 to January 2016. Corresponding MLS water vapour values increased at the same time by about 20 % to 30%. The capability of FORUM to capture such inter-annual variability is investigated, based on these averaged values to derive the order of magnitude of the signals to be expected. Regional perturbations may be larger (e.g. for the West Pacific or Indian Ocean) or smaller.

To estimate the impact of such disturbances on the OLR spectrum and to check on its detectability by FORUM, the approach of Y. Huang et al. (2010) is followed (Fig. 2.2). The authors show in a theoretical study that individual greenhouse gas forcings and climate feedbacks have distinct spectral signatures in the outgoing longwave radiation (OLR). Y. Huang et al. use a climate model experiment with a doubling CO₂ scenario as a proxy for climate change, taking representative profiles before and after the doubling as input to radiative transfer calculations to diagnose the CO₂ forcing and feedbacks of temperature, water vapour, and clouds. Based on optimal detection technique, fingerprints of different contributors and their associated contributions to total OLR changes are isolated not only in clear-sky but also for all-sky conditions. They show that a spectral resolution of about 1 cm⁻¹ is sufficient to account for any nonlinearity effects (sum of individual changes not equal to the total change) and to reconstruct individual contributions to OLR changes with minimal biases (order of 1 %). The method is directly transferable to FORUM, which provides an even better spectral resolution for the extraction of fingerprints of single contributors.

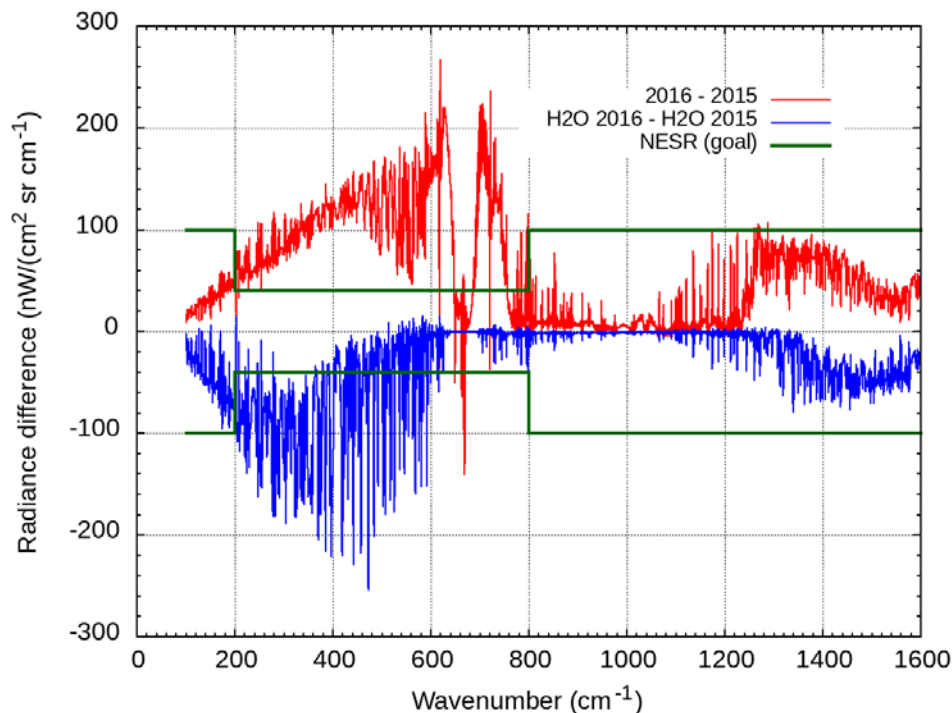


Figure 7.27 Spectral fingerprints of water vapour and temperature changes from January 2015 to January 2016 in the tropical UTLS. The red curve shows the combined fingerprint of atmospheric temperature and water vapour changes, while the blue curve shows the fingerprint of water vapour changes alone. Straight horizontal lines indicate the noise level for an individual observation. (B. M. Dinelli, CNR, Italy)

Fig. 7.27 shows spectral residuals representing changes in the OLR corresponding to the above mentioned atmospheric temperature and water vapour changes ($50^{\circ}\text{S} - 50^{\circ}\text{N}$) from January 2015 to January 2016. The red line corresponds to the total fingerprint of atmospheric temperature and water vapour changes, while the blue line shows the fingerprint of water vapour changes only. Straight horizontal lines represent the goal noise level for single FORUM observations. The fingerprint signals evidently exceed the FORUM noise level of a single observation in the long wavelength part of the spectrum.

7.3.2.5 FORUM Systematic Error Assessment

Systematic errors originate from the uncertainties on the different instrumental, atmospheric and auxiliary parameters that will not be targets of the retrievals in the Level-2 analyses. They include the concentration of the various interfering species whose spectral signatures overlap the ones of the target molecules, the spectroscopic data and water vapour continuum model employed, and instrumental effects. FORUM Level-2 clear sky retrieval are the vertical profile of water vapour and temperature, surface temperature and spectrally resolved emissivity.

Systematic errors affecting FORUM Level-2 products are estimated using the simulation of the retrieval procedure and the error spectra calculation, as in Dudhia et al. (2002). the method used for the error assessment is briefly outlined below. As reported in Chapter 6, at any step of the retrieval iterative process, the solution is expressed by the equation

$$x = x_0 + ((K^T S_y^{-1} K) + S_a^{-1})^{-1} [K^T S_y^{-1} n + S_a^{-1} (x_0 - x_a)]$$

where \mathbf{x} is the state vector of the parameters to be retrieved, \mathbf{x}_0 the vector of the parameters at the previous step of the iterations, \mathbf{x}_a the a-priori state vector, \mathbf{K} the Jacobian matrix, \mathbf{S}_y and \mathbf{S}_a the Variance Covariance Matrices (VCM) of the measurements and of the a-priori state respectively. The vector \mathbf{n} , the so-called residual, contains the difference between the observation and the simulation performed by the forward model inside the retrieval code with the set of parameters \mathbf{x}_0 . In the presence of a systematic error, the observed radiances will differ from the real radiances by a contribution due to the considered systematic error and the new residuals $\hat{\mathbf{n}}$ will be affected by the same systematic contribution. Calling the new solution $\hat{\mathbf{x}}$, the estimate of the systematic error that affects the retrieved state vector can be calculated as the difference $\Delta\mathbf{x} = \hat{\mathbf{x}} - \mathbf{x}$.

Defining \mathbf{G} (the information gain matrix) as:

$$G = ((K^T S_y^{-1} K) + S_a^{-1})^{-1} K^T S_y^{-1}$$

and

$$\Delta x = G \cdot (\hat{n} - n)$$

The quantity $(\hat{\mathbf{n}} - \mathbf{n})$ can be evaluated with simulations as the difference between the spectra at the top of the atmosphere obtained with unperturbed conditions and with each parameter perturbed by its systematic uncertainty.

To have a complete picture of the expected systematic components of the error, simulations using the IG2 climatological atmospheres (Remedios et al. 2007) have been performed. The IG2 database contains yearly climatological profiles estimated for four seasons and six latitude bands from 2002 to 2012 and their climatological variability at 1σ . In this work, the IG2 profiles for four seasons of 2012 in six latitudinal bands were applied, polar North ($90^\circ\text{N} - 65^\circ\text{N}$), mid-latitude North ($65^\circ\text{N} - 30^\circ\text{N}$), tropical North ($30^\circ\text{N} - 0^\circ$), tropical South ($0^\circ - 30^\circ\text{S}$), mid-latitude South ($30^\circ\text{S} - 65^\circ\text{S}$) and polar South ($65^\circ\text{S} - 90^\circ\text{S}$).

The following set of systematic error sources have been considered: VMR of interfering species, instrumental line shape uncertainty, spectroscopy, forward model errors, ARA. The

Table 7.10 A priori errors for water vapour and temperature profiles.

Height (km)	A priori error for H ₂ O (%)	A priori error for temperature (K)
120.0	10.0	1.4
64.6	10.0	1.4
32.1	10.0	0.6
15.8	10.0	0.6
8.0	30.0	0.5
2.6	30.0	0.5
0.0	3.0	0.5

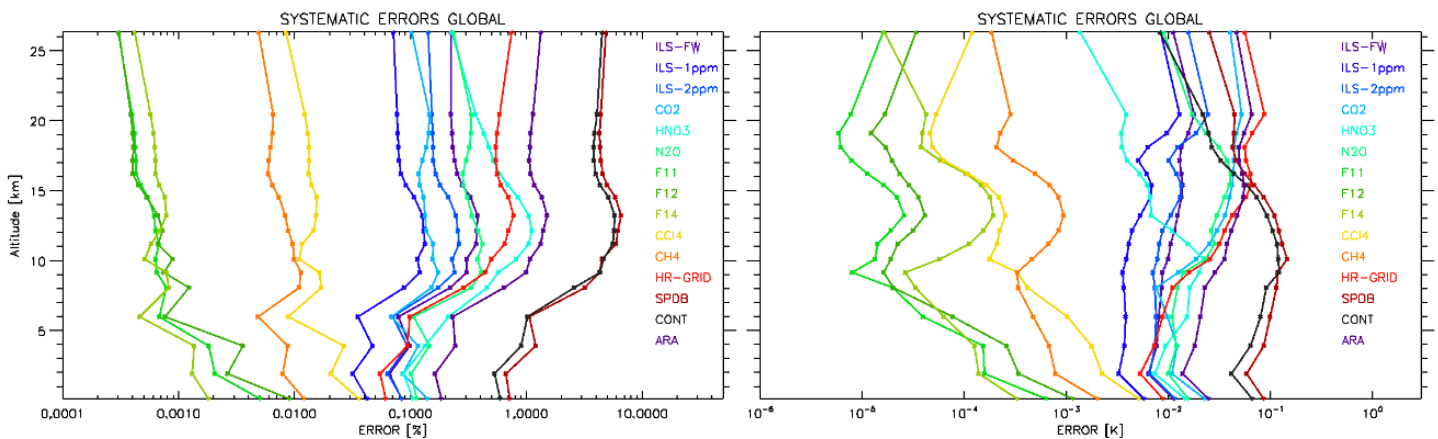


Figure 7.28 Global average systematic errors on retrieved water vapour (left panel) and temperature (right panel) as a function of altitude. (A. Di Roma, CNR, Italy)

sources of the systematic errors along with the values used in the analysis are listed in the following

- VMR of interfering species → The systematic component was set to the 1 σ climatologic variability estimated for MIPAS for mid-latitude, equator and polar winter and summer. The following gases have been considered: CO₂, N₂O, CH₄, HNO₃, CFC-11, CFC-12, CFC-14, CFC-22, CCl₄ marked correspondingly as **[CO₂, N₂O, CH₄, HNO₃, F11, F12, F14, F22, CCl₄]**
- Uncertainties on the knowledge of the instrumental line shape (ILS) function → The error spectra are created from the difference between spectra calculated with the perturbed ILS function and with the unperturbed one. The systematic errors due to the following parameters are accounted for separately: Frequency shift error (goal value, 1 ppm **[ILS_1ppm]** and threshold value, 2 ppm **[ILS_2ppm]**); maximum width error (Full Width Half Maximum (FWHM) perturbed by 0.6%) **[ILS FW]**
- Water Vapour Continuum Model → differences between spectra computed with the MT_CKDV2.5 model and MT_CKDV3.0 model. **[CONT]**
- Frequency grid in the Forward Model → difference between spectra computed with a very fine spectral resolution 0.0005 cm⁻¹ (that enables to model all the line centers correctly) and spectra with the resolution used in the retrievals (reduced to reduce the CPU time) (0.0025 cm⁻¹) **[HR-GRID]**
- Uncertainties on spectroscopic parameters → random perturbation in line strength and pressure broadening coefficients (HWHM) of HITRAN2016 transitions, according to the errors reported in the database **[SPDB]**

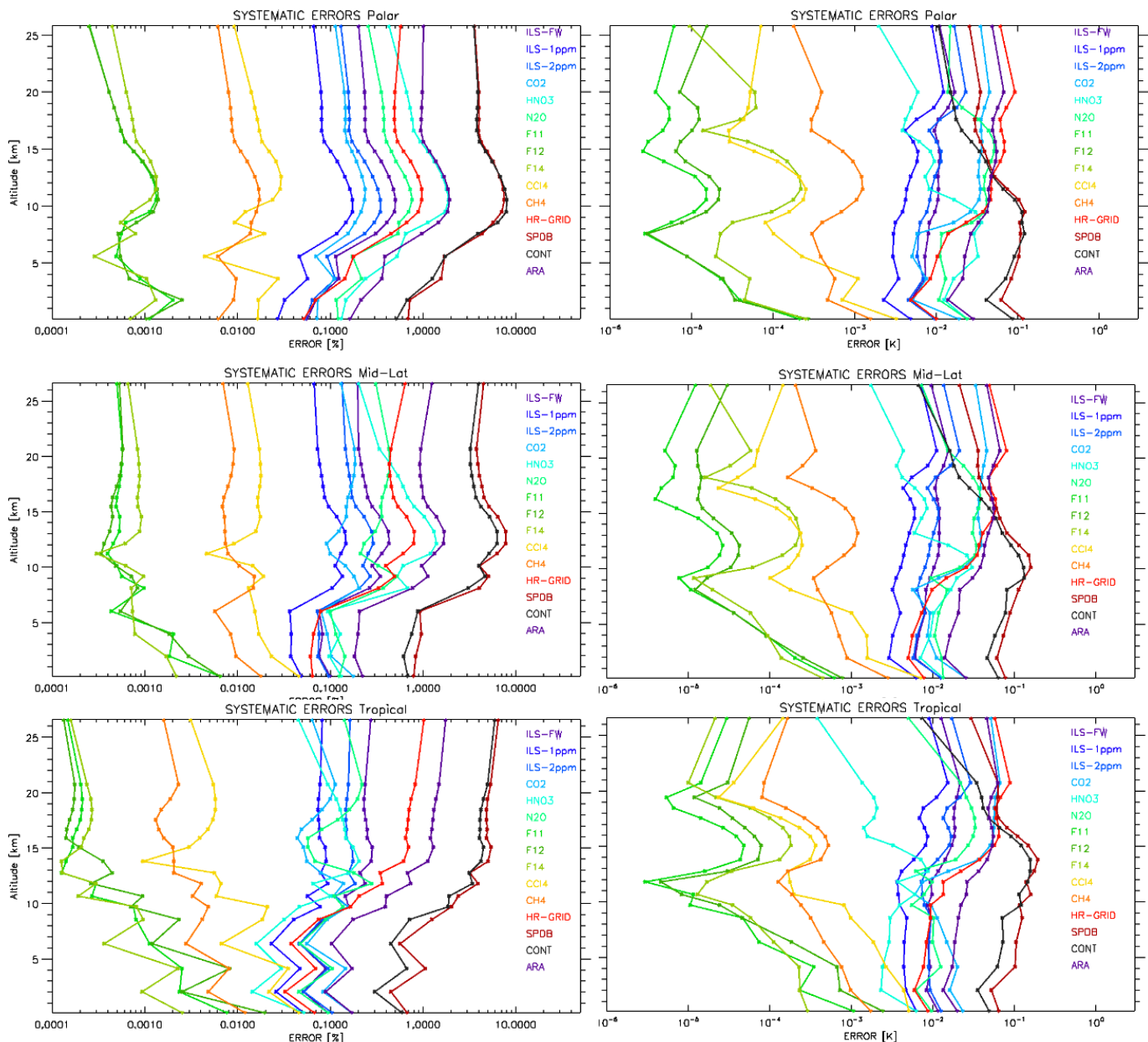


Figure 7.29 Average systematic errors on retrieved water vapour (left panels) and temperature (right panels) as a function of altitude for the different latitudinal bands: top polar, middle mid-latitudes and bottom tropical. (A. Di Roma, CNR, Italy)

The systematic error assessment has been performed using a vertical grid with a 2 km step from ground level to 8 km altitude, 1 km step from 8 km up to 20 km altitude and 5 km step from 20 km up to the top of the atmosphere. The surface emissivity is retrieved at 30 evenly spaced spectral points covering the full FORUM spectral range from 100 to 1600 cm^{-1} . Table 7.10 reports the a-priori errors used for each retrieved variable. For water vapour, the error is expressed as percentage error of the a-priori profile, while for temperature the absolute error in Kelvin is reported. For the ground emissivity, the a-priori error was set to 0.1 for all the selected spectral points. The VCM of the observations (S_y matrix) was set to FORUM goal NESR (Noise Equivalent Spectral Radiance).

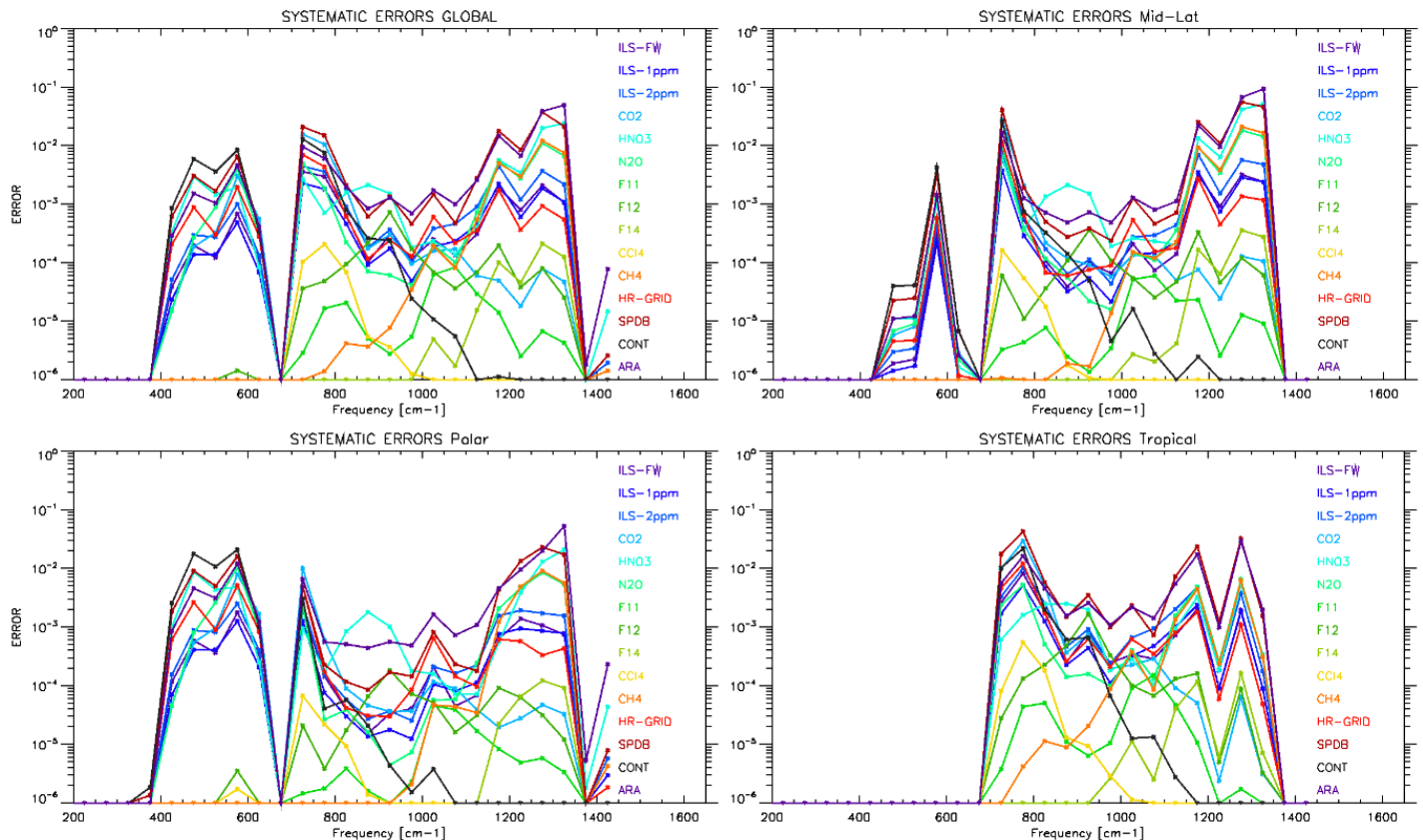


Figure 7.30 Systematic errors on the retrieved ground emissivity. Top left panel: global average, Top right panel: mid-latitude average, Bottom left panel: Polar average Bottom right panel: Tropical average (A. Di Roma, CNR, Italy)

The systematic errors have been averaged over all seasons and latitudinal bands to produce a global estimate of their magnitude. The results are shown in Fig. 7.28 for water vapour and temperature. The errors are expressed as percentage errors for water vapour and as absolute error for temperature in the altitude range from 0 to 25 km. For both water vapour and temperature retrievals, systematic errors due to the trace gases CFCs, CH₄, and CCl₄ are negligible (below 0.01 % for water and 0.01 K for temperature), while CO₂, N₂O and HNO₃ produce systematic uncertainties between 0.1 % and 1 % for water vapour and between 0.01 K and 0.1 K for temperature. Similar uncertainties result from the error on the ILS, the frequency grid used in the forward model (HR-GRID) and the absolute radiometric accuracy. The dominant sources of systematic error are the uncertainties associated with the spectroscopic database and with the water vapour continuum model.

The impact of the systematic errors has a latitudinal dependence, as shown in Fig. 7.29. The impact of interfering species varies with latitude. A special case is HNO₃ which shows the maximum contribution in the polar regions at winter time (not shown here) due to the ozone hole chemistry. However, in all latitudinal bands, the major error sources are still due to the spectroscopic errors and the continuum model.

The impact of the systematic error sources on the retrieved surface emissivity (shown in Fig. 7.30) is always very small, below 0.01. The errors in frequency regions not sensitive to the surface emissivity are set to zero, therefore the plots in Fig. 7.30 also show the spectral regions where FORUM will be sensitive to the surface emissivity. The width of the spectral sensitivity increases going from the tropics to the Poles, where it reaches its maximum extent because of the increasing transparency of the overlying atmosphere as the water vapour concentration reduces (Fig. 2.6).

The size of the systematic errors on the water vapour and temperature profiles due to the interfering species suggests that FORUM measurements are sensitive to their variability and therefore could be used to retrieve the abundance of several trace gases, like HNO₃, N₂O and CO₂. The impact of the spectroscopic errors and continuum model on the retrievals suggests that FORUM measurements are sensitive to spectroscopy and can therefore be used to improve the quality of spectroscopic data.

7.4 Campaign Data Analysis

The Earth's outgoing longwave radiation can only be measurements at the top of the atmosphere with a satellite mission like FORUM. However, the effects of the atmospheric state and surface parameters on the far-infrared can be investigated in ground-based campaigns and airborne field experiments. In the next two sections, results from field campaigns that investigated the sensitivity to parameters such as temperature, water vapour, surface emissivity and cloud parameters including sensitivity to the habit of ice cloud crystals, are shown. These results complement the synthetic performance tests as presented in the previous section.

7.4.1 Ground-based Campaign at Zugspitze

A new instrument called far-infrared radiation mobile observation system (FIRMOS) was developed, build, tested, and successfully deployed in a field experiment during the FORUM Phase A studies. Because of the high opacity of the atmosphere in the FIR, caused by the high concentration of water vapour (see Fig. 2.6), field measurements require a high altitude site where a dry atmosphere is sufficiently transparent in the FIR. The Observatory Zugspitze Summit, Germany (47.4°N, 11.0°E, 2962 m above sea level) offers excellent facilities in the vicinity providing independent validation of the geophysical data products.

The instrument was operated on the terrace of the Summit, for two months in November-December 2018 and January-February 2019 acquiring measurements when the weather conditions were appropriate. The instrument covered the 100-1000 cm⁻¹ spectral range with a resolution of 0.36 cm⁻¹ and 36 s acquisition time. The calibrated spectral measurements were validated using the Extended-range Atmospheric Emitted Radiance Interferometer (E-AERI) (ABB Bomem Inc., Quebec, Canada), an operational instrument installed permanently at the Summit covering the 400 to 3000 cm⁻¹ spectral range with 0.6 cm⁻¹ of resolution (Sussmann et al., 2016). This instrument was fitted with two new calibration blackbodies for this campaign. Here, only the comparison for the integrated water vapour is shown (Fig. 7.31), both retrieved from the spectral measurements using the same technique adapted from Serio et al. (2008). Good agreement is found. The very small mean difference

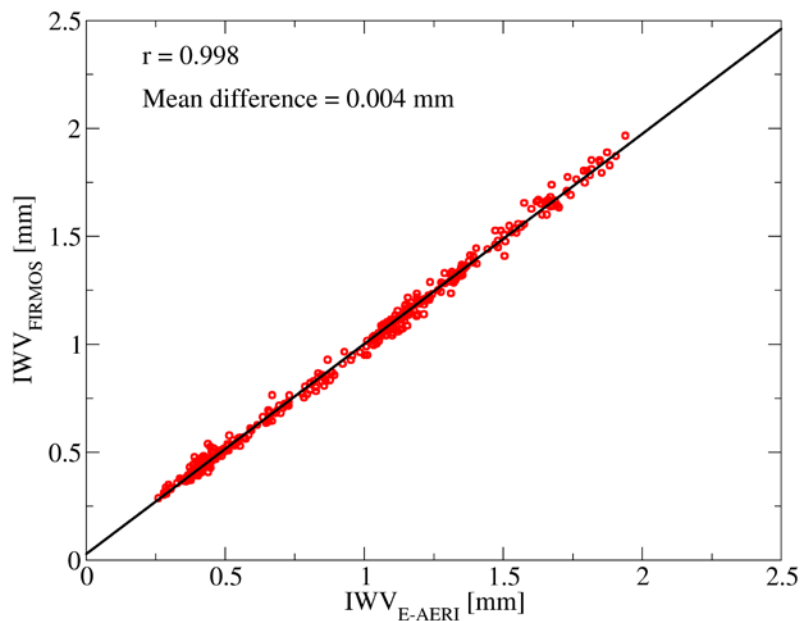


Figure 7.32 scatterplot for the integrated water vapour measured by the FIRMOS and E-AERI instruments. The same retrieval code was used for both instruments. Good agreement is found. The small mean difference can be assigned to a 4 m height difference of the two instruments. (L. Palchetti, CNR, Italy)

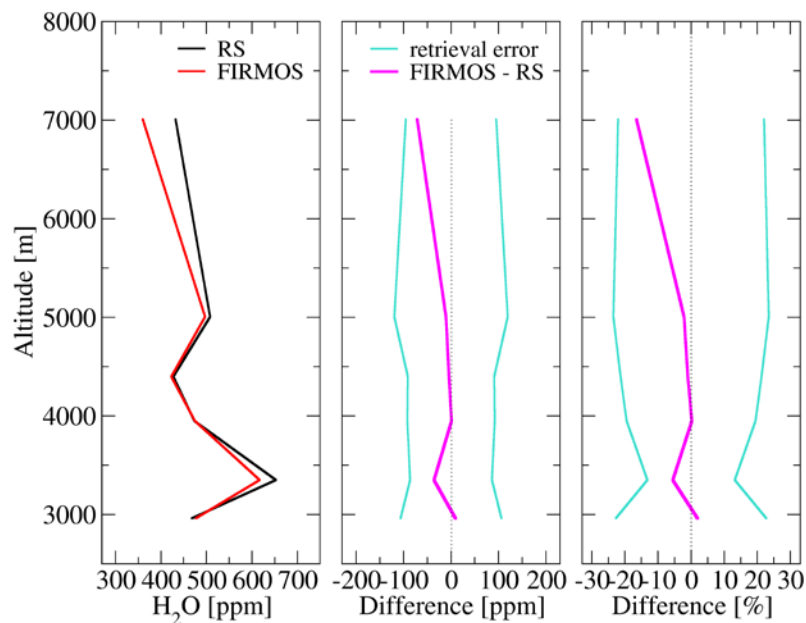


Figure 7.31 Comparison between FIRMOS water vapour retrievals and radiosonde (RS) profiles. The left-hand panel shows the average RS profile in red and the average coincident FIRMOS profiles in black. The other two panels show the average difference, both in volume mixing ratio (central panel) and in percentage difference (right panel) together with the average FIRMOS retrieval error (cyan curves). (C. Belotti, CNR, Italy)

between the two datasets can be explained by the 4 m difference in altitude of the two instruments.

In order to derive profiles of water vapour and temperature, and the CO₂ total column, the FIRMOS measurements were analysed with the KLIMA code (Del Bianco et al. 20), and for cloudy scenes, with the SACR code (Di Natale et al. 2017). Both codes are based on the Levenberg-Marquardt iterative method of the optimal estimation approach (see Section 6.1). SACR allows the retrieval of clouds parameters, such as the optical depth, the effective sizes of ice crystals (or alternatively the ice water path), the ice-to-water fraction, the liquid droplets sizes, and the cloud bottom layer. As for the FEES, the a priori information for the initial guess is taken from the IG2 climatology (Remedios et al. 2007). The SACR forward model is able to treat the multiple scattering effect on the radiation due to multi-layered clouds and uses the optical coefficients for the ice particles from databases provided by P. Yang for different habits (Yang et al. 2013, see also Section 6.1).

Though the comparison with the E-AERI showed excellent results, the underlying water vapour spectroscopy is the same. For completely independent validation, radiosoundings are ideal and four were performed during 5 - 6 February 2019. The sondes were launched from Garmisch-Partenkirchen, about 10 km from the Zugspitze summit, though with a height difference of about 2200 m. The balloon sondes were equipped with a standard radiosonde and a cryogenic frostpoint hygrometer (CFH) for measuring water vapour profiles.

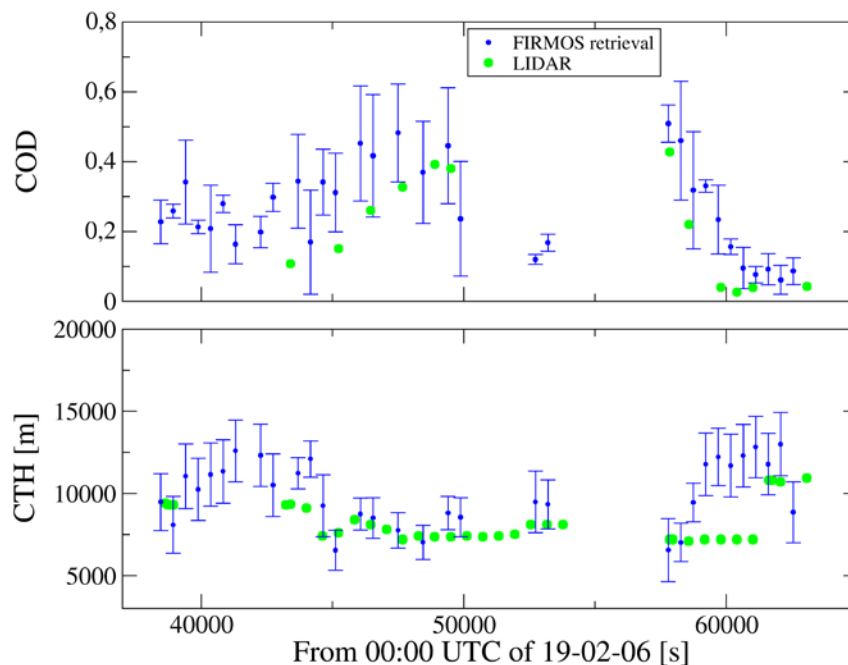


Figure 7.33 Comparison of Lidar and FIRMOS measurements for cloud optical depth and cloud bottom height. (G. Di Natale, CNR, Italy)

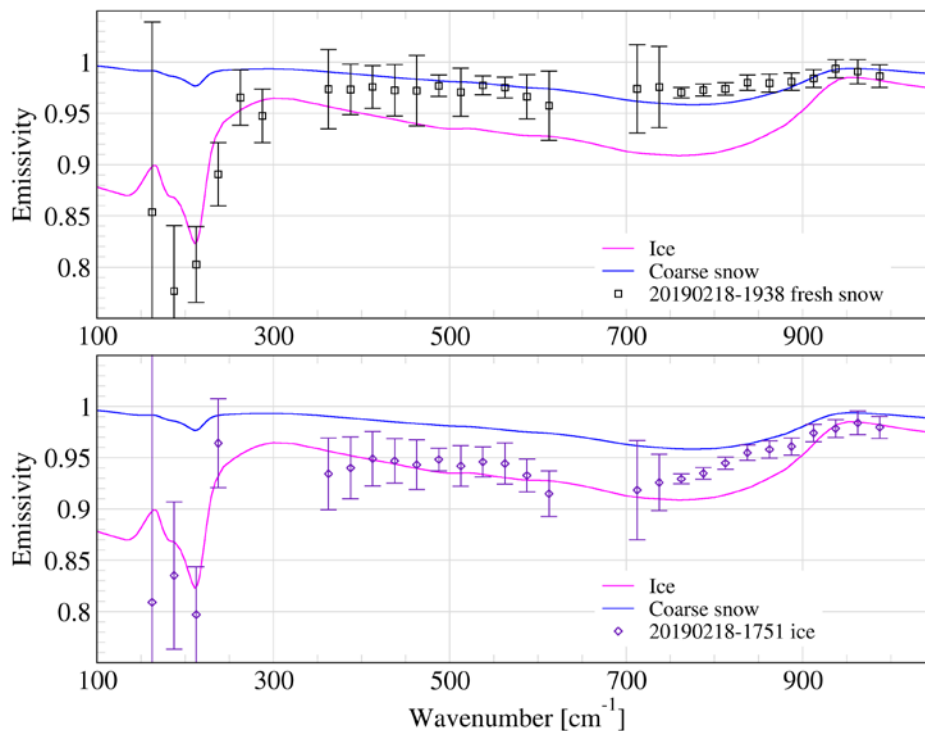


Figure 7.34 top panel: emissivity retrieved from FIRMOS measurement (squares) of a fresh snow sample (taken on 18 Feb 2019 19:38). bottom panel: emissivity retrieved from FIRMOS measurement (diamonds) of an ice sample (taken on 18 Feb 2019 17:51). The two curves on both panels are model data for ice (magenta) and coarse snow (blue). (C. Belotti, CNR, Italy)

The Level-2 retrieval products for clear sky cases are the profiles of water vapour. The quality of the retrievals was evaluated by comparison with the closest radio soundings. The radiosonde profiles have a fine vertical resolution. Therefore, they were convolved with the FIRMOS averaging kernels. Fig. 7.32 shows the average difference between all coincident FIRMOS and radiosonde water vapour profiles. The results show that the average difference falls well within the retrieval error range.

The FIRMOS retrieved cloud parameters were compared with the standard product of a backscattering Lidar operated from the nearby research station of the Schneefernerhaus at about 600 m away from the Summit. Fig. 7.33 shows the good agreement between the retrieved values and the Lidar measurements for the optical depths and cloud bottom height. These comparisons show that passive measurements in the FIR are as good as active measurements for cloud properties.

In the last part of the campaign, the instrument was modified for nadir observations. Emissivity was retrieved from FIRMOS measurements of upwelling and downwelling radiances taking into account the contribution of the atmosphere between the sample and the instrument. Fig. 7.34 shows the retrieved spectral emissivity values for two different snow sample, one for fresh snow (snow density of 200 kg/m^3 , total surface of air/ice interface $40 \text{ m}^2/\text{kg}$) and another one for an ice sample (snow density 850 kg/m^3 , the total surface of air/ice interface cannot be measured for ice). As a reference both panels also show emissivity model values (Chen et al. 2014) for *ice* and *coarse snow* from 100 to 1000 cm^{-1} .

The measurements confirm that the emissivity is different from 1. More measurements are needed to investigate the accuracy of the emissivity model.

7.4.2 Airborne Measurements

Here airborne measurements of upwelling nadir radiance covering the 100-1400 cm^{-1} spectral range are exploited in order to show how FORUM will be able to (a) test and improve the ability to accurately model the radiative signature of ice cloud consistently across the infrared and (b) infer surface emissivity in suitable atmospheric conditions. In both cases measurements from the TAFTS (Canas et al., 1997) and the Airborne Research Interferometer Evaluation System (ARIES, Wilson et al., 1999) were used, both mounted on the UK Facility for Atmospheric Airborne Measurements (FAAM) BAe-146 aircraft which was also equipped with a Leosphere ALS450 backscatter lidar (Marenco 2010) and an array of cloud microphysical instrumentation (O'Shea et al., 2016). TAFTS nominally covers the FIR in two bands from 80-300 and 330-600 cm^{-1} with a spectral resolution of 0.12 cm^{-1} , while ARIES has a resolution of 1 cm^{-1} and spans the range 550-3000 cm^{-1} . In comparison, the goal spectral resolution for FORUM is 0.5 cm^{-1} .

7.4.2.1 Testing Current Cirrus Bulk-Scattering Models

The goal is to determine whether radiance spectra in the presence of cirrus cloud can be consistently modelled across the infrared within measurement uncertainties using state-of-the-art line-by-line radiative transfer codes and cirrus optical property databases. The observations are from a single flight on the 13th March 2015 off the north-east coast of Scotland, UK focusing on a straight and level run (SLR) made above an optically thin cirrus cloud. During the SLR, in addition to the radiance measurements, a 355 nm lidar provided continuous profiling of the cloud while profiles of temperature and humidity were obtained

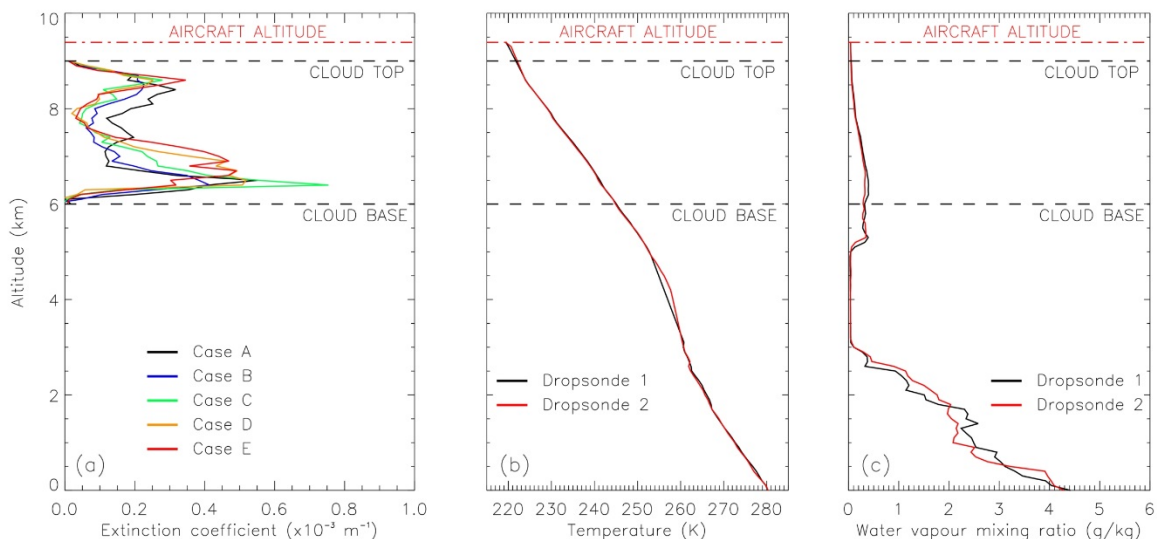


Figure 7.35 (a) Example lidar extinction coefficient profiles obtained during the SLR, indicating the variability in the cirrus structure along the run; (b) Dropsonde temperature profiles from the two dropsondes deployed approximately 3 minutes apart during the SLR; (c) As centre panel, but for the water vapour mixing ratio profiles. The altitude of the aircraft and the upper and lower boundaries of the cirrus cloud layer are indicated by the dashed lines. (R. Bantges, Imperial College, London)

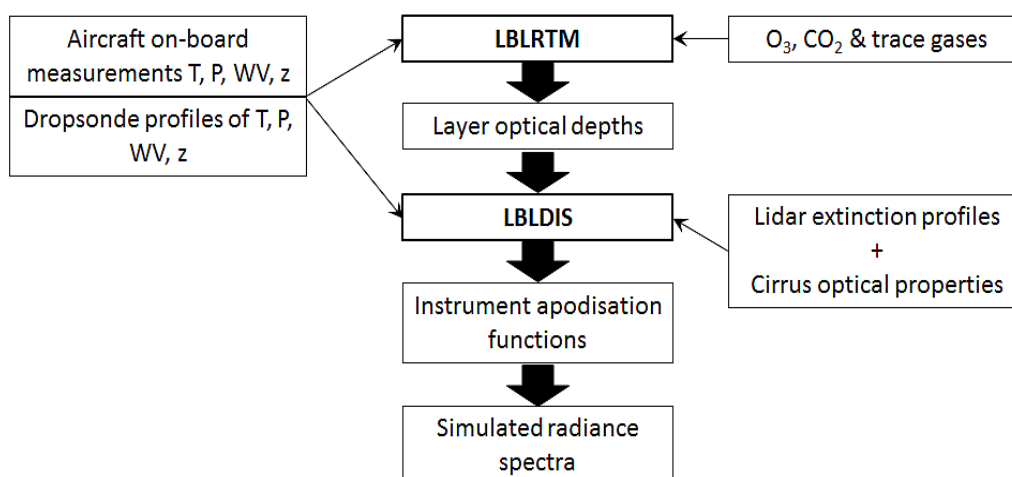


Figure 7.36 Schematic of the ARIES and TAFTS radiance simulation methodology. T, P, WV and z refer to temperature, pressure, water vapour and altitude, respectively. CO₂ and trace gas profiles assumed standard Mid-Latitude Winter profiles (Anderson et al., 1986) scaled to present day concentrations. O₃ was taken from ERA interim reanalyses data. (R. Bantges, Imperial College, London)

from dropsonde launches from the aircraft (Fig. 7.35). Subsequent to the SLR the aircraft descended to within the cloud deck, where dedicated cloud probes characterised the cirrus particle size distribution (O'Shea et al., 2016).

The simulation methodology followed the procedure shown in Fig. 7.36, utilising version 12.8 of the Line by Line Radiative Transfer Model (LBLRTM, Clough et al., 2005) and version 3.0 of the Line by Line Discrete Ordinates Radiative Transfer Model (LBLDIS, Turner, 2005). Cirrus optical properties were either taken directly from Baum et al. (2014), representing one fixed size distribution and a variety of crystal habits or habit mixtures, or were derived from the measured size distribution combined with the single scattering properties of specific crystal habits from Yang et al. (2013). Assuming the temperature and water vapour profiles and the cloud height to be well constrained by the dropsondes and lidar, for each crystal habit or habit mix the cirrus optical depth and effective radius were varied until optimal agreement between the ARIES observations and simulations in the main atmospheric window (800-1200 cm⁻¹, excluding the 1041 cm⁻¹ ozone band) was achieved. Using the same combination of optical depth and effective radius the simulations were then extended to the FIR and the agreement with TAFTS assessed.

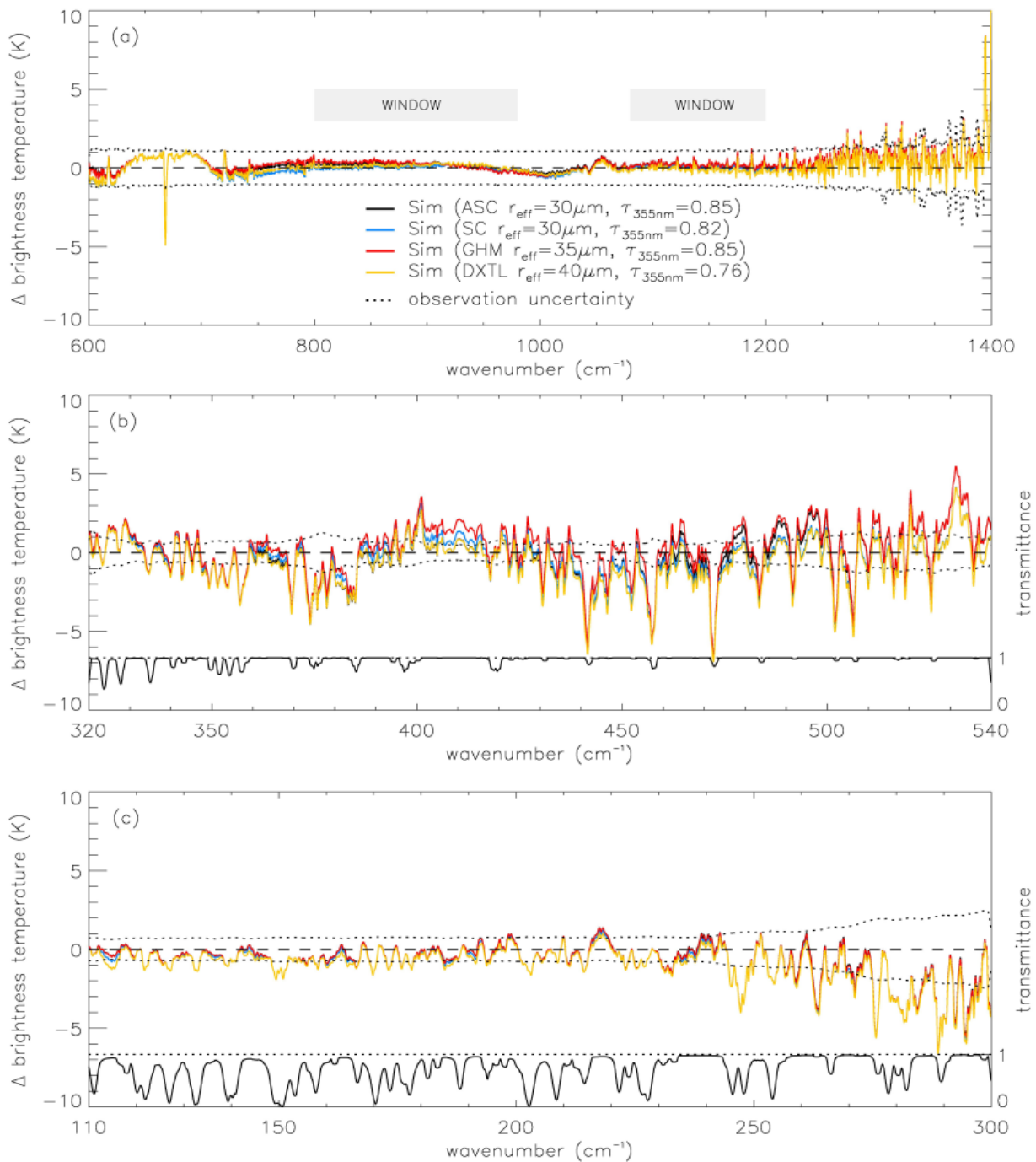
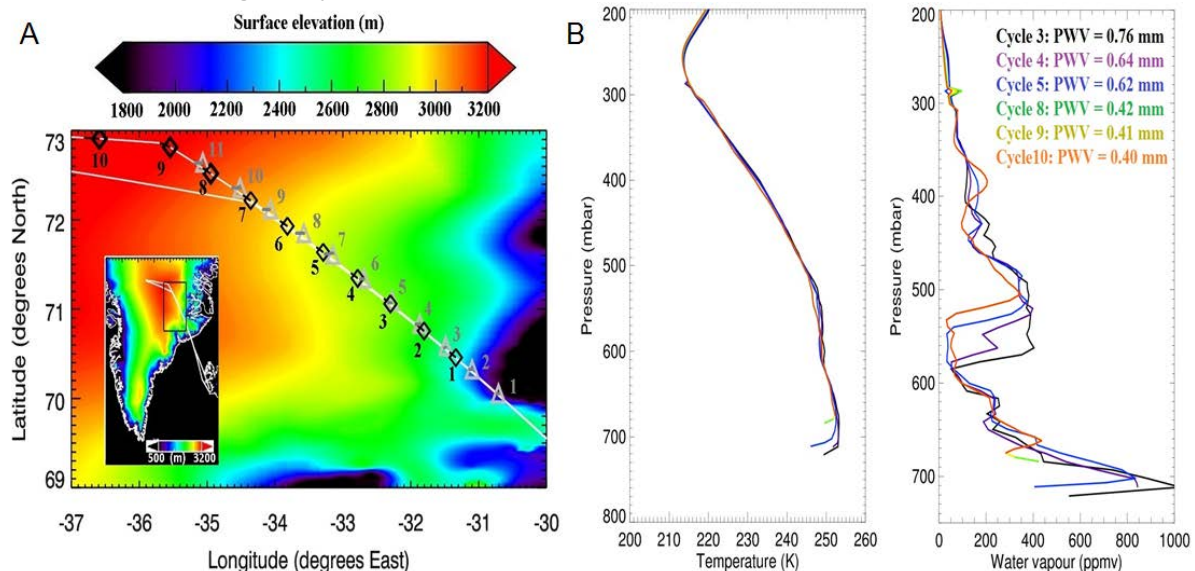


Figure 7.37 Infrared brightness temperature differences between aircraft observed radiances and simulations for Case A in Fig. 7.36, with cirrus optical depth and effective radius constrained to provide the best match in the MIR for the Single Column (SC), Aggregate Single Column (ASC) and General Habit Mix (GHM) habits of Baum et al (2014) or for the in-situ particle size distribution assuming droxtals (DXTL) (panel (a)). In panels (b) and (c) the transmittance of the layer between the top of the cirrus cloud and aircraft is also shown by the solid black line. Micro-windows where the transmittance is close to 1.0 show the largest sensitivity to habit/size distribution. The dotted lines indicate the level of instrumental uncertainty. (R. Bantges, Imperial College, London)

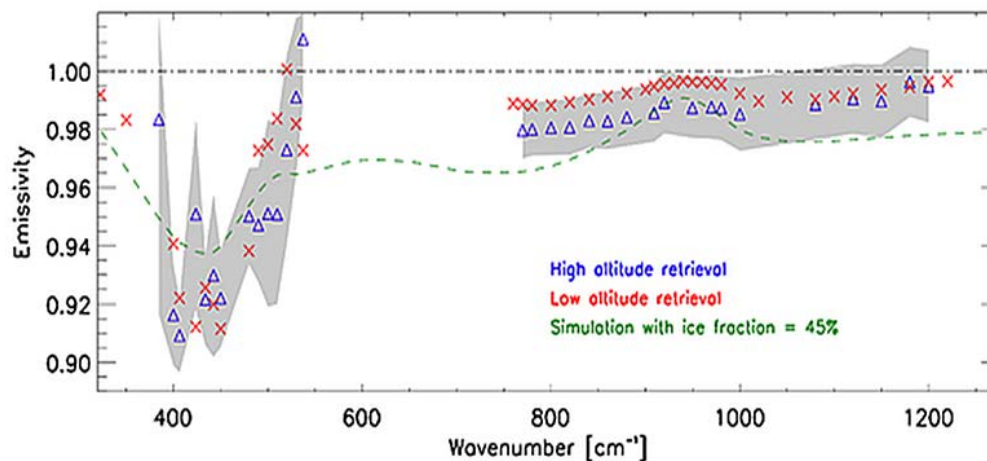
Fig. 7.37 shows the differences between the observed and simulated radiances, for Case A, across the MIR (a) and FIR (b and c). As noted above, by design, the agreement in the MIR window is very good and well within the ARIES uncertainty. In the FIR, the effects of changes in cirrus microphysics can be masked by the overlying water vapour in the atmospheric layer between the cloud top and aircraft. However, in highly transparent micro-windows (e.g. between 362-368, 402-416, 473-482 cm^{-1} etc.) the simulations tend to diverge from each other, showing an enhanced sensitivity to cirrus microphysics compared to that seen in the MIR window. Moreover, none of the optical property models tested, including those using the observed size distribution, agree with the TAFTS measurements within uncertainties across all the micro-windows sampled. Conclusions consistent with these are drawn from analysis of the results from the other four cases (B to E). These results reinforce the need for FORUM measurements in order to (a) build up the global radiance dataset needed to thoroughly test and improve ice-cloud scattering models and parameterisations across the FIR and (b) exploit these improvements to better constrain global estimates of crystal habit and size. This approach will directly benefit climate modelling by developing a consistent representation of ice cloud and its radiative impact across the infrared and thus give greater confidence in change predictions.

7.4.2.2 Retrieving FIR Surface Emissivity over the Greenland Plateau

Bellisario et al. (2017) were able to provide the first airborne estimates of FIR surface emissivity of snow, exploiting TAFTS and ARIES measurements from a near surface (300 m above ground level) FAAM flight over the Greenland Plateau. Here measurements are analysed, taken during the same flight but from the UTLS at ~ 9.2 km above ground level, a configuration which is more representative of the atmospheric path FORUM will encounter. Fig. 7.38 (A) shows the FAAM flight path over the Plateau, proceeding in a north-west direction from the coast with the periodic TAFTS nadir scan cycles highlighted in black. Dropsondes were regularly launched from the plane to characterise the atmospheric state,



7.38 Inset: FAAM flight track and surface elevation. Black box indicates the region highlighted in the main image. Main Image: Dropsonde release points (grey triangles) and location of TAFTS nadir scan cycles (black diamonds). (B) Selected dropsonde temperature and water vapour profiles. Precipitable water vapour (PWV) for each profile is also shown in the legend. (J. Murray, Imperial College, London)



7.39 Surface emissivity retrieved by Bellisario et al. (2017) for low altitude flight (red crosses) and from the UTLS flight analysed here (blue triangles). The shading represents the uncertainty on the high level retrievals. The green curve is a theoretical model of snow emissivity assuming surface ice crusting. (J. Murray, Imperial College, London)

and show a systematic decrease in precipitable water vapour as the aircraft progressed towards the interior of the Plateau (Fig. 7.38 (B)).

Emission from the surface is governed by a combination of the surface emissivity and the surface temperature, T_s . These can either be retrieved jointly or one can be obtained assuming the other is known. The approach taken here was to estimate T_s from ARIES measurements in the MIR following Knuteson et al. (2004), before applying the technique of Bellisario et al. (2017) to infer the surface emissivity. Fig. 7.39 shows the resulting surface emissivity inferred for scan cycle 10, closest in time and location to the near surface retrievals of Bellisario et al. (2017). These latter retrievals are over-plotted for comparison. No retrievals are attempted in either case between 550-750 cm^{-1} due to both the reduced sensitivity to surface emission in this region as a consequence of strong CO_2 absorption and increasing instrument noise towards the edges of the TAFTS and ARIES detectors. Given the marked difference in path length, and the small offsets in location and timing, the overall agreement between the low and high altitude flights, within the associated uncertainty, is highly encouraging.

7.4.2.3 Testing Cirrus Classification Using Aircraft Data

The machine-learning algorithm for cloud detection (Section 6.1) of the FORUM end-to-end simulator (Section 7.1.4) has been adapted for TAFTS and ARIES data. For this, a new training data set has to be created. Because of limited data availability from this aircraft campaign, the training data set was augmented with synthetic data. The same climatologies and radiative transfer codes as for the end-to-end simulator were used for this. Here, the cloud detection algorithm was limited to only two options, clear sky or cirrus cloud. The parameters for this specific training data set are listed in Table 7.11.

For different wavenumber intervals were used to investigate the performance of the algorithm. Results highlight the advantage of using the optimised range that accounts for both the FIR and the MIR part of the spectrum (see Table 7.12). The methodology applied to

the full test set and using the 300-1300 cm^{-1} spectral range allows identifying thin cirrus clouds corresponding to optical depth as low as 0.03. The detection performances using only the MIR or the FIR (respectively ARIES and TAFTS spectral ranges) are significantly lowered. Key information for the clear/cirrus identification is derived mainly from the 300–1300 cm^{-1} spectral range rather than the full spectrum covered by both sensors available. This is mostly due to the large noise in the data at wavenumbers below 300 cm^{-1} and above 1300 cm^{-1} , and low sensitivity to cirrus clouds parameters.

FORUM	Range
Day	1 – 31 March 2015
Cloud top height	5.1 – 9.3 km
Geometric thickness	0.2 – 3.0 km
Cloud optical depth	0.03 – 2.0
Particle effective radius	2 – 40 μm

Table 7.11. Range for cloud parameters used for the synthetic data set

Wavenumber range (cm^{-1})	Hit rate clear/ cloudy/ total (%)
80 – 2180 (TAFTS + ARIES)	100/ 19/ 47
300 – 1300 (optimised TAFTS + ARIES)	91/ 100/ 98
80 – 540 (TAFTS)	100/ 47/ 61
600 – 2180 (ARIES)	100/ 50/ 63

Table 7.12. Classification results summary

7.4.2.4 Retrieving Atmospheric Humidity during the PknMix Campaign

During March 2019 TAFTS and ARIES were again flown together on the FAAM aircraft under the auspices of the Met Office PknMix campaign based out of Stornoway, Scotland. Two flights dedicated to the characterisation and retrieval of upper tropospheric humidity were performed. More than 2 hours of observations of upwelling nadir radiance were obtained from flight altitudes at or above 30000 ft. These measurements are currently being analysed by the Met Office to assess whether they can be exploited to improve knowledge of the humidity profile relative to forecasts from their Unified Model using the approach described by Thelen et al. (2009). Particular emphasis will be placed on assessing the additional benefit of the TAFTS FIR measurements compared to the quality of the ARIES only retrievals. This new data will also be incorporated into the training and test data set for the cloud identification algorithm for improving the detection abilities.

8 MISSION CONTEXT

This chapter describes the impact FORUM's observations and products will have on various applications and highlights potential interactions with planned operational satellites and research missions. It also identifies the scientific user community for FORUM and outlines some possible spin off applications for FORUM data.

8.1 Science and Societal Impact

The importance of understanding the climate, and the ability to predict how this will change in the future for safeguarding the well-being of humanity, has been highlighted in Chapter 2. With observations already showing that some of the most fragile regions of the globe are changing at an alarming rate, there comes an even greater urgency to ensure improvement in the ability to predict climate and its variability over longer timescales. To achieve these aims, it is essential that key processes in the Earth system models that are used to predict future climate are accurately represented.

FORUM will resolve part of the electromagnetic spectrum that satellite measurements have not previously explored, despite the fact that it contains around half of the Earth's outgoing energy. The accurate, stable FIR top of the atmosphere spectra FORUM will obtain will provide unique information on the Earth's atmosphere and surface, addressing key gaps in the understanding of direct relevance to climate research and weather prediction. Its observations will

- enable uncertainties in the spectroscopy of water vapour and its radiative effect in the atmosphere to be resolved,
- enable retrieval of FIR surface emissivity in dry regions such as the poles where it is radiatively important,
- provide a unique ability to remotely sense ice cloud properties, address uncertainties in the radiative impact of thin ice cloud and allow ice cloud optical models to be tested and improved,
- provide unique information for NWP with the potential to enhance forecasting and enable temperature and water vapour profile retrievals with greater sensitivity to upper tropospheric and lower stratospheric conditions which are currently poorly sampled,
- provide currently missing information for climate monitoring and attribution, complementing existing MIR hyperspectral measurements and enabling forcing and feedback signals to be diagnosed.

Thus FORUM data tackle some of the biggest issues identified by the IPCC (Stocker et al., 2013) in the ability to predict the future of the changing climate by providing “accurate descriptions of the properties of clouds and the distribution of water and ice in the atmosphere” and “a better understanding of the role of clouds in the climate system, including cloud–radiation feedback”.

The spectrally resolved FIR measurements FORUM will obtain will complement existing hyperspectral measurements in the MIR. At a fundamental level the OLR spectrum contains

the fingerprints of where energy is being emitted and absorbed by the surface and atmosphere. Comparing model simulations against these spectra will thus provide both a stringent test of multiple model parameters and a means of diagnosing the cause of any differences (Section 8.3.1). Furthermore, the improved spectroscopy, surface emissivity and cloud models that will result from FORUM products, (Sect 8.3.2, 8.3.3), will advance the ability to capture key climate processes and their radiative effect. Besides being scientifically important in its own right, this information will feed through to improvements to NWP and global climate models enabling them to better capture the distribution of energy within the atmosphere and thus better represent the local and global circulation (Khan et al. 2016) and provide a more realistic response to change. In this way FORUM will contribute to climate and NWP model improvement as both a unique tool for model evaluation and by providing missing information that will directly impact the fidelity with which key climate components are represented. It will be a valuable resource for climate change attribution and monitoring and enable NWP models to better capture water and temperature profile information with the potential for future operational applications that will improve weather forecasting skill (Section 8.3.4).

GCOS ECV	Application				
	Improved Spectroscopy	Prescribed Boundary Conditions	NWP Data Assimilation	Model Development and Validation	Climate Monitoring/ Attribution
Atmospheric					
TOA radiation budget				X	X
Temperature profile			x	x	X
Water vapour profile	X		X	X	X
Cloud properties				X	
Carbon dioxide	X		x	x	X
Methane	X		x	x	X
Ozone	X		x	x	X
Other GHG	X			x	X
Terrestrial					
LST (emissivity)		X			x
Snow cover		x			x

Table 8.1 Scientific applications of FORUM data listed according to the GCOS Essential Climate Variables. All the shaded boxes (green and grey) indicate possible areas of contribution, with the green boxes indicating where there is also a stated requirement by scientists in the user survey for the data and products FORUM will provide.

That the missing information FORUM will provide is needed by the community is confirmed by a user survey carried out to identify which scientific areas users expect the new data from FORUM to contribute to (Section 8.2). The results are summarised in Table 8.1 which shows



how FORUM data could contribute to benefit ten essential climate variables (ECVs). The shaded boxes indicate applications where FORUM can contribute, those shaded green are where this expectation is backed up by responses from the user survey and interviews with key scientists in the field, indicating the readiness of the user community to exploit the data. Of the ten GCOS ECVs identified, there is only one where the user community is not yet ready to exploit FORUM data. In addition for most of the ECVs it is expected that the FORUM data will contribute in multiple ways.

As well as filling key knowledge gaps and addressing the needs of the science community, FORUM's observations will result in measurable societal impacts. Improved climate models and improved climate monitoring and attribution will reduce uncertainty in climate predictions producing a direct societal impact. Hope (2015) has shown that approximately halving the uncertainty range for transient climate response has a net value of about \$10.3 trillion (year 2005 US\$) if accomplished in time for emissions to be adjusted in 2020, falling to \$9.7 trillion if accomplished by 2030. This shows there is potential for large savings through improved climate model projections by quantifying the mitigation strategies early enough for policy makers to implement them.

8.2 Global Mission Context

Obvious synergies exist between FORUM observations and a number of missions that are expected to be operating in the FORUM timeframe. These missions will provide complementary information from which FORUM can benefit and FORUM measurements will, in turn, offer the opportunity to enhance their science value. This section puts the FORUM mission in the global context of other missions expected to be operating at the same time, and outlines some of the mutual benefits that will be gained by their joint exploitation.

FORUM will fly in a polar orbit, in the 2022-2043 timeframe, with the next generation European Meteorological satellites, EPS-SG, which will have a new suite of innovative instruments. The EPS-SG mission is composed of two series of spacecraft, Metop-SG A and B, flying on the same mid-morning orbit, similar to the current Metop satellites. The orbit height is in the range 823-848 km (dependent on latitude). There will be three satellites each of Metop-SG A and Metop-SG B. The objective is to fly FORUM in close formation with the first Metop-SG A satellite which has IASI-NG, a Microwave Sounder (MWS), METimage, GNSS radio occultation (RO), 3MI and Sentinel-5 on board.

FORUM observations provide excellent complementarity to those anticipated from the MetOp-SG A payload. FORUM ice cloud and water vapour and temperature profile products will be analysed in the context of IASI-NG, MWS and GNSS RO products which will all provide complementary information about cloud and the atmospheric state. METimage will contribute to the cloud detection capabilities for FORUM which will provide confidence in the FORUM "clear sky" measurements as well as in the retrieval of cloud top layer altitude. Thanks to its multi-viewing and polarisation capability, 3MI will help cloud phase detection in complex scenes like the presence of a super-cooled water layer above an ice layer, frequently observed in polar regions, or in detecting multi-layer clouds. Characterisation of cloud altitude and extent should also benefit from the synergy between 3MI and FORUM. Finally, Sentinel-5 will provide a standard against which ozone or HNO₃ retrievals from



FORUM can be compared, with a view to their possible ingestion into air quality forecast models.

The MetOp-SG-B satellite will be at least 30 minutes apart from the 'A' satellite but it has the Ice Cloud Imager (ICI) on board measuring from 183 to 664 GHz. This will enable an interesting comparison with the FORUM ice cloud measurements at least for monthly averages. Ice clouds will appear more transparent to ICI than FORUM, the former will be able to 'see' through optically thin cirrus cloud whereas FORUM will be more sensitive to the cloud top. Thus they provide unique perspectives of the cloud. Insights and model improvements to ice cloud derived from the ICI products can be tested from a radiative perspective against the FORUM and IASI-NG spectra and conversely improvements derived from the FORUM radiances evaluated against ICI results.

The Meteosat Third Generation (MTG) satellites, in geostationary orbit over Europe, will include an IR hyperspectral sounder (MTG-IRS) and collocations between FORUM and this instrument will be of interest especially for cloud studies where the time evolution of the clouds can be monitored by the geostationary satellite with both the imager and the sounder. Other geostationary satellites around the globe include the Chinese FY-4 series which has a hyperspectral sounder (GIIRS) and the U.S. GOES and Japanese Himawari series which have high quality imagery for cloud studies. Such observations will provide a diurnal context for the FORUM observations.

PREFIRE (Polar Radiant Energy in the Far-InfraRed Experiment) is a NASA sponsored mission focused on the Arctic designed to address the impact uncertainties in far infrared emission have on the ability to predict Arctic climate. It consists of two 3U CubeSats with IR miniaturised spectrometers to observe the 0–45 μm spectral range at 0.84 μm resolution. Expected to fly for a year, the exact launch date is uncertain but instrument delivery is scheduled for 2021. More speculatively the Thin Ice Clouds in the Far Infrared Experiment (TICFIRE) sponsored by the Canadian Space Agency (ASC) covering the spectral range 8-50 μm using eight narrow bands designed to study thin ice clouds, is not yet scheduled but discussions are ongoing between NASA and ASC. If these missions launch before FORUM they can act as pathfinders furthering the FORUM prelaunch activities. If either are flying at the time of FORUM there will be obvious benefits to compare the radiances where collocated measurements can be obtained. The more stable and accurate FORUM observations can provide a calibration reference for the CubeSat observations, improving their quality. The broader spectral range and higher spectral detail of the FORUM observations will also enable the data from the CubeSats to be put in a broader context with potential to enhance their interpretation and products. The interest in both of these missions in the US and Canada will lead to enhanced opportunities for future collaboration on FIR science, benefiting FORUM preparation.

There are also other relevant research missions which may be flying at the time of FORUM which offer the potential for joint data exploitation. The ESA EarthCARE mission is one example where detailed 3D measurements of clouds, aerosols and radiation will be made with several instruments. Currently expected to launch in the early 2020s EarthCARE will fly in a low earth orbit with 14:00 local crossing time and so collocations will be possible at high latitudes. FORUM data are ideally placed to enhance the EarthCARE mission objective



to improve the understanding of clouds. In turn, EarthCARE data will provide cloud microphysical information (ice water content, cloud particle effective radius, cloud optical depth) and cloud position and extent invaluable for the interpretation of the FORUM and IASI-NG spectral measurements across the IR. Collocations would also offer valuable case studies for the cloud and surface communities exploiting the EarthCARE data. For example, the FORUM and IASI-NG spectral detail across the IR can provide a sensitive, detailed evaluation of simulations that have been tightly constrained by the EarthCARE cloud property and broadband flux measurements. Sensors specifically designed to measure broadband OLR radiances and fluxes will also be flying: potential examples include GERB, CERES and the NASA Earth Venture Continuity-1 mission, designed to ensure continuous ERB measurements. The collocations of the combined FORUM and IASI-NG observations with these instruments offers the potential for cross-calibration and, given its high absolute accuracy, the possibility that FORUM could act as a transfer standard between instruments.

8.3 User Community Readiness

A comprehensive user survey has been conducted amongst the prospective users of FORUM data and it is summarised in Fig. 8.1 which shows that Climate, NWP and spectroscopy users are the main categories with equal weight and atmospheric chemistry is a minor application area. An assessment of how the user community will exploit FORUM for these different applications is given here.

The first candidates to consider as early adopters of FORUM data are the leading global NWP Centres so that a routine monitoring of the FORUM Level-1 radiances can be setup during the commissioning phase to identify any instrument calibration or geolocation issues. Sudden changes, if they occur, will be observed by comparing the measured radiances with those simulated from the model 6 hour forecast in near real time. This feedback to the data providers can be extremely valuable. Once there is sufficient confidence in the quality of the measurements, the NWP Centres will be in a good position to carry out data assimilation experiments to assess the impact of FORUM on the model analyses and forecasts. A number of different options (e.g. with and without IASI-NG) can be explored. Results of the impact of FORUM in at least two different NWP models should be obtained. The European Centre for Medium-Range Weather Forecasts (ECMWF), the Met Office, the German Weather Service and MétéoFrance are all well positioned to do the real time monitoring and make impact assessments. ECMWF is also responsible for implementation of the Copernicus Atmosphere Monitoring Service (CAMS) and of the Copernicus Climate Change Service (C3S), which are both key application areas for FORUM. The CAMS will provide the focus for any atmospheric chemistry applications which FORUM can contribute to.

The user survey recognises that FORUM will make important contributions to climate modelling through the improved representation of ice cloud, more robust radiation schemes and better surface characteristics in very dry regions, as well as providing unique measurements for model evaluation and the identification of climate feedback mechanisms. There are at least seven global climate modelling centres in Europe who will be able to make use of the improvements to their models provided by FORUM.

The third application area sees the benefit of FORUM for improving the molecular spectroscopic databases for terrestrial and planetary atmospheres, such as HITRAN, GEISA,

Survey Responses on FORUM applications

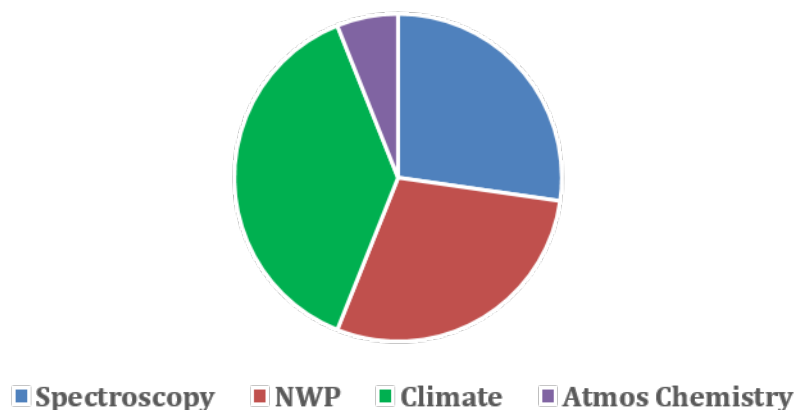


Figure 8.1 Summary of on-line survey of 84 potential FORUM data users completed during six weeks in June–July 2018. (R. Saunders, UK Met Office)

etc. Updates will not be immediate as it will take time for the impact of the new measurements to feed through into more accurate parameters in the FIR. This is because it requires the analysis of the differences between measurements and radiative transfer models to be completed before the updated parameters can confidently be added to the databases. However, once added the entire radiation community will benefit from the improved accuracy the updates provide.

8.4 Applications

As shown in Section 8.2, FORUM will provide data and products that are particularly desirable to a number of different groups. These include climate scientists and those working in climate/Earth system modelling; the NWP community; those interested in evaluating and improving spectroscopy and its associated applications; and the atmospheric chemistry community. In the following sections it is outlined how these groups will benefit from FORUM.

8.4.1 Evaluating and Improving Earth-System Models using FORUM Level-1 Radiances

One emerging method to assess Earth-system model performance is through the comparison of spectrally resolved radiances (X. Huang et al., 2008, 2010). Variability in the Earth's spectrally resolved OLR contains signatures of how the surface and atmospheric temperatures, greenhouse gases, some aerosol species, and clouds are varying with time (e.g. Y. Huang et al., 2010). Global observations of the spectrally resolved FIR OLR from FORUM will provide the first opportunity to evaluate the performance of NWP and climate models in this energetically critical region, through the direct comparison with model output using existing satellite simulator tools (Bodas-Salcedo et al., 2011) coupled with recently developed fast radiative transfer codes (Saunders, pers. comm. 2019). Furthermore, when combined with spectrally resolved radiances from IASI-NG, there will be the opportunity to compare



modelled and observed spectral radiances over almost the entire infrared frequency range. These spectrally resolved measurements will provide a much stronger constraint on model performance than can be obtained from conventional broadband observations of OLR because of their ability to identify compensating differences which can be masked in the spectrally integrated signal. Moreover, by examining differences between the observed and modelled spectra, insight will be gained into those components / processes within an individual model that require further development – and these developments can then be re-evaluated against the observations.

For example, FIR spectrally resolved radiances are strongly influenced by mid-upper tropospheric water vapour concentrations, contain unique information about ice cloud crystal shape and size, can be used to sense surface emission in the highly sensitive polar environments and are fundamentally linked to the vertical heating profile of the atmosphere. Model comparisons with the FORUM L1 radiances thus have the potential to lead to improved representations of water vapour – particularly in the poorly constrained UTLS region; ice cloud - whose climate feedback is currently poorly understood; and FIR surface properties – which are currently based on theoretical estimates. This in turn will lead to improvements in key model processes, such as the radiative heating within atmospheric layers; atmospheric dynamics, including convection and anvil outflow; and precipitation.

The variability of the spectrally resolved radiances over time will contain valuable signals of climate forcings and resultant feedbacks. These signals are typically small but, as discussed in Chapters 2 and 3, the highly accurate measurements made by FORUM, coupled with the spectral range and resolution is sufficient to diagnose and differentiate between proposed feedback signals and will also help to constrain current forcing estimates. Comparison of the modelled and observed variability over the mission lifetime will further enhance model development, ensuring improved capability to correctly capture future climate variability and change.

8.4.2 The role of FORUM Level-2 Products for Climate

8.4.2.1 Water Vapour Vertical Distribution

Water vapour is the most important greenhouse gas. Although water vapour amounts in the UTLS are small, because of the temperature contrast between this part of the atmosphere and the surface, changes to concentrations here have a disproportionately large impact on the Earth's OLR, playing the dominant role in water vapour feedback and hence the surface temperature response. Much of the radiative impact is realised in the FIR. For this reason, spectrally resolved radiance measurements across the FIR implicitly contain information about UTLS water vapour.

FORUM will thus provide new information which can be exploited to improve the current estimates of water vapour concentrations in the UTLS. When exploited in conjunction with the spectroscopic improvements that the mission is expected to deliver (Section 8.3.3) the measurements may show an improvement over existing observations in the region. Work reported in Section 7.3 using the existing modelling tools and in-built spectroscopic assumptions already indicates that the synergistic use of FORUM and IASI-NG has promise for reducing retrieval uncertainties not only in the UTLS but throughout the troposphere. In

this way it is envisaged FORUM measurements making a unique contribution to initiatives such as the GEWEX Water Vapor assessment G-VAP (Schroder et al., 2016), the ESA Water Vapour Climate Change Initiative and the WCRP/SPARC Water Vapour Assessment 2 (WAVAS-2).

FORUM will not only enable a more accurate representation of the vertical profile of water vapour, but will critically tie this to its radiative impact across the IR spectrum. Work in Section 7.3 already shows how these data can be used to probe the variability associated with important large scale climate oscillations such as ENSO. Similar studies can easily be envisaged for other important modes of variability.

8.4.2.2 Ice Cloud Occurrence and Properties

The development of ice cloud microphysical models, capable of representing the radiative properties consistent across the mid- and far- infrared, will ultimately lead to a better parameterisation of ice cloud radiative properties in Earth system models. This will have a major impact on local heating / cooling rates, thus modifying dynamics, cloud formation and dispersion and the Earth's radiation balance (e.g. Baran et al., 2014) and will improve confidence in the quantification of ice-cloud feedback, currently a major source of uncertainty in climate predictions (IPCC report, Stocker et al., 2013). In this way the observations speak directly to the WCRP Grand Challenge on Clouds and Climate Sensitivity.

The enhanced sensitivity of the FIR to ice cloud occurrence (especially thin ice cloud), as demonstrated in Chapter 7 also implies that the observations will be of benefit for the construction of ice cloud climatologies (e.g. ISCCP, Young et al., 2018) which currently suffer from the limited capability of MIR/visible passive sensors to detect these thin ice cloud and the limited sampling of active sensors.

8.4.2.3 FIR Surface Emissivity

FIR surface emissivity measurements can be used by Earth system and NWP models to enable a better representation of the energy balance in dry areas such as polar regions, high altitude locations and deserts. Surface emissivity has a major impact on the surface energy budget, affecting the surface temperature and exchanges of sensible and latent heat. The impact is not localised, affecting vertical and horizontal transport. As noted in Chapter 2, a more realistic representation of surface emissivity in Earth system models has been shown to have marked implications for both surface temperature seasonality and change. This has obvious knock-on implications for other components of the Earth-system: for example, the accurate representation of surface temperature in Arctic regions is key for ensuring realistic predictions of sea-ice melt and re-growth which are themselves coupled to oceanic temperature, salinity and hence circulation.

8.4.2.4 Spectroscopy

Improved water vapour spectroscopy in the FIR will enable its better representation in the spectroscopic databases used by the international community, feeding through into state-of-the-art radiative transfer codes. As outlined in Chapter 2 these radiative transfer tools play a fundamental role in both weather and climate prediction by modelling the flow of radiation through the Earth's atmosphere and its interaction with the surface. Accurate radiative



transfer is also key for the retrieval of atmospheric constituents – hence improved water vapour spectroscopy will directly enhance the quality of retrievals of both its vertical distribution and total column amount. This will enable a superior picture of the vertical and global distribution of water vapour to be developed.

8.4.2.5 Numerical Weather Prediction

The impact of infrared sounder measurements on numerical weather prediction models (Chap 2) will directly benefit society by providing more accurate and timely warnings of severe weather and other hazards. Studies carried out for the EPS-SG business case have shown that there is a benefit to cost ratio of at least 5 and maybe as high as 20, for the EPS-SG investment, and FORUM can potentially increase this benefit in the longer term if it demonstrates FIR measurements should be added to future operational platforms. Given the sensitivity of the FIR to UTLS water vapour it is anticipated that FORUM measurements should help to constrain NWP water vapour forecasts in this region. It is also feasible that FORUM all-sky radiances may be beneficial for improving the representation of LS water vapour in the presence of optically thick cloud as anticipated by Jing and Huang (2017).

8.4.2.6 Spin-off Applications

There are a number of potential spin off applications that FORUM data might be useful for but are not key aims of the mission. Firstly if trials of assimilating a subset of the FORUM radiances (or equivalent representations of them) in operational NWP models shows positive benefits to the analyses and forecasts then if the data can be made available to the Centres in less than 3 hours it could be used operationally for numerical weather prediction having an immediate impact. Simulations have shown an improved representation of the UTLS water vapour will be possible when assimilated with the IASI-NG radiances. There may also be indirect benefit through the FORUM data providing a better cloud detection capability for the IASI-NG observations due to the increased scattering from ice cloud at FIR wavelengths.

Another potential application will be in the production of atmospheric chemistry and air quality forecasts such as those provided by the Copernicus Atmospheric Monitoring Service (CAMS). Studies undertaken for this report indicate that FORUM will have benefit for ozone retrievals. Since the FIR also contains the signature of HNO₃ (nitric acid), FORUM will permit investigations into whether the spectral range can be exploited to improve the knowledge of its atmospheric concentration. FORUM will be in formation with Sentinel-5 and total column measurements of ozone and nitric acid from FORUM can be made and compared with the Sentinel-5 data and potentially exploited by CAMS either for assimilation in addition to Sentinel-5 data or for an independent validation of the CAMS output fields.

Although not a specified science goal, FORUM's spectral coverage will also allow the spectroscopy of the complete 15 μm CO₂ band to be analysed observationally for the first time, with potential benefit for both temperature and CO₂ retrievals. The latter may be particularly useful at night when the passive near infrared measurements exploited by instruments such as GOSAT, OCO-2 and 3 and MicroCarb are not available.



If there is a major volcanic eruption during the FORUM mission similar to Pinatubo where the aerosols remain in the stratosphere for more than a week there are two potential areas of interest to investigate with FORUM measurements. The first is to see if FORUM with IASI-NG can mitigate some of the impact the aerosol has on the IR spectrum that will strongly affect IASI-NG's ability to sound the atmosphere. If the impact of the aerosol at FORUM wavelengths is less it may help to reduce the impact of the aerosols on the soundings. If on the other hand the impact of the aerosols is significant on FORUM measurements then more information on the ash optical depth and size distribution may be retrieved. Both of these measures are important for aviation applications.

9 PROGRAMMATICS

This chapter presents the maturity (including similarity/heritage), critical areas and risks associated with the mission-level scientific concepts (Section 9.1) and the programmatic and system level technical concepts (Section 9.2) as developed in the frame of the scientific and industrial Phase A studies. The development approach and the schedule are presented and discussed in Section 9.3 with respect to the compatibility of a target launch for the ninth Earth Explorer mission by the end of 2025.

9.1 Scientific Maturity, Critical Areas and Risks

9.1.1 *Scientific Maturity: key questions for SRL*

At the end of the Phase A, scientific readiness level 5 is required. The key questions pertinent to the assessment of the scientific maturity are addressed in the following (ESA, 2015c):

1. Is an end-to-end simulator in place and are the most important processes and input parameters (including uncertainty estimates) properly represented?

An End-to-End performance simulator has been put in place (see section 7.1, 7.2 and 7.3). The simulator models the end-to-end performance chain, starting with the observed Earth - atmosphere scene and its geophysical phenomena, at a resolution suitable to simulate real-world atmospheres and Earth's surface variations, and ending with an automated comparison of the simulated level 2 products with the input quantities. Realistic uncertainty estimates for the instrument implementation have been tested in the simulator. The end-to-end simulator has been developed to distinguish between clear sky and cloudy conditions, and apply the corresponding retrieval; determining clear sky atmospheric parameters, i.e. water vapour and temperature profiles, precipitable water vapour, and surface temperature or for the cloudy sky case, cloud optical depth, cloud particle effective radius, cloud top height, and ice water path. In the Phase B1 the simulator will be expanded to also include flux calculations (draft algorithm outline in Section 6.1.3) and in the case of low atmospheric humidity, retrievals of surface emissivity.

2. Is an error propagation model in place allowing the rigorous computation of uncertainties for measurements and observations?

In each of the steps of the end-to-end simulator, relevant errors and uncertainties are either generated (e.g. off-axis effects, calibration errors, effects of scene heterogeneity) or ingested (e.g. attitude errors, climatological covariance matrices), depending on what is the most relevant and rigorous method to achieve an end-to-end performance simulator representative of the observation method and the technical concept derived from Phase A industrial and scientific activities. For some cases, as for example the NESR, two methods for the computation of this uncertainty have been implemented: one in which the NESR is computed internally by simulating the effect of the beamsplitter and a generic but representative detection chain and another in which a high fidelity externally computed NESR can be directly introduced into the chain. The internally generated NESR allows the end-to-end performance simulator to perform parametric analysis to assess the impact of varying NESR errors in the Level-1 and 2, while the externally provided NESR allows to run



the simulator in a mode highly representative of the industrial concepts. The latter allowing for instance introducing an NESR derived from measurements of pre-development activities on the beamsplitter and the detection chain.

The optimal estimation technique by Rodgers (2000) is the tool of choice for atmospheric retrievals owing to its rigorous treatment of uncertainties especially for multi-target retrievals since it naturally takes the co-variant effects into account and also provides a comprehensive framework for assessing information content Sections 6.1.2 and 7.1.4.

3. Has a set of realistic test scenarios been established and are they scientifically justified?

The test scenarios are described in Sections 7.1.2 and 7.1.6. Twelve scenes have been selected which broadly capture the wide range of the environments that will be encountered by FORUM. The surface types range from snow cover to desert and half of the scenes include cloud. The simulations of the selected scenarios are based on information derived from ERA-Interim reanalysis and monthly averaged surface properties derived from satellite measurements and thus represent realistic observational conditions. The selected scenarios are:

- a desert case for evaluating the effects on the profile retrievals (temperature and humidity) of a large temperature gradient between surface temperature and atmospheric/cloud layers
- an ocean case is a very common case and is a typical observational condition. When in presence of a very thin cirrus cloud (optical depth is set to 0.3) it represents a scientifically relevant case for cloud identification and properties retrieval.
- an ocean case with stratus is common, but challenging. It is suitable to evaluate the errors in the retrieval of atmospheric properties when the stratus is not identified due to its low altitude and its properties similar to the ocean layer.
- a continental case in clear sky or in presence of an altocumulus cloud, allowing a verification of the clear/cloudy retrieval algorithm over land.
- a snow surface representative of Arctic conditions that are observed every orbit by FORUM. When accounting for an ice cloud with moderately thick opacity (optical depth of 3) it is a very challenging case owing to the similarity of the cloud properties to the atmospheric background.
- a Po Valley case with a cumulonimbus is relevant for the study of extremely thick clouds and also archetypal of hurricane conditions.

Six of the scenes account for cloud cover and six are in clear sky condition but with the same surface and atmospheric properties of a corresponding cloudy case. This was done in order to:

- provide a challenging dataset for cloud identification/classification
- allow the evaluation of the errors associated with the retrieved geophysical parameters when misclassification are assumed.

Furthermore, the simulator's scene generator provides a high level of flexibility for creating user-input scenes owing to a simple, but effective configuration where scenes can be selected based on climatologies and then augmented with levels of heterogeneity of different shapes



(e.g. a sector) and nature (e.g. a coastline). The simulator is also capable of ingesting input scenes based on MODIS measurements with 1 km horizontal resolution, thus accounting for a high level of heterogeneity in terms of atmospheric profile, cloud and surface properties.

4. Is the simulator tested and validated and applied for the predefined set of scenarios?

The full end-to-end chain of the simulator, as well as each individual module, has been tested and verified (see 7.1 for more details). The end-to-end performance simulator has also been validated with the predefined set of scenarios. The tests demonstrate that retrieval results and error estimates are consistent across the input scenes. See sections 7.2 and 7.3.1.

5. Are all assumptions of the performance simulator documented and critically discussed?

The underlying assumptions of the performance simulator are documented and critically discussed in Section 7.1 and in the draft ATBDs of the end-to-end simulator study.

6. Has the robustness of the simulator been demonstrated against independent observations (e.g. campaign data)?

The simulator is designed for analysing top-of-atmosphere radiances and cannot be easily adapted for ground-based zenith-looking geometry. However, the machine learning code of the cloud identification and classification module of the simulator has been adjusted with a different training data set from airborne data and has been successfully tested as shown in Section 7.4.2.3. Ingestion of airborne data to test the simulator performance is planned in phase B.

7. Is a draft instrument calibration strategy available and properly described?

The comprehensive validation strategy for Level-1 and Level-2 science products is described in Section 6.2. A complete on-ground characterization and in-flight calibration strategy of both instruments has been described in Sections 5.3.3.5.7. and 5.3.3.5.8 for both technical concepts, based on results of the Phase A. The instruments will be characterized on ground radiometrically, spectrally and geometrically. In-flight the FSI will be characterised radiometrically, spectrally and geometrically while the FEI will only be calibrated radiometrically and geometrically. During the Phase A, special attention has been paid to come up, and describe (Chapter 5), a radiometric calibration strategy accurate enough to achieve the required FSI performance in terms of Absolute Radiometric Accuracy (Chapter 5 and 7).

8. Is there a demonstrated interest of users?

Numerous studies demonstrating the theoretical impact of FIR radiances and fluxes for weather and climate are outlined in Chapter 2. A diverse range of researchers (climate scientists, NWP and climate modellers, atmospheric chemists, spectroscopists) are eagerly anticipating real measurements to test and improve the current understanding, which was demonstrated by the participation of about 90 international researchers for the first FORUM



user workshop held for two days in October last year. A user survey that was open for 6 weeks during summer 2018 saw over 80 participants indicating interest in FORUM.

9. Is there a first evaluation of (simulated or measured data) in applications?

FIR radiation plays a fundamental role in modulating the current climate and holds critical information about key climate components and processes. Theory suggests that systematic, global observations of Earth's outgoing FIR spectrum will provide new insight into the radiative cooling of the planet and its controls, testing and refining the understanding of how these operate from the local to global scale, and how they respond in a changing climate. There is ample evidence for the significant impact of actual FIR radiance measurements as outlined in Section 2.1 and 7.3.2.4.

In summary, with respect to the scientific readiness, the mission and research objectives have remained stable in comparison to the original proposal. However they have been significantly refined within dedicated science activities and can be considered consolidated. During the Phase A, two measurement campaigns were performed, one ground-based at Zugspitze summit in Germany, and one airborne over the UK. The results will undergo further investigation. Additionally, the first ever measurements of far-infrared emissivity of snow samples with simultaneous in-field characterisation, already delivered impressive results confirming in parts theoretical calculations. A complex and representative end-to-end performance simulator, able to model the full observation chain, including autonomous scene classification based on machine learning algorithms, has been developed. Simulations indicate that the main mission objectives can be met. Further refinements and expansions to also include flux calculations and, in the case of low atmospheric humidity, retrievals of surface emissivity will be implemented in Phase B.

On the basis of the above, it is considered that FORUM has reached the expected scientific readiness level of 5 at the end of Phase A.

9.1.2 Critical Scientific Areas and Risks

FORUM's primary research objectives (Chapter 3):

- building a highly accurate global dataset of FIR radiances to validate the present-day climate state as captured by Earth system models
- using these measurements to understand and constrain the processes that control FIR radiative transfer and hence Earth's greenhouse effect
- updating the parametrisations of these processes for implementation in radiative transfer codes, and ultimately in Earth system models
- characterising critical feedback mechanisms.

require only highly accurate Level-1 radiances. In fact, in the ESAC recommendation for implementing FORUM as one of the EE9 candidate missions, the clear explorer nature of FORUM was recognized, simply by providing the first-ever systematic observation of the outgoing spectrum of far-infrared radiation from space. Spectral coverage beyond 1600 cm^{-1}

will be provided by IASI-NG. Since MetOp-SG is an operational programme there is no risk associated with the availability of IASI-NG radiances.

For the retrieval of geophysical parameters (Level 2 products), as outlined in the introduction to Chapter 6, the methods and tools for data processing are based on experience with mid-infrared (MIR) sensors. The methods, such as the use of inversion techniques to obtain atmospheric profiles from radiances, are well-understood and transferrable. However, underlying assumptions used within these inversions, such as the spectroscopic data bases for water vapour, models of FIR surface emissivity, or parameterisations of the optical properties of ice cloud have only been tested in a very limited number of field and laboratory experiments. As detailed in the following section, more dedicated work focused on testing, and where possible updating, the retrieval codes and the underlying models prior to launch.

An airborne demonstrator which is fully representative of the FORUM mission will have to be developed during Phase B1.

9.1.3 Scientific Roadmap

The Phase A studies documented in this report have shown that FORUM has the capability to deliver Level-2 products, such as H₂O profiles and cirrus cloud properties, with the required accuracy, over the range of conditions that the mission will encounter. This was demonstrated using synthetic measurements and scientific analysis tools, and the first prototype of the end-to-end simulator. FIR measurements from air-borne and ground campaigns have also been exploited to provide a first demonstration of the ability to retrieve H₂O profiles, ice cloud properties and surface emissivity from real observations.

Starting from this maturity level, the prototype processor of the end-to-end simulator will be improved to study the performance of the retrieval of additional Level-2 products such as surface emissivity, the calculation of outgoing longwave radiation flux and the synergistic retrieval of H₂O using IASI-NG products. A further early modification will be the addition of a module capable of ingesting airborne campaign data such as those that have already been collected during Phase A. Similarly the simulator will be modified to allow the generation of high-order products, such as zonal monthly means, to be used for the comparison with analogous products provided by other satellites. In such a way, the prototype processor will be upgraded to a first operational processor for the detailed system review to be addressed during Phase C.

An airborne demonstrator will be developed. Dedicated field campaigns with FIR spectrometers from high altitude airborne platforms, such as TAFTS and ARIES on the UK-FAAM aircraft (or an alternative platform) and FIRMOS on stratospheric balloons, will be planned for the next study phases to provide the scientific community with exemplar precursor measurements. These campaigns should be focused on sampling conditions relevant for the FORUM scientific goals that have, to date, either not been explored with FIR instrumentation or only in an extremely limited way. Potential examples include, but are not limited to: (a) flights over high latitude snow/ice, including marginal ice zones, ideally including overflying well-instrumented in-situ ground sites; (b) flights over tropical cirrus:



to date there are no published FIR measurements sampling these types of ice cloud with coincident measurements of the cloud vertical extent and microphysical properties. A further campaign should consider the use of the same (or alternative) FIR spectrometers on the ground to characterize snow/ice surface emissivity over an extended period to characterise both short term responses to precipitation/melt and seasonal behavior of the surface. Ideally this could complement the more time-limited campaign (a). In addition to these new field campaigns, work should continue to assess and optimize the information available from the campaign measurements undertaken during Phase A, particularly the PknMix flights (Section 7.4.2.4).

Finally, laboratory measurements of refractive indices of ice, including its temperature dependence, should be undertaken in order to improve cloud optical property models. These currently assume no temperature dependence in the ice refractive index yet compilations of available measurements suggest it may be marked (Iwabuchi and Yang, 2011), with significant impact on the optical properties of upper tropospheric ice clouds, particularly in the FIR (Anthony Baran, pers. comm., 2019).

These pre-launch activities will ensure that the scientific community is able to exploit the potential of FORUM at the earliest possible opportunity.

9.1.4 Scientific Concluding Remarks

This report has highlighted how radiation within the far infrared part of the electromagnetic spectrum plays a fundamental role in modulating Earth's climate, containing critical information about key climate components and processes. Theory suggests that the region contributes more than 50 % to Earth's total outgoing longwave radiation in the global mean, containing unique information about water vapour, ice cloud and surface properties. Systematic, global observations of Earth's outgoing FIR spectrum will thus provide new insight into the radiative cooling of our planet and its controls, testing and refining our understanding of how these operate from the local to global scale, and, importantly, how they respond in a changing climate. Despite this, there are still no dedicated satellite based measurements of outgoing FIR radiation beyond a few isolated spectra from the 1970s, and even these only extend a limited way into the region. By providing highly accurate measurements of the OLR spectrum across the FIR, FORUM will address this long-term observational shortcoming, making a truly unique contribution to our knowledge of the climate and how it is responding to change.

The FORUM objective to exploit the FIR to understand the radiation processes involving water vapour, clouds, and surface properties and to attribute the observed variability and change in the spectral radiances to the relevant climatic variables, is one of the main themes of the ESA Earth Observation Science Strategy (EOSS). The proposed spectral observation was underlined in the ESA document "The Changing Earth" (ESA, 2006, p. 42), and is strongly in line with the key elements of the EOSS for ESA (ESA, 2015a). In particular, FORUM meets the request for developing "observations to understand and attribute trends beyond the expected variability", and for an "optimised Earth observing system that can fill gaps in observational needs and build new capabilities in a cost-effective way (ESA, 2015a)."



A further goal of this mission, relevant for the ESA EOSS, is the implementation in space of a measurement scenario which is “carefully designed” to exploit the possible “complementarity and to maximise measurement synergies with other satellites and satellite-borne instruments (ESA, 2015a, p. 12)”. In particular, the FORUM mission will be able to demonstrate the improvements expected by means of the exploitation of the FIR spectral region of the OLR with respect to operative missions measuring only the total broadband longwave radiance (not the spectrum), such as CERES or GERB, or the mid-infrared spectrum, such as IASI-NG. This goal will be realized by flying in loose formation with MetOp-SG(1A), where IASI-NG will be accommodated.

Finally, the FORUM mission directly addresses several of ESA’s Living Planet Challenges. These include:

Challenge A1: [Water vapour, cloud, aerosol and radiation processes and the consequences of their effects on the radiation budget and the hydrological cycle.](#) The mission will supply multi-annual “accurate and stable measurements of the long-wave radiation at the top of the atmosphere to assess the contributions of clouds and aerosols, greenhouse gases, in particular water vapour, and surface optical properties to the radiation budget”, which are required to reduce the “largest uncertainty (still present) to estimates and interpretations of Earth’s changing energy budget” (IPCC, 2013). The “accurate descriptions of the properties of clouds and the distribution of water and ice in the atmosphere”, supplied by FORUM, will give “a better understanding of the role of clouds in the climate system, including cloud–radiation feedback” (ESA, 2015b, pp. 12).

Challenge A4: [Interactions between changes in large-scale atmospheric circulation and regional weather and climate.](#) This challenge identifies that “much better observational capabilities are required in regions of strong temperature and moisture gradients” such as those found in the upper troposphere/ lower stratosphere. FORUM has high sensitivity to the upper troposphere/ lower stratosphere with studies in chapter 7 highlighting how the measurements may be used to probe water vapour signatures associated with large-scale modes of circulation variability such as El Niño southern oscillation and the quasi-biennial oscillation.

Challenge C4: [Effects of changes in the cryosphere on the global oceanic and atmospheric circulation.](#) Although there have been major advances in the representation of the cryosphere in GCMs there are “still major deficits in the parameterisation and integration of cryospheric processes in these models”. Studies have already shown how the incorporation of more realistic FIR surface emissivity estimates in Earth System models has a marked impact on the surface (and top of atmosphere) energy budget in polar regimes, with particular implications for Arctic surface temperatures and sea ice response (Feldman et al., 2014, Kuo et al., 2018). FORUM will provide observationally based estimates of FIR emissivity and its inter-annual variability.

Other indirect benefits such as improved trace gas (CO₂, HNO₃, O₃) spectroscopy also have the potential to contribute to Challenges A2 (Interactions between the atmosphere and Earth’s surface) and A3 (Changes in atmospheric composition and air quality, including interactions with climate), although not part of the primary or secondary mission goals.

Measurements of the outgoing FIR spectrum are long overdue and, as noted in Sections 8.3 and 9.1.1, the wider community is ready to exploit the data. Via responses to the user survey and attendance at the FORUM Workshop, representatives from the climate modelling and Numerical weather Prediction community see a clear utility for FORUM in evaluating their model output in several ways. Direct comparison with the FORUM radiances, assessment of ice cloud parameterisations, implementation of improved surface emissivity estimates and assessment of their impact, and the potential benefit of Level-1 and Level-2 products for understanding upper troposphere/ lower stratosphere processes are seen as particular applications of FORUM. Tools which will permit early uptake of the measurements for these purposes are already in place (e.g. RTTOV, Saunders 2019). This buy-in from the wider community will help to ensure that the overarching research goal of the mission, to evaluate the role of the FIR in shaping the current climate and thus reduce uncertainty in predictions of future climate change, can be realised.

FORUM will contribute to several planned operational space programs, operative during the mission. Its unprecedented radiometric accuracy and spectral coverage, extending into the MIR means that it can be used both synergistically and for cross-validation with MIR sounders (including, but not limited to IASI-NG, e.g. IRS on MTG). Coverage across the full OLR spectrum with IASI-NG means that the measurements could also be used synergistically with broadband observations from instruments such as CERES and GERB, potentially informing their calibration (especially during daytime) and scene identification. Since there will be no dedicated broadband sensor on MTG, FORUM may also provide a valuable means of assessing the quality of any attempted narrow-to-broadband conversion.

Dependent on launch dates, FORUM could efficiently complement the EarthCARE mission, which will make global observations of clouds, aerosols, and the ERB. It will also leverage any insights provided by PREFIRE, whose main goal is to address the impact uncertainties in FIR surface emission have on the ability to predict Arctic climate. The insights gained on ice cloud presence and microphysics also have the potential to benefit the interpretation of observations from ICI and MWS. Similarly, since the surface emissivity of snow is dependent on grain size and density (e.g. Chen et al., 2014), FORUM is ideally placed to leverage new findings from active and passive instruments on Sentinels 1-3.

By improving our understanding of the current and future state of our climate we enhance and strengthen society's basis for decision making, benefiting people and communities worldwide. The economic implications alone associated with reducing uncertainty in our predictions of future climate are huge, with studies estimating that a factor of two improvement in our knowledge of climate sensitivity would have an economic benefit ranging from \$US 5-20 trillion (Hope et al., 2015, Cooke et al., 2014, 2017). Research has also shown how a warming climate may exacerbate natural disasters such as drought, heatwaves, storm and hurricane intensity, and wildfire occurrence (Van Aalst, 2006, Fischer and Knutti, 2015, Walsh et al., 2016, Schoennagel et al., 2017). Better constraining future climate predictions would thus directly benefit policy makers working towards meeting the Sustainable Development Goal on Climate Action of the Sendai Framework for Disaster Risk Reduction (<https://www.unisdr.org/we/monitor/indicators/sendai-framework-sdg>).



Because of the interdependencies of the different components of the Earth system, a reduction in the uncertainty of future climate prediction will also positively impact decision makers working in all of the Global Earth Observation System of Systems (GEOSS) Societal Benefit Areas including: Disaster Resilience; Public Health Surveillance; Energy and Mineral Resource Management; Water Resources Management; Infrastructure and Transportation Management; Food Security and Sustainable Agriculture and Biodiversity and Ecosystem Sustainability (<https://www.earthobservations.org/sbas.php>).

In this way, FORUM will make a valuable and unique contribution to tackling arguably the greatest challenge facing this generation.

9.2 Technical maturity, Critical Areas and Risks

9.2.1 Summary

FORUM is considered a technically feasible mission but challenging within the programmatic constraints applicable to the EE9.

The FORUM Mission has two competitive industrial consortia for the platform and for the two instruments. Both consortia have a balanced make or buy approach. The proposed re-use of standard platform products is considered beneficial for the development of the mission within the programmatic constraints applicable to the EE9 mission.

For the satellite platform both concepts are based on extensive re-use of heritage and technologically mature designs. Instruments are decoupled from platform design, which will help to allow the parallel design, development, assembly, integration and test (AIT) of Platform and Instruments. For concept A the re-use of the platform developed for the Copernicus Sentinel-5P and the Astrobus-M family – including the same structure design – is proposed with minor modifications, offering a solution that provides comfortable margins for the payload accommodation and for the platform resources and performances required by the mission. This will allow flexibility with regard to potential evolution of the instruments design. The platform for concept B is also based on heritage designs, either flight proven (Proteus 150/300 standard platforms and Copernicus Sentinel-3) or under an advanced development status (FLEX Earth Explorer mission), though a custom platform structure will need to be developed for FORUM. In both cases the platform design and the envisaged modifications are based on the use of mature technologies and will not require the implementation of any early pre-developments.

The FORUM payload complement, consisting of the FORUM Sounding Instrument (FSI) and the FORUM Embedded Imager (FEI), will re-use – in both concepts, which became very similar at end of Phase A – mature technologies with heritage from flight-proven instrument designs. For the FEI no criticalities have been identified. The FSI interferometer re-uses the design of the TANSO-FTS instrument flying on GOSAT-2, with mission specific adaptations. On one hand, the FSI can benefit from relevant heritage designs for the main instruments subsystems based on mature technologies. On the other hand, due to the unprecedented spectral range of the instrument and the demanding performance requirements, it requires



specific technology pre-developments for the beam splitters and the calibration blackbody, which have been implemented in the course of the Phase A in parallel of the two contracts, including an assessment of several coating materials. Early breadboard of the detection chain and of the interferometer mechanism have also been developed during the phase A to assess and characterize critical performance aspects and provide early feedback for the optimization of the design aim to reach at least TRL 5 (and 6 whenever possible) by the end of phase B1. The instrument(s) design and technology heritage together with on-going and planned pre-development activities provide good confidence about the technical feasibility of the instruments and the robustness of the risk mitigation strategy.

No criticalities have been identified for the ground segment. The loose formation flying with MetOp-SG will require interaction between ESA and EUMETSAT in future Phases of the mission.

Both consortia are compliant with Vega C in dual launch configuration, on upper or lower position, with suitable margins.

9.2.2 *Satellite and Platform*

The platform design in Concept A is based on the full re-use of the platform developed for a Copernicus mission (Sentinel-5P). This low-risk solution offers comfortable margins for what concern the mission specific needs in terms of the payload accommodation, the resources available and the required performance, while is still compatible – with margins – with a dual launch on VEGA-C. Most platform subsystems and equipment will be re-used without modification and can therefore be considered already at TRL 9, pending confirmation of similar thermal-mechanical loads. The few elements requiring mission specific adaptation (e.g. the structure, thermal control, harness, the central software) are all based on modification of existing equipment/products and are therefore assessed to have a TRL >6.

Also for concept B the platform design is based on extensive heritage designs from the Proteus 150/300 LEO platforms, on-going developments in the frame of the other Earth Explorer (FLEX) platform development and re-use of equipment flight proven in the context of other programmes (e.g. Copernicus Sentinel-3). The new structure to be developed specifically for the FORUM mission is based on mature technology and does not present any criticality, it is currently assessed at TRL 6. Most subsystems/equipment are assessed currently at TRL 9. The few elements requiring mission specific adaptation (e.g. the structure, Thermal control, harness, the central software, the PDHU) are all based on modification of existing equipment/products and are therefore assumed to have a TRL >6.

For both concepts, compliance with the Space Debris mitigation requirements has been analysed and an uncontrolled re-entry is baselined. A detailed analysis will continue to confirm the Phase A analysis, with only pending issue the instrument materials final selection.

9.2.3 FORUM Sounding Instrument and FORUM Embedded Imager

As outlined in the summary no critical items/technologies have been identified for the FEI (for both concepts) thanks to the re-use of COTS microbolometer detectors and bandpass filter with similar requirement as for the EarthCARE Multi-Spectral Imager or Sentinel-3 SLSTR instruments. All FEI subsystems/equipment, including the detectors, are assessed at $TRL \geq 5$ or above and no specific pre-developments are required. The following sections describe the FSI subsystems/equipment for which the TRL assessment is lower than 5, including a description of the on-going/planned pre-developments and the assessment of the TRL achieved at the end of the relevant pre-developments in relation to the Phase A and Phase B1 schedule, recalling that the objective is to reach at least TRL 5 (and 6 whenever possible) for the critical technologies at the end of Phase B1.

9.2.3.1 FSI Beam splitter

The beam splitter was identified as a critical technology due to the lack of demonstrated European technologies that would guarantee the required spectral transmission and reflection properties in the FSI wide spectral range (100 - 1600 cm^{-1}). Different technologies have been identified, all assessed at TRL 3 (based on European technology) at the start of the phase A, namely:

- Germanium coated wedged diamond plate
- Germanium coated Polypropylene membrane
- Germanium coated Mylar membrane

The wedged diamond plate technology has been selected as a baseline for concept B after manufacturing of a full scale plate and testing for transmission, reflection and Wave Front Errors, before and after environmental test, reaching a TRL of 4/5 (due to partial completion of the environmental tests). Manufacturing and testing of diamond samples with anti-reflection micro-structure has also been performed, showing improvements in the transmittance. The application of the process on the full scale plate remains to be assessed as part of the on-going Phase A activities in order to reach TRL 4 and during early Phase B1 to reach TRL 5.

For concept A, a diamond plate beam splitter with Germanium coating and anti-reflection micro-structure based on US technology has been selected as a baseline. Such beam splitter has been used in the OTEs instrument flying in the NASA mission OSIRIS-REx. Characterisation of diamond samples to confirm the feasibility for FORUM has been undertaken in the course of the phase A with the aim of raising the TRL to 4. Further activities for characterizing and testing a full scale sample and reaching TRL 5 are planned for Phase B1.

The membrane (Polypropylene and Mylar) beam splitters have been manufactured and tested in the context of dedicated pre-developments. The results of the tests show that the process of Germanium deposition on the membrane introduce defects that led to lower transmission/reflection performance and higher WFE than predicted, especially in the case of Polypropylene, which at this moment is not considered a suitable solution. Mylar also exhibit absorption features, as expected, in the FSI spectral range that would lead to non-

compliance to the instrument NESR performance, although pending additional activities it is retained as a backup.

9.2.3.2 FSI Calibration blackbody

The performance of the calibration blackbody (emissivity, stability, homogeneity) is fundamental to achieve the on-board high calibration accuracy required to meet the demanding radiometric performance requirements of the instrument. The design and assessment of the blackbody cavities in relation to the candidate coatings identified has been performed in the course of the Phase A studies for both consortia. The candidate black coating materials have been selected based on tested performance and heritage. Candidate materials such as Nextel, Vantablack, ... have been subject to pre-developments in the course of the phase A to characterize their performance in the FSI spectral range. The selected baseline coating has flight heritage from the calibration blackbody of the HIRLDS instrument embarked on the NASA EOS Chem satellite. For the baseline coating, coated samples have been manufactured and submitted to environmental tests. It is planned at completion of the Phase A activities that the analysis of the cavity design in combination with the characterized properties of the coating material the blackbody will allow to reach TRL 4/5 (due to partial completion of the environmental tests). For concept B it is foreseen to breadboard a full scale sample of the emissivity plate and a simplified baffle to test the manufacturability and homogeneity of the coating. It is also planned to test the assembly in vacuum.

For Concept A, a pre-development of a phase change cell for the absolute calibration in orbit of the blackbody thermal sensors has been pursued. The planned activity aims to reach TRL 4 at the end of Phase A and TRL 5 by the end of Phase B1.

9.2.3.3 Pointing and Scan mechanism

Pointing and scan mechanism for Concept B is at TRL 4 at this moment with a plan to reach TRL 5 in Phase B1 via a dedicated pre-development. For concept A a re-use of the pointing mechanisms from the MetImage instrument on board MetOp-SG is planned with minor modification. No specific pre-developments have been envisaged. Accordingly, the pointing and scan mechanism is not considered critical.

9.2.3.4 FSI Detection Chain

The baseline pyroelectric detectors selected for FORUM have flight heritage (TRL 9, concept B) or are an evolution of the flight proven series, already assessed at high TRL (TRL 6, concept A). Though the detectors themselves are not considered critical and have a very high TRL, an early prototyping of the complete detection chain (detectors and prototype Front End Electronics) has been undertaken by both consortia with the aim of improving the characterization of the detectors in terms of noise and responsivity properties, perform an assessment of the different operation modes and investigate the optimal operating conditions concerning the detector temperature. The results of the pre-development confirm the achievement of TRL 4/5 (due to partial completion of the environmental tests) for the FSI detection chain. The manufactured and tested prototypes of the detection chain will also evolve during Phase B1 into a breadboard to be tested for achieving TRL 5 and for

developing an Instrument Elegant Breadboard, consisting of the detector chain breadboard combined with the FSI interferometer breadboard (see next Section and Section 9.4).

9.2.3.5 FSI Interferometer mechanism

The double pendulum interferometer mechanisms selected as a baseline for both concepts, after some trade-offs, use a double pivot point mechanisms (Concept A), with heritage from commercial (non-space qualified) interferometers. A prototype of the double pivot point mechanism is undergoing space qualification for the Large Aperture Dual Pivot (LADP), an internal development program, partially funded by the Canadian Space Agency, expected to reach TRL \geq 6 before the end of 2019. Concept B baselines a single pivot point mechanisms, with flight heritage from the TANSO-FTS interferometer on board GOSAT and the ACE-FTS on board SciSat (Canadian Space Agency). The current TRL of the interferometer mechanisms is assessed at 4 for both concepts. For concept B an interferometer mechanism breadboard has been manufactured and will be tested for speed stability and susceptibility to micro-vibrations, aiming to reach TRL 4 by the end of Phase A. The mechanism breadboard has been conceived with a modular approach aiming at being developed incrementally into a complete interferometer breadboard (including beam splitter, laser metrology and detection chain) to be completed and tested during Phase B1 with the aim of achieving TRL 5 of the full assembly/subsystem. For concept A the interferometer mechanisms breadboard is under manufacturing and will be assembled and tested during Phase A, to be integrated later (in Phase B1) into a complete interferometer breadboard that will later become part of the Sounding Instrument Elegant Breadboard (SIEBB).

Pre-development activity	Technology Readiness Level (TRL)		
	Start of Phase A	End of Phase A	End of Phase B1
Beam splitter			
Germanium coated Diamond Plate with micro-structured anti-reflection layer (Concept A)	3	4	5
Germanium coated Wedged Diamond Plate (Concept B)	3	4/5	5
Germanium coated Mylar membrane (both concepts)	3	4	Further activities depending on performance results
Germanium coated Polypropylene membrane (both concepts)	3	4	-
Germanium coated Diamond Plate with micro-structured anti-reflection layer (Concept B)	3	4	5
Calibration blackbody			
Coating material (both concepts)	3	4/5	5
Blackbody cavity (both concepts)	3	4	5

Phase Change Cell (Concept A)	3	4	5
Pointing and Scan mechanism (concept B)	4	4	5
Detection Chain (both concepts)	3	4/5	5
Interferometer mechanism (both concepts)	3/4	4	5

Table 9-1: FORUM FSI pre-developments

9.3 Development Approach and Schedule

9.3.1 Overall Development Approach and Model Philosophy

FORUM will follow a phased development process (Phases B2/C/D/E1) with system reviews (System Requirements Review (SRR at end of Phase B1), Preliminary Design Review (PDR at end of Phase B2), Critical Design Review (CDR at the end of Phase C), etc.) to verify the status of the system design, development, procurement and integration of development and flight models. For concept A, a “fast track” approach is proposed for some instrument and lower level reviews as optimization of the traditional review approach and organization. In order to establish a robust development schedule, the instrument and platform developments can be decoupled. As reference planning to minimise project cost and schedule, both industrial consortia have proposed parallel development activities on the instrument, platform and satellite levels, with integration performed at the two different levels, full Instrument AIT, full Platform AIT and finally the satellite combined AIT. The instrument development has been assessed as driving the overall schedule. Different approaches have been proposed to minimize the instrument development duration, such as reducing the number of intermediate development models at unit level for low development risk units or at instrument level, developing in parallel intermediate development models, performing testing or achieving qualification at satellite level.

The proposed platform/satellite model philosophy is derived from the risk analysis and the level of maturity of technologies envisaged for the programme.

Both concepts rely on extensive (though to a different extent) re-use of heritage design for the platform, leading to the following development approaches:

For concept A, it is proposed for the platform to follow a direct PFM approach. Thanks to the re-use of flight proven design and modelling approaches no structural/thermal model have been assessed as necessary to reduce risks. The full mechanical and thermal qualification will take place at Satellite PFM level. No Electrical Functional Model of the avionics has been considered due to the re-use of equipment that were fully integrated and tested in previous programmes, but a functional bench and Software Validation Facility (SVF) will be used. Electrical integration and test of new/modified equipment for which EMs or EFM will be developed will take place via integration and test with the equipment they directly interface with. Instrument to platform interfaces will be verified on functional bench. A Simulated Electrical Functional Model where new/modified HW EM/EFM could be integrated and tested in the loop is considered when deemed necessary. This is planned in particular with an instrument electrical and functional EGSE simulating the Instrument Control Unit.



Modification of the AOCS control algorithms will be validated in the existing Functional Validation Bench and SVF. Validation of the FORUM Central Software will take place in the existing SVF as well – customised for FORUM – prior to loading on the on board computer. The full functional qualification of the payload/platform interfaces will take place at Satellite PFM level.

For the instrument, the development and model philosophy considered for concept A consists in early breadboarding of the instrument to address operation, data processing and performance under ambient and thermal vacuum conditions. The detailed need for further breadboards in extension to the proposed pre-development will have to be confirmed during Phase B1. An Instrument Electrical Functional Model, consisting of the ICU, harness and detection chain EMs, will be developed for the electrical and functional tests at instrument level and shall be later used for the payload/platform interface validation against a representative platform interface. The instrument and its subsystems will follow a PFM approach. The instrument EMC, Mechanical and Thermal qualification as well as performance characterisation in representative environment are proposed to be achieved during the satellite PFM testing.

For concept B a robust and low risk approach has been baselined, both at platform/satellite and instrument level. Due to the development of a FORUM specific platform structure, a Structure and Thermal Model at satellite level consisting of the platform STM and the instrument STM, both structurally and thermally representative of the flight hardware will be developed and used for the mechanical and thermal qualification of the structure and performance evaluation. The platform STM will be refurbished as platform flight structure. An Avionic Test Bench (ATB) will be developed/adapted to allow early verification of the avionics design and the software and hardware/software integration using EM equipment. It will also allow to verify the AOCS subsystem design/performance, the data handling design and the flight software enabling avionics interface testing. The ATB will then be extended into a functional test bed to complete the electrical and functional verification at satellite level (including the software) and to verify the payload/platform interfaces using an instrument E(Q)M. At instrument level all instrument subsystems/assemblies will follow an EQM/FM approach, with full qualification achieved at subsystem level. At instrument level, an Engineering Model is foreseen with the main objective to rehearse the integration and alignment procedures. The instrument PFM will have achieved full qualification and characterisation prior to the delivery for integration in the satellite PFM.

9.3.2 Schedule

The schedule for the FORUM development assumes the Phase B1 to start in October 2019 for a 1 year duration and that the Phase B2/C/D/E1 could start in March 2021 following the bidding and negotiation phase.

The instrument kick-off is assumed to take place at the same time as the System Phase B2 KO. 6 months of contingency at prime level have been included. The schedule is driven by the instrument development after instrument PDR (instrument phases C/D), in particular the development of the instrument detection chain and interferometer PFM. A launch for FORUM by the end of 2025 is not considered feasible with adequate margin. A launch by



mid-2026 is considered feasible but challenging and will require an optimisation of the development approach and schedule taking into due account the associated risks.

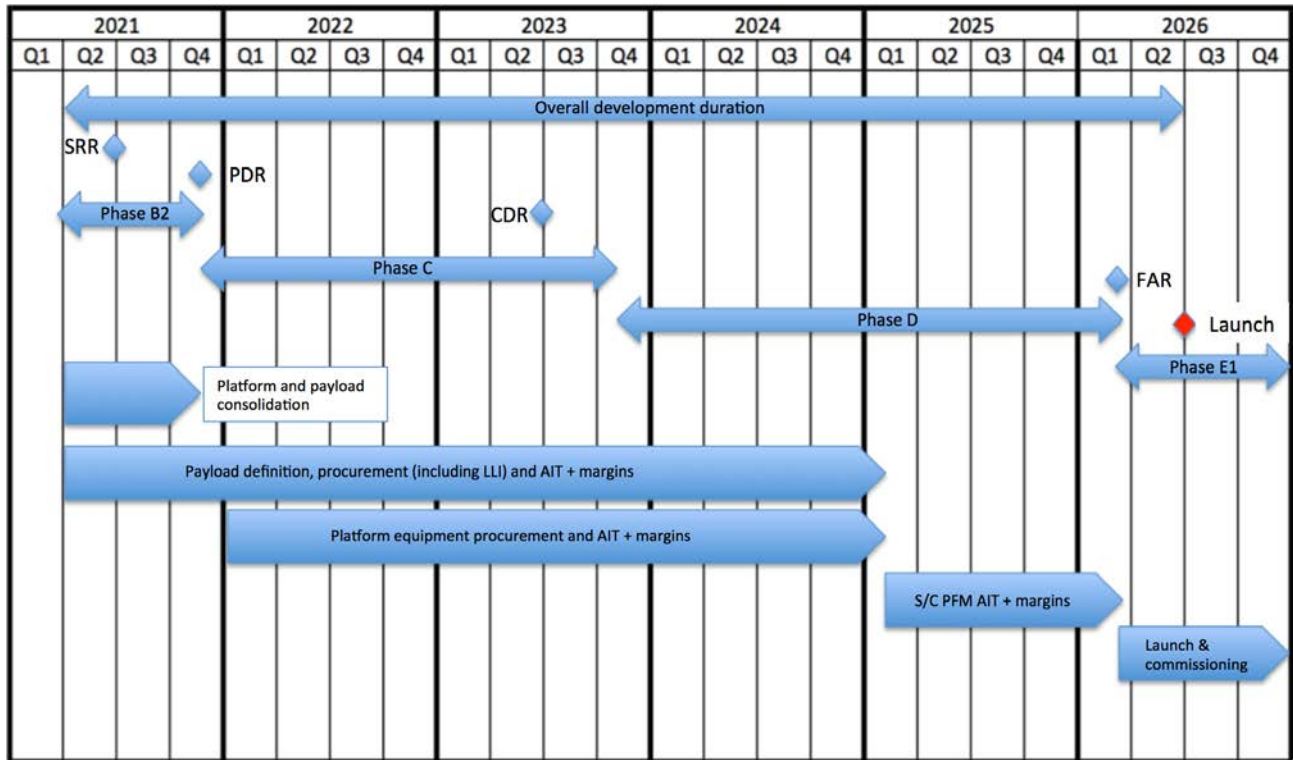


Figure 9.1 FORUM Development Schedule

9.4 Conclusion

The critical scientific areas of maturity and risk have been assessed and there are no major issues of concern to the scientific development of FORUM. The mission and research objectives have remained stable with respect to the original proposal. Based on the results of the End-to-End performance simulations, the scientific campaigns and studies conducted during the Phase A, it is considered that the FORUM mission concept has reached Scientific Readiness Level 5 at the end of Phase A.

Assuming the expected successful outcome of on-going and planned technology pre-developments, the maturity of critical technologies will reach the required level prior to the start of the implementation phase. The development schedule is driven by the instrument development, calibration & characterization and test phases. The Design Development and Validation Plan and the associated schedule is not yet fully consolidated and further improvements would be necessary to recover - with margins - the launch date by the end of 2025.

FORUM will be the first satellite mission to provide spectrally-resolved measurements in the far-infrared range, enabling climate research and acquiring knowledge with which to reduce uncertainty in predictions of future climate change.



It is judged that the FORUM mission concept has reached the expected scientific and technical readiness level at the end of Phase A, and is sufficiently mature for implementation as Earth Explorer 9. The development schedule is compatible with a launch in the 2026 timeframe.

REFERENCES

- Allan, R. P., Shine, K. P., Slingo, A., and Pamment, J. A. (1999). The dependence of clear-sky outgoing long-wave radiation on surface temperature and relative humidity. *Quarterly Journal of the Royal Meteorological Society*, 125(558), 2103–2126. <https://doi.org/10.1002/qj.49712555809>
- Ackerman, S. A., Holtz R. E., Frey R., Eloranta E. W., Maddux B. C. and McGill M. (2008). Cloud detection with MODIS, part II: Validation, JAOT, doi: 10.1175/2007/JTECHA1053.1.
- Ackerman, S. A., A. D. Collard, X. L. Ma, H. E. Revercomb, and R. O. Knuteson (1995). Cirrus cloud properties derived from High Spectral Resolution Infrared Spectrometry during FIREII. Part II: Aircraft HIS results, *J. Atmos. Sci.*, 52, 4246–4263.
- Allan, R. P. (2004). Simulation of the Earth's radiation budget by the European Centre for Medium-Range Weather Forecasts 40-year reanalysis (ERA40). *Journal of Geophysical Research*, 109(D18). <https://doi.org/10.1029/2004JD004816>
- Amato, U., Lavanant, L., Liuzzi, G., Masiello G., Serio C., Stuhlmann, R., and Tjemkes, S.A. (2014). Cloud mask via cumulative discriminant analysis applied to satellite infrared observations: scientific basis and initial evaluation. *Atm.Meas.Tech.*, vol. 7, p. 3355-3372, ISSN: 1867-1381, doi: 10.5194/amt-7-3355-2014.
- Anderson, G.P., Clough, S.A., Kneizys, F.X., Chetwynd, J.H., and Shettle, E.P. (1986). AFGL Atmospheric constituent profiles (0-120km). Air Force Geophysics Laboratory, AFGL-TR-86-0110, No. 964.
- Aumann, H. H., Elliott, D., and Manning, E. (2016). Comparison of the AIRS, IASI, and CrIS 900 cm⁻¹ channel for Dome Concordia. In J. J. Butler, X. (Jack) Xiong, and X. Gu (Eds.) (p. 997209). Presented at the SPIE Optical Engineering + Applications, San Diego, California, United States. <https://doi.org/10.1117/12.2235945>
- Aumann, H. H., Jiang, Y., and Elliott, D. A. (2011). Evaluation of cloudy data as stable references for climate research using AIRS and IRIS data. In J. J. Butler, X. Xiong, and X. Gu (Eds.) (p. 815304). Presented at the SPIE Optical Engineering + Applications, San Diego, California, USA. <https://doi.org/10.1117/12.892797>
- Baker, N. C., and Taylor, P. C. (2016). A Framework for Evaluating Climate Model Performance Metrics. *Journal of Climate*, 29(5), 1773–1782. <https://doi.org/10.1175/JCLI-D-15-0114.1>
- Bantges, R. J., Brindley, H. E., Chen, X. H., Huang, X. L., Harries, J. E., and Murray, J. E. (2016). On the Detection of Robust Multidecadal Changes in Earth's Outgoing Longwave Radiation Spectrum. *Journal of Climate*, 29(13), 4939–4947. <https://doi.org/10.1175/JCLI-D-15-0713.1>
- Baran, A. J. (2012). From the single-scattering properties of ice crystals to climate prediction: A way forward. *Atmospheric Research*, 112, 45–69. <https://doi.org/10.1016/j.atmosres.2012.04.010>

- Baran, A. J., and Labonnote, L.-C. (2007). A self-consistent scattering model for cirrus. I: The solar region. *Quarterly Journal of the Royal Meteorological Society*, 133(629), 1899–1912. <https://doi.org/10.1002/qj.164>
- Baran, A. J., Cotton, R., Furtado, K., Havemann, S., Labonnote, L.-C., Marengo, F., et al. (2014). A self-consistent scattering model for cirrus. II: The high and low frequencies: Self-consistent Scattering Model for Cirrus: Part II. *Quarterly Journal of the Royal Meteorological Society*, 140(680), 1039–1057. <https://doi.org/10.1002/qj.2193>
- Baran, A. J., Hill, P., Furtado, K., Field, P., and Manners, J. (2014). A Coupled Cloud Physics–Radiation Parameterization of the Bulk Optical Properties of Cirrus and Its Impact on the Met Office Unified Model Global Atmosphere 5.0 Configuration. *Journal of Climate*, 27(20), 7725–7752. <https://doi.org/10.1175/JCLI-D-13-00700.1>
- Barkstrom, B. R. (1984). The Earth Radiation Budget Experiment (ERBE). *Bulletin of the American Meteorological Society*, 65(11), 1170–1185. [https://doi.org/10.1175/1520-0477\(1984\)065<1170:TERBE>2.0.CO;2](https://doi.org/10.1175/1520-0477(1984)065<1170:TERBE>2.0.CO;2)
- Bates, J. J., and Privette, J. L. (2012). A maturity model for assessing the completeness of climate data records. *Eos, Transactions American Geophysical Union*, 93(44), 441–441. <https://doi.org/10.1029/2012EO440006>
- Baum, B., P. Yang, A. Heymsfield, A. Bansemir, B. Cole, A. Merrelli, C. Schmitt and C. Wang (2014), Ice cloud single-scattering property models with the full phase matrix at wavelengths from 0.2 to 100 μ m, *J. Quant. Spectrosc. Radiat. Transf.*, 146, 123–139, doi:10.1016/j.jqsrt.2014.02.029.
- Bellisario, C., Brindley, H. E., Murray, J. E., Last, A., Pickering, J., Harlow, R. C., et al. (2017). Retrievals of the Far Infrared Surface Emissivity Over the Greenland Plateau Using the Tropospheric Airborne Fourier Transform Spectrometer (TAFTS): Article TAFTS FIR Surface Emissivity. *Journal of Geophysical Research: Atmospheres*, 122(22), 12,152–12,166. <https://doi.org/10.1002/2017JD027328>
- Bellisario, C., Brindley, H. E., Tett, S. F. B., Rizzi, R., Di Natale, G., Palchetti, L., and Bianchini, G. (2018). Can downwelling far-infrared radiances over Antarctica be estimated from mid-infrared information? *Atmospheric Chemistry and Physics Discussions*, 1–17. <https://doi.org/10.5194/acp-2018-729>
- Bellisario, C., H. Brindley, J. Murray, A. Last, J. Pickering, R. Harlow, S. Fox, C. Fox, S. Newman, M. Smith, D. Anderson, X. Huang and X. Chen (2017), Retrievals of the far infrared surface emissivity over the Greenland Plateau using the Tropospheric Airborne Fourier Transform Spectrometer (TAFTS), *J. Geophys. Res.*, 122, 12,152–12,166.
- Bianchini, G., Carli, B., Cortesi, U., Del Bianco, S., Gai, M., and Palchetti, L. (2008). Test of far-infrared atmospheric spectroscopy using wide-band balloon-borne measurements of the upwelling radiance. *Journal of Quantitative Spectroscopy and Radiative Transfer*, 109(6), 1030–1042. <https://doi.org/10.1016/j.jqsrt.2007.11.010>
- Bianchini, G., Castagnoli, F., Di Natale, G., and Palchetti, L. (2019). A Fourier transform spectroradiometer for ground-based remote sensing of the atmospheric downwelling long-wave radiance. *Atmospheric Measurement Techniques*, 12(1), 619–635. <https://doi.org/10.5194/amt-12-619-2019>



- Bianchini, G., Palchetti, L., Carli, B. (2009). Vectorial combination of signals in Fourier transform spectroscopy", *Infrared Physics and Technologies*, 52, 19-21.
- Blanchet, J.-P., Royer, A., Châteauneuf, F., Bouzid, Y., Blanchard, Y., Hamel, J.-F., et al. (2011). TICFIRE: a far infrared payload to monitor the evolution of thin ice clouds. In R. Meynart, S. P. Neeck, and H. Shimoda (Eds.) (p. 81761K). Presented at the SPIE Remote Sensing, Prague, Czech Republic. <https://doi.org/10.1117/12.898577>
- Bodas-Salcedo, A., Webb, M. J., Bony, S., Chepfer, H., Dufresne, J.-L., Klein, S. A., et al. (2011). COSP: Satellite simulation software for model assessment. *Bulletin of the American Meteorological Society*, 92(8), 1023–1043. <https://doi.org/10.1175/2011BAMS2856.1>
- Bojinski, S., Verstraete, M., Peterson, T. C., Richter, C., Simmons, A., and Zemp, M. (2014). The Concept of Essential Climate Variables in Support of Climate Research, Applications, and Policy. *Bulletin of the American Meteorological Society*, 95(9), 1431–1443. <https://doi.org/10.1175/BAMS-D-13-00047.1>
- Bony, S., Stevens, B., Coppin, D., Becker, T., Reed, K. A., Voigt, A., and Medeiros, B. (2016). Thermodynamic control of anvil cloud amount. *Proceedings of the National Academy of Sciences*, 113(32), 8927–8932. <https://doi.org/10.1073/pnas.1601472113>
- Bony, S., Stevens, B., Frierson, D. M. W., Jakob, C., Kageyama, M., Pincus, R., et al. (2015). Clouds, circulation and climate sensitivity. *Nature Geoscience*, 8, 261.
- Brindley, H. and Russell, J. (2018). Top of Atmosphere Broadband Radiative Fluxes from Geostationary Satellite Observations, in *Comprehensive Remote Sensing, Vol 5: Earth's Energy Budget*, pp 85-113, Ed. S. Liang, Elsevier
- Brindley, H. E., and Harries, J. E. (1998). The impact of far i.r. absorption on clear sky greenhouse forcing: sensitivity studies at high spectral resolution. *Journal of Quantitative Spectroscopy and Radiative Transfer*, 60(2), 151–180. [https://doi.org/10.1016/S0022-4073\(97\)00152-0](https://doi.org/10.1016/S0022-4073(97)00152-0)
- Canas, T. A., Murray, J. E., and Harries, J. E. (1997). Tropospheric airborne Fourier transform spectrometer (TAFTS). In J. D. Haigh (Ed.) (p. 91). Presented at the Aerospace Remote Sensing '97, London, United Kingdom. <https://doi.org/10.1117/12.301139>
- Carleton, T. A., and Hsiang, S. M. (2016). Social and economic impacts of climate. *Science*, 353(6304), aad9837–aad9837. <https://doi.org/10.1126/science.aad9837>
- Cess, R.D., M.-H. Zhang, G.L. Potter, H.W. Barker, R.A. Colman, D.A. Dazlich, A.D. Del Genio, M. Esch, J.R. Fraser, V. Galin, W.L. Gates, J.J. Hack, W.J. Ingram, J.T. Kiehl, A.A. Lacis, H. Le Treut, Z.-X. Li, X.-Z. Liang, J.-F. Mahfouf, B.J. McAvaney, V.P. Meleshko, J.-J. Morcrette, D.A. Randall, E. Roeckner, J.-F. Royer, A.P. Sokolov, P.V. Sporyshev, K.E. Taylor, W.-C. Wang, and R.T. Wetherald, 1993: Uncertainties in carbon dioxide radiative forcing in atmospheric general circulation models. *Science*, 262, 1252-1255, doi:10.1126/science.262.5137.1252.

- Chahine, M. T., Gunson, M., Aumann, H. H., Strow, L. L., Hagan, D., Hofstadter, M., et al. (2000). THE AIRS TEAM SCIENCE DATA VALIDATION PLAN (No. JPL D-16822). JPL.
- Chahine, M. T., Pagano, T. S., Aumann, H. H., Atlas, R., Barnett, C., Blaisdell, J., et al. (2006). AIRS: Improving Weather Forecasting and Providing New Data on Greenhouse Gases. *Bulletin of the American Meteorological Society*, 87(7), 911–926. <https://doi.org/10.1175/BAMS-87-7-911>
- Chen, X., Huang, X., and Flanner, M. G. (2014). Sensitivity of modeled far-IR radiation budgets in polar continents to treatments of snow surface and ice cloud radiative properties. *Geophysical Research Letters*, 41(18), 6530–6537. <https://doi.org/10.1002/2014GL061216>
- Chen, X., Huang, X., Dong, X., Xi, B., Dolinar, E. K., Loeb, N. G., et al. (2018). Using AIRS and ARM SGP clear-sky observations to evaluate meteorological reanalyses: A hyperspectral radiance closure approach. *Journal of Geophysical Research: Atmospheres*, 123, 11,720–11,734. <https://doi.org/10.1029/2018JD028850>
- Chen, X., Huang, X., Loeb, N. G., and Wei, H. (2013). Comparisons of Clear-Sky Outgoing Far-IR Flux Inferred from Satellite Observations and Computed from the Three Most Recent Reanalysis Products. *Journal of Climate*, 26(2), 478–494. <https://doi.org/10.1175/JCLI-D-12-00212.1>
- Chou, C., Neelin, J. D., Chen, C.-A., and Tu, J.-Y. (2009). Evaluating the “Rich-Get-Richer” Mechanism in Tropical Precipitation Change under Global Warming. *Journal of Climate*, 22(8), 1982–2005. <https://doi.org/10.1175/2008JCLI2471.1>
- Chou, M.-D. (1999). Parameterization for Cloud Longwave Scattering for Use in Atmospheric Models. *Journal of Climate*, 12(1), 159–169. [https://doi.org/10.1175/1520-0442\(1999\)012<0159:PFCLSF>2.0.CO;2](https://doi.org/10.1175/1520-0442(1999)012<0159:PFCLSF>2.0.CO;2)
- Christensen, P. R., Hamilton, V. E., Mehall, G. L., Pelham, D., O'Donnell, W., Anwar, S., Bowles, H., Chase, S., Fahlgren, J., Farkas, Z., Fisher, T., James, O., Kubik, I., Lazbin, I., Miner, M., Rassas, M., Schulze, L., Shamordola, K., Tourville, T., West, G., Woodward, R. and Lauretta, D. (2018). The OSIRIS-REx Thermal Emission Spectrometer (OTES) Instrument, *Space Science Reviews*, vol. 214, no. 5, 87. <https://doi.org/10.1007/s11214-018-0513-6>
- Chung, E.-S., and Soden, B. J. (2015a). An Assessment of Direct Radiative Forcing, Radiative Adjustments, and Radiative Feedbacks in Coupled Ocean–Atmosphere Models*. *Journal of Climate*, 28(10), 4152–4170. <https://doi.org/10.1175/JCLI-D-14-00436.1>
- Chung, E.-S., and Soden, B. J. (2015b). An assessment of methods for computing radiative forcing in climate models. *Environmental Research Letters*, 10(7), 074004. <https://doi.org/10.1088/1748-9326/10/7/074004>
- Chung, E.-S., Soden, B. J., Sohn, B.-J., and Schmetz, J. (2011). Model-simulated humidity bias in the upper troposphere and its relation to the large-scale circulation. *Journal of Geophysical Research*, 116(D10). <https://doi.org/10.1029/2011JD015609>

- Chung, E.-S., Soden, B., Sohn, B. J., and Shi, L. (2014). Upper-tropospheric moistening in response to anthropogenic warming. *Proceedings of the National Academy of Sciences*, 111(32), 11636–11641.
<https://doi.org/10.1073/pnas.1409659111>
- Clough, S. A., Iacono, M. J., and Moncet, J.-L. (1992). Line-by-line calculations of atmospheric fluxes and cooling rates: Application to water vapor. *Journal of Geophysical Research*, 97(D14), 15761.
<https://doi.org/10.1029/92JD01419>
- Clough, S. A., Shephard, M. W., Mlawer, E. J., Delamere, J. S., Iacono, M. J., Cady-Pereira, K., et al. (2005). Atmospheric radiative transfer modeling: a summary of the AER codes. *Journal of Quantitative Spectroscopy and Radiative Transfer*, 91(2), 233–244. <https://doi.org/10.1016/j.jqsrt.2004.05.058>
- Collard, A. D., and McNally, A. P. (2009). The assimilation of Infrared Atmospheric Sounding Interferometer radiances at ECMWF. *Quarterly Journal of the Royal Meteorological Society*, 135(641), 1044–1058.
<https://doi.org/10.1002/qj.410>
- Collins, W. D. (2002). An updated parameterization for infrared emission and absorption by water vapor in the National Center for Atmospheric Research Community Atmosphere Model. *Journal of Geophysical Research*, 107(D22).
<https://doi.org/10.1029/2001JD001365>
- Committee on the Decadal Survey for Earth Science and Applications from Space, Space Studies Board, Division on Engineering and Physical Sciences, and National Academies of Sciences, Engineering, and Medicine. (2018). *Thriving on Our Changing Planet: A Decadal Strategy for Earth Observation from Space*. Washington, D.C.: National Academies Press. <https://doi.org/10.17226/24938>
- Comstock, J. M., Ackerman, T. P., and Turner, D. D. (2004). Evidence of high ice supersaturation in cirrus clouds using ARM Raman lidar measurements: ICE SUPERSATURATION IN CIRRUS CLOUDS. *Geophysical Research Letters*, 31(11), n/a-n/a. <https://doi.org/10.1029/2004GL019705>
- Conrath, B. J., Hanel, R. A., Kunde, V. G., and Prabhakara, C. (1970). The Infrared Interferometer Experiment on Nimbus 3. *Journal of Geophysical Research*, 75(30), 5831–5857. <https://doi.org/10.1029/JC075i030p05831>
- Cooke, R., Golub, A., Wielicki, B. A., Young, D. F., Mlynchak, M. G., and Baize, R. R. (2017). Using the social cost of carbon to value earth observing systems. *Climate Policy*, 17(3), 330–345.
<https://doi.org/10.1080/14693062.2015.1110109>
- Cooke, R., Wielicki, B. A., Young, D. F., and Mlynchak, M. G. (2014). Value of information for climate observing systems. *Environment Systems and Decisions*, 34(1), 98–109. <https://doi.org/10.1007/s10669-013-9451-8>
- Cortesi, U., Del Bianco, S., Gai, M., Laurenza, L. M., Ceccherini, S., Carli, B., Barbara, F., and Buchwitz M., (2014). Sensitivity analysis and application of KLIMA algorithm to GOSAT and OCO validation - KLIMA-IASI, Final Report of Project ESA-ESRIN/Contract n. 21612/08/I-OL, IFAC-TSRR, vol. 6, pp. 1-153

- Coudert, L. H., Martin-Drumel, M.-A., and Pirali, O. (2014). Analysis of the high-resolution water spectrum up to the Second Triad and to $J = 30$. *Journal of Molecular Spectroscopy*, 303, 36–41.
<https://doi.org/10.1016/j.jms.2014.07.003>
- Cox, C. V., Harries, J. E., Taylor, J. P., Green, P. D., Baran, A. J., Pickering, J. C., et al. (2010). Measurement and simulation of mid- and far-infrared spectra in the presence of cirrus. *Quarterly Journal of the Royal Meteorological Society*, n/a-n/a. <https://doi.org/10.1002/qj.596>
- Crevoisier, C., Clerbaux, C., Guidard, V., Phulpin, T., Armante, R., Barret, B., Camy-Peyret, C., Chaboureaud, J.-P., Coheur, P.-F., Crépeau, L., Dufour, G., Labonnote, L., Lavanant, L., Hadji-Lazaro, J., Herbin, H., Jacquinet-Husson, N., Payan, S., Péquignot, E., Pierangelo, C., Sellitto, P., and Stubenrauch, C. (2014): Towards IASI-New Generation (IASI-NG): impact of improved spectral resolution and radiometric noise on the retrieval of thermodynamic, chemistry and climate variables, *Atmos. Meas. Tech.*, 7, 4367-4385, <https://doi.org/10.5194/amt-7-4367-2014>.
- Davis, S. M., Rosenlof, K. H., Hassler, B., Hurst, D. F., Read, W. G., Vömel, H., et al. (2016). The Stratospheric Water and Ozone Satellite Homogenized (SWOOSH) database: a long-term database for climate studies. *Earth System Science Data*, 8(2), 461–490. <https://doi.org/10.5194/essd-8-461-2016>
- Dee, D. P., Uppala, S. M., Simmons, A. J., Berrisford, P., Poli, P., Kobayashi, S., Andrae, U., Balmaseda, M. A., Balsamo, G., Bauer, P., Bechtold, P., Beljaars, A. C., van de Berg, L., Bidlot, J., Bormann, N., Delsol, C., Dragani, R., Fuentes, M., Geer, A. J., Haimberger, L., Healy, S. B., Hersbach, H., Hólm, E. V., Isaksen, I., Kållberg, P., Köhler, M., Matricardi, M., McNally, A. P., Monge-Sanz, B. M., Morcrette, J., Park, B., Peubey, C., de Rosnay, P., Tavolato, C., Thépaut, J. and Vitart, F. (2011), The ERA-Interim reanalysis: configuration and performance of the data assimilation system. *Q.J.R. Meteorol. Soc.*, 137: 553-597. doi:10.1002/qj.828
- Del Bianco, S., Carli, B., Gai, M., Laurenza, L.M., Cortesi, U. (2014), XCO₂ retrieved from IASI using KLIMA algorithm, *Annals of Geophysics*, 56, doi:10.4401/ag-6331
- Delamere, J. S., Clough, S. A., Payne, V. H., Mlawer, E. J., Turner, D. D., and Gamache, R. R. (2010). A far-infrared radiative closure study in the Arctic: Application to water vapor. *Journal of Geophysical Research*, 115(D17).
<https://doi.org/10.1029/2009JD012968>
- Delanoë, J., and Hogan, R. J. (2008). A variational scheme for retrieving ice cloud properties from combined radar, lidar, and infrared radiometer. *Journal of Geophysical Research*, 113(D7). <https://doi.org/10.1029/2007JD009000>
- Desmons, M., Ferlay, N., Parol, F., Mcharek, L. and Vanbauce, C. (2013), Improved information about the vertical location and extent of monolayer clouds from POLDER3 measurements in the oxygen A-band. *Atmos. Meas. Tech.*, 6(8), 2221-2238. [10.5194/amt-6-2221-2013](https://doi.org/10.5194/amt-6-2221-2013)



- Dessler, A. E., Schoeberl, M. R., Wang, T., Davis, S. M., and Rosenlof, K. H. (2013). Stratospheric water vapor feedback. *Proceedings of the National Academy of Sciences*, 110(45), 18087–18091. <https://doi.org/10.1073/pnas.1310344110>
- Dessler, A. E., Zhang, Z., and Yang, P. (2008). Water-vapor climate feedback inferred from climate fluctuations, 2003–2008. *Geophysical Research Letters*, 35(20). <https://doi.org/10.1029/2008GL035333>
- Dewitte, S., Clerbaux, N., Cornelis, J., (2019), Decadal Changes of the Reflected Solar Radiation and the Earth Energy Imbalance, *Remote Sensing*, 2072-4292, V. 11, N P 663, doi:10.3390/rs11060663
- Di Natale, G., Palchetti, L., Bianchini, G., and Del Guasta, M. (2017). Simultaneous retrieval of water vapour, temperature and cirrus clouds properties from measurements of far infrared spectral radiance over the Antarctic Plateau. *Atmospheric Measurement Techniques*, 10(3), 825–837. <https://doi.org/10.5194/amt-10-825-2017>
- Diallo, M., Riese, M., Birner, T., Konopka, P., Müller, R., Hegglin, M. I., Santee, M. L., Baldwin, M., Legras, B., and Ploeger, F. (2018). Response of stratospheric water vapor and ozone to the unusual timing of El Niño and the QBO disruption in 2015–2016, *Atmos. Chem. Phys.*, 18, 13055-13073, <https://doi.org/10.5194/acp-18-13055-2018>.
- Dirksen, R. J., Sommer, M., Immler, F. J., Hurst, D. F., Kivi, R., and Vömel, H. (2014). Reference quality upper-air measurements: GRUAN data processing for the Vaisala RS92 radiosonde. *Atmospheric Measurement Techniques*, 7(12), 4463–4490. <https://doi.org/10.5194/amt-7-4463-2014>
- Divakarla, M. G., Barnet, C. D., Goldberg, M. D., McMillin, L. M., Maddy, E., Wolf, W., et al. (2006). Validation of Atmospheric Infrared Sounder temperature and water vapor retrievals with matched radiosonde measurements and forecasts. *Journal of Geophysical Research*, 111(D9). <https://doi.org/10.1029/2005JD006116>
- Dudhia, A., Jay, V. L., Rodgers, C. D. (2002). Microwindow Selection for High-Spectral-Resolution Sounders. *Applied optics*. 41. 3665-73. 10.1364/AO.41.003665.
- Dyroff, C., Zahn, A., Christner, E., Forbes, R., Tompkins, A. M., and van Velthoven, P. F. J. (2015). Comparison of ECMWF analysis and forecast humidity data with CARIBIC upper troposphere and lower stratosphere observations: ECMWF Humidity/CARIBIC Observation Comparison. *Quarterly Journal of the Royal Meteorological Society*, 141(688), 833–844. <https://doi.org/10.1002/qj.2400>
- Eliasson, S., Buehler, S. A., Milz, M., Eriksson, P., and John, V. O. (2011). Assessing observed and modelled spatial distributions of ice water path using satellite data. *Atmospheric Chemistry and Physics*, 11(1), 375–391. <https://doi.org/10.5194/acp-11-375-2011>
- ESA (2006) *The Changing Earth: New Scientific Challenges for ESA's Living Planet Programme*. ESA SP-1304, European Space Agency, Noordwijk, The Netherlands.



- ESA (2015a). Earth Observation Science Strategy for ESA: A New Era for Scientific Advances and for Societal Benefits. ESA SP-1329/1 (2 volumes), European Space Agency, Noordwijk, The Netherlands.
- ESA (2015b). ESA's Living Planet Programme: Scientific Achievements and Future Challenges - scientific context of the Earth Observation Science Strategy for ESA, ESA SP-1329/2 (2 volumes), European Space Agency, Noordwijk, The Netherlands.
- ESA (2015c). Scientific Readiness Levels Handbook. Mission Science Division (EOP-SM), EOP-SM/2776, V1.1, European Space Agency, Noordwijk, The Netherlands.
- Feister, U. (1980). The determination of atmospheric total ozone using infrared radiation measurements made with the Fourier spectrometer SI-1 onboard METEOR 28. *Zeitschrift Für Meteorologie*, 30.5, 279–295.
- Feldman D, Collins W, Paige J. Pan-spectral observing system simulation experiments of shortwave reflectance and longwave radiance for climate model evaluation. *Goesci Model Dev.* 2015;8:1943–54. doi:10.5194/gmd-8-1943-2015.
- Feldman, D. R., Collins, W. D., Pincus, R., Huang, X., and Chen, X. (2014). Far-infrared surface emissivity and climate. *Proceedings of the National Academy of Sciences*, 111(46), 16297–16302. <https://doi.org/10.1073/pnas.1413640111>
- Ferlay, N., Thieuleux, F., Cornet, C., Davis, A. B., Dubuisson, P., Ducos, F., Parol, F., Riedi, J., and Vanbaue, C.: Toward New Inferences about Cloud Structures from Multidirectional Measurements in the Oxygen A Band: Middle-of-Cloud Pressure and Cloud Geometrical Thickness from POLDER-3/PARASOL, *J. Appl. Meteorol. Clim.*, 49, 2492–2507, 2010.
- Field, P. R., Heymsfield, A. J., and Bansemmer, A. (2007). Snow Size Distribution Parameterization for Midlatitude and Tropical Ice Clouds. *Journal of the Atmospheric Sciences*, 64(12), 4346–4365. <https://doi.org/10.1175/2007JAS2344.1>
- Fischer, E. and Knutti, R. (2015). Anthropogenic contribution to global occurrence of heavy-precipitation and high-temperature extremes, *Nature Climate Change*, 5, 560–564.
- Flato, G., Marotzke, J., Abiodun, B., Braconnot, P., Chou, S. C., Collins, W., et al. (2013). Evaluation of Climate Models.
- Fusina, F., Spichtinger, P., and Lohmann, U. (2007). Impact of ice supersaturated regions and thin cirrus on radiation in the midlatitudes. *Journal of Geophysical Research*, 112(D24). <https://doi.org/10.1029/2007JD008449>
- Goldberg, M. D., Zhou, L., Wolf, W. W., Barnet, C., and Divakarla, M. G. (2005). Applications of principal component analysis (PCA) on AIRS data. In A. M. Larar, M. Suzuki, and Q. Tong (Eds.) (p. 479). Presented at the Fourth International Asia-Pacific Environmental Remote Sensing Symposium 2004: Remote Sensing of the Atmosphere, Ocean, Environment, and Space, Honolulu, HI. <https://doi.org/10.1117/12.578939>

- Gordon, I. E., Rothman, L. S., Hill, C., Kochanov, R. V., Tan, Y., Bernath, P. F., et al. (2017). The HITRAN2016 molecular spectroscopic database. *Journal of Quantitative Spectroscopy and Radiative Transfer*, 203, 3–69.
<https://doi.org/10.1016/j.jqsrt.2017.06.038>
- Green, P. D., Newman, S. M., Beeby, R. J., Murray, J. E., Pickering, J. C., and Harries, J. E. (2012). Recent advances in measurement of the water vapour continuum in the far-infrared spectral region. *Philosophical Transactions of the Royal Society A: Mathematical, Physical and Engineering Sciences*, 370(1968), 2637–2655.
<https://doi.org/10.1098/rsta.2011.0263>
- Han, Y., Revercomb, H., Cromp, M., Gu, D., Johnson, D., Mooney, D., et al. (2013). Suomi NPP CrIS measurements, sensor data record algorithm, calibration and validation activities, and record data quality: CRIS SENSOR DATA RECORD QUALITY. *Journal of Geophysical Research: Atmospheres*, 118(22), 12,734–12,748.
<https://doi.org/10.1002/2013JD020344>
- Hanel, R. A., Conrath, B. J., Kunde, V. G., Prabhakara, C., Revah, I., Salomonson, V. V., and Wolford, G. (1972). The Nimbus 4 infrared spectroscopy experiment: 1. Calibrated thermal emission spectra. *Journal of Geophysical Research*, 77(15), 2629–2641. <https://doi.org/10.1029/JC077i015p02629>
- Hansen, J. (2005). Earth's Energy Imbalance: Confirmation and Implications. *Science*, 308(5727), 1431–1435.
<https://doi.org/10.1126/science.1110252>
- Harries, J. E., Russell, J. E., Hanafin, J. A., Brindley, H., Futyan, J., Rufus, J., et al. (2005). The Geostationary Earth Radiation Budget Project. *Bulletin of the American Meteorological Society*, 86(7), 945–960.
<https://doi.org/10.1175/BAMS-86-7-945>
- Harries, J., Carli, B., Rizzi, R., Serio, C., Mlynczak, M., Palchetti, L., et al. (2008). The Far-infrared Earth. *Reviews of Geophysics*, 46(4). <https://doi.org/10.1029/2007RG000233>
- Hegglin M., Schröder M., Brogniez H., Hubert D., (2019), User Requirements Document (URD), Water Vapour Climate Change Initiative (WV_cci) - Phase One, Ref: D1.1, Date: 28 January 2019, Issue: 1.1, ESA / ECSAT, Ref: CCIWV.REP.001
- Hegglin, M. I., et al. (2013), SPARC Data Initiative: Comparison of water vapor climatologies from international satellite limb sounders, *J. Geophys. Res. Atmos.*, 118, 11,824–11,846, doi:10.1002/jgrd.50752.
- Hegglin, M. I., Plummer, D. A., Shepherd, T. G., Scinocca, J. F., Anderson, J., Froidevaux, L., et al. (2014). Vertical structure of stratospheric water vapour trends derived from merged satellite data. *Nature Geoscience*, 7(10), 768–776. <https://doi.org/10.1038/ngeo2236>
- Held, I. M., and Soden, B. J. (2000). WATER VAPOR FEEDBACK AND GLOBAL WARMING. *Annual Review of Energy and the Environment*, 25(1), 441–475. <https://doi.org/10.1146/annurev.energy.25.1.441>

- Hess, M., Koepke, P., and Schult, I. (1998). Optical Properties of Aerosols and Clouds: The Software Package OPAC. *Bulletin of the American Meteorological Society*, 79(5), 831–844. [https://doi.org/10.1175/1520-0477\(1998\)079<0831:OPOAAC>2.0.CO;2](https://doi.org/10.1175/1520-0477(1998)079<0831:OPOAAC>2.0.CO;2)
- Hilton, F., Armante, R., August, T., Barnet, C., Bouchard, A., Camy-Peyret, C., et al. (2012). Hyperspectral Earth Observation from IASI: Five Years of Accomplishments. *Bulletin of the American Meteorological Society*, 93(3), 347–370. <https://doi.org/10.1175/BAMS-D-11-00027.1>
- Hollmann, R. (2018). ESA Cloud_cci Product validation and intercomparison report (Applicable to Cloud_cci version 2.0 products). Issue 5 Revision 1. Retrieved from http://www.esa-cloud-cci.org/sites/default/files/documents/public/Cloud_cci_D4.1_PVIR_v5.1.pdf
- Hong, Y., and Liu, G. (2015). The Characteristics of Ice Cloud Properties Derived from CloudSat and CALIPSO Measurements. *Journal of Climate*, 28(9), 3880–3901. <https://doi.org/10.1175/JCLI-D-14-00666.1>
- Hong, Y., Liu, G., and Li, J.-L. F. (2016). Assessing the Radiative Effects of Global Ice Clouds Based on CloudSat and CALIPSO Measurements. *Journal of Climate*, 29(21), 7651–7674. <https://doi.org/10.1175/JCLI-D-15-0799.1>
- Hope, C. (2015). The \$10 trillion value of better information about the transient climate response. *Philosophical Transactions of the Royal Society A: Mathematical, Physical and Engineering Sciences*, 373(2054), 20140429. <https://doi.org/10.1098/rsta.2014.0429>
- Huang, X., Chen, X., Flanner, M., Yang, P., Feldman, D., and Kuo, C. (2018). Improved Representation of Surface Spectral Emissivity in a Global Climate Model and Its Impact on Simulated Climate. *Journal of Climate*, 31(9), 3711–3727. <https://doi.org/10.1175/JCLI-D-17-0125.1>
- Huang, X., Chen, X., Zhou, D. K., and Liu, X. (2016) An Observationally Based Global Band-by-Band Surface Emissivity Dataset for Climate and Weather Simulations. *J. Atmos. Sci.*, 73, 3541–3555, <https://doi.org/10.1175/JAS-D-15-0355.1>
- Huang, X., Cole, J. N. S., He, F., Potter, G. L., Oreopoulos, L., Lee, D., et al. (2013). Longwave Band-By-Band Cloud Radiative Effect and Its Application in GCM Evaluation. *Journal of Climate*, 26(2), 450–467. <https://doi.org/10.1175/JCLI-D-12-00112.1>
- Huang, X., Loeb, N. G., and Yang, W. (2010). Spectrally resolved fluxes derived from collocated AIRS and CERES measurements and their application in model evaluation: 2. Cloudy sky and band-by-band cloud radiative forcing over the tropical oceans. *Journal of Geophysical Research*, 115(D21). <https://doi.org/10.1029/2010JD013932>
- Huang, X., Yang, W., Loeb, N. G., and Ramaswamy, V. (2008). Spectrally resolved fluxes derived from collocated AIRS and CERES measurements and their application in model evaluation: Clear sky over the tropical oceans. *Journal of Geophysical Research*, 113(D9). <https://doi.org/10.1029/2007JD009219>

- Huang, Y. and Ramaswamy, V. (2008). Observed and simulated seasonal co-variations of outgoing longwave radiation spectrum and surface temperature. *Geophysical Research Letters*, 35(17).
<https://doi.org/10.1029/2008GL034859>
- Huang, Y, Leroy, S., Gero, P. J., Dykema, J., and Anderson, J. (2010). Separation of longwave climate feedbacks from spectral observations. *Journal of Geophysical Research*, 115(D7). <https://doi.org/10.1029/2009JD012766>
- Huang, Y, Ramaswamy, V., Huang, X., Fu, Q., and Bardeen, C. (2007). A strict test in climate modeling with spectrally resolved radiances: GCM simulation versus AIRS observations. *Geophysical Research Letters*, 34(24).
<https://doi.org/10.1029/2007GL031409>
- Huang, Y., Leroy, S., and Goody, R. M. (2011). Discriminating between climate observations in terms of their ability to improve an ensemble of climate predictions. *Proceedings of the National Academy of Sciences*, 108(26), 10405–10409. <https://doi.org/10.1073/pnas.1107403108>
- Hurst, D. F., Oltmans, S. J., Vömel, H., Rosenlof, K. H., Davis, S. M., Ray, E. A., et al. (2011). Stratospheric water vapor trends over Boulder, Colorado: Analysis of the 30 year Boulder record. *Journal of Geophysical Research*, 116(D2). <https://doi.org/10.1029/2010JD015065>
- Iacono, M. J., Mlawer, E. J., Clough, S. A., and Morcrette, J.-J. (2000). Impact of an improved longwave radiation model, RRTM, on the energy budget and thermodynamic properties of the NCAR community climate model, CCM3. *Journal of Geophysical Research: Atmospheres*, 105(D11), 14873–14890.
<https://doi.org/10.1029/2000JD900091>
- Illingworth, A. J., Barker, H. W., Beljaars, A., Ceccaldi, M., Chepfer, H., Clerbaux, N., et al. (2015). The EarthCARE Satellite: The Next Step Forward in Global Measurements of Clouds, Aerosols, Precipitation, and Radiation. *Bulletin of the American Meteorological Society*, 96(8), 1311–1332. <https://doi.org/10.1175/BAMS-D-12-00227.1>
- Inoue T. (1985). On the temperature and effective emissivity determination of semi-transparent cirrus clouds by bi-spectral measurements in the 10 μm window region, *J Meteorol Soc Jpn*, 63, 88–98.
- IPCC (1990). *Climate Change: The IPCC Scientific Assessment*. Eds. Houghton, Jenkins and Ephraums, Cambridge University Press.
- IPCC (2013). *Climate Change 2013: The Physical Science Basis*. Cambridge University Press, 1535 pp.
- Iwabuchi, H. and Yang, P., (2011). Temperature dependence of ice optical constants: Implications for single scattering properties of cold ice clouds, *J. Quant. Spectrosc. Rad. Trans.*, 112, 2520-2525.
- Jacquinet-Husson, N., Armante, R., Scott, N. A., Chédin, A., Crépeau, L., Boutammine, C., et al. (2016). The 2015 edition of the GEISA spectroscopic database. *Journal of Molecular Spectroscopy*, 327, 31–72.
<https://doi.org/10.1016/j.jms.2016.06.007>

- Jensen, E. J., Smith, J. B., Pfister, L., Pittman, J. V., Weinstock, E. M., Sayres, D. S., et al. (2005). Ice supersaturations exceeding 100% at the cold tropical tropopause: implications for cirrus formation and dehydration. *Atmospheric Chemistry and Physics*, 5(3), 851–862. <https://doi.org/10.5194/acp-5-851-2005>
- Jiang, J. H., Su, H., Zhai, C., Perun, V. S., Del Genio, A., Nazarenko, L. S., et al. (2012). Evaluation of cloud and water vapor simulations in CMIP5 climate models using NASA “A-Train” satellite observations: EVALUATION OF IPCC AR5 MODEL SIMULATIONS. *Journal of Geophysical Research: Atmospheres*, 117(D14), n/a-n/a. <https://doi.org/10.1029/2011JD017237>
- Jiang, J. H., Su, H., Zhai, C., Wu, L., Minschwaner, K., Molod, A. M., and Tompkins, A. M. (2015). An assessment of upper troposphere and lower stratosphere water vapor in MERRA, MERRA2, and ECMWF reanalyses using Aura MLS observations: H₂O IN REANALYSES AND MLS OBSERVATION. *Journal of Geophysical Research: Atmospheres*, 120(22), 11,468-11,485. <https://doi.org/10.1002/2015JD023752>
- Jing, F. and Y. Huang (2017), Cloud-assisted retrieval of lower stratospheric water vapor from nadir view satellite measurements, *J. Atmos. Ocean. Tech.*, 35, 541-553
- John, V. O., Holl, G., Allan, R. P., Buehler, S. A., Parker, D. E., and Soden, B. J. (2011). Clear-sky biases in satellite infrared estimates of upper tropospheric humidity and its trends. *Journal of Geophysical Research*, 116(D14). <https://doi.org/10.1029/2010JD015355>
- Jones, G. S., Stott, P. A., and Christidis, N. (2013). Attribution of observed historical near-surface temperature variations to anthropogenic and natural causes using CMIP5 simulations: ATTRIBUTION OF TEMPERATURES WITH CMIP5. *Journal of Geophysical Research: Atmospheres*, 118(10), 4001–4024. <https://doi.org/10.1002/jgrd.50239>
- Joo, S., Eyre, J., and Marriott, R., (2013). The Impact of MetOp and Other Satellite Data within the Met Office Global NWP System Using an Adjoint-Based Sensitivity Method. *Mon. Wea. Rev.*, 141, 3331–3342, <https://doi.org/10.1175/MWR-D-12-00232.1>
- Kahn, B. H., Huang, X., Stephens, G. L., Collins, W. D., Feldman, D. R., Su, H., et al. (2016). ENSO regulation of far- and mid-infrared contributions to clear-sky OLR: CLEAR-SKY SPECTRAL INFRARED. *Geophysical Research Letters*, 43(16), 8751–8759. <https://doi.org/10.1002/2016GL070263>
- Karlsson, K.-G., and Devasthale, A. (2018). Inter-Comparison and Evaluation of the Four Longest Satellite-Derived Cloud Climate Data Records: CLARA-A2, ESA Cloud CCI V3, ISCCP-HGM, and PATMOS-x. *Remote Sensing*, 10(10), 1567. <https://doi.org/10.3390/rs10101567>
- Kaufmann, S., Voigt, C., Heller, R., Jurkat-Witschas, T., Krämer, M., Rolf, C., et al. (2018). Intercomparison of midlatitude tropospheric and lower-stratospheric water vapor measurements and comparison to ECMWF

- humidity data. *Atmospheric Chemistry and Physics*, 18(22), 16729–16745. <https://doi.org/10.5194/acp-18-16729-2018>
- Kiehl, J. T. (1983). Satellite Detection of Effects Due to Increased Atmospheric Carbon Dioxide. *Science*, 222(4623), 504–506. <https://doi.org/10.1126/science.222.4623.504>
- Klein, S. A., and Hall, A. (2015). Emergent Constraints for Cloud Feedbacks. *Current Climate Change Reports*, 1(4), 276–287. <https://doi.org/10.1007/s40641-015-0027-1>
- Knuteson, R., Best, F., DeSlover, D., Osborne, B., Revercomb, H., and Smith, W. (2004), Infrared land surface remote sensing using high spectral resolution aircraft observations, *Adv. Space Res.*, 33, 1114–1119, doi:10.1016/S0273-1177(03)00752-X.
- Knutti, R., and Sedláček, J. (2013). Robustness and uncertainties in the new CMIP5 climate model projections. *Nature Climate Change*, 3(4), 369–373. <https://doi.org/10.1038/nclimate1716>
- Krijger, J.M., van Weele, M., Aben, I., and Frey, R., (2007) Technical Note: The effect of sensor resolution on the number of cloud-free observations from space, *Atmos. Chem. Phys.*, 7, 2881-2891.
- Kunde, V. G., Conrath, B. J., Hanel, R. A., Maguire, W. C., Prabhakara, C., and Salomonson, V. V. (1974). The Nimbus 4 infrared spectroscopy experiment: 2. Comparison of observed and theoretical radiances from 425-1450 cm⁻¹. *Journal of Geophysical Research*, 79(6), 777–784. <https://doi.org/10.1029/JC079i006p00777>
- Kuo, C., Feldman, D. R., Huang, X., Flanner, M., Yang, P., and Chen, X. (2018). Time-Dependent Cryospheric Longwave Surface Emissivity Feedback in the Community Earth System Model. *Journal of Geophysical Research: Atmospheres*, 123(2), 789–813. <https://doi.org/10.1002/2017JD027595>
- Kursinski, E. R., and Gebhardt, T. (2014). A Method to Deconvolve Errors in GPS RO-Derived Water Vapor Histograms. *Journal of Atmospheric and Oceanic Technology*, 31(12), 2606–2628. <https://doi.org/10.1175/JTECH-D-13-00233.1>
- Lacour, A., Chepfer, H., Miller, N. B., Shupe, M. D., Noel, V., Fettweis, X., et al. (2018). How Well Are Clouds Simulated over Greenland in Climate Models? Consequences for the Surface Cloud Radiative Effect over the Ice Sheet. *Journal of Climate*, 31(22), 9293–9312. <https://doi.org/10.1175/JCLI-D-18-0023.1>
- Latvakoski, H., Mlynczak, M. G., Cageao, R. P., Johnson, D. G., and Kratz, D. P. (2014). Far-infrared spectroscopy of the troposphere: calibration with a cold background. *Applied Optics*, 53(24), 5425. <https://doi.org/10.1364/AO.53.005425>
- Latvakoski, H., Mlynczak, M. G., Johnson, D. G., Cageao, R. P., Kratz, D. P., and Johnson, K. (2013). Far-infrared spectroscopy of the troposphere: instrument description and calibration performance. *Applied Optics*, 52(2), 264. <https://doi.org/10.1364/AO.52.000264>

- Lavanant L, Roquet P. (2013), Method to generate a reference cloud mask for MTG-IRS Technical Memorandum n°1, Météo-France/DP/CMS/R&D.
- Leroy, S., Anderson, J., Dykema, J., and Goody, R. (2008). Testing Climate Models Using Thermal Infrared Spectra. *Journal of Climate*, 21(9), 1863–1875. <https://doi.org/10.1175/2007JCLI2061.1>
- Li, J.-L. F., Waliser, D. E., Chen, W.-T., Guan, B., Kubar, T., Stephens, G., et al. (2012). An observationally based evaluation of cloud ice water in CMIP3 and CMIP5 GCMs and contemporary reanalyses using contemporary satellite data: CMIP3, CMIP5, IWC, CloudSat, GCM. *Journal of Geophysical Research: Atmospheres*, 117(D16), n/a-n/a. <https://doi.org/10.1029/2012JD017640>
- Li, J.-L. F., Waliser, D. E., Stephens, G., Lee, S., L'Ecuyer, T., Kato, S., et al. (2013). Characterizing and understanding radiation budget biases in CMIP3/CMIP5 GCMs, contemporary GCM, and reanalysis: RADIATION BUDGET BIASES IN CMIP3/CMIP5. *Journal of Geophysical Research: Atmospheres*, 118(15), 8166–8184. <https://doi.org/10.1002/jgrd.50378>
- Liuzzi, G. Masiello, C. Serio, S. Venafra, C. Camy-Peyret, Physical inversion of the full IASI spectra (2016): Assessment of atmospheric parameters retrievals, consistency of spectroscopy and forward modelling, *Journal of Quantitative Spectroscopy and Radiative Transfer*, 182, 128-157, <http://dx.doi.org/10.1016/j.jqsrt.2016.05.022>.
- Liuzzi, G., Masiello, G., Serio, C., Palchetti, L., and Bianchini, G. (2014). Validation of H₂O continuum absorption models in the wave number range 180–600 cm⁻¹ with atmospheric emitted spectral radiance measured at the Antarctica Dome-C site. *Optics Express*, 22(14), 16784. <https://doi.org/10.1364/OE.22.016784>
- Lodi, L., and Tennyson, J. (2012). Line lists for H₂18O and H₂17O based on empirical line positions and ab initio intensities. *Journal of Quantitative Spectroscopy and Radiative Transfer*, 113(11), 850–858. <https://doi.org/10.1016/j.jqsrt.2012.02.023>
- Maestri, T., Cossich, W., and Sbrolli, I. (2019). Cloud identification and classification from high spectral resolution data in the far and mid infrared. *Atmospheric Measurement Techniques Discussions*, 1–32. <https://doi.org/10.5194/amt-2019-28>
- Maestri, T., Rizzi, R., and Smith, J. A. (2005). Spectral infrared analysis of a cirrus cloud based on Airborne Research Interferometer Evaluation System (ARIES) measurements: SPECTRAL INFRARED ANALYSIS OF A CIRRUS CLOUD. *Journal of Geophysical Research: Atmospheres*, 110(D6), n/a-n/a. <https://doi.org/10.1029/2004JD005098>
- Malinowski, E. R. (2002). *Factor analysis in chemistry* (3rd ed). New York: Wiley.
- Marenco, F., Johnson, B., Turnbull, K., Newman, S., Haywood, J., Webster, H., Ricketts, H.. (2011). Airborne lidar observations of the 2010 Eyjafjallajökull volcanic ash plume. *Journal of Geophysical Research (Atmospheres)*. 116. [10.1029/2011JD016396](https://doi.org/10.1029/2011JD016396).

- Mast, J. C., Mlynczak, M. G., Cageao, R. P., Kratz, D. P., Latvakoski, H., Johnson, D. G., et al. (2017). Measurements of downwelling far-infrared radiance during the RHUBC-II campaign at Cerro Toco, Chile and comparisons with line-by-line radiative transfer calculations. *Journal of Quantitative Spectroscopy and Radiative Transfer*, 198, 25–39. <https://doi.org/10.1016/j.jqsrt.2017.04.028>
- McCarthy, M. P., Thorne, P. W., and Titchner, H. A. (2009). An Analysis of Tropospheric Humidity Trends from Radiosondes. *Journal of Climate*, 22(22), 5820–5838. <https://doi.org/10.1175/2009JCLI2879.1>
- McCarthy, M. P., Titchner, H. A., Thorne, P. W., Tett, S. F. B., Haimberger, L., and Parker, D. E. (2008). Assessing Bias and Uncertainty in the HadAT-Adjusted Radiosonde Climate Record. *Journal of Climate*, 21(4), 817–832. <https://doi.org/10.1175/2007JCLI1733.1>
- Merrelli, A., and Turner, D. D. (2012). Comparing Information Content of Upwelling Far-Infrared and Midinfrared Radiance Spectra for Clear Atmosphere Profiling. *Journal of Atmospheric and Oceanic Technology*, 29(4), 510–526. <https://doi.org/10.1175/JTECH-D-11-00113.1>
- Merrelli, A., and Turner, D. D. (2013). Information content for cloud ice microphysics in the FIR radiance spectrum (pp. 348–351). Presented at the RADIATION PROCESSES IN THE ATMOSPHERE AND OCEAN (IRS2012): Proceedings of the International Radiation Symposium (IRC/IAMAS), Dahlem Cube, Free University, Berlin. <https://doi.org/10.1063/1.4804778>
- Miloshevich, L. M., Vömel, H., Whiteman, D. N., Lesht, B. M., Schmidlin, F. J., and Russo, F. (2006). Absolute accuracy of water vapor measurements from six operational radiosonde types launched during AWEX-G and implications for AIRS validation. *Journal of Geophysical Research*, 111(D9). <https://doi.org/10.1029/2005JD006083>
- Mlawer, E. J., Turner, D. D., Paine, S. N., Palchetti, L., Bianchini, G., Payne, V. H., et al. (2019). Analysis of water vapor absorption in the far-infrared and submillimeter regions using surface radiometric measurements from extremely dry locations. *Journal of Geophysical Research: Atmospheres*. <https://doi.org/10.1029/2018JD029508>
- Mlynczak, M. G., Cageao, R. P., Mast, J. C., Kratz, D. P., Latvakoski, H., and Johnson, D. G. (2016). Observations of downwelling far-infrared emission at Table Mountain California made by the FIRST instrument. *Journal of Quantitative Spectroscopy and Radiative Transfer*, 170, 90–105. <https://doi.org/10.1016/j.jqsrt.2015.10.017>
- Mlynczak, M. G., Johnson, D. G., Latvakoski, H., Jucks, K., Watson, M., Kratz, D. P., et al. (2006). First light from the Far-Infrared Spectroscopy of the Troposphere (FIRST) instrument. *Geophysical Research Letters*, 33(7). <https://doi.org/10.1029/2005GL025114>
- NESDIS, Report from the Workshop on Continuity of Earth Radiation Budget (CERB) Observations: Post-CERES Requirements. NOAA Tech. Report NESDIS 134 (2011)

- O'Shea, S. J., Choularton, T. W., Lloyd, G., Crosier, J., Bower, K. N., Gallagher, M., et al. (2016). Airborne observations of the microphysical structure of two contrasting cirrus clouds: Microphysical Structure of Cirrus Clouds. *Journal of Geophysical Research: Atmospheres*, 121(22), 13,510-13,536. <https://doi.org/10.1002/2016JD025278>
- Palchetti, L., Belotti, C., Bianchini, G., Castagnoli, F., Carli, B., Cortesi, U., et al. (2006). Technical note: First spectral measurement of the Earth's upwelling emission using an uncooled wideband Fourier transform spectrometer. *Atmospheric Chemistry and Physics*, 6(12), 5025–5030. <https://doi.org/10.5194/acp-6-5025-2006>
- Palchetti, L., Bianchini, G., Carli, B., Cortesi, U., and Del Bianco, S. (2008). Measurement of the water vapour vertical profile and of the Earth's outgoing far infrared flux. *Atmospheric Chemistry and Physics*, 8(11), 2885–2894. <https://doi.org/10.5194/acp-8-2885-2008>
- Palchetti, Luca, Bianchini, G., Di Natale, G., and Del Guasta, M. (2015). Far-Infrared Radiative Properties of Water Vapor and Clouds in Antarctica. *Bulletin of the American Meteorological Society*, 96(9), 1505–1518. <https://doi.org/10.1175/BAMS-D-13-00286.1>.
- Parol, F., Buriez J. C., Brogniez G., and Fouquart, Y. (1991). Information Content of AVHRR Channels 4 and 5 with Respect to the Effective Radius of Cirrus Cloud Particles, *J. Appl. Meteorol.*, 30, 973–984, doi:10.1175/1520-0450-30.7.973.
- Peña, O. and Pal, U. (2009). Scattering of electromagnetic radiation by a multilayered sphere, *Computer Physics Communications*, Volume 180, Issue 11, November 2009, Pages 2348-2354 <https://doi.org/10.1016/j.cpc.2009.07.010>
- Pincus, R., Mlawer, E. J., Oreopoulos, L., Ackerman, A. S., Baek, S., Brath, M., et al. (2015). Radiative flux and forcing parameterization error in aerosol-free clear skies: RADIATION PARAMETERIZATION ERRORS. *Geophysical Research Letters*, 42(13), 5485–5492. <https://doi.org/10.1002/2015GL064291>
- Ploeger, F., Günther, G., Konopka, P., Fueglistaler, S., Müller, R., Hoppe, C., et al. (2013). Horizontal water vapor transport in the lower stratosphere from subtropics to high latitudes during boreal summer: HORIZONTAL WATER VAPOR TRANSPORT. *Journal of Geophysical Research: Atmospheres*, 118(14), 8111–8127. <https://doi.org/10.1002/jgrd.50636>
- Poshyvailo, L., Müller, R., Konopka, P., Günther, G., Riese, M., Podglajen, A., and Ploeger, F. (2018). Sensitivities of modelled water vapour in the lower stratosphere: temperature uncertainty, effects of horizontal transport and small-scale mixing. *Atmospheric Chemistry and Physics*, 18(12), 8505–8527. <https://doi.org/10.5194/acp-18-8505-2018>
- Pougatchev, N. (2008). Validation of atmospheric sounders by correlative measurements. *Applied Optics*, 47(26), 4739. <https://doi.org/10.1364/AO.47.004739>

- Prabhakara, C., Fraser, R. S., Dalu, G., Wu, M.-L. C., Curran, R. J., and Styles, T. (1988). Thin Cirrus Clouds: Seasonal Distribution over Oceans Deduced from Nimbus-4 IRIS. *Journal of Applied Meteorology*, 27(4), 379–399.
[https://doi.org/10.1175/1520-0450\(1988\)027<0379:TCCSDO>2.0.CO;2](https://doi.org/10.1175/1520-0450(1988)027<0379:TCCSDO>2.0.CO;2)
- Prabhakara, C., Rodgers, E. B., and Salomonson, V. V. (1973). Remote sensing of the global distribution of total ozone and the inferred upper-tropospheric circulation from Nimbus IRIS experiments. *Pure and Applied Geophysics*, 106–108(1), 1226–1237. <https://doi.org/10.1007/BF00881075>
- Prabhakara, C., Yoo, J.-M., Dalu, G., and Fraser, R. S. (1990). Deep Optically Thin Cirrus Clouds in the Polar Regions. Part I: Infrared Extinction Characteristics. *Journal of Applied Meteorology*, 29(12), 1313–1329.
[https://doi.org/10.1175/1520-0450\(1990\)029<1313:DOTCCI>2.0.CO;2](https://doi.org/10.1175/1520-0450(1990)029<1313:DOTCCI>2.0.CO;2)
- Raval, A., and Ramanathan, V. (1989). Observational determination of the greenhouse effect. *Nature*, 342(6251), 758–761. <https://doi.org/10.1038/342758a0>
- Remedios, J. J., Leigh, R. J., Waterfall, A. M., Moore, D. P., Sembhi, H., Parkes, I., Greenhough, J., Chipperfield, M. P., and Hauglustaine, D. (2007). MIPAS reference atmospheres and comparisons to V4.61/V4.62 MIPAS level 2 geophysical data sets, *Atmos. Chem. Phys. Discuss.*, 7, 9973–10017, doi:10.5194/acpd-7-9973-2007
- Riedi, J., Marchant, B., Platnick, S., Baum, B., Thieuleux, F., Oudard, C., Parol, F., Nicolas, J. M. and Dubuisson, P. (2010). Cloud thermodynamic phase inferred from merged POLDER and MODIS data. *Atmos. Chem. Phys.*, 10(23), 11851–11865. [10.5194/acp-10-11851-2010](https://doi.org/10.5194/acp-10-11851-2010)
- Riese, M., Ploeger, F., Rap, A., Vogel, B., Konopka, P., Dameris, M., and Forster, P. (2012). Impact of uncertainties in atmospheric mixing on simulated UTLS composition and related radiative effects: IMPACT OF MIXING ON RADIATIVE EFFECTS. *Journal of Geophysical Research: Atmospheres*, 117(D16), n/a-n/a.
<https://doi.org/10.1029/2012JD017751>
- Rizzi, R., Arosio, C., Maestri, T., Palchetti, L., Bianchini, G., and Del Guasta, M. (2016). One year of downwelling spectral radiance measurements from 100 to 1400 cm⁻¹ at Dome Concordia: Results in clear conditions: SPECTRAL FIR MEASUREMENTS AT DOME C. *Journal of Geophysical Research: Atmospheres*, 121(18), 10,937–10,953.
<https://doi.org/10.1002/2016JD025341>
- Rizzi, R., Maestri, T., and Arosio, C. (2018). Estimate of Radiosonde Dry Bias From Far-Infrared Measurements on the Antarctic Plateau. *Journal of Geophysical Research: Atmospheres*, 123(6), 3205–3211.
<https://doi.org/10.1002/2017JD027874>
- Roca, R., Brogniez, H., Chambon, P., Chomette, O., ClochÃ©, S., Gosset, M. E., et al. (2015). The Megha-Tropiques mission: a review after three years in orbit. *Frontiers in Earth Science*, 3.
<https://doi.org/10.3389/feart.2015.00017>

- Rodgers, C. D. (2000). *Inverse Methods for Atmospheric Sounding: Theory and Practice (Vol. 2)*. WORLD SCIENTIFIC.
<https://doi.org/10.1142/3171>
- Sassen, K., and Cho, B. S. (1992). Subvisual-Thin Cirrus Lidar Dataset for Satellite Verification and Climatological Research. *Journal of Applied Meteorology*, 31(11), 1275–1285. [https://doi.org/10.1175/1520-0450\(1992\)031<1275:STCLDF>2.0.CO;2](https://doi.org/10.1175/1520-0450(1992)031<1275:STCLDF>2.0.CO;2)
- Saunders, R. W., Blackmore, T. A., Candy, B., Francis, P. N., and Hewison, T. J. (2013). Monitoring Satellite Radiance Biases Using NWP Models. *IEEE Transactions on Geoscience and Remote Sensing*, 51(3), 1124–1138.
<https://doi.org/10.1109/TGRS.2012.2229283>
- Saunders, R., Hocking, J., Turner, E., Rayer, P., Rundle, D., Brunel, P., et al. (2018). An update on the RTTOV fast radiative transfer model (currently at version 12). *Geoscientific Model Development*, 11(7), 2717–2737.
<https://doi.org/10.5194/gmd-11-2717-2018>
- Saunders, R., Matricardi, M., and Brunel, P. (1999). An improved fast radiative transfer model for assimilation of satellite radiance observations. *Quarterly Journal of the Royal Meteorological Society*, 125(556), 1407–1425.
<https://doi.org/10.1002/qj.1999.49712555615>
- Saunders, Roger, Hocking, J., Turner, E., Rayer, P., Rundle, D., Brunel, P., et al. (2018). An update on the RTTOV fast radiative transfer model (currently at version 12). *Geoscientific Model Development*, 11(7), 2717–2737.
<https://doi.org/10.5194/gmd-11-2717-2018>.
- SCC (Social Cost of Carbon, U.S. Government, Interagency Working Group). 2010. Technical Support Document: Social Cost of Carbon for Regulatory Impact Analysis—Under Executive Order 12866.
<https://obamawhitehouse.archives.gov/sites/default/files/omb/inforeg/for-agencies/Social-Cost-of-Carbon-for-RIA.pdf>.
- Schoennagel, T. et al., (2017). Adapt to more wildfire in western North American forests as climate changes, *PNAS*, 114, 4582–4590
- Schroder, M et al., (2016), The GEWEX Water Vapor Assessment: Results from intercomparison, trend and homogeneity analysis of total column water vapor, *J. Appl. Met. Climatology*, 55, 1633-1649
- Scott, D. C., Herman, R. L., Webster, C. R., May, R. D., Flesch, G. J., and Moyer, E. J. (1999). Airborne Laser Infrared Absorption Spectrometer (ALIAS-II) for in situ atmospheric measurements of N₂O, CH₄, CO, HCL, and NO₂ from balloon or remotely piloted aircraft platforms. *Applied Optics*, 38(21), 4609.
<https://doi.org/10.1364/AO.38.004609>
- Serio, C., Masiello, G., Camy-Peyret, C., and Liuzzi, G. (2019). CO₂ spectroscopy and forward/inverse radiative transfer modelling in the thermal band using IASI spectra. *Journal of Quantitative Spectroscopy and Radiative Transfer*, 222–223, 65–83. <https://doi.org/10.1016/j.jqsrt.2018.10.020>

- Serio, C., Masiello, G., Camy-Peyret, C., Jacquette, E., Vandermarcq, O., Bermudo, F., et al. (2018). PCA determination of the radiometric noise of high spectral resolution infrared observations from spectral residuals: Application to IASI. *Journal of Quantitative Spectroscopy and Radiative Transfer*, 206, 8–21.
<https://doi.org/10.1016/j.jqsrt.2017.10.022>
- Serio, C., Masiello, G., Esposito, F., Di Girolamo, P., Di Iorio, T., Palchetti, L., Bianchini, G., Muscari, G., Pavese, G., Rizzi, R., Carli, B., and Cuomo, V.: Retrieval of foreign-broadened water vapor continuum coefficients from emitted spectral radiance in the H₂O rotational band from 240 to 590cm⁻¹, *Opt. Express*, 16, 15816–15833, doi:10.1364/OE.16.015816, 2008.
- Shephard, M. W., Clough, S. A., Payne, V. H., Smith, W. L., Kireev, S., and Cady-Pereira, K. E. (2009). Performance of the line-by-line radiative transfer model (LBLRTM) for temperature and species retrievals: IASI case studies from JAIVEx. *Atmospheric Chemistry and Physics*, 9(19), 7397–7417. <https://doi.org/10.5194/acp-9-7397-2009>
- Sherwood, S. C., Roca, R., Weckwerth, T. M., and Andronova, N. G. (2010). Tropospheric water vapor, convection, and climate. *Reviews of Geophysics*, 48(2). <https://doi.org/10.1029/2009RG000301>
- Shi, L., and Bates, J. J. (2011). Three decades of intersatellite-calibrated High-Resolution Infrared Radiation Sounder upper tropospheric water vapor. *Journal of Geophysical Research*, 116(D4).
<https://doi.org/10.1029/2010JD014847>
- Shine, K. P., Ptashnik, I. V., and Rädcl, G. (2012). The Water Vapour Continuum: Brief History and Recent Developments. *Surveys in Geophysics*, 33(3–4), 535–555. <https://doi.org/10.1007/s10712-011-9170-y>
- Sinha, A., and Harries, J. E. (1995). Water vapour and greenhouse trapping: The role of far infrared absorption. *Geophysical Research Letters*, 22(16), 2147–2150. <https://doi.org/10.1029/95GL01891>
- Slingo, A., and Webb, M. (1997). The spectral signature of global warming. *Quarterly Journal of the Royal Meteorological Society*, 123(538), 293–307. <https://doi.org/10.1256/smsqj.53802>
- Soden, B. J., and Held, I. M. (2006). An Assessment of Climate Feedbacks in Coupled Ocean–Atmosphere Models. *Journal of Climate*, 19(14), 3354–3360. <https://doi.org/10.1175/JCLI3799.1>
- Soden, B. J., Collins, W. D., and Feldman, D. R. (2018). Reducing uncertainties in climate models. *Science*, 361(6400), 326–327. <https://doi.org/10.1126/science.aau1864>
- Solomon, S., Rosenlof, K. H., Portmann, R. W., Daniel, J. S., Davis, S. M., Sanford, T. J., and Plattner, G.-K. (2010). Contributions of Stratospheric Water Vapor to Decadal Changes in the Rate of Global Warming. *Science*, 327(5970), 1219–1223. <https://doi.org/10.1126/science.1182488>
- Sourdeval, O., C.-Labonnote, L., Baran, A. J., Mülmenstädt, J. and Brogniez, G. (2016). A methodology for simultaneous retrieval of ice and liquid water cloud properties. Part 2: Near-global retrievals and evaluation against A-Train products. *Q.J.R. Meteorol. Soc.*, 142(701), 3063-3081. [10.1002/qj.2889](https://doi.org/10.1002/qj.2889)

- Spankuch, D. (1980). Studies made in the meteorological service of the GDR in indirect sounding. *Zeitschrift Für Meteorologie*, 30.4, 205–214.
- Spurr, R. (2008). LIDORT and VLIDORT: Linearized pseudo-spherical scalar and vector discrete ordinate radiative transfer models for use in remote sensing retrieval problems. *Light Scattering Reviews*, Volume 3, ed. A. Kokhanovsky, Springer.
- Stamnes, K., Tsay, C. S., Wiscombe, W. and Jayaweera, K. (1988). Numerically stable algorithm for discrete-ordinate-method radiative transfer in multiple scattering and emitting layered media. *Applied optics*. 27. 2502-9.
- Stephens, G. L., Li, J., Wild, M., Clayson, C. A., Loeb, N., Kato, S., et al. (2012). An update on Earth's energy balance in light of the latest global observations. *Nature Geoscience*, 5, 691.
- Stephens, G. L., Tsay, S.-C., Stackhouse, P. W., and Flatau, P. J. (1990). The Relevance of the Microphysical and Radiative Properties of Cirrus Clouds to Climate and Climatic Feedback. *Journal of the Atmospheric Sciences*, 47(14), 1742–1754. [https://doi.org/10.1175/1520-0469\(1990\)047<1742:TROTMA>2.0.CO;2](https://doi.org/10.1175/1520-0469(1990)047<1742:TROTMA>2.0.CO;2)
- Stocker, T. F., Qin, D., Plattner, G.-K., Tignor, M., Allen, S. K., Boschung, J., et al. (2013). *Climate Change 2013: The Physical Science Basis. Contribution of Working Group I to the Fifth Assessment Report of the Intergovernmental Panel on Climate Change*. Cambridge, UK.
- Su, W., Corbett, J., Eitzen, Z., and Liang, L. (2015). Next-generation angular distribution models for top-of-atmosphere radiative flux calculation from CERES instruments: methodology. *Atmospheric Measurement Techniques*, 8(2), 611–632. <https://doi.org/10.5194/amt-8-611-2015>
- Su, Z., Timmermans, W., Zeng, Y., Schulz, J., John, V. O., Roebeling, R. A., et al. (2018). An Overview of European Efforts in Generating Climate Data Records. *Bulletin of the American Meteorological Society*, 99(2), 349–359. <https://doi.org/10.1175/BAMS-D-16-0074.1>
- Sun, B., Reale, A., Tilley, F. H., Pettay, M. E., Nalli, N. R., and Barnet, C. D. (2017). Assessment of NUCAPS S-NPP CrIS/ATMS Sounding Products Using Reference and Conventional Radiosonde Observations. *IEEE Journal of Selected Topics in Applied Earth Observations and Remote Sensing*, 10(6), 2499–2509. <https://doi.org/10.1109/JSTARS.2017.2670504>
- Susskind, J., Molnar, G., Iredell, L., and Loeb, N. G. (2012). Interannual variability of outgoing longwave radiation as observed by AIRS and CERES: OLR OBSERVED BY AIRS AND CERES. *Journal of Geophysical Research: Atmospheres*, 117(D23), n/a-n/a. <https://doi.org/10.1029/2012JD017997>
- Sussmann, R., Reichert, A., and Rettinger, M. (2016), The Zugspitze radiative closure experiment for quantifying water vapor absorption over the terrestrial and solar infrared – Part 1: Setup, uncertainty analysis, and assessment of far-infrared water vapor continuum, *Atmos. Chem. Phys.*, 16, 11649-11669, doi:10.5194/acp-16-11649-2016.

- Tan, I., Storelvmo, T., and Zelinka, M. D. (2016). Observational constraints on mixed-phase clouds imply higher climate sensitivity. *Science*, 352(6282), 224–227. <https://doi.org/10.1126/science.aad5300>
- Thelen J-C, Havemann S, Newman SM, Taylor JP. (2009). Hyperspectral retrieval of land surface emissivities using ARIES. *Q J R Meteorol Soc* 2009;135(645, B, SI):2110–24. doi: 10.1002/qj.520 .
- Théodore, B., Coppens, D., Döhler, W., Damiano, A., Oertel, D., Klaes, D., et al. (2015). In A glimpse into the past: rescuing hyperspectral SI-1 data from Meteor-28 and 29. Toulouse, France.
- Tobin, D. C., Best, F. A., Brown, P. D., Clough, S. A., Dedecker, R. G., Ellingson, R. G., et al. (1999). Downwelling spectral radiance observations at the SHEBA ice station: Water vapor continuum measurements from 17 to 26 μ m. *Journal of Geophysical Research: Atmospheres*, 104(D2), 2081–2092. <https://doi.org/10.1029/1998JD200057>
- Tobin, D. C., Revercomb, H. E., Knuteson, R. O., Lesht, B. M., Strow, L. L., Hannon, S. E., et al. (2006). Atmospheric Radiation Measurement site atmospheric state best estimates for Atmospheric Infrared Sounder temperature and water vapor retrieval validation. *Journal of Geophysical Research*, 111(D9). <https://doi.org/10.1029/2005JD006103>
- Tobin, D., Revercomb, H., and Antonelli, P. (2009). Principal Component Analysis of IASI Spectra with a Focus on Non-Uniform Scene Effects on the ILS (pp. 16–19). Presented at the CURRENT PROBLEMS IN ATMOSPHERIC RADIATION (IRS 2008): Proceedings of the International Radiation Symposium (IRC/IAMAS), Foz do Iguaçú (Brazil). <https://doi.org/10.1063/1.3116941>
- Trenberth, K. E., and Fasullo, J. T. (2013). An apparent hiatus in global warming?, *Earth's Future*, 1, 19–32, doi:10.1002/2013EF000165
- Trent, T., Schröder, M., and Remedios, J. (2019). GEWEX Water Vapor Assessment: Validation of AIRS Tropospheric Humidity Profiles With Characterized Radiosonde Soundings. *Journal of Geophysical Research: Atmospheres*, 124(2), 886–906. <https://doi.org/10.1029/2018JD028930>
- Turner, D. D., and Mlawer, E. J. (2010). The Radiative Heating in Underexplored Bands Campaigns. *Bulletin of the American Meteorological Society*, 91(7), 911–924. <https://doi.org/10.1175/2010BAMS2904.1>
- Turner, D. D., Knuteson, R. O., Revercomb, H. E., Lo, C., and Dedecker, R. G. (2006). Noise Reduction of Atmospheric Emitted Radiance Interferometer (AERI) Observations Using Principal Component Analysis. *Journal of Atmospheric and Oceanic Technology*, 23(9), 1223–1238. <https://doi.org/10.1175/JTECH1906.1>
- Turner, D. D., Merrelli, A., Vimont, D., and Mlawer, E. J. (2012). Impact of modifying the longwave water vapor continuum absorption model on community Earth system model simulations: IMPACT OF A WATER VAPOR CONTINUUM CHANGE. *Journal of Geophysical Research: Atmospheres*, 117(D4), n/a-n/a. <https://doi.org/10.1029/2011JD016440>

- Turner, D., (2005), Arctic mixed phase cloud properties from AERI lidar observations: Algorithm and results from SHEBA, *J. Appl. Met.*, 44, 427-444
- United Nations. (2015). 2030 Agenda for Sustainable Development (No. A/RES/70/1). United Nations. Retrieved from https://www.un.org/ga/search/view_doc.asp?symbol=A/RES/70/1andLang=E
- Van Aalst, M. K. (2006), The impacts of climate change on the risk of natural disasters. *Disasters*, 30: 5-18.
doi:10.1111/j.1467-9523.2006.00303.x
- Veglio, P. and Maestri, T. (2009) Statistics of vertical backscatter profiles of cirrus clouds, *Atmos. Chem. Phys.*, 11, 12925-12943, <https://doi.org/10.5194/acp-11-12925-2011>.
- Vial, J., Dufresne, J.-L., and Bony, S. (2013). On the interpretation of inter-model spread in CMIP5 climate sensitivity estimates. *Climate Dynamics*, 41(11–12), 3339–3362. <https://doi.org/10.1007/s00382-013-1725-9>
- Vidot, J., Baran, A. J., and Brunel, P. (2015). A new ice cloud parameterization for infrared radiative transfer simulation of cloudy radiances: Evaluation and optimization with IIR observations and ice cloud profile retrieval products: ICE CLOUD PARAMETERIZATION FOR IR RTM. *Journal of Geophysical Research: Atmospheres*, 120(14), 6937–6951. <https://doi.org/10.1002/2015JD023462>
- Vidot, J., Labonnote, L.-C., Baran, A. J., Matricardi, M., and Brunel, P. (2019). Evaluation of the RTTOV scattering parameterization with LIDORT for hyperspectral IR cloudy radiances and Jacobians. *Geoscientific Model Development*, to be submitted.
- Voosen, P. (2019). New climate models forecast a warming surge. *Science*, 364(6437), 222.
<https://doi.org/10.1126/science.364.6437.222>
- Waliser, D. E., Li, J.-L. F., Woods, C. P., Austin, R. T., Bacmeister, J., Chern, J., et al. (2009). Cloud ice: A climate model challenge with signs and expectations of progress. *Journal of Geophysical Research*, 114.
<https://doi.org/10.1029/2008JD010015>
- Walsh, K. J., McBride, J. L., Klotzbach, P. J., Balachandran, S., Camargo, S. J., Holland, G., Knutson, T. R., Kossin, J. P., Lee, T., Sobel, A. and Sugi, M. (2016), Tropical cyclones and climate change. *WIREs Clim Change*, 7: 65-89.
doi:10.1002/wcc.371
- Whiteway, J. (2004). Anatomy of cirrus clouds: Results from the Emerald airborne campaigns. *Geophysical Research Letters*, 31(24). <https://doi.org/10.1029/2004GL021201>
- Wielicki, B. A., Barkstrom, B. R., Harrison, E. F., Lee, R. B., Louis Smith, G., and Cooper, J. E. (1996). Clouds and the Earth's Radiant Energy System (CERES): An Earth Observing System Experiment. *Bulletin of the American Meteorological Society*, 77(5), 853–868. [https://doi.org/10.1175/1520-0477\(1996\)077<0853:CATERE>2.0.CO;2](https://doi.org/10.1175/1520-0477(1996)077<0853:CATERE>2.0.CO;2)



- Wielicki, B. A., Young, D. F., Mlynchzak, M. G., Thome, K. J., Leroy, S., Corliss, J., et al. (2013). Achieving Climate Change Absolute Accuracy in Orbit. *Bulletin of the American Meteorological Society*, 94(10), 1519–1539.
<https://doi.org/10.1175/BAMS-D-12-00149.1>
- Wielicki, B.A., D.F. Young, M.G. Mlynchzak, K.J. Thome, S. Leroy, J. Corliss, J.G. Anderson, C.O. Ao, R. Bantges, F. Best, K. Bowman, H. Brindley, J.J. Butler, W. Collins, J.A. Dykema, D.R. Doelling, D.R. Feldman, N. Fox, X. Huang, R. Holz, Y. Huang, Z. Jin, D. Jennings, D.G. Johnson, K. Jucks, S. Kato, D.B. Kirk-Davidoff, R. Knuteson, G. Kopp, D.P. Kratz, X. Liu, C. Lukashin, A.J. Mannucci, N. Phojanamongkolkij, P. Pilewskie, V. Ramaswamy, H. Revercomb, J. Rice, Y. Roberts, C.M. Roithmayr, F. Rose, S. Sandford, E.L. Shirley, W.L. Smith, B. Soden, P.W. Speth, W. Sun, P.C. Taylor, D. Tobin, and X. Xiong, 2013: Achieving Climate Change Absolute Accuracy in Orbit. *Bull. Amer. Meteor. Soc.*, 94, 1519–1539, <https://doi.org/10.1175/BAMS-D-12-00149.1>
- Wilson, S., Atkinson, N., and Smith, J. (1999). The development of an airborne infrared interferometer for meteorological sounding studies. *J. Atmos. Ocean. Tech.*, 16, 1912–1927.
- WMO (2016), The Global Observing System for Climate: Implementation Needs, GCOS- No. 200,
https://library.wmo.int/index.php?lvl=notice_display&id=19838#.XO-fIZypVhF
- Yang, P., Bi, L., Baum, B. A., Liou, K.-N., Kattawar, G. W., Mishchenko, M. I., and Cole, B. (2013). Spectrally Consistent Scattering, Absorption, and Polarization Properties of Atmospheric Ice Crystals at Wavelengths from 0.2 to 100 μ m. *Journal of the Atmospheric Sciences*, 70(1), 330–347. <https://doi.org/10.1175/JAS-D-12-039.1>
- Yang, P., Liou, K.-N., Bi, L., Liu, C., Yi, B., and Baum, B. A. (2015). On the radiative properties of ice clouds: Light scattering, remote sensing, and radiation parameterization. *Advances in Atmospheric Sciences*, 32(1), 32–63.
<https://doi.org/10.1007/s00376-014-0011-z>
- Young, A., et al., (2018), The International Satellite Cloud Climatology Project H-Series climate data record product, *Earth Syst. Sci. Data*, 10, 583-593
- Yu, S., Pearson, J. C., Drouin, B. J., Martin-Drumel, M.-A., Pirali, O., Vervloet, M., et al. (2012). Measurement and analysis of new terahertz and far-infrared spectra of high temperature water. *Journal of Molecular Spectroscopy*, 279, 16–25. <https://doi.org/10.1016/j.jms.2012.07.011>
- Zelinka, M. D., and Hartmann, D. L. (2011). The observed sensitivity of high clouds to mean surface temperature anomalies in the tropics: TEMPERATURE SENSITIVITY OF HIGH CLOUDS. *Journal of Geophysical Research: Atmospheres*, 116(D23), n/a-n/a. <https://doi.org/10.1029/2011JD016459>
- Zhang, Y., Rossow, W. B., Lacis, A. A., Oinas, V., and Mishchenko, M. I. (2004). Calculation of radiative fluxes from the surface to top of atmosphere based on ISCCP and other global data sets: Refinements of the radiative transfer model and the input data, *J. Geophys. Res.*, 109, D19105, doi:10.1029/2003JD004457.



Zhou, C., Dessler, A. E., Zelinka, M. D., Yang, P., and Wang, T. (2014). Cirrus feedback on interannual climate fluctuations: Cirrus feedback on climate fluctuations. *Geophysical Research Letters*, 41(24), 9166–9173.
<https://doi.org/10.1002/2014GL062095>

ACRONYMS

AIRS	Atmospheric Infrared Sounder
ASC	Canadian Space Agency
3MI	Multi-viewing, Multi-channel, Multi-polarization Imager
ADM	Angular Distribution Model
AIT	Assembly Integration and Test
AOCS	Attitude and Orbit Control Subsystem
ARA	Absolute Radiometric Accuracy
BT	Brightness Temperature
CALIOP	<i>Cloud-Aerosol Lidar with Orthogonal Polarization</i>
CBH	Cloud Bottom Height
CCI	Climate Change Initiative
CERES	Cloud's and the Earth's Radiant Energy Systems
CESM	Community Earth System Model
CH ₄	Methane
CIC	Cloud Identification and Classification
CMIP5, CMIP6	Coupled Model Intercomparison Project 5/6
CO ₂	Carbon Dioxide
COTS	Commercial Off-The-Shelf
CrIS	Cross-Track Infrared Sounder
CTH	Cloud Top Height
CTOP	Cloud Top Pressure
CVD	Chemical Vapor Deposition
DARDAR	Radar/Lidar Project
DET	Direct Energy Transfer
ΔF	Radiative Forcing
DLaTGS	Deuterated L-alanine Dopped Triglycine Sulphate
DoD	Depth of Discharge
ECMWF	European Centre for Medium-Range Weather Forecasts
ECV	Essential Climate Variable
EMS	Estrack Management and Schedule System
ENSO	El Niño Southern Oscillation
EO-CFI	Earth Observation Custom Furnished Item
ERB	Earth Radiation Budget
ESA	European Space Agency
ESA-CCS	European Space Agency Constellation Coordination Tool
ESOC	European Space Operation Center
EUMETSAT	European Organisation for the Exploitation of Meteorological Satellites
FD	Flight Dynamics
FDIR	Failure Detection Isolation and Recovery
FEE	Front End Electronics



FEI	FORUM Embedded Imager
FEM	Finite Element Model
FIR	Far InfraRed
FIRST	Far-InfraRed Spectroscopy of the Troposphere
FM	Forward Model
FOCC	Flight Operations Control Centre
FORUM	Far-infrared-Outgoing-Radiation Understanding and Monitoring
FOS	Flight Operations Segment
FoV	Field of View
FPA	Focal Plane Array
FSI	FORUM Sounding Instrument
FTS	Fourier Transform Spectrometer
FWHM	Full Width Half Maximum
G	goal
GCM	General Circulation Model
GCOS	Global Climate Observing System
GERB	Geostationary Earth Radiation Budget
GEWEX	Global Energy and Water cycle Experiment
GFRP	Glass Fiber Reinforced Polymer
GM	Geometry Module
GNSS	Global Navigation Satellite System
GPS	Global Positioning System
GRUAN	GCOS Reference Upper Air Network
GS	Ground Station
GSD	Ground Sampling Distance
HIRDLS	High Resolution Dynamics Limb Sounder
HK	HouseKeeping
HKTM	HouseKeeping and TeleMetry
IASI	Infrared atmospheric sounding interferometer
IASI-NG	Infrared Atmospheric Sounding Interferometer-Next Generation
ICU	Instrument Control Unit
ILS	Instrument Line Shape
IPCC	Intergovernmental Panel on Climate Change
IR	Infrared
IRIS	Infrared Interferometer Spectrometer
IRS	InfRared Sounder
ISRF	Instrument Spectral Response Function
IWP	Ice Water Path
LEOP	Launch and Early Operation Phase
LM	Levenberg-Marquardt
LoS	Line of Sight



MAG	Mission Advisory Group
MAP	Maximum A-posteriori Probability
MetOp-SG	Meteorological Operational Satellite - Second Generation
MIR	Mid-Infrared
MLI	Multi Layer Insulation
MLST	Mean Local Solar Time
MODIS	MODERate Imaging Spectroradiometer
MOPD	Maximum Optical Path Difference
MoS	Margins of Safety
MPS	Mission Planning System
MTF	Modulation Transfer Function
MTG	Meteosat Third Generation
N2O	Nitrous Oxide
NASA	National Aeronautics and Space Administration
NEdT	Noise Equivalent delta Temperature
NESR	Noise Equivalent Spectral Radiance
NWP	Numerical Weather Prediction
O3	Ozone
OBC	On-Board Computer
OBSW	On-Board SoftWare
OGSE	Optical Ground Support Equipment
OLR	Outgoing Longwave Radiation
OOB	Out-Of-Band
OPAC	Optical Properties of Aerosols and Clouds: The Software Package
OPD	Optical Path Difference
OSCAR	Optimized Spacecraft Computer Architecture with Reconfiguration
OSCAR	Observing Systems Capability Analysis and Review Tool
OSS	Observation System Simulator
PCDU	Power Conditioning and Distribution Unit
PDGS	Payload Data Ground Segment
PDHT	Payload Data Handling and Transmission
PDHU	Payload Data Handling Unit
ppm	parts per million
PREFIRE	Polar Radiant Energy in the Far Infrared Experiment
PRR	Preliminary Requirements Review
PRT	Platinum Resistance Thermometer
PTB	Physikalisch-Technische Bundesanstalt
PUS	Packet Utilization Standard
PVT	Position Velocity and Time
QBO	Quasi-Biennial Oscillation
RAAN	Right Angle of Ascending Node



REFIR-PAD	Radiation Explorer in the Far InfraRed – Prototype of Applications and Development
RF	Radio Frequency
RHUBC-II	Radiative Heating in the Underexplored Bands Campaign – II
RIU	Remote Interface Unit
RT	Radiative Transfer
RTTOV	Radiative Transfer for TOVS
RU	Reconfiguration Unit
RXRA	Relative Spatial Radiometric Accuracy
S5p	Sentinel-5 precursor
ScaRaB	French/Indian Scanner for Radiation Budget
SDO	Space Debris Office
SEDF	System Energy Distribution Function
SGM	Scene Generation Module
SI	International System of Units - Système international d'unités
SI-1	Spektrometer Interferometer-1
SIE	System Integrated Energy
sinc	sine cardinal
SMU	Satellite Management Unit
SPARC	Stratosphere-troposphere Processes And their Role in Climate
SRL	Scientific Readiness Level
SSD	Spatial Sampling Distance
SSM	Secondary Surface Mirror
SSO	Sun-Synchronous Orbit
STOP	Structural Thermal Optical Performance
T	Threshold
TAFTS	Tropospheric Airborne Fourier Transform Spectrometer
TICFIRE	Thin Ice Clouds in the Far Infrared Experiment
TOA	Top Of the Atmosphere
ToD	True of Date
TOVS	Tiros-N Operational Vertical Sounder
TRL	Technology Readiness Level
TT&C	Telemetry, Tracking and Command
TWTA	Travelling Wave Tube Amplifier
UCM	User Consultation Meeting
UTLS	Upper Troposphere/ Lower Stratosphere
WFE	Wave Front Error
VMR	Volume Mixing Ratio
WAVAS-2	Water Vapour Assessment 2
WCRP	World Climate Research Programme
WMO	World Meteorological Organization



ZPD	Zero Path Difference
χ^2	chi-square
(G)	Goal
(T)	Threshold